

6-9-2016

# Differential Interactions of Lipopolysaccharides with Lipid Bilayers: Applications for Pathogen Detection

Loreen R. Stromberg

Follow this and additional works at: [https://digitalrepository.unm.edu/bme\\_etds](https://digitalrepository.unm.edu/bme_etds)

---

## Recommended Citation

Stromberg, Loreen R.. "Differential Interactions of Lipopolysaccharides with Lipid Bilayers: Applications for Pathogen Detection." (2016). [https://digitalrepository.unm.edu/bme\\_etds/9](https://digitalrepository.unm.edu/bme_etds/9)

This Dissertation is brought to you for free and open access by the Engineering ETDs at UNM Digital Repository. It has been accepted for inclusion in Biomedical Engineering ETDs by an authorized administrator of UNM Digital Repository. For more information, please contact [disc@unm.edu](mailto:disc@unm.edu).

Loreen R. Stromberg

*Candidate*

Biomedical Engineering

*Department*

This dissertation is approved, and it is acceptable in quality and form for publication:

*Approved by the Dissertation Committee:*

Steven W. Graves, Ph.D., Chairperson

Harshini Mukundan, Ph.D., Co-Chairperson

Gabriel A. Montaña, Ph.D.

Andrew P. Shreve, Ph.D.

Douglas J. Perkins, Ph.D.

**DIFFERENTIAL INTERACTIONS OF  
LIPOPOLYSACCHARIDES WITH LIPID BILAYERS:  
APPLICATIONS FOR PATHOGEN DETECTION**

**by**

**LOREEN R. STROMBERG**

B.S., Biochemistry, University of New Mexico, 2012

**DISSERTATION**

Submitted in Partial Fulfillment of the  
Requirements for the Degree of

**Doctor of Philosophy  
Engineering**

The University of New Mexico  
Albuquerque, New Mexico

**May 2016**

## ACKNOWLEDGEMENTS

I would like to thank my advisor Dr. Harshini Mukundan for her advice, both personal and professional, which has helped me reach this milestone. She granted me an enormous amount of autonomy in the lab which helped me grow tremendously as scientist. As a result of her input and positive outlook, I can now view my data from multiple angles, not just the negative ones that I normally see. Additionally I would like to thank my co-advisor Dr. Steven Graves, for facilitating the relationship between Los Alamos National Laboratory and the University of New Mexico. I would never have been able to successfully jump through all the necessary hoops without his guidance and direction. I also need to thank Dr. Gabriel Montaña, who has become my honorary advisor, for his guidance and direction for my projects while I worked in his lab. His enthusiasm for science combined with a good sense of humor and balance helped me continue on days when I was ready to quit, for which I am ever grateful. Additionally, I thank Dr. Andrew Shreve for his input in regards to data analysis and experimental design. His suggestions have helped me to develop a deeper understanding of data collection, which has only strengthened this project and my skills as a scientist. Lastly, I need to thank Dr. Douglas Perkins for his amazing knowledge in cytokine expression and innate immunity. He was a great encouragement and resource while I developed this project. Only now can I look back and fully appreciate his insight in developing proper controls and strategies for analysis.

There are a great deal of other researchers and students that I must also thank for the role they played in my development and growth. Firstly, I must thank Dr. Peter Adams, who was kind enough to train me and allow me to work with him. His attention to detail was critical to my development as a scientist, and he was a great mentor, probably without realizing it. I also need to acknowledge Aaron Anderson, who was always there to discuss technical problems, perform computer updates, and lend an open ear for complaints. If it wasn't for his friendship in the lab, I might have given up long ago. There is also a long list of people who have provided both technical and emotional support during this time. Specifically, I would like to

thank Matt Rush, Kirstie Swingle, and Heather Mendez for their help. Additionally, I need to thank the former and current students and post-docs of the Graves lab, Shreve lab, and Montaña lab who have aided me throughout the years- your help, suggestions, and discussions of data have always been appreciated.

Finally, I need to thank my family and friends who have given me support and love throughout the years. My parents have provided unending support to me in many forms, my appreciation for them cannot be overstated. In every literal sense, this accomplishment would not have been possible without them. I need to thank my husband, Dr. Zachary Stromberg, for his love, patience, and humor, as well as his professional contributions to my work. Also, I would like to acknowledge Nishta Mukundan, who will one day realize the relevance of this. Her sense of joy and wonder lifted my spirits, encouraged me to set aside work in the evening, and provided therapy for my soul, but I am still waiting for that glitter laden card I was promised.

Lastly, this dissertation would not have been possible, or nearly as complete, without the wonderful staff at the UNM Interlibrary Loan and the modern wonders of caffeine, ibuprofen, and the internet.

**DIFFERENTIAL INTERACTIONS OF LIPOPOLYSACCHARIDES WITH LIPID  
BILAYERS:  
APPLICATIONS FOR PATHOGEN DETECTION**

by

**Loreen R. Stromberg**

**B.S. Biochemistry, University of New Mexico, 2012**

**Ph.D. Biomedical Engineering, University of New Mexico, 2016**

**ABSTRACT**

This dissertation describes the development of new tailored methods for the discriminative detection of amphiphilic lipopolysaccharide (LPS) antigens, so as to improve screening methodologies for food-safety applications, and detection of amphiphiles in general. LPS is associated with the outer membrane of Gram-negative bacteria, and is a primary virulence biomarker of several pathogens. Direct detection of amphiphilic LPS in the aqueous matrices of the host/sample requires an appreciation of the complex biochemistry of the molecule, and forms the basis for this research. The unique structure of this molecule can be used for identification of both the serogroup and strain of pathogen. However, current detection methods lack sensitivity, and are also not serogroup specific. To achieve discriminative detection, we have first created a unique repertoire of associated reagents by isolating amphiphilic LPS from seven strains of Shiga toxin-producing *Escherichia coli*, and developing highly specific monoclonal antibodies against the O antigen regions of the same. We demonstrate the use of a targeted detection technique, called membrane insertion, which facilitates the physiological presentation of LPS by inserting the hydrophobic lipid A portion of the molecule into a lipid bilayer, leaving the O antigen exposed. This method is advantageous because it minimizes exposure of the highly conserved lipid A epitopes, and maximizes exposure of the serogroup specific O antigens. In addition, we present the first comprehensive biophysical analysis of the interaction of LPS with supported lipid bilayer

architectures, and identify several novel and interesting effects of the same. Further characterization of these effects reveals the role or impact of membrane proteins and complexity on the interactions between host and pathogen biomarkers and significantly questions the design and execution of cell studies and *in vitro* platforms for amphiphilic targets like LPS. Cell studies clearly reveal that presentation of LPS either in buffer or in serum dramatically alters associated cytokine profiles. Our conclusions indicate that the biochemistry of amphiphilic molecules, like LPS, and their presentation, should always be considered when interfacing with physiological systems.

## TABLE OF CONTENTS

<b>LIST OF FIGURES</b> .....	xi
<b>LIST OF TABLES</b> .....	xv
<b>Chapter 1. Introduction</b> .....	1
1.1 <i>Considerations for universal bacterial detection systems</i> .....	1
1.2 <i>Sources of lipopolysaccharides</i> .....	3
1.3 <i>Lipopolysaccharide structures and conformations</i> .....	5
1.4 <i>Detection methods for lipopolysaccharides and similar amphiphiles</i> .....	10
1.4.1 <i>Limulus amoebocyte lysate assay and the rabbit pyrogen test</i> .....	10
1.4.2 <i>Immunoassays for LPS detection and antibody screening</i> .....	14
1.4.3 <i>Biological and chemical-based LPS sensing</i> .....	18
1.4.4 <i>Cell-based LPS detection platforms</i> .....	24
1.5 <i>Present studies</i> .....	25
1.6 <i>References</i> .....	31
<b>Chapter 2. Goals and Overview of this Work</b> .....	48
<b>Chapter 3. Purification and characterization of lipopolysaccharides from six strains of non-O157 Shiga toxin-producing <i>Escherichia coli</i></b> .....	58
3.1 <i>Abstract</i> .....	59
3.2 <i>Introduction</i> .....	59
3.3 <i>Materials and methods</i> .....	62
3.3.1 <i>Materials</i> .....	62
3.3.2 <i>Growth of STEC</i> .....	63
3.3.3 <i>Phenol extraction</i> .....	64
3.3.4 <i>Purification of LPS</i> .....	64
3.3.5 <i>Precipitation of nucleic acids from purified extracts</i> .....	64
3.3.6 <i>Hydrolysis of lipid A</i> .....	65
3.3.7 <i>Sodium dodecyl sulfate – polyacrylamide gel electrophoresis</i> .....	65
3.3.8 <i>Inverse staining with eosin B</i> .....	66
3.3.9 <i>Antibodies and immunoblotting</i> .....	66
3.3.10 <i>Western-type blotting of lipopolysaccharides</i> .....	67
3.3.11 <i>Image processing</i> .....	67
3.4 <i>Results and Discussion</i> .....	68
3.4.1 <i>Bacterial growth and purification of lipopolysaccharides</i> .....	68
3.4.2 <i>Gel electrophoresis</i> .....	68
3.4.3 <i>Western-type and immunoblotting</i> .....	69
3.5 <i>Conclusions</i> .....	73
3.6 <i>Conflict of Interest</i> .....	73
3.7 <i>Acknowledgements</i> .....	74
3.8 <i>References</i> .....	75
<b>Chapter 4. O Antigen Monoclonal Antibodies For Shiga Toxin-Producing <i>Escherichia coli</i> Serogroups O26, O45, O103, O111, O121, and O145</b> .....	79
4.1 <i>Abstract</i> .....	80

4.2	<i>Introduction</i>	80
4.3	<i>Materials and Methods</i>	82
4.3.1	Bacterial strains and serum screening	82
4.3.2	Hybridoma production and screening	84
4.3.3	Developing assays to test antibody specificity	85
4.4	<i>Results and discussion</i>	86
4.4.1	Serum screening and immunoblotting	86
4.4.2	Assays for testing antibody specificity	92
4.5	<i>Conclusion</i>	95
4.6	<i>Future directions</i>	95
4.7	<i>Acknowledgments</i>	95
4.8	<i>References</i>	97
<b>Chapter 5. Lipopolysaccharide-induced dynamic lipid membrane reorganization: tubules, perforations and stacks</b>		100
5.1	<i>Abstract</i>	101
5.2	<i>Introduction</i>	101
5.3	<i>Materials and Methods</i>	105
5.3.1	Materials	105
5.3.2	Liposome and Supported Lipid Bilayer Formation	105
5.3.3	Treatment of surfaces with LPS	106
5.3.4	Microscopy of LPS-treated sLBAs	106
5.4	<i>Results</i>	107
5.4.1	Lipid tubule formation is induced by LPS in PBS	108
5.4.2	Hole formation in the sLBA after LPS treatment in PBS and washing	110
5.4.3	LPS in Ca <sup>2+</sup> buffer induces lamellar sheet formation instead of lipid tubules	113
5.5	<i>Discussion</i>	116
5.5.1	Considerations of the model membrane system	116
5.5.2	Membrane effects induced by LPS-Na <sup>+</sup>	117
5.5.3	Membrane effects induced by LPS-Ca <sup>2+</sup>	120
5.5.4	Understanding LPS-sLBA interaction	122
5.6	<i>Conclusions</i>	124
5.7	<i>Acknowledgements</i>	124
5.8	<i>References</i>	126
<b>Chapter 6. Membrane Insertion for the Detection of Lipopolysaccharides: Exploring the Dynamics of Amphiphile-in-Lipid Assays</b>		131
6.1	<i>Abstract</i>	132
6.2	<i>Introduction</i>	132
6.3	<i>Materials and Methods</i>	136
6.3.1	Materials	136
6.3.2	Waveguide preparation	137
6.3.3	Micelle preparation	138
6.3.4	Lipopolysaccharides, beef samples, and antibodies	138
6.3.5	LPS membrane insertion assays	139
6.3.6	Imaging inside of a flow cell	140
6.3.7	Imaging LPS on glass slides	141

6.3.8 Data processing .....	141
6.3.9 Statistical Analysis .....	142
6.4 <i>Results and Discussion</i> .....	142
6.4.1 Detection of LPS with membrane insertion .....	142
6.4.2 Imaging LPS-lipid bilayer interactions inside a flow cell .....	148
6.4.3 Imaging LPS subtypes on glass slides.....	149
6.5 <i>Conclusion</i> .....	150
6.6 <i>Acknowledgments</i> .....	151
6.7 <i>References</i> .....	153
<b>Chapter 7. Understanding the <i>in vitro</i> effects of differential LPS presentation</b>	
.....	158
7.1 <i>Introduction</i> .....	158
7.1.1 Model sLBAs.....	160
7.1.2 Cell lines with and without TLR4 .....	161
7.2 <i>Materials and Methods</i> .....	161
7.2.1 Materials .....	161
7.2.2 Lipid and bilayer preparations .....	162
7.2.3 LPS interactions with sLBAs .....	163
7.2.4 Microscopy.....	163
7.2.5 Preparation of IMS beads .....	163
7.2.6 Immunodepletion of serum proteins from mouse serum .....	164
7.2.7 Cell lines .....	165
7.2.8 LPS induced cytokine expression in TLR4(+) and TLR4(-) cell lines.....	165
7.3 <i>Results and discussion</i> .....	167
7.3.1 Model sLBAs: Increasing the complexity of sLBAs .....	167
7.3.2 Cholesterol model bilayers.....	168
7.3.3 Spingomyelin model bilayers .....	168
7.3.4 Mixed sphingomyelin and cholesterol model bilayers .....	169
7.3.5 Effect of temperature and LPS serogroup on hole formation in DOPC bilayers .....	170
7.3.6 Cell studies: effect of murine serum on LPS-induced cytokine expression .....	172
7.4 <i>Conclusion</i> .....	179
7.5 <i>Future Directions</i> .....	179
7.6 <i>References</i> .....	182
<b>Chapter 8. Conclusions and Future Directions</b> .....	188
8.1 <i>Conclusions</i> .....	188
8.1.1 Development of antibodies and antigens for assay development .....	188
8.1.2 Implication of LPS-induced hole formation in sLBAs.....	188
8.1.3 Membrane insertion of LPS.....	189
8.1.4 Differential presentation LPS in vitro .....	190
8.2 <i>Future directions</i> .....	190
8.2.1 Advancements for screening antibody clones.....	190
8.2.2 Improved membrane insertion methods for LPS detection .....	191
8.2.3 Membrane insertion for detection of Shiga toxin .....	192
8.3 <i>References</i> .....	194

<b>Appendix 1</b> .....	195
<i>Section A1.1 Additional information for Chapter 1</i> .....	195
<b>Appendix 2</b> .....	196
<i>Section A2.1 Chapter 3 supplementary tables and figures</i> .....	196
<b>Appendix 3</b> .....	199
<i>Section A3.1 Longitudinal results for mouse serum screens</i> .....	199
<i>Section A3.2 Serum lipoprotein capture ELISAs for LPS</i> .....	249
<b>Appendix 4</b> .....	251
<i>Section A4.1 Supporting images for Chapter 5</i> .....	251
<i>Section A4.2 Information for supporting video files</i> .....	258
<b>Appendix 5</b> .....	259
<i>Section A5.1 Supporting information for Chapter 6</i> .....	259
A5.1.1 Statistical results.....	259
<i>Section A5.2 Data processing methods</i> .....	265
A5.2.1 Data processing algorithm .....	265
A5.2.2 Integrated spectral values and data processing method .....	266
A5.2.3 Raw data of spectral curves .....	266
<b>Appendix 6</b> .....	267
Section A6.1 LPS interactions with complex supported lipid bilayers .....	267
Section A6.2 Effect of murine serum on LPS-induced cytokine expression.....	271
Section A6.3 The effect of FBS on cytokine expression .....	276

## LIST OF FIGURES

<b>Figure 1.1.</b>	Physiology of bacteria.	4
<b>Figure 1.2.</b>	Representative structure of the components of lipopolysaccharide.	7
<b>Figure 1.3.</b>	Factors that influence micelle conformation.	8
<b>Figure 1.4.</b>	Summary mechanism of the <i>Limulus</i> amoebocyte lysate pathway.	11
<b>Figure 1.5.</b>	Schematics of ELISA types.	15
<b>Figure 1.6.</b>	Functionalized surfaces for detection of biomarkers.	22
<b>Figure 3.1.</b>	Western-type blotting of LPS purified extracts.	72
<b>Figure 4.1.</b>	ELISA results from a C57BL/6 mouse immunized with O45 bacterial antigens.	87
<b>Figure 4.2.</b>	Signal to noise ratios of O45 hybridomas.	88
<b>Figure 4.3.</b>	ELISA results for serum screens from BALB/c mice.	91
<b>Figure 4.4.</b>	Serogroup specific LPS membrane insertion assays.	94
<b>Figure 4.5.</b>	Performance of mAb O26 for O-ag targeted detection.	94
<b>Figure 5.1.</b>	Comparison of the chemical structure of lipopolysaccharide from <i>E. coli</i> serotype O111 and the phospholipid 1,2-dioleoyl- <i>sn</i> -glycero-3-phosphocholine (DOPC).	103
<b>Figure 5.2.</b>	Lipid tubule formation induced by LPS in PBS.	109
<b>Figure 5.3.</b>	Holes in sLBAs after LPS treatment and washing.	111
<b>Figure 5.4.</b>	LPS concentration and time dependence on hole formation.	112
<b>Figure 5.5.</b>	LPS in Ca <sup>2+</sup> buffer causes formation and growth of multilamellar stacks.	114
<b>Figure 5.6.</b>	Schematic of the mechanism of LPS-induced lipid bilayer deformation.	115
<b>Figure 6.1.</b>	Representative structure of the molecular components of LPS.	134
<b>Figure 6.2.</b>	Membrane insertion for detection of LPS O157.	144
<b>Figure 6.3.</b>	Concentration dependent detection of LPS O157 in 1 mg/mL beef lysates.	146
<b>Figure 6.4.</b>	Concentration dependent detection of LPS O157 in 1 mg/mL beef lysates.	147
<b>Figure 6.5.</b>	Assay performance inside flow cells.	149
<b>Figure 6.6.</b>	Imaging LPS O157 with lipid bilayers.	150
<b>Figure 7.1.</b>	DOPC lipid bilayers with 25% cholesterol.	168
<b>Figure 7.2.</b>	DOPC lipid bilayers with 15% sphingomyelin.	169
<b>Figure 7.3.</b>	DOPC lipid bilayers with 5% sphingomyelin and 50% cholesterol.	170
<b>Figure 7.4.</b>	The effect of temperature and serogroup on LPS-induced hole formation in sLBAs.	171
<b>Figure 7.5.</b>	The effect of serum on LPS induced cytokine expression.	174
<b>Figure 7.6.</b>	Subset graphs of LPS-induced cytokine expression.	176
<b>Figure A1.1.</b>	Structures of Gram-negative lipid A molecules.	195
<b>Figure A2.1.</b>	Immunoblots of LPS antigens.	196
<b>Figure A2.2.</b>	Eosin stained SDS-PAGE of LPS extracts.	198
<b>Figure A3.1.</b>	ELISA results for a BALB/C mouse in O45 serogroup.	199
<b>Figure A3.2.</b>	Images of longitudinal dot blots for a BALB/c mouse in O45 serogroup.	200

<b>Figure A3.3.</b> ELISA results for a C57BL/6 mouse in O45 serogroup.	201
<b>Figure A3.4.</b> Images of longitudinal dot blots for a C57BL/6 mouse in O45 serogroup.	202
<b>Figure A3.5.</b> ELISA results for a Swiss Webster mouse in O45 serogroup.	203
<b>Figure A3.6.</b> Images of longitudinal dot blots for a Swiss Webster mouse in O45serogroup.	204
<b>Figure A3.7.</b> ELISA results for a BALB/C mouse in O26 serogroup.	205
<b>Figure A3.8.</b> Images of longitudinal dot blots for a BALB/c mouse in the O26 serogroup.	206
<b>Figure A3.9</b> (A-B). ELISA results for a C57BL/6 mouse in O26 serogroup.	207
<b>Figure A3.9</b> (C-D). ELISA results for a C57BL/6 mouse in O26 serogroup.	208
<b>Figure A3.10.</b> Images of longitudinal dot blots for a C57BL/6 mouse in the O26 serogroup.	210
<b>Figure A3.11</b> (A-B). ELISA results for Swiss Webster mouse in O26 serogroup.	211
<b>Figure A3.11</b> (C-D). ELISA results for Swiss Webster mouse in O26 serogroup.	211
<b>Figure A3.12.</b> Images of longitudinal dot blots for Swiss Webster mouse in the O26 serogroup.	214
<b>Figure A3.13</b> (A-B). ELISA results for a BALB/c mouse in O103 serogroup.	215
<b>Figure A3.13</b> (C-D). ELISA results for a BALB/c mouse in O103 serogroup.	216
<b>Figure A3.14.</b> Images of longitudinal dot blots for a BALB/c mouse in the O103 serogroup.	218
<b>Figure A3.15.</b> ELISA results for a C57BL/6 mouse in the O103 serogroup.	220
<b>Figure A3.16.</b> Images of longitudinal dot blots for a C57BL/6 mouse in the O103 serogroup.	222
<b>Figure A3.17.</b> ELISA results for Swiss Webster mouse in the O103 serogroup.	224
<b>Figure A3.18.</b> Images of longitudinal dot blots for a Swiss Webster mouse in the O103 serogroup.	226
<b>Figure A3.19.</b> ELISA results for a BALB/c mouse in O111 serogroup.	227
<b>Figure A3.20.</b> Images of longitudinal dot blots for a BALB/C mouse in the O111 serogroup.	228
<b>Figure A3.21.</b> ELISA results for a C57BL/6 mouse in O111 serogroup.	229
<b>Figure A3.21.</b> ELISA results for a C57BL/6 mouse in O111 serogroup.	230
<b>Figure A3.22.</b> Images of longitudinal dot blots for a C57BL/6 mouse in the O111 serogroup.	232
<b>Figure A3.23.</b> (A-B). ELISA results for a Swiss Webster mouse in O111 serogroup.	233
<b>Figure A3.23.</b> (C-D). ELISA results for a Swiss Webster mouse in O111 serogroup.	234
<b>Figure A3.24.</b> Images of longitudinal dot blots for a Swiss Webster mouse in the O111 serogroup.	236
<b>Figure A3.25.</b> ELISA graphs for a BALB/c mouse in O121 serogoup.	237
<b>Figure A3.26.</b> Images of longitudinal dot blots for a BALB/c mouse in the O121 serogroup.	238
<b>Figure A3.27.</b> ELISA results for a C57BL/6 mouse in the O121 serogroup.	239
<b>Figure A3.28.</b> Images of longitudinal dot blots for a C57BL/6 mouse in the O121 serogroup.	240

<b>Figure A3.29.</b> ELISA results for a Swiss Webster mouse in the O121 serogroup.	241
<b>Figure A3.30.</b> Images of longitudinal dot blots for a Swiss Webster mouse in the O121 serogroup.	242
<b>Figure A3.31.</b> ELISA results for a BALB/c mouse in the O145 serogroup.	243
<b>Figure A3.32.</b> Images of longitudinal dot blots for a BALB/c mouse in the O145 serogroup.	244
<b>Figure A3.33.</b> ELISA results for a C57BL/6 mouse in the O145 serogroup.	245
<b>Figure A3.34.</b> Images of longitudinal dot blots for a C57BL/6 mouse in the O145 serogroup.	246
<b>Figure A3.35.</b> ELISA results for Swiss Webster mouse in the O145 serogroup.	247
<b>Figure A3.36.</b> Images of longitudinal dot blots for a Swiss Webster mouse in the O145 serogroup.	248
<b>Figure A3.37.</b> ELISA results for serum functionalized plates.	249
<b>Figure A3.38.</b> ELISA results for LPS O26 on a serum functionalized plate.	250
<b>Figure A4.1.</b> Size of surface-associated lipid vesicles.	251
<b>Figure A4.2.</b> Elongation of lipid tubules.	252
<b>Figure A4.3.</b> Fluorescence time-course showing that holes are stable.	253
<b>Figure A4.4.</b> Dual channel LSCM fluorescence images tracking FITC-LPS its hole formation.	253
<b>Figure A4.5.</b> FRAP studies on LPS (Ca <sup>2+</sup> ) planar lamellar sheets.	254
<b>Figure A4.6.</b> LPS concentration dependence of planar sheet formation.	255
<b>Figure A4.7.</b> Cation concentration effects on LPS membrane disruption.	256
<b>Figure A4.8.</b> Reduction in lipid tubules and similar hole formation by multiple cycles of LPS treatment.	257
<b>Movie A4.1.</b> Mobility of surface-associated lipid vesicles.	258
<b>Movie A4.2.</b> Lipid tubule formation.	258
<b>Movie A4.3.</b> Lipid tubule mobility.	258
<b>Movie A4.4.</b> Lipid sheet formation and growth.	258
<b>Figure A5.1.</b> Integrated intensities of O-ag targeted detection of LPS.	261
<b>Figure A5.2.</b> High concentration of LPS O157 in a flow cell.	261
<b>Figure A5.3.</b> Lateral fluidity of bilayers after incubation with 100 µg/mL LPS O157 inside a flow cell.	262
<b>Figure A5.4.</b> Specific and non-specific binding of pAb O157-af647 inside a flow cell.	263
<b>Figure A5.5.</b> Effects of multiple serogroups of LPS on lipid bilayers.	264
<b>Figure A6.1.</b> DOPC sLBA controls.	267
<b>Figure A6.2.</b> DOPC lipid bilayers with 50% cholesterol.	267
<b>Figure A6.3.</b> Lipid bilayers labeled with TR enriched with 50% NBD-cholesterol.	268
<b>Figure A6.4.</b> DOPC lipid bilayers with 5% Sphingomyelin.	268
<b>Figure A6.5.</b> Zoomed out image of lipid bilayers with 5% sphingomyelin and 50% cholesterol.	268
<b>Figure A6.6.</b> Bilayers enriched with 5% sphingomyelin and 25% cholesterol.	271
<b>Figure A6.7.</b> Lipid bilayers controls for elevated temperature studies.	270
<b>Figure A6.8.</b> LPS-induced cytokine expression in IC-21 cells.	271

<b>Figure A6.9.</b> Cytokine expression of IC-21 cells when LPS is presented to cells in serum.	272
<b>Figure A6.10.</b> Standard curves for murine cytokines using the Milliplex XMap 25-plex kit.	274
<b>Figure A6.11.</b> Standard curves for other murine cytokines/chemokines.	276
<b>Figure A6.12.</b> The effect of 50% FBS on cytokine expression.	278

## LIST OF TABLES

<b>Table 1.1.</b>	Survey of Methods and Reported Sensitivities of Assays Against Bacterial Endotoxins and Similar Amphiphiles	26
<b>Table 3.2.</b>	Commercial Antibodies.	63
<b>Table 3.3.</b>	Immunoblotting antibody activity against LPS antigens	70
<b>Table 4.1.</b>	Immunoblot summary analysis of C57BL/6 mouse inoculated with O45 bacterial antigens.	88
<b>Table 4.2.</b>	Immunoblot summary analysis of BALB/c mice inoculated with O26, O103, and O111 bacterial antigens.	92
<b>Table 6.1.</b>	Signal to Noise Ratios of LPS Membrane Insertion Assays	146
<b>Table 7.1.</b>	Experimental groups for cytokine studies.	166
<b>Table 7.2.</b>	Murine macrophage cytokine responses seen as a result of <i>E. coli</i> LPS stimulation	177
<b>Table 7.3.</b>	Calculated cytokine/chemokine expression (pg/mL) in IC-21 and 23ScCr serum/'no serum' LPS groups.	179
<b>Table A2.1.</b>	Extracted and purified amounts of LPS from dried bacteria.	196
<b>Table A2.2.</b>	Immunoblotting antibody activity against isolated lipid A fractions from LPS antigens.	196
<b>Table A3.1.</b>	Immunoblot summary analysis of BALB/c mouse inoculated with O45 bacterial antigens.	200
<b>Table A3.2.</b>	Immunoblot summary analysis of C57BL/6 mouse inoculated with O45 bacterial antigens.	202
<b>Table A3.3.</b>	Immunoblot summary of Swiss Webster mouse inoculated with O45 bacterial antigens.	204
<b>Table A3.4.</b>	Immunoblot summary of a BALB/c mouse inoculated with O26 bacterial antigens.	206
<b>Table A3.5.</b>	Immunoblot summary analysis of C57BL/6 mouse inoculated with O26 bacterial antigens.	209
<b>Table A3.6.</b>	Immunoblot summary analysis of a Swiss Webster mouse inoculated with O26 bacterial antigens.	213
<b>Table A3.7.</b>	Immunoblot summary analysis of a BALB/c mouse inoculated with O103 bacterial antigens.	217
<b>Table A3.8.</b>	Immunoblot summary analysis of C57BL/6 mouse inoculated with O103 bacterial antigens.	221
<b>Table A3.9.</b>	Immunoblot summary analysis of a Swiss Webster mouse inoculated with O103 bacterial antigens.	225
<b>Table A3.10.</b>	Immunoblot summary analysis of a BALB/c mouse inoculated with O111 bacterial antigens.	228
<b>Table A3.11.</b>	Immunoblot summary analysis of a C57BL/6 mouse inoculated with O111 bacterial antigens.	231
<b>Table A3.12.</b>	Immunoblot summary analysis for a Swiss Webster mouse inoculated with O111 bacterial antigens.	235
<b>Table A3.13.</b>	Immunoblot summary analysis of a BALB/c mouse inoculated with O121 bacterial antigens.	238

<b>Table A3.14.</b> Immunoblot summary analysis of a C57BL/6 mouse inoculated with O121 bacterial antigens.	240
<b>Table A3.15.</b> Immunoblot summary analysis of a Swiss Webster mouse inoculated with O121 bacterial antigens.	242
<b>Table A3.16.</b> Immunoblot summary analysis of a BALB/c mouse inoculated with O145 bacterial antigens.	244
<b>Table A3.17.</b> Immunoblot summary analysis of a C57BL/6 mouse inoculated with O145 bacterial antigens.	246
<b>Table A3.18.</b> Immunoblot summary analysis of a Swiss Webster mouse inoculated with O145 bacterial antigens.	248
<b>Table A5.1.</b> ANOVA of variable significance (5%) in relation to logarithm of integrated intensity.	259
<b>Table A5.2.</b> ANOVA of absolute values of residuals.	260
<b>Table A5.3.</b> Regression analysis of residuals for LPS concentration detection.	260
<b>Table A6.1.</b> Values for the variables in the cytokine standards determined from the 5 parameter logistic fit using the controls on the 23ScCr plate.	273
<b>Table A6.2.</b> Values for the variables in the cytokine standards determined from the 5 parameter logistic fit using the controls on the IC-21 plate.	274
<b>Table A6.3.</b> Calculated cytokine expression in pg/mL using serum variants	275
<b>Table A6.4.</b> Values for the variables in chemokine standards determined from the 5 parameter logistic fit using the controls on the IC-21 plate.	275
<b>Table A6.5.</b> Calculated cytokine expression in pg/mL using FBS and normal murine serum	277

## **Chapter 1. Introduction**

### **1.1 Considerations for universal bacterial detection systems**

The increasing occurrence of infectious diseases is a global issue. Newly emergent diseases and re-emerging pathogens with increasing levels of drug resistance are a continuing danger to both public health and agriculture. Accurate and rapid detection of pathogens is critical for our ability to implement preventative measures and treatment procedures to mitigate this problem. Despite the need for rapid analytical detection measures, conventional methods for bacterial detection require the use of cell culture and serology, which can take up to several weeks for a confirmed result. As new pathogens emerge, it is ever more important that our detection technologies evolve to keep pace with the need to discriminate pathogen from host flora in a variety of complex sample backgrounds. To achieve discriminative detection, it is necessary to understand the biology of pathogens, the types of samples they occur in, and how pathogens interact with their hosts upon infection. Effective detection strategies involve a critical characterization of the bacteria and their biological signatures that interact with the host, attach or enter cells, and trigger (or evade) immune response<sup>1</sup>.

There are many methods for detection of pathogens. However, each technique has problems associated with it. For many pathogens, culturing for positive identification is the gold standard, but this can take up to a week, or even longer depending on the bacteria.<sup>2,3</sup> In most cases, waiting a week or more is not a viable option, especially if patient treatment is delayed. Other techniques for detection of bacteria and viruses, screen for the presence of pathogen virulence factors or other biomarkers present in clinical samples,<sup>1,3</sup> but not all methods are capable of discriminating pathogen from non-pathogenic near neighbors. These techniques include traditional methods like bacterial plating, culturing and biochemical testing,<sup>4,5</sup> immunological assays, as well as newer methods which use polymerase chain reaction (PCR), DNA microarrays, mass spectrometry, flow cytometry, and different biosensors.<sup>3,4,6</sup> Some methods such as polymerase chain reaction (PCR) are highly sensitive, but target isolated pathogen DNA, and therefore

are not capable of determining viable from non-viable pathogens without utilizing special enzymes.<sup>3</sup> Immunological methods, like the well-established enzyme-linked immunosorbent assay (ELISAs) or immunomagnetic separation methods take advantage of antibody-antigen interactions to measure antibody titers or identify pathogens. These methods rely heavily on antibodies, which can be highly cross-reactive and can denature on hydrophobic surfaces. One reason for poor antibody performance is due to the conformational differences in antigen presentation between the antibody-selection process, and the detection assay platforms. In many cases, reliable antibodies have not even been developed due to the large diversity of antigens.<sup>7-10</sup> ELISAs also suffer sensitivity issues due to inconsistent sample processing and variation in protocols.<sup>11</sup> In fact, many of these techniques suffer from limitations. They are either time consuming, expensive, yield false positives, have low throughput, or do not selectively detect viable bacteria.

The human innate immune system is able to discriminate pathogens from non-pathogenic strains, and rapidly sense pathogen biomarkers in the complex milieu of the host. Exploiting this recognition via the measurement of pathogenic molecular signatures produced by bacteria can provide a universal strategy for biodetection, and help discriminate pathogens from near neighbors. Molecules associated with the presence of pathogens in the host are called pathogen-associated molecular patterns (PAMPs).<sup>12</sup> PAMPs are evolutionarily conserved molecular signatures that bind pattern-recognition receptors in the mammalian host, and activate the innate immune response.<sup>13,14</sup> Due to their role in innate immune recognition, targeted detection methods for PAMPs could provide a means to facilitate both early and specific detection of pathogens. Also, the short half-life<sup>15</sup> of these signatures in the infected host ensures that detection results in positive identification of viable bacteria for diagnostic applications. There are a diverse array of proteins, lipopeptides, lipoglycans, peptidoglycans, teichoic acids, and nucleic acids associated with different species of pathogens that present as PAMPs upon infection.<sup>16</sup>

Aside from proteins and nucleic acid PAMPs, there are many other virulence markers associated with early onset disease<sup>14,17,18</sup> that have until recently been

ignored in detection methods as their small size, unique biochemistry, and low concentration in samples makes them difficult to detect in gold standard screening methods, such as immunoassays.<sup>19,20</sup> One of these classes of virulence biomarkers are lipoglycans, which are small molecules that have an amphiphilic biochemistry.<sup>21</sup> A classic example of this is the molecule lipopolysaccharide (LPS), which is associated with Gram-negative pathogens. As detection platforms advance, so do our capabilities to detect LPS as an early indicator of infection.<sup>22</sup> With an understanding of host-pathogen biology, biomimetic capture surfaces can be optimized to bind these amphiphilic molecules in conformations that are physiologically relevant, which not only optimizes the capability to detect low concentrations, but also maximizes the specificity with which antibodies can bind conformationally viable epitopes.<sup>23</sup> Developing systems with incorporated biomimicry has given rise to a large array of biosensors, with multiple detection capabilities. However, current strategies for the detection of amphiphiles, like LPS, are not optimized and do not consider the biochemistry of this category of virulence signatures. LPS is also much more stable than its protein counterparts, which is clear advantage for food safety applications. Coupling sensitive detection platforms with surfaces designed to maximize the binding of amphiphilic PAMPs is a potential solution to facilitate the early and specific detection of pathogens.

## 1.2 Sources of lipopolysaccharides

Bacteria are historically classified into two categories, Gram-negative, and Gram-positive<sup>24</sup> (**Figure 1.1**). All bacteria are single-cell organisms with a cell membrane, and an exterior peptidoglycan layer on the outside of the membrane. However, Gram-negative bacteria have an additional cell membrane outside of the peptidoglycan layer, creating a periplasmic space sandwiched between<sup>25</sup> the two cell walls. Gram-negative bacteria are characteristically named due to the inability of the cell to retain a crystal violet dye during the Gram staining procedure.<sup>25</sup> This inability is a result of the peptidoglycan layer being 'too thin' to retain enough dye. In Gram-positive bacteria, the peptidoglycan layer is much thicker, and readily absorbs and retains the crystal violet after a subsequent alcohol wash. Both Gram-positive and

Gram-negative bacteria secrete amphiphilic virulence factors such as LPS, lipoarabinomannan (LAM), and lipoteichoic acid (LTA) that are associated with the bacterial outer membrane (**Figure 1.1**).

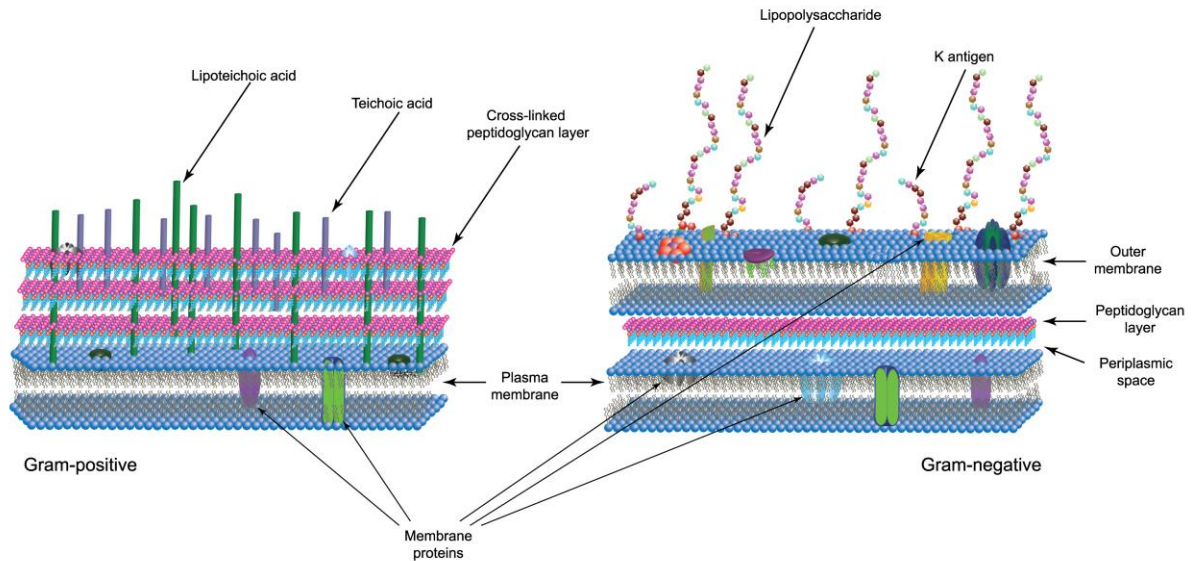


**Figure 1.1. Physiology of bacteria.** Gram-positive bacteria are single cell organisms with one cell membrane and a thick, heavily cross-linked peptidoglycan layer on the outside of that membrane. Gram-negative bacteria share the same structure with Gram-positive, but have an additional cell wall surrounding the peptidoglycan layer. Due to this additional cell wall, Gram-negative bacteria do not retain the crystal violet “Gram-stain” after washing. Both LTA and LPS are considered amphiphilic biomarkers associated with each type of bacteria.

Species of pathogenic Gram-negative bacteria of concern to human health, include, but are not limited to *Acinetobacter*,<sup>26</sup> *Burkholderia*,<sup>27</sup> *Bordetella*,<sup>28</sup> *Campylobacter*,<sup>2,3,29</sup> *Chlamydia*,<sup>30,31</sup> *Escherichia coli (E. coli)*,<sup>3,32</sup> *Helicobacter*,<sup>33,34</sup> *Hemophilus*,<sup>35</sup> *Klebsiella*,<sup>36</sup> *Legionella*,<sup>3,37</sup> *Moraxella*,<sup>38</sup> *Neisseria*,<sup>39</sup> *Pseudomonas*,<sup>40</sup> *Proteus*,<sup>41</sup> *Salmonella*,<sup>3,42</sup> *Shigella*,<sup>43</sup> *Yersinia*,<sup>44</sup> and others, grouped into the Enterobacteriaceae family. These pathogens can be found as contaminants in food, water, and soil; used as agents of bioterrorism, or be the cause of nosocomial infections.<sup>4</sup> Detection and differentiation of these organisms is an important aspect not only for epidemiology, but also for disease control and treatment.

Detection of these bacteria by measuring associated protein and nucleic biomarkers is well reviewed in the literature.<sup>6,45-49</sup> However, a largely ignored category of detection techniques uses PAMPs, and more specifically lipoglycans, as diagnostics for detection and identification of bacterial infections. This discussion

specifically addresses current methods and challenges for detection of LPS, as LPS is a strain-specific antigen<sup>50-52</sup> and an ideal target for differential diagnostics. Briefly mentioned are some of the methods to detect other PAMPs with similar molecular structures,<sup>20</sup> such as LAM and LTA from Gram-positive bacteria. Since *E. coli* is an intensely studied Gram-negative organism, it often serves as the basis for this discussion surrounding LPS. While many detection methods for LPS can be extremely sensitive, only a few of these are capable of identifying strain specific LPS antigens, and are therefore useful as a true diagnostics of infections.

### 1.3 Lipopolysaccharide structures and conformations

One of the primary challenges for developing detection assays for LPS is the unique amphiphilic structure of the molecule. Lipopolysaccharides have been the subject of intense study for over half a century.<sup>53-55</sup> LPS is the prototypical lipoglycan<sup>16</sup> and the primary component of the outer membrane of nearly all Gram-negative bacteria.<sup>50</sup> It is a key bacterial PAMP that stimulates the mammalian innate immune system through activation of Toll-like receptor 4 (TLR4).<sup>56</sup> The bacterial membrane of each *E. coli* cell is comprised of approximately  $10^6$  lipid A moieties and  $10^7$  glycerophospholipid molecules, comprising approximately three-quarters of the outer membrane.<sup>57-59</sup> This implies that there is approximately 62 picograms of LPS per cell (for *E. coli* in log phase growth).<sup>60</sup>

In general, LPS is a complex molecule with an overall net negative charge.<sup>61-63</sup> It has an amphipathic tripartite structure (**Figure 1.2**). Lipid A is the most conserved portion of the LPS molecule, and consists of 6, sometimes 7, fatty acid tails (*E. coli* and *Salmonella* respectively), which gives the molecule its hydrophobic properties. Lipid A is often referred to as 'endotoxin',<sup>58</sup> as it is the part of the LPS molecule responsible for the biological effects in the host.<sup>59,64,65</sup> Structurally, lipid A is covalently bound to the core polysaccharide, which is further divided into the inner and outer core polysaccharides, with the outer core being less conserved in both sugar moiety composition and location of glycosidic linkages compared to the inner core.<sup>66-68</sup>

There are two main forms of LPS, designated smooth (S-form) and rough (R-form).<sup>63,69</sup> In S-form LPS, the distal end of the molecule extends to an O-polysaccharide antigen (O-ag(s)). Smooth form LPS is considered an indicator of virulence of bacteria,<sup>70,71</sup> while R-form LPS is devoid of the O-ag,<sup>72</sup> but can still induce an immunogenic response.<sup>73</sup> The O-ag is hyper-variable, and made up of repeating subunits, each composed of 1-7 glycosyl residues.<sup>74,75</sup> As many as 40 size variations in subunit repeats of the O-ag have been reported just for *E. coli* O111:B4,<sup>76</sup> and 180 O-ag have been identified for *E. coli* species.<sup>64,77</sup> The sugars that help make the O-ag unique are seldom found elsewhere. These include moieties such as colitose, paratose, tyvelose, and abequose.<sup>78</sup> Other variations to the polysaccharide chain are implemented through the addition of non-carbohydrate entities such as acetyl or methyl groups.<sup>78</sup> This variability in sugar repeats and degree of branching of the glycosyl residues in the O-ag makes distinction between serotypes within strains a possibility.<sup>74</sup> However, this variability of LPS structure also poses a challenge for its characterization. Due to the heterogenous presentation of LPS, often in micelle conformation in aqueous solutions, it is impossible to determine the exact molecular weight of S-form LPS. As such, LPS concentrations are reported in weight per volume, or in Endotoxin Units (EU), a measure of activity rather than concentration. As degree of endotoxicity can vary according to bacterial origin, a rough estimate of 100 pg = 1 EU is used in many cases to facilitate unit conversion.<sup>79,80</sup> Due to the abundance on Gram-negative bacteria, the highly conserved nature of the lipid A molecule, and the variability of the O-ag, LPS is an ideal target for the early detection and identification of Gram-negative pathogens.

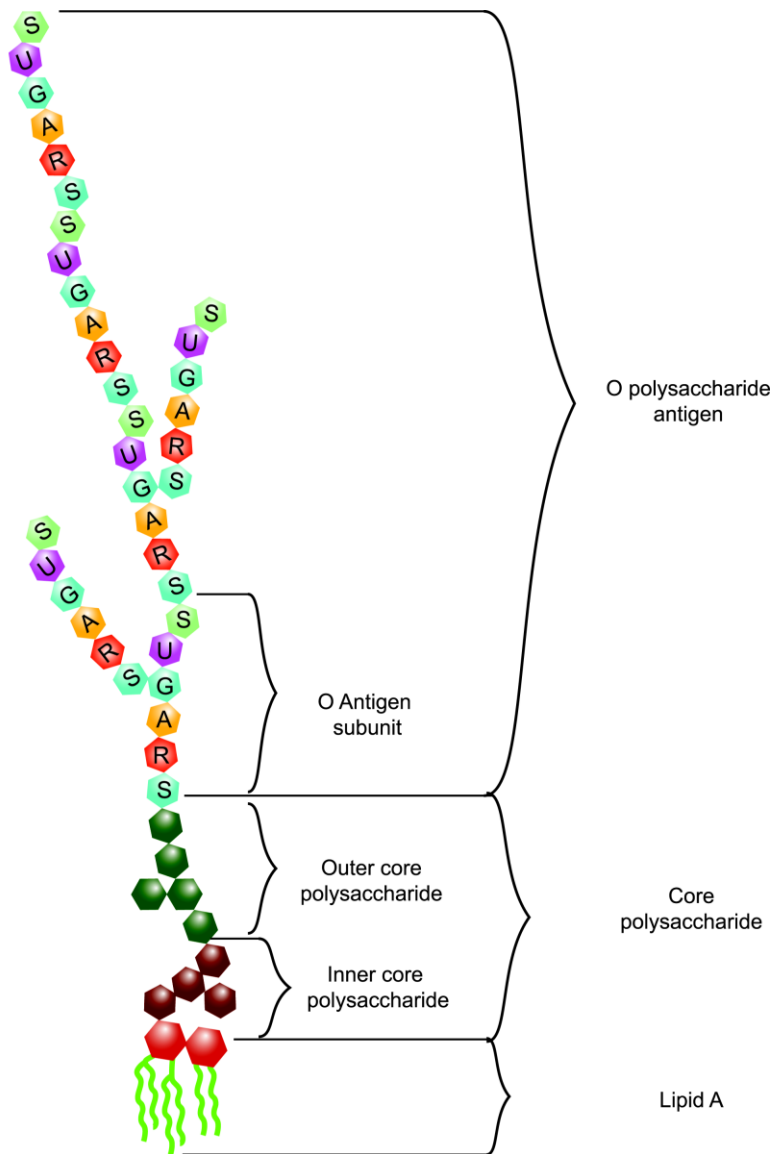


**Figure 1.2. Representative structure of the components of lipopolysaccharide.** LPS is divided into three distinct molecular components. The highly conserved, hydrophobic lipid A group, the moderately conserved core polysaccharide (inner and outer core), and the hypervariable O polysaccharide antigen which is made up of repeating sugar subunits.

The physiological conformation of an amphiphilic molecule should be considered for the design and execution of both synthetic and *in vivo* detection schemes. In aqueous solutions, amphiphiles like LPS can present in a micellar conformation,<sup>65,76,81,82</sup> as the hydrophobic lipid A region is sequestered away from the hydrophilic medium.<sup>83</sup> This occurs at a concentration specific to the amphiphile in question,<sup>76</sup> and is known as the critical micelle concentration (CMC). When the CMC is reached, it does not imply that all amphiphiles present in solution exist as

micelles.<sup>76</sup> Instead, at or above the CMC, there is an equilibrium state between monomers, micelles or supramolecular aggregates,<sup>62,65,81,84-89</sup> depending on the environmental conditions.

The structure and orientation of the hydrophobic lipid A moiety is the primary driving factor for shaping the LPS micelle<sup>90-92</sup> (**Figure 1.3**). Although fairly conserved amongst species, lipid A can vary between species both in the number of fatty acid chains, as well as the degree of saturation<sup>59,91</sup> within those chains.<sup>30,64,93</sup> Many structures of lipid A have been identified to date<sup>64</sup> (**Figures 1.3A** and **A1.1**). These structural variations influence the shape of micelles formed in aqueous media.<sup>94</sup> Aggregate shapes that have been recorded for LPS micelles include cubic, lamellar, and hexagonal inverted structures.<sup>95-98</sup>

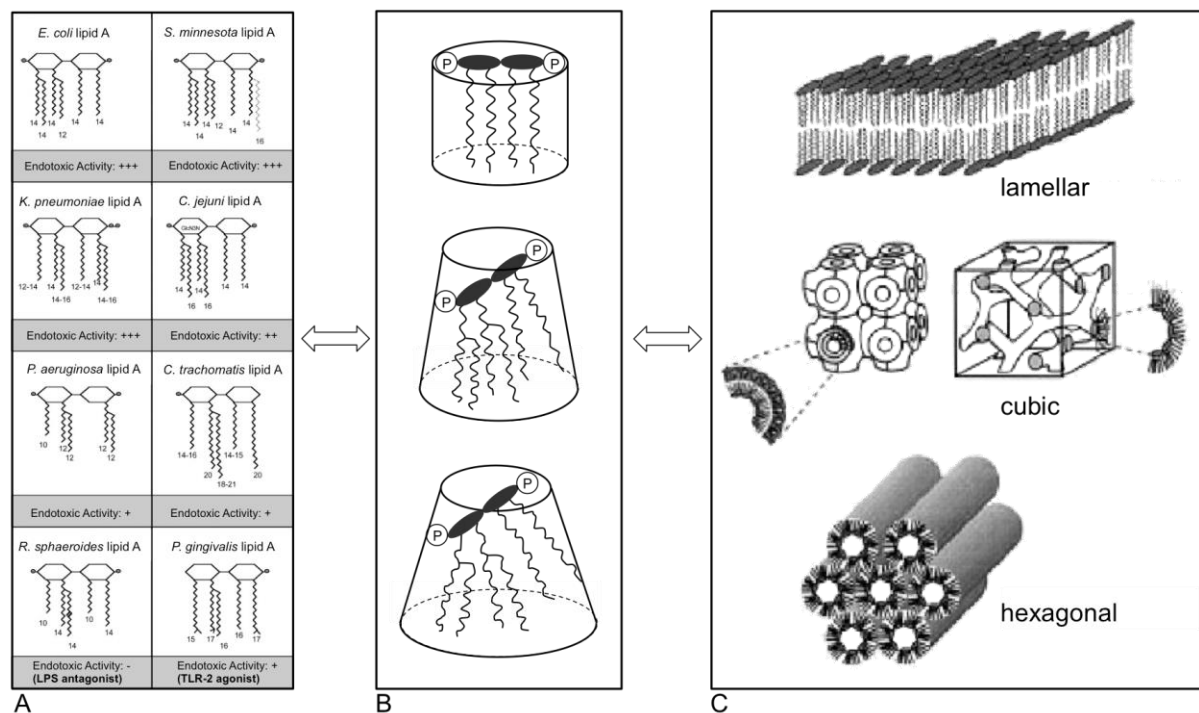


**Figure 1.3. Factors that influence micelle conformation.** Micelle conformations of LPS are governed by the orientation and structure of the lipid A group. A. Multiple structures of lipid A associated with various bacteria have been documented and studied. Common substitutions are indicated by grey lines (*S. minnesota*). Endotoxic activities are indicated by '+++' for strongest activity and '-' for no activity. Scale is intended as a qualitative guide only. (Adapted from Erridge et al. 2002 and reprinted with permission from Elsevier). B. The angle of orientation of the lipid A group affects the hydrophobic interface and therefore the shape of the lipid A molecule and the aggregate micelle. C. The aggregate shapes that have been recorded for LPS include lamellar, cubic, and hexagonal inverted structures. (B-C were reprinted from Seydel et al. 2000, with permission from Karger Publishers.)

While some sources point to LPS aggregates as being the form required for activation of innate immunity,<sup>98,99</sup> others indicate that it is a monomer.<sup>100</sup> Both states may induce immune response, however, since LPS-mediated toxicity and immune activation occur in aqueous blood, it is unlikely that the molecule is presented as a monomer, until it becomes associated with serum binding proteins. In any case, since samples like blood and serum are aqueous, detection strategies should take into account the variability due to micelle conformations of LPS. This is predominantly driven by the shape of the lipid A molecule,<sup>69,89,98,101,102</sup> but other factors can also influence the shape and size of aggregates. R-form LPS is composed of lipid A and core polysaccharide,<sup>103</sup> and is therefore primarily hydrophobic.<sup>72,104</sup> However, the large oligosaccharide region on S-form LPS makes the molecule amphipathic in nature,<sup>78</sup> which influences the overall shape of micelles in solution. This variation in the shape of LPS micelles<sup>76</sup> in solution can modify the presentation of O-ag specific epitopes for detection, making quantitative immune-based detection of LPS challenging.<sup>105,106</sup> This is specifically true when the heterogenous presentation of linear<sup>107</sup> and conformational epitopes<sup>67,108</sup> present on LPS are considered.

Additional driving forces regulate the shape of LPS micelles.<sup>88</sup> In addition to structural variance in the lipid A and O-ag regions, the primary structure of the LPS molecule also varies within the core polysaccharide, both within and between species.<sup>64,76</sup> Core polysaccharides are primarily made up of common sugars such as heptose and 2-deoxy-D-*manno*octulosonic acid (a.k.a. KDO), which can be functionalized with components such as phosphate or ethanolamine groups.<sup>66,68,109</sup> It has been demonstrated that a KDO molecule bound to a lipid A group is the minimum requirement for growth in Gram-negative bacteria.<sup>58,59,64,72</sup> This additional degree of variability can contribute to varying charge distributions. It can also vary the size ratio of the cross-sectional area of the hydrophobic to hydrophilic regions; influencing the assembly of micelles.<sup>83,90,103,110</sup> Other factors that contribute to LPS micelle assembly<sup>90,103</sup> are pH,<sup>85</sup> ion concentration,<sup>111-116</sup> and temperature.<sup>86</sup> When developing detection strategies for LPS, all of the variability issues related to structure and micelle conformation are especially important to consider.

## 1.4 Detection methods for lipopolysaccharides and similar amphiphiles

Due to the endotoxic nature of the LPS, there have been many efforts to establish rapid and reliable detection methods for the molecule.<sup>117,118</sup> The detection of endotoxin is critical not only for bacterial detection, but also important for testing pharmacological products such as infusion fluids, sterile injectables, medical device implants, and other biological supplies.<sup>119</sup> In 1980, McCabe<sup>120</sup> reported that as many as 20 different methods for the detection of endotoxin were currently in existence, and that number has only grown higher with passing time.<sup>118</sup> Analysis of the methods reveals that they can be broadly divided into six overlapping categories: *in vivo* and *in vitro* tests, immunoassays and their derivatives, biosensors, chemical sensors, and cell-based sensors. These assays have a broad range of sensitivity for endotoxin, but most of them lack the ability to differentiate LPS O-ag.

### 1.4.1 *Limulus amoebocyte lysate assay and the rabbit pyrogen test*

There is surprisingly very little information available on the first type of endotoxin test. The first method approved by the US Food and Drug Administration for LPS detection was called the rabbit pyrogen test.<sup>121-123</sup> Since endotoxin is a pyrogen (a fever inducing compound), a rabbit was inoculated with the material in question and its body temperature recorded over time. Any pyrogenic activity was attributed to contamination of the material with endotoxin.<sup>122-124</sup> The test, clearly, is activity based, and non-specific. However in the case of some types of vaccine manufacturing, the rabbit pyrogen test is still the standard method for determining contamination with endotoxin.<sup>124</sup> As an *in vivo* assay, the rabbit pyrogen test is cost prohibitive and is minimally utilized in present day, except for detecting endotoxin in some parenteral devices.<sup>118</sup>

In 1956, Frederick Bang discovered that amoebocytes from *Limulus polyphemus* (a.k.a. horseshoe crab) agglutinate upon addition of endotoxin,<sup>125</sup> as a result of a protease cascade<sup>118</sup> (**Figure 1.4**). Realizing the medical relevance of this discovery, Bang and Levin<sup>126,127</sup> subsequently developed an assay for the detection of endotoxin in clinical samples. Since the lysates of amoebocytes were required, it was called the limulus amoebocyte lysate (LAL) assay, and has since been the gold

standard for detection of lipid A (endotoxin). The LAL assay is prone to variability and can be inhibited through several mechanisms. The United States Pharmacopeia and the Code of Federal Regulations have consequently published guidances for both the manufacturing and testing required when using these assays for testing of human products.<sup>128,129</sup> However, despite challenges, the LAL assay is reportedly 300 times more sensitive,<sup>117</sup> and much more cost effective as rapid compared to the rabbit pyrogen test, so it has largely displaced the *in vivo* test.<sup>130</sup>

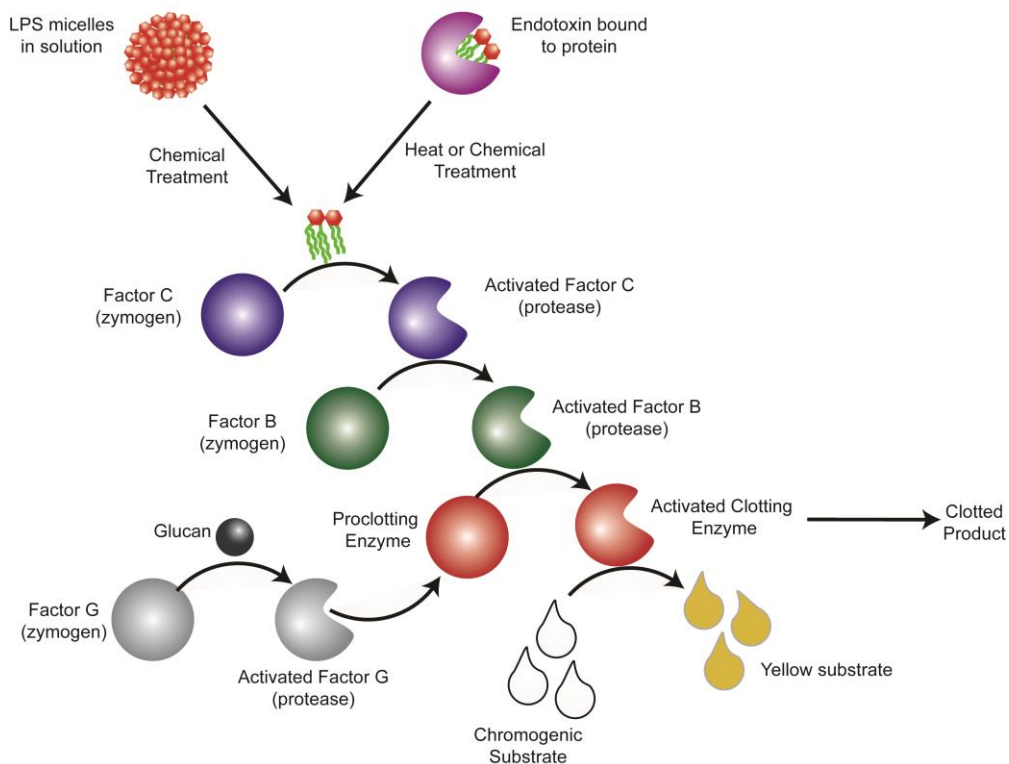


**Figure 1.4. Summary mechanism of the Limulus amoebocyte lysate pathway.** Blood is drawn from the horseshoe crab and the amoebocytes are isolated *via* centrifugation and then lysed and the clotting enzymes are purified to use in the assay. Factor C is a protease zymogen, which is activated through interaction with endotoxin. Factor C activates Factor B, which activates the pro-clotting enzyme, which can activate creates clotting or converts the substrate. False positives result when the pro-clotting enzyme is alternatively activated by Factor G, which is activated by glucans. Results can be determined by visual evaluation of the clot, measuring the optical density of the solution, or by adding a colorimetric *p*-nitroaniline substrate, which is cleaved by the activated clotting enzyme.

Several variants of the LAL assay use turbidimetric,<sup>131</sup> chromogenic,<sup>132</sup> or viscosity<sup>133</sup> readings to determine results.<sup>117,118</sup> A turbidimetric gel clot has more coagulen and evaluates the change in turbidity over time, but does not form a solid

clot.<sup>117,131</sup> The viscosity assay works in much the same way, but by measuring the degree of clotting *via* the change in viscosity. The chromogenic assay can be an endpoint or kinetic readout and varies from the former in that a *p*-nitroaniline substrate, which is cleaved by an LAL proenzyme, is added and results in increasing color intensity over time.<sup>134</sup> The sensitivity of LAL assays are largely dependent on the sample type, processing method and time, as well as the dilution factor.<sup>117</sup> Additionally, the source of the LAL reagent plays a factor, as is apparent when comparing the different limits of detection (LoD) that are reported for endotoxin standards. A survey of the relative sensitivities of the LAL assay as compared to other LPS detection methods is reported in **Table 1.1**.

As research progressed, more knowledge about the LAL assay came to light. In 1970, Levin did multiple studies on the LAL assay in the blood of patients. Initially, he discovered that samples tested in whole blood would not render a positive result,<sup>135</sup> but if the plasma was extracted in chloroform and diluted 1-10%, then the endotoxin reactivity could be detected in the 0.5-5 ng•mL<sup>-1</sup> range.<sup>127,135</sup> Levin correctly assumed that components of whole blood were bound to endotoxin, therefore inhibiting the reaction with the LAL reagent,<sup>135-137</sup> or changing the kinetics of the reaction.<sup>138</sup> This is immediately apparent when the amphiphilic nature of LPS and the aqueous media of blood are considered. Therefore, by implementing different processing methods to degrade serum proteins and release the LPS, one could improve the sensitivity of endotoxin measurement.

In addition to blood or plasma of septic patients,<sup>127,135,139,140</sup> the LAL assay has also been used in other clinical samples such as: urine,<sup>132,141</sup> cerebral spinal fluid,<sup>140,142,143</sup> synovial fluid,<sup>143</sup> ascites fluid,<sup>144</sup> vaginal and cervical fluids,<sup>145</sup> broncho-alveolar lavage samples,<sup>146</sup> seawater,<sup>60</sup> and even agricultural samples like bovine milk<sup>147</sup> and beef tissue<sup>148,149</sup>. Virtually all of these have reported ng•mL<sup>-1</sup> LoDs, for endotoxin, but none are serotype specific to facilitate bacterial detection. Many researchers have used different methods such as heat,<sup>150,151</sup> chemical treatment with chloroform,<sup>152</sup> acids,<sup>153,154</sup> alkalali,<sup>155,156</sup> or ether<sup>157</sup> to improve the sensitivity of the LAL test, with some successes in improving sensitivity when using heat or chemical extraction of endotoxin prior to running an assay.<sup>158,159</sup> However, when

comparing samples of purified endotoxin standards, different researchers achieved highly varied results even when using similar preparation methods (**Table 1.1**). Yin and Galanos<sup>155</sup> reported a sensitivity of  $10^{-11}$  ng•mL<sup>-1</sup> for *Salmonella spp.* while Cooper and Levin<sup>122</sup> reported a sensitivity of 1.0 ng•mL<sup>-1</sup> for *E. coli* endotoxin. While some variation is expected between species, this disparity leaves a lot of questions, especially when considering that the structure of *E. coli* endotoxin is considered to be the most biologically active type of LPS.<sup>89,90,92,98,103,160</sup> Thus, in an activity-based assay, the *E. coli* endotoxin should theoretically demonstrate the better sensitivity. However, as seen in **Table 1.1**, this is not always the case and the source organism, reagents, and processing methods play a heavy role in determining assay sensitivity. Even small changes in preparation methods, such as heat or chemical treatments, the usage of plastics instead of silanized glass, or the addition of surfactants can result in altered sensitivity of assays. This variation in sensitivity could also be explained by the variable structure of the *Salmonella* lipid A molecule as a result of biosynthesis,<sup>161</sup> as discussed by Erridge *et al.*<sup>64</sup> (**Figure A1.1**). There are also cross reactivity issues as the LAL can show false positives upon reacting with other polysaccharides or  $\beta$ -(1,3)-glucans.<sup>162,163</sup> However, the main reason for variability is the source bacteria of the endotoxin. LPS/endotoxin varies in toxicity levels,<sup>89,90,92,103</sup> especially in regards to stimulation of the immune system.<sup>62,160,164</sup> It is therefore a safe assumption that an assay such as the LAL assay or the rabbit pyrogen test, which are both based on the native immune responses of the horseshoe crab or rabbit, would therefore vary accordingly in the reported sensitivities with respect to the toxicity level of the LPS being detected.

Despite these variabilities, there are many instances when a rapid test such as LAL is useful for quickly determining whether contamination exists. For example, in 1981, Jay<sup>149</sup> used the LAL test to determine both microbial counts and endotoxin load in 153 samples of store bought ground beef. He reported a mean sensitivity of 7.9  $\mu$ g•mL<sup>-1</sup> (endotoxin/beef sample), and a processing time of 1 hour. In 1985, Nachum and Shanbrom<sup>132</sup> reported using a chromogenic LAL system to detect between 2-175 ng•mL<sup>-1</sup> of endotoxin in 324 patient urine samples, with an assay taking between 2-4 hours. Obviously timely detection in these scenarios is valuable

to both patient care and product viability. Despite being an ideal test for the presence of endotoxin, determining identity of the pathogens in the sample still requires culture identification. While the LAL assay is extremely sensitive for detection of nanogram quantities of endotoxin contamination in parenteral injections, or on medical devices, the assay lacks specificity and therefore is not a good diagnostic method for determining bacterial species or serogroup.

#### *1.4.2 Immunoassays for LPS detection and antibody screening*

Many researchers have made attempts to develop specific and sensitive ELISAs that target LPS O-ag. Developed in 1971,<sup>165-167</sup> the ELISA is an established method for the detection of antigens or antibodies in many sample types. Schematics of standard types of ELISAs are seen in **Figure 1.5**. Since ELISAs are based on an immune reaction between an antigen-antibody pair, each assay must be specifically developed for the unique antigen being tested. This can lead to a highly specific result if appropriate reagents are available. ELISAs were specifically designed and optimized for the detection of proteins, but the importance of LPS as a biomolecule of wide significance is further illustrated by the fact that some of the earliest research using ELISAs was investigating targeted antibody binding to *Salmonella* O-ag.<sup>168</sup> However, ELISAs for lipoglycans such as LPS and LAM, suffer from low sensitivity and reproducibility.<sup>169-171</sup> One of the primary reasons for this is the structure of said molecules, which in addition to being amphipathic, are heterogenous and micellar, leading to inconsistent binding on ELISA plates,<sup>172</sup> and variable conformations of epitope binding sites.<sup>51,173</sup>

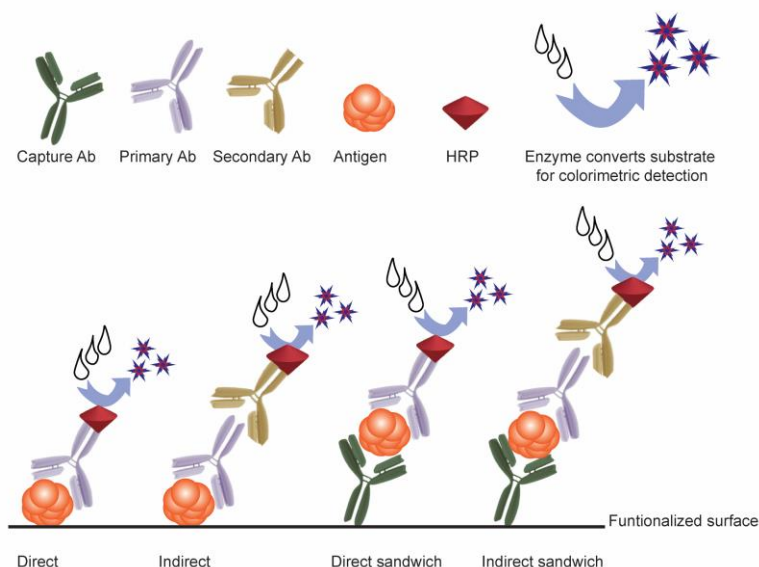


**Figure 1.5. Schematics of ELISA types.** A. Direct ELISA where antigen is coated directly to the plate and then detected with an enzyme-linked primary antibody. The enzyme is often horseradish peroxidase (HRP). An indirect ELISA adds an additional enzyme-linked secondary antibody to a direct ELISA. A direct sandwich and an indirect sandwich are based on the same detection methods, but a capture antibody against the antigen is used to pull down the target from the medium.

Despite challenges with lipoglycan binding, there exist two primary types of LPS-ELISAs, each with many experimental variations. The first is designed to directly detect the LPS antigen (**Figure 1.5**), and the other uses serology to measure LPS antibody titers. For direct detection, the surface of the plate is typically coated with a primary capture antibody specific to LPS. Alternatively, the plate can be directly coated with the sample being tested for LPS.<sup>172</sup> After antigen capture, an epitope-specific antibody is used to detect LPS. The detection antibody can be directly labeled with an enzyme to facilitate colorimetric detection.<sup>167</sup> Alternatively, a secondary antibody can be used.<sup>174,175</sup> In 1998, Mackenzie *et al.*<sup>176</sup> reported on the effectiveness of a commercial assay to screen stool samples for *E. coli* O157 antigens, and found that re-testing samples provided inconsistent results in some cases. It was speculated that this was due to inefficient washing of the micro-wells between assay steps, but the inconsistency in amphiphilic antigen preparation and its presentation to antibodies was not discussed. In clinical samples, the association of amphiphilic LPS with host carrier molecules may affect its ability to adhere/associate with capture surfaces. It was also not considered that LPS is

notorious for causing non-specific and inconsistent binding on microplates.<sup>170,172,177</sup> Some groups have also reported cross reactivity or false positives when developing sandwich ELISAs for LPS antigens.<sup>178,179</sup> Choi *et al.*<sup>179</sup> developed a sensitive capture ELISA, but it was found to cross react with 24 species of *Salmonella*. To mitigate cross reactivity and non-specific interactions, attempts have been made to substitute antibodies with other ligands more apt to physiologically bind LPS. Grallert *et al.*<sup>180,181</sup> coated microplates with proteins from bacteriophages, which are specific to core polysaccharides, in order to capture LPS, and then perform detection with Factor C (a component from the LAL assay, see **Figure 1.4**). This resulted in the development of the sandwich ENDOLisa<sup>®</sup>, a microplate assay for direct detection of endotoxin which was tested in various buffers and detergents, and reports sensitivities between 0.05-500 endotoxin units (EU) per milliliter. At present, ENDOLisa<sup>®</sup> technology is sold as the Endotoxin Sample Preparation (ESP<sup>™</sup>) Kit, and is one of the few kits available for the direct detection of endotoxin in blood or serum.<sup>182</sup> Even though the ENDOLisa is sensitive, it is not serogroup specific due to the semi-conserved nature of the core polysaccharide between different subtypes.

For determining exposure in clinical samples, a modified immunoassay is used to screen for LPS antibody titers. This is one of the most common methods for determining exposure to specific Gram-negative pathogens. To perform the assay, the surface of the plate is functionalized with the antigen in order to pull down the antibodies from serum (**Figure 1.5**). Since this method is based on adaptive immunity there is a lag between initial exposure to a pathogen, and increased antibody titers,<sup>183</sup> which makes early detection difficult. In contrast, directly targeting LPS antigen (as in the first type of ELISA discussed) facilitates early and specific detection. Because this is an indirect method to assess for LPS-induced immune activation, and cannot be correlated with active infection, it is of limited use. Furthermore, many LPS antigens have not been isolated from their respective bacterial strains<sup>10</sup> and are not available for development of screening assays.

Screening for LPS antibody titers (Immunoglobulins A, G, and M (IgG, IgA, IgM)) has been used in many studies to monitor population health and track epidemiology of infectious diseases. For example, it has been used to detect

exposure of military personnel to *Shigella*,<sup>184</sup> obstetric patients to *Chlamydia spp.*,<sup>185</sup> and *Salmonella* patients from Vietnam,<sup>186</sup> as well as many other species of pathogens.<sup>168,187-191</sup> Suthienkul *et al.*<sup>188</sup> used an indirect ELISA (**Figure 1.5**) to passively adsorb LPS to the surface of polystyrene plates, and screen patient serum samples for IgG and IgM titers against the LPS of *Vibrio cholera*. However, the results indicated some possible discrepancies between the titers of IgG and IgM in young versus older patients. This could either be due to the inconsistency of LPS coating on the surface of the microplate, or the issues with cross reactivity of IgMs.<sup>192</sup> Suthienkul also acknowledged that antibody levels in the infants screened could be inherited from the mother's exposure, since said antibodies are known to cross the placental barrier.<sup>188,193</sup>

Functionalizing ELISA plates with the amphiphilic LPS antigens is a technical challenge,<sup>51</sup> since the surfaces are optimized for protein binding. Researchers have examined methods for increasing adherence of LPS to the surfaces of microtiter plates. In the late 1970's, it was discovered that polymyxin B (an antibiotic, PmB) interacted with LPS monomers in a 1-to-1 ratio,<sup>116,194</sup> and can be used to functionalize surfaces for Gram-negative detection schemes.<sup>173</sup> However, PmB recognizes the lipid A group of LPS in much the same manner as other LPS recognition proteins, and does not allow for discriminative detection. Takahashi *et al.*<sup>172</sup> studied methods for increasing the adsorption of LPS from samples directly to microtiter plates. By pre-coating the plate with high molecular weight poly-L-lysine, they determined that LPS from *Klebsiella* O3 could be selectively detected at 1  $\mu\text{g}\cdot\text{mL}^{-1}$ , with no cross reactivity with other O-groups. Others have studied the effects of ions such as calcium and magnesium,<sup>195</sup> trichloroacetic acid,<sup>196</sup> mixing the antigen in chloroform/ethanol and drying on the plate surface,<sup>187</sup> or complexing LPS with a protein such as bovine serum albumin.<sup>197</sup> Functionalization of ELISA plates with other proteins known to bind LPS, such as high- or low- density lipoproteins (HDL, LDL), chylomicrons, and LPS Binding Protein (LBP), have been performed, to study the preferred binding associations of LPS with these proteins.<sup>198,199</sup> However, using molecules known to bind LPS, like PmB, HDL, LDL, LBP<sup>200</sup>, chylomicrons, peptides, and lectins, are potential ways to optimize detection assays, and present

LPS in physiologically relevant conformations, to enable binding of antibodies to their preferred epitopes.

There are other drawbacks to using classical schemes for detection of LPS. In some cases, antigens are not readily available, and thus antibodies with high affinity for the target cannot be developed.<sup>10,201</sup> Additionally, ELISAs can suffer from high background noise due to non-specific interactions with both the sample matrix to the polystyrene plate or the antibodies sticking to non-specific targets.<sup>176,177,187,202</sup> There is also a concern that endogenous endotoxin present in reagents, on glassware, or plastics<sup>203</sup> can add to the problem.

To mitigate this, researchers have worked to develop better antibodies against both the O-ag of LPS, as well as the conserved epitopes within the molecule.<sup>9,204-208</sup> However, the main problem with developing antibodies against O-ag lies in the technique used. While there are variations of the procedure,<sup>177</sup> ELISA plates are typically functionalized with whole dead bacteria to screen monoclonal antibody cultures,<sup>9,204,208</sup> giving rise to potentially cross reactive antibody clones.<sup>10,177</sup> To minimize undesired cross reactivity, potential clones are screened against a multitude of bacterial strains.<sup>204,205,207</sup> However, it is impossible to screen clones against all epitopes of LPS. In 2000, Jauho *et al.*<sup>51</sup> addressed this issue by covalently linking purified LPS O-ag to polystyrene ELISA plates using anthraquinone and UV irradiation. This technique could prove immensely useful in developing serogroup specific antibodies against LPS, as conserved antigens like lipid A and core polysaccharide, are absent. Alternative methods for antibody screening and epitope affinity have utilized immunoblotting techniques<sup>10,205,209-211</sup> and flow cytometry.<sup>212-215</sup> These techniques allow for careful analysis of epitopes being bound by antibodies, and can help minimize cross reactivity.

#### 1.4.3 Biological and chemical-based LPS sensing

As biotechnology advances, the development of many sensing capabilities such as electrochemical impedance spectroscopy (EIS)<sup>216-218</sup>, antimicrobials,<sup>106,219</sup> aptamers,<sup>220</sup> synthetic polymers,<sup>221</sup> optical immunoassays,<sup>176,178,222</sup> waveguide technology,<sup>106,223,224</sup> lipid bilayers,<sup>20,105,225</sup> and *in vitro*<sup>226-228</sup> assays have all been

used to study LPS interactions and develop sensitive and/or specific detection methods. These technologies, similar to older ones, use a common strategy of functionalizing biosensors with proteins or molecules to pull down LPS from a sample matrix. The researchers typically utilize one of many specialized proteins and ligands that interact with LPS, as discussed above, for this purpose.

A primary protein that binds LPS is the LPS Binding Protein (LBP),<sup>229</sup> a relatively small protein (~60 kDa) that transports LPS in the bloodstream. LBP passes LPS off to the cluster of differentiation 14 (CD14) protein, located in the extracellular matrix, or on the membrane of immune cells, such as macrophages.<sup>229</sup> After LPS binds CD14, it is passed to the hydrophobic binding pocket of myeloid differentiation factor 2 (MD-2),<sup>18,104</sup> which is a necessary cofactor for activation of the innate immune receptor, TLR4. In addition to these, LPS has been demonstrated to bind aptamers,<sup>216,217</sup> various peptides,<sup>119,219,230-232</sup> and metal/cation complexes.<sup>114,116,218,233-235</sup> All of these molecules, along with the serum carriers (HDL and LDL) of LPS, are potential receptors for capturing LPS on surfaces, and have been evaluated in that context.

Electrochemical and fluorescence-based sensors for detection of LPS have been developed. Existing methods are based on the idea that LPS must be pulled down from the sample matrix to a receptor molecule on the sensing surface. Electrochemical sensing of LPS requires a recognition ligand (similar to ELISA) and a transducer to measure the variation in signal.<sup>218</sup> For fluorescence-based sensing, a receptor is required to capture LPS while another molecule emits a fluorescent signal when bound to the antigen. Burkhardt *et al.*<sup>236</sup> used solubilized LBP to transfer LPS to a CD14 functionalized surface, and detected it at a LoD of 10 ng•mL<sup>-1</sup> using an electro-chemiluminescent assay. This method enforces the role of LBP as a lipid transfer protein, as previously demonstrated by Wurfel *et al.*<sup>237,238</sup> and that CD14 can bind monomeric LPS in the absence of TLR4.<sup>239</sup> Highly sensitive (LoD = 0.0005 EU) electrochemical sensors have also been developed using a recombinant innate immune (TLR4 + MD-2) receptor complex for recognition of LPS.<sup>240</sup> However, such an assay has no capability for O-ag specificity, unless a recognition molecule could be used to bind the exposed O-ag.

Priano *et al.*<sup>230,231</sup> functionalized an electrochemical sensor with a recombinant endotoxin neutralizing protein on a dextran matrix to perform a competitive LPS assay, and achieved a detection range of 1-100 ng•mL<sup>-1</sup>. Endotoxin neutralizing protein has also been used in a capacitive biosensor with an extremely low LoD ( $1.0 \times 10^{-13}$  M).<sup>241</sup> As mentioned in *Section 1.4.1*, small changes in the preparation of LPS can lead to large changes in sensitivity of assays. The disparity in detection signals between these two assays can perhaps be explained by the method of surface functionalization. Priano *et al.*<sup>230,231</sup> used the dextran matrix, and Limbut *et al.*<sup>241</sup> used self assembled monolayers (SAMs), which are known to have particularly low background interference.<sup>242-244</sup> Inoue and Takano<sup>245,246</sup> used a recombinant factor C (a protein from the LAL enzyme pathway)<sup>247</sup> to make an electrochemical-based hybrid LAL-biosensor chip with a reported sensitivity range of  $5 \times 10^{-4}$  – 1.0 EU/mL. This strategy would work well for detection in ground beef and patient urine. However, the inability to detect bacterial species leaves health care providers with little information on treatment strategies.

An interesting adaptation of LPS pull down with PmB was performed by Kato<sup>119</sup> and Iijima.<sup>248</sup> PmB was labeled with ferrocene-bound LPS in solution, and then captured on a nanocarbon-film electrode to measure bound LPS. This electrochemical sensor reported a detection range of 2-50 ng•mL<sup>-1</sup> in as little as 5 minutes.<sup>248</sup> However, previously, Ding *et al.*<sup>219</sup> functionalized an electrode with PmB and performed EIS with a detection range of 0.2-0.8 ng•mL<sup>-1</sup> which is sufficiently more sensitive, but has a much smaller range. A broader detection range was demonstrated by Rahman *et al.*,<sup>232</sup> who were able to functionalize interdigital sensors with PmB and tested 0.1-1000 µg/mL of LPS O111:B4 in various food samples, using impedance spectroscopy.

A special category of protein functionalization is the usage of lectins (sugar binding proteins) to pull down and bind LPS. Lectins have been covalently linked to the surface of a luminescent biosensor, resulting in a sensitivity of ~200 ng•mL<sup>-1</sup> LPS,<sup>249</sup> and also to polyaniline coated electrodes to detect both LPS and a similar amphiphilic PAMP, LTA.<sup>250</sup> This method indicates the importance of being able to detect both Gram-positive and Gram-negative pathogens, however the ability to

differentiate between the two amphiphiles was not a capability of this particular platform. Similar methodology was used to functionalize the surface of an EIS sensor with the lectin, CramoLL, to develop a proof of concept assay with a detection range of 25-200  $\mu\text{g}/\text{mL}$ .<sup>251</sup>

Other biosensor platforms have used gold electrodes or surfaces functionalized with LPS-binding materials to develop assays capable of detecting LPS O-ag. Su *et al.*<sup>217,252,253</sup> used aptamers attached to gold nanoparticles to detect LPS using EIS, and achieved an impressive detection limit of 0.1  $\text{pg}/\text{mL}$ .<sup>253</sup> Aptamers have also been used in a magnetic aptasensor, where two different aptamers were used in a sandwich format to detect LPS in complex medias containing BSA, sucrose, glucose, or RNA.<sup>220</sup> The range of detection for the aptasensor was determined to be  $0.01 - 1.0 \times 10^6 \text{ ng}\cdot\text{mL}^{-1}$  (LPS O55:B5) using a flow cytometer within 1 minute. Bai *et al.*<sup>254</sup> developed an electrochemical sensor where aptamers that bind LPS were hybridized with capture probes, and then the capture probes were hybridized to complementary DNA sequences on gold nanoparticles. This method reported a very sensitive detection range of  $10 \text{ fg}\cdot\text{mL}^{-1}$  up to  $50 \text{ ng}\cdot\text{mL}^{-1}$ , and is arguably the most sensitive endotoxin assay. Such a sensitive method could also have high potential as a discriminative assay, especially because multiplexing with LPS aptamer probes is feasible. However, multiple aptamer libraries against O-ag would be essential before this method could be implemented on a broader scale.

Some researchers have used more specialized surfaces for detection. In some cases, SAMs have been used to functionalize sensors with peptides,<sup>255</sup> PmB,<sup>219</sup> antibodies,<sup>256</sup> and aptamers,<sup>216</sup> to develop pull down assays for LPS detection. A schematic of SAMs for detection can be seen in **Figure 1.6A**. Nieradka *et al.*<sup>256</sup> used strain specific antibodies attached to SAMs on the surface of microcantilevers for detection of LPS from *Hafnia* strains, but the LoD was in the  $\mu\text{g}\cdot\text{mL}^{-1}$  range. Kim *et al.*<sup>216</sup> performed sensitive detection of LPS O55:B5 ( $0.01 - 1.0 \text{ ng}\cdot\text{mL}^{-1}$ ) using SAMs functionalized with aptamers, but the decreased detection range could prove a limiting factor. Both antibodies and aptamers are advantageous

methods for specific detection, however they can both be cost prohibitive given the sero-diversity of LPS.

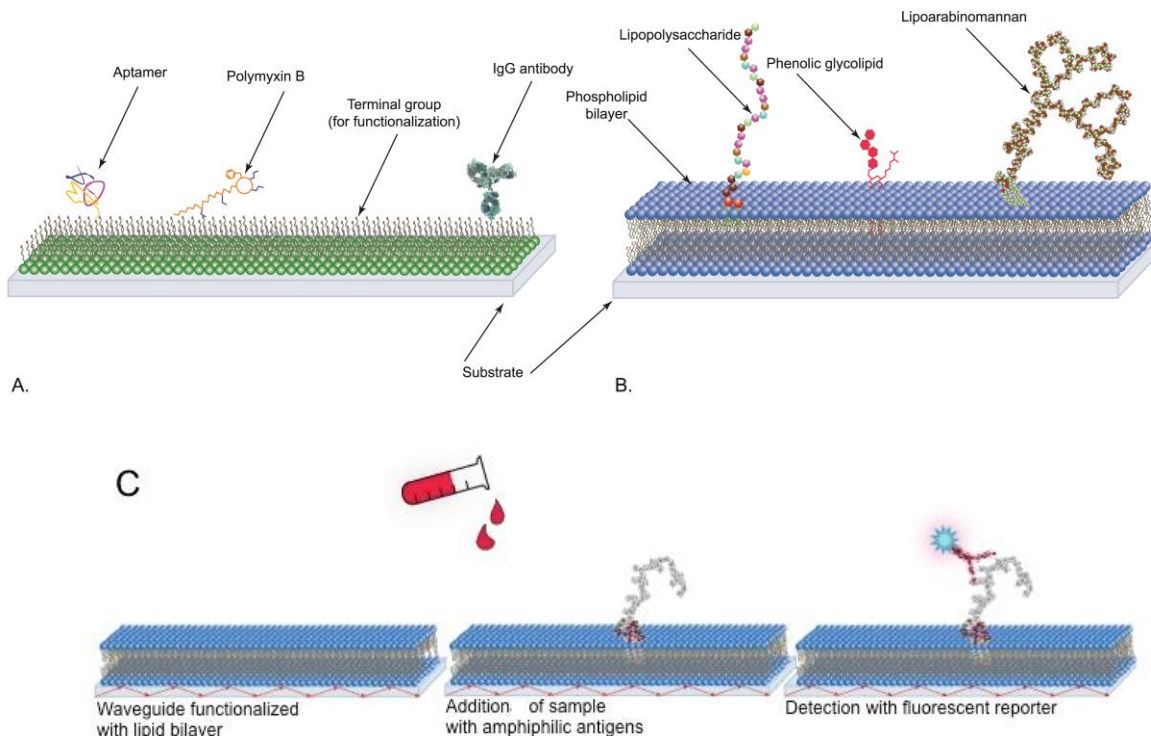


**Figure 1.6 – Functionalized surfaces for detection of biomarkers.** A. Self-assembled monolayers (SAMs) can be put on the surface of detection platforms to minimize the background noise associated with detection in complex bilayers. SAMs can be functionalized with a multitude of moieties, including aptamers, antibodies, or polymyxin B. B. Membrane insertion uses a substrate functionalized with supported lipid bilayers and the target amphiphile diffuses into the bilayer due to hydrophobic associations. C. Detection with membrane insertion in which the waveguide is functionalized with a lipid bilayer, the amphiphile diffuses into the bilayer and is detectable with a fluorescently labeled antibody. (Figure B (LAM structure) was adapted from Mukundan et al. 2012 and reprinted with permission from Elsevier.)

Other research groups have exploited the chemical nature of LPS by demonstrating interactions with other synthetic systems such as copolythiophene copolymers<sup>221</sup> and polydiacetylene liposomes,<sup>257,258</sup> both of which generate a fluorescent signal in solution when associated with LPS. Johnson *et al.*<sup>259</sup> demonstrated an endotoxin capture technique by functionalizing a bead matrix with proanthocyanidins and binding with fluorescein isothiocyanate-labeled LPS. While the technique was developed as a purification system, it could potentially be applied to detection of endotoxin as proanthocyanidins have a high affinity for lipid A.<sup>259</sup>

Pyrenyl-derived quaternary ammonium probes, developed by Zeng *et al.*,<sup>260</sup> exhibited fluorescence when bound to LPS and were able to detect nanomolar concentrations, and fluorescently labeled CD14 synthetic peptides demonstrated an increase in Förster resonance energy transfer when bound to LPS, but were only able to detect  $\mu\text{M}$  concentrations of the antigen.<sup>261</sup> Lim *et al.*<sup>262</sup> functionalized a graphene oxide surface with a fluorescently labeled LPS binding peptide, which when bound to the graphene oxide was quenched. Upon binding of 130 pM LPS, fluorescence recovery occurred due to release of the peptide from the surface. While this method was tested with many types of LPS, it is a method specific to the biological activity of lipid A, and not the O-ag. Thompson *et al.*<sup>263</sup> designed a tandem system to both detect ( $\text{LoD} = 1.0 \text{ ng}\cdot\text{mL}^{-1}$ ) and filter LPS from blood using piezo electric quartz discs functionalized with PmB. These separation and concentration approaches have accounted for the biochemistry of LPS, and such lessons should be transitioned into detection schemes for effective assay design.

Other methods for detection of LPS have taken advantage of its unique amphipathic nature. Harmon *et al.*<sup>264</sup> demonstrated that disrupting the hydrophobic association of LPS with lipid liposomes increases the sensitivity of the LAL assay. In contrast to lipid disruption, Sakamuri *et al.*<sup>19</sup> was able to detect 0.8 pM of amphiphilic LAM in patient serum on a waveguide biosensor using a technique called membrane insertion. In this technique, the amphiphile partitions into a lipid bilayer, and fluorescence detection with a labeled antibody is performed within an evanescent field,<sup>225,265</sup> resulting in very sensitive detection. A schematic of membrane insertion of amphiphilic biomarkers can be seen in **Figure 1.6 B** and **1.6 C**. Membrane insertion uses the natural association of amphiphiles with a lipid bilayer to facilitate detection, and is particularly applicable to LPS since the native form of the molecule is associated with the outer membrane of Gram-negative bacteria. An additional advantage of membrane insertion is that it is not exclusive to pathogen biomarkers, but universally adaptable to many types of amphiphiles, such as carcinoembryonic antigen from tumor cells.<sup>266</sup> Most sensor platforms report exquisite sensitivity, even down to the picogram<sup>221</sup> and femtomolar<sup>20,225,265</sup> range, but very few are capable of physiological presentation of amphiphiles to facilitate discriminative detection of O-

ag groups. The detection of LPS associated with a membrane takes advantage of physiological presentation to minimize cross reactivity with the conserved lipid A epitopes, and maximize binding of O-ag specific antibodies.

#### 1.4.4 Cell-based LPS detection platforms

More specialized systems for detection of LPS look at the *in vitro* effects of the molecule on cell systems. While cells are the systems best built to recognize endotoxin, interpreting the signal response can be challenging in some instances, making for a more qualitative strategy rather than a quantitative one. Bouafsoun *et al.*<sup>226</sup> functionalized the surface of an impedance biosensor with endothelial cells and measured the decrease in impedance with endotoxin binding. This system could detect  $500 \text{ ng}\cdot\text{mL}^{-1}$  of endotoxin by measuring the decrease in resistivity of the monolayer, which was attributed to the LPS-induced formation of pores in the endothelial layer. Veiseh *et al.*<sup>267</sup> patterned macrophage cells onto gold electrodes (silicon oxide substrates) to detect LPS concentrations of  $0.1\text{-}10 \text{ }\mu\text{g}\cdot\text{mL}^{-1}$ . However, cells were concurrently stained with necrosis and apoptosis markers in parallel studies, and no staining effect could be seen in cells using concentrations less than  $10 \text{ }\mu\text{g}\cdot\text{mL}^{-1}$ . This is an interesting effect as many *in vitro* studies on innate immune response use much lower concentrations of LPS and still document increased levels of pro-inflammatory cytokines.<sup>137,268,269</sup> However, while not specified, it can be deduced that Veiseh used serum supplemented media in the experiments, and the lipoproteins and LBP in serum could have a protective effect on cells.<sup>136,269,270</sup> The most sensitive cell-based detection system was developed by Inoue *et al.*,<sup>227</sup> and could detect LPS between  $0.1\text{-}1.0 \text{ ng}\cdot\text{mL}^{-1}$ . In this system, cells were engineered to secrete alkaline phosphatase in the presence of endotoxin, and then patterned on the surface of an amperometric biosensor. Cells were incubated in the presence of LPS and *p*-aminophenyl phosphate (substrate). When the expressed alkaline phosphatase oxidized the substrate, a concentration dependent increase in voltage was recorded. Despite sensitivity and physiological relevance, cell-based *in vitro* assays are notoriously prone to errors and contamination, so developing a robust and fieldable assay based on this technology is not plausible. However, by studying

LPS in cell-based systems, a lot of knowledge about interactions with receptors and cell membranes can be gained, which can facilitate detection. It becomes obvious as one looks at the advancing research that the ability to detect low concentrations of endotoxin increases over time as new LPS binding molecules are discovered, and used to functionalize the surfaces of biosensors. However, while the detection of endotoxin is of critical importance, the new focus needs to look at the early discriminative detection of the pathogen to facilitate early response, preventing further infection and transmission in both epidemics and food safety scenarios.

### **1.5 Present studies**

Shiga-toxin producing *E. coli* (STEC) is a virulent Gram-negative pathogen that commonly presents as a contaminant in the food chain, especially in beef. Upon infection, STEC can cause severe symptoms in humans, such as gastroenteritis and hemolytic uremic syndrome. The increasing occurrence of non-O157 STEC in both cattle<sup>271</sup> and humans<sup>272</sup> has caused the United States Department of Agriculture Food Safety Inspection Service to require that all non-intact cattle products be screened for the presence of seven serotypes of STEC. The detection and differentiation of STEC strains from one another and from non-pathogenic near neighbors is essential to ensuring the safety of the food supply. However, developing strain specific detection methods for STEC predominantly relies on the identification of the LPS O-ag biomarker. For most strains of STEC, these antigens were not available for assay development. As such, in the work presented here, we show the isolation and antigen characterization of a set of LPS antigens and commercial antibodies to use for development of discriminative LPS O-ag assays. This involved bacterial culturing, antigen extraction, purification, and testing of LPS subgroups including the whole antigen molecule as well as O-ag, and lipid A components from multiple strains of STEC. We demonstrate techniques for assessing cross reactivity between O-ag using available antibodies, and then use these methods in turn to develop monoclonal antibodies with higher specificity. To develop discriminative detection methods for LPS, we applied the previously established waveguide biosensor technology using SLBs and performed detection of

LPS antigens inserted into the membrane using fluorescently labeled antibodies. An advantage of this system is the physiological presentation of LPS in a mimetic membrane system, which leaves the O-ag exposed in the aqueous matrix for detection. While this approach exploited the current knowledge that LPS passively diffuses into DOPC bilayers, we were also able to shed new light on the dynamic effects of LPS in bilayer systems. To ensure the validity of our detection platform, we extensively characterized the effects of various subtypes of LPS under multiple conditions. Understanding the physical ramifications of LPS-SLBs interactions not only aids in the development of better biosensors for detection of amphiphilic biomarkers, but also gives deeper understanding of the bioactivity of endotoxins *in vivo*. Finally we explore the ramifications that this knowledge has on our current understanding of endotoxin activity in biomimetic complex lipid systems, as well as the optimal presentation methods of LPS used in *in vitro* studies.

**Table 1.1 Survey of Methods and Reported Sensitivities of Assays Against Bacterial Endotoxins and Similar Amphiphiles**

Description	Sample	Detection Method	Species	CFU/mL	Sensitivity	Specific*	Reference
Rabbit Pyrogen	Purified endotoxin	Febrile Response	----	----	----	No	122
LAL	Plasma	Gelation	multiple species	----	0.5-5.0 ng•mL <sup>-1</sup>	No	273
LAL	Spiked Blood/ Serum Plasma	Gelation	<i>E. coli</i>	----	0.5-5.0 ng•mL <sup>-1</sup>	No	135
LAL	Serum/Plasma	Optical Density	<i>E. coli</i>	----	0.025-0.5 ng•mL <sup>-1</sup>	No	139
LAL	Spiked Urine	Gelation	<i>E. coli</i> (standard)	>10 <sup>5</sup>	0.5 ng•mL <sup>-1</sup>	No	141
LAL	Urine	Optical Density	multiple species	≥10 <sup>5</sup>	2.0 ng•mL <sup>-1</sup>	No	132
LAL	Cerebral Spinal Fluid	Gelation	<i>Haemophilus influenzae B</i>	----	0.03 ng•mL <sup>-1</sup>	No	142
LAL	Cerebral Spinal Fluid/Plasma	Optical Density	<i>Haemophilus influenzae B</i> , <i>E. coli</i> (standard)	10 <sup>7</sup>	0.01 (CSF) 0.1 (plasma) ng•mL <sup>-1</sup>	No	140
LAL	Bronchoalveolar lavage	Chromogenic	<i>Pseudomonas Haemophilus influenzae B</i>	≤10 <sup>2</sup>	0.005 ng•mL <sup>-1</sup>	No	146

Description	Sample	Detection Method	Species	CFU/mL	Sensitivity	Specific*	Reference
LAL	Cervical and urethral exudates	Chromogenic	----	----	0.07 (cervix) 0.14 (vagina) ng•mL <sup>-1</sup>	No	145
LAL	Ascites	Gelation	<i>E. coli</i> (standard)	----	0.5 ng•mL <sup>-1</sup>	No	144
LAL	Cerebral /Synovial	----	<i>E. coli</i> (standard)	----	1.0 ng•mL <sup>-1</sup>	No	143
LAL	Seawater	Optical Density	<i>E. coli</i> (standard)	4.23	2.3 ng•mL <sup>-1</sup>	No	60
LAL	Purified endotoxin	Gelation	<i>E. coli</i>	----	1.0 ng•mL <sup>-1</sup>	No	122
LAL	Purified endotoxin	Gelation	<i>Klebsiella</i>	----	0.1 ng•mL <sup>-1</sup>	No	122
LAL	Purified endotoxin	Gelation	<i>Salmonella minnesota</i>	----	10 <sup>-11</sup> ng•mL <sup>-1</sup>	No	155
LAL	Ground Beef	Gelation	<i>Enterobacter aerogenes</i>	3.5 <sup>5</sup>	----	No	274
LAL	Ground Beef	Gelation	multiple species	5.24 <sup>5</sup>	51.0 ng•g <sup>-1</sup>	No	148
LAL	Milk	Chromogenic	<i>Pseudomonas putida</i>	1.4*10 <sup>2</sup>	0.01 ng•mL <sup>-1</sup>	No	147
LAL	Purified endotoxin	Gelation	<i>E. coli</i> O114	----	100 ng•mL <sup>-1</sup>	No	275
LAL-Magnetoelastic sensor	Purified LPS	changes in resonant frequency of the sensor	<i>E. coli</i> O111:B4	----	0.0105 EU•mL <sup>-1</sup>	No	276
ENDOLisa® (LAL)	Purified endotoxin	Fluorescence	<i>E. coli</i> spp. <i>Salmonella</i> spp. and others	----	0.05-500 EU•mL <sup>-1</sup>	No	277
ELISA - LAM	Urine	Abs @ 450 nm	<i>Mycobacterium tuberculosis</i>	----	----	Yes	171
ELISA	Milk	Abs @ 405 nm	<i>E. coli</i>	----	100-200 ng•mL <sup>-1</sup>		222
LPS pull down - Sandwich ELISA	Pure cultures	Abs at 450nm	<i>E. coli</i> O157	10 <sup>5</sup>	----		178
LPS pull down - Sandwich ELISA	Purified LPS and pure cultures	Abs at 450 nm	<i>Salmonella</i> spp. (31 total)	1120	1.0 ng•mL <sup>-1</sup>	Yes	179
ELISA	Purified LPS in PBS buffer	Abs at 492nm	<i>Klebsiella</i> O3	----	1000 ng•mL <sup>-1</sup>	Yes	172

Description	Sample	Detection Method	Species	CFU/mL	Sensitivity	Specific	Reference
Premier EIA <i>E. coli</i> O157	human stool extract	Spectrophotometric	<i>E. coli</i> O157	----	----	Yes	176
LPS pull down	Purified endotoxin	RIA	<i>E. coli</i> O114	----	300 ng•mL <sup>-1</sup>	No	275
LPS pull down - ion capture (NTA-Cu)	Purified LPS	EIS	<i>E. coli</i> O55:B5	----	0.0001–0.1 ng•mL <sup>-1</sup>	No	218
Electrochemical - diaphorase functionalized surface	Purified LPS	chemically amplified current	<i>E. coli</i> O127:B8	----	50 ng•mL <sup>-1</sup>	Maybe	119
Electrochemical competitive	Purified LPS	amperometric	<i>E. coli</i> O26:B6 <i>Salmonella minnesota</i>	----	1.0-100 ng•mL <sup>-1</sup>	No	231
LPS pull down - SAMs with synthetic peptide capture	Purified LPS	Electrochem.	<i>E. coli</i> ATCC 35218	----	21.8 pg•mL <sup>-1</sup>	No	255
LPS pull down - SAMs with aptamer capture	Purified LPS	EIS	<i>E. coli</i> O55:B5	----	0.1-1.0 ng•mL <sup>-1</sup>	Maybe	216
LPS pull down - gold electrode with aptamer capture	Purified LPS	EIS & cyclic voltammetry	<i>E. coli</i> O55:B5	----	0.001-1.0 ng•mL <sup>-1</sup>	No	217
LPS aptamer sandwich	Purified LPS in BSA, glucose or RNA	Electrochem.	----	----	10 fg•mL <sup>-1</sup>	Maybe	254
LPS pull down - gold electrodes w/ PmB capture	Purified LPS	EIS	<i>E. coli</i> O111:B4	----	0.2 ng•mL <sup>-1</sup>	No	219
Polydiacetylene Liposomes	Purified LPS (5 groups)	Change in Abs - electronic tongue	<i>E. coli spp</i> and <i>Salmonella spp</i>	----	2.22 mg•mL <sup>-1</sup>	Yes	258,278
Impedance entothelial biosensor	Purified LPS in culture medium*	Electrical resistivity of endothelial monolayer	----	----	500 ng•mL <sup>-1</sup>	No	226
Macrophage microarrays on gold electrodes	Purified LPS in culture medium*	FTIR	<i>E. coli</i> O111:B4	----	0.1 µg•mL <sup>-1</sup>	No	267
Primary culture HDME cells	Purified LPS	Fluorescent labeling of E-selectin with antibody	<i>E. coli</i> O111:B4	----	1.0 µg•mL <sup>-1</sup>	No	228

Description	Sample	Detection Method	Species	CFU/mL	Sensitivity	Specific <sup>a</sup>	Reference
Engineered cells secrete alkaline phosphatase in the presence of LPS	Purified LPS in culture medium <sup>*</sup>	Electrochem. Oxidation of substrate	----	----	0.1 ng•mL <sup>-1</sup>	No	227
LPS pull down - PmB capture	Purified labeled & unlabeled LPS	Evanescent sensing - competitive replacement by LPS	<i>E. coli</i> O128:B12	----	25 ng•mL <sup>-1</sup>	No	106
LPS pull down - TLR4/MD2 complex on gold electrodes	Purified LPS	Electrochem.	<i>E. coli</i> O55:B5	----	0.0005 EU•mL <sup>-1</sup>	No	240
LAM pull down - membrane insertion	Infected patient serum (LAM)	Evanescent sensing - fluorescence	<i>Mycobacterium tuberculosis</i>	----	0.8 pM	Yes	19
PGL pull down - membrane insertion	Purified phenolic glycolipid	Evanescent sensing - fluorescence	<i>Mycobacterium leprae</i>	----	500 nM	Yes	20
LAM pull down - membrane insertion	Purified LAM	Evanescent sensing - fluorescence	<i>Mycobacterium tuberculosis</i>	----	10 fM	Yes	225
LPS pull down - membrane insertion	Purified LPS (3 groups)	Evanescent sensing - fluorescence	<i>E. coli</i>	----	4.20 µg•mL <sup>-1</sup>	Yes	105
LPS pull down - antibody capture	Pure cultures in ground beef	Evanescent sensing - fluorescence	<i>E. coli</i> O157	520/g	----	Yes	223
LPS pull down - proanthocyanidin on beads	FITC-labeled LPS	Fluorescence	<i>E. coli</i> O55:B5	----	----	No	259
Copolythiophene interacts with LPS	Purified LPS	Fluorometric - conformational change in copolythiophene backbone	<i>E. coli</i> O55:B5		2.5E <sup>-5</sup> – 2.0 µM <sup>#</sup>	No	221
Polydiacetylene liposomes	----	Fluorometric - Binding of LPS to PDA liposomes turns on fluorescence	----	----	0.1 µM <sup>#</sup>	No	257
Peptide-based fluorescence	Purified LPS	FRET - increase	<i>E. coli</i> O111:B4	----	0.15-2.0 µM <sup>#</sup>	No	261
Pyrenyl-derived long-chain quaternary ammonium probe	Purified LPS	Fluorescence - probe binds to LPS	<i>E. coli</i> O55:B5		100 nM <sup>#</sup>	No	260

Description	Sample	Detection Method	Species	CFU/mL	Sensitivity	Specific <sup>*</sup>	Reference
LPS pull down – peptide functionalized Graphene Oxide	Purified LPS (4 groups)	Fluorescence turn on	Several species	----	130 pM <sup>#</sup>	No	262
LPS pull down PmB capture	Purified LPS spiked in blood	High frequency acoustic sensing	<i>E. coli</i> O55:B5		1.0 ng•mL <sup>-1</sup>	No	263
LPS pull down CD14 capture	Biotinylated LPS	Luminescence	----	----	10.0 ng•mL <sup>-1</sup>	No	236
LPS pull down Concanavalin-A	Purified LPS in buffer and pure cultures	Changes in luminescence	<i>Hafnia alvei</i>	4.0*10 <sup>6</sup>	0.2 µg•mL <sup>-1</sup>	No	249
LPS pull down Polyaniline + Concanavalin-A	Purified LPS and LTA	EIS	<i>E. coli aureus</i> S.	----	50.0 µg•mL <sup>-1</sup>	No	250
LPS pull down specific antibodies on SAMs	Purified LPS (2 strains)	Change in resonant frequency of microcantilever	<i>Hafnia alvei</i>	----	50 µg•mL <sup>-1</sup>	Yes	256
Aptamer sandwich on beads	Purified LPS	Flow cytometry, fluorescence	<i>E. coli</i> O55:B5	----	0.01 ng•mL <sup>-1</sup>	Maybe	220
LPS pull down Endotoxin neutralizing protein capture	Purified LPS	Change in capacitance	<i>E. coli</i>	----	1.0•10 <sup>-13</sup> M <sup>#</sup>	No	241
LPS pull down CramoLL lectin	Purified LPS (4 types)	EIS	<i>E. coli</i> <i>Salmonella</i> <i>Klebsiella</i> <i>Serratia</i>	----	25.0 µg•mL <sup>-1</sup>	No	251

\* Where specificity refers to ability to detect specific O-antigens of LPS, or differentiate between species, Maybe = indicates that specificity could be achieved, but was not tested with multiple LPS types; <sup>#</sup> Authors assumed a homogenous molecular weight (10 kDa) for LPS; <sup>\*</sup>Indicates that based on methods description, culture medium was positive for serum  
 ---- Indicates a values not specified by the author or not applicable to a given situation

## 1.6 References

- (1) Love, T. E. and Jones, B. Chapter 1. Introduction to Pathogenic Bacteria. In *Principles of Bacterial Detection*; Zourob, M., Elwary, S., Turner, A. P. F., Eds.; Springer Science & Business Media, **2008**, 1–14.
- (2) Brooks, B.W. *et al.* Evaluation of a Monoclonal Antibody-Based Enzyme-Linked Immunosorbent Assay for Detection of *Campylobacter Fetus* in Bovine Preputial Washing and Vaginal Mucus. *Vet Microbiol*, **2004** 103(1), 77-84.
- (3) Lazcka, O. *et al.* Pathogen Detection: a Perspective of Traditional Methods and Biosensors. *Biosens Bioelectron* **2007**, 22(7), 1205–1217.
- (4) Deisingh, A.K. and Thompson, M. Biosensors for the Detection of Bacteria. *Can. J. Microbiol.* **2004**, 50(2), 69–77.
- (5) Kretzer, J.W. *et al.* Sample Preparation: an Essential Prerequisite for High-Quality Bacteria Detection. In *Principles of Bacterial Detection*; Zourob, M., Elwary, S., Turner, A. P. F., Eds.; Springer Science & Business Media, 2008; pp 15–30.
- (6) Ivnitski, D. *et al.* E. Biosensors for Detection of Pathogenic Bacteria. *Biosens Bioelectron* **1999**, 14(7), 599–624.
- (7) Ngai, P.K. *et al.* Protein a Antibody-Capture ELISA (PACE): an ELISA Format to Avoid Denaturation of Surface-Adsorbed Antigens. *J Immunol Methods* **1993**, 158(2), 267–276.
- (8) Jayasena, S.D. Aptamers: an Emerging Class of Molecules That Rival Antibodies in Diagnostics. *Clin. Chem.* **1999**, 45(9), 1628–1650.
- (9) Brooks, B.W. *et al.* Monoclonal Antibodies to Lipopolysaccharide O Antigens of Enterohemorrhagic *Escherichia coli* Strains in Serogroups O26, O45, O103, O111, O121, and O145. *J Food Prot*, **2015**, 78(7), 1252-1258.
- (10) Stromberg, L.R. *et al.* A. Purification and Characterization of Lipopolysaccharides From Six Strains of Non-O157 Shiga Toxin-Producing *Escherichia coli*. *J Microbiol Methods* **2015**.
- (11) Moudallal, A.Z. *et al.* Comparative Sensitivity of Different ELISA Procedures for Detecting Monoclonal Antibodies. *J Immunol Methods* **1984**, 68 (1-2), 35–43.
- (12) Kumagai, Y. *et al.* Pathogen Recognition by Innate Receptors. *J. Infect. Chemother.* **2008**, 14 (2), 86–92.
- (13) Broz, P. and Monack, D.M. Newly Described Pattern Recognition Receptors Team Up Against Intracellular Pathogens. *Nat Rev Immunol* **2013**, 13(8), 551–565.
- (14) Akira, S. *et al.* Pathogen Recognition and Innate Immunity. *Cell* **2006**, 124(4), 783–801.
- (15) Gegner, J.A *et al.* Lipopolysaccharide (LPS) Signal Transduction and Clearance. Dual Roles for LPS Binding Protein and Membrane CD14. *J Biol Chem* **1995**, 270(10), 5320–5325.
- (16) Miyake, K. Innate Recognition of Lipopolysaccharide by Toll-Like Receptor 4–MD-2. *Trends Microbiol* **2004**, 12(4), 186–192.
- (17) Kawai, T. and Akira, S. TLR Signaling. *Semin Immunol* **2007**, 19(1), 24–32.
- (18) Park, B.S. *et al.* The Structural Basis of Lipopolysaccharide Recognition by

- the TLR4–MD-2 Complex. *Nature* **2009**, 458(7242), 1191–1195.
- (19) Sakamuri, R.M. *et al.* Association of Lipoarabinomannan with High Density Lipoprotein in Blood: Implications for Diagnostics. *Tuberculosis (Edinb)* **2013**, 93(3), 301–307.
- (20) Sakamuri, R.M. *et al.* Detection of Stealthy Small Amphiphilic Biomarkers. *J Microbiol Methods* **2014**, 103, 112-117.
- (21) Gutschmann, T. *et al.* The Physicochemistry of Endotoxins in Relation to Bioactivity. *Int J Med Microbiol* **2007**, 297(5), 341–352.
- (22) Kumar, H. *et al.* Pathogen Recognition by the Innate Immune System. *Int Rev Immunol* **2011**, 30(1), 16–34.
- (23) Schreiber, A. *et al.* 3D-Epitope-Explorer (3DEX): Localization of Conformational Epitopes Within Three-Dimensional Structures of Proteins. *J Comput Chem* **2005**, 26(9), 879–887.
- (24) Beveridge, T.J. Use of the Gram Stain in Microbiology. *Biotech Histochem* **2001**, 76 (3), 111–118.
- (25) Beveridge, T.J. Structures of Gram-Negative Cell Walls and Their Derived Membrane Vesicles. *J Bacteriol* **1999**, 181(16), 4725–4733.
- (26) Joly-Guillou, M.L. Clinical Impact and Pathogenicity of *Acinetobacter*. *Clin Microbiol Infect* **2005**, 11(11), 868–873.
- (27) Wiersinga, W.J. *et al.* Melioidosis: Insights Into the Pathogenicity of *Burkholderia pseudomallei*. *Nat Rev Microbio* **2006**, 4(4), 272–282.
- (28) Mattoo, S. *et al.* Mechanisms of *Bordetella* Pathogenesis. *Front Biosci* **2001**, 6, E168–E186.
- (29) Ketley, J.M. Pathogenesis of Enteric Infection by *Campylobacter*. *Annu Rev Microbiol* **1997**, 143(1), 5–21.
- (30) Lüderitz, O. *et al.* Lipopolysaccharides of Gram-Negative Bacteria. *Curr Top Membr*, **1982**, 17(79) 339.
- (31) Belland, R.J. *et al.* *Chlamydia pneumoniae* and Atherosclerosis. *Cell Microbiol*, **2004**, 6(2), 117-127.
- (32) Leimbach, A. *et al.* *E. coli* as an All-Rounder: the Thin Line Between Commensalism and Pathogenicity. *Curr Top Microbiol Immunol* **2013**, 358 (Chapter 303), 3–32.
- (33) Moran, A. P. *et al.* Structural Characterization of the Lipid a Component of *Helicobacter pylori* Rough- and Smooth-Form Lipopolysaccharides. *J Bacteriol* **1997**, 179(20), 6453–6463.
- (34) Yamaoka, Y. and Graham, D.Y. *Helicobacter pylori* virulence and Cancer Pathogenesis. *Future Oncol* **2014**, 10(8), 1487–1500.
- (35) Livorsi, D.J. *et al.* Invasive *Haemophilus influenzae* in the United States, 1999-2008: Epidemiology and Outcomes. *J Infect* **2012**, 65(6), 496–504.
- (36) Meatherall, B.L. *et al.* Incidence, Risk Factors, and Outcomes of *Klebsiella pneumoniae* Bacteremia. *Amer J Med* **2009**, 122(9), 866-873.
- (37) Newton, H.J. *et al.* Molecular Pathogenesis of Infections Caused by *Legionella pneumophila*. *Clin Microbiol Rev* **2010**, 23(2), 274–298.
- (38) Perez Vidakovics, M.L. and Riesbeck, K. Virulence Mechanisms of *Moraxella* in the Pathogenesis of Infection. *Curr Opin Infect Dis* **2009**, 22(3), 279–285.

- (39) Stephens, D.S. Biology and Pathogenesis of the Evolutionarily Successful, Obligate Human Bacterium *Neisseria meningitidis*. *Vaccine* **2009**, 27 Suppl 2, B71–B77.
- (40) Mahajan-Miklos, S. *et al.* Molecular Mechanisms of Bacterial Virulence Elucidated Using a *Pseudomonas aeruginosa*-*Caenorhabditis Elegans* Pathogenesis Model. *Cell* **1999**, 96(1), 47–56.
- (41) Mobley, H.L. and Belas, R. Swarming and Pathogenicity of *Proteus mirabilis* in the Urinary Tract. *Trends Microbiol* **1995**, 3(7), 280–284.
- (42) Mather, A.E. *et al.* Distinguishable Epidemics of Multidrug-Resistant *Salmonella typhimurium* DT104 in Different Hosts. *Science*, **2013**, 341(6153), 1514-1517.
- (43) Caboni, M. *et al.* An O Antigen Capsule Modulates Bacterial Pathogenesis in *Shigella sonnei*. *PLoS Pathog* **2015**, 11(3), e1004749.
- (44) Fàbrega, A. and Vila, J. *Yersinia enterocolitica*: Pathogenesis, Virulence and Antimicrobial Resistance. *Enferm Infecc. Microbiol Clin* **2012**, 30(1), 24–32.
- (45) Iqbal, S.S. *et al.* A Review of Molecular Recognition Technologies for Detection of Biological Threat Agents. *Biosens Bioelectron* **2000**, 15(11-12), 549–578.
- (46) Mairhofer, J. *et al.* Microfluidic Systems for Pathogen Sensing: a Review. *Sensors* **2009**, 9 (6), 4804–4823.
- (47) Skottrup, P.D. *et al.* Towards on-Site Pathogen Detection Using Antibody-Based Sensors. *Biosens Bioelectron* **2008**, 24(3), 339–348.
- (48) Uttamchandani, M. *et al.* Applications of Microarrays in Pathogen Detection and Biodefence. *Trends Biotech* **2009**, 27 (1), 53–61.
- (49) Mandal, P.K. *et al.* Methods for Rapid Detection of Foodborne Pathogens: an Overview. *Amer J Food Tech* **2011**, 6(2), 87–102.
- (50) Alexander, C. and Rietschel, E.T. Invited Review: Bacterial Lipopolysaccharides and Innate Immunity. *J Endotoxin Res* **2001**, 7(3), 167–202.
- (51) Jauho, E.S. *et al.* New Technology for Regiospecific Covalent Coupling of Polysaccharide Antigens in ELISA for Serological Detection. *J Immunol Methods* **2000**, 242(1-2), 133–143.
- (52) Munford, R.S. Sensing Gram-Negative Bacterial Lipopolysaccharides: a Human Dischoiease Determinant? *Infect Immun* **2008**, 76(2), 454–465.
- (53) Bennett, I.L. and Cluff, L.E. Bacterial Pyrogens. *Pharmacol Rev*, **1957**, 9(4), 427–429.
- (54) Westphal, O. *et al.* The History of Pyrogen Research. *Microbiol*, **1978**, 221–238.
- (55) Beutler, B. and Rietschel, E.T. Innate Immune Sensing and Its Roots: the Story of Endotoxin. *Nat Rev Immunol* **2003**, 3(2), 169–176.
- (56) Beutler, B. Tlr4: Central Component of the Sole Mammalian LPS Sensor. *Curr Opin Immunol* **2000**, 12(1), 20–26.
- (57) Galloway, S.M. and Raetz, C.R. A Mutant of *Escherichia coli* Defective in the First Step of Endotoxin Biosynthesis. *J Biol Chem* **1990**, 265(11), 6394–6402.

- (58) Meredith, T.C. *et al.* Redefining the Requisite Lipopolysaccharide Structure in *Escherichia coli*. *ACS Chem Biol*, **2006**, 1(1), 33–42.
- (59) Raetz, C.R.H. *et al.* Discovery of New Biosynthetic Pathways: the Lipid a Story. *J Lipid Res* **2009**, 50 S103–S108.
- (60) Watson, S.W. *et al.* Determination of Bacterial Number and Biomass in the Marine Environment. *J Appl Environ Microbiol* **1977**, 33(4), 940–946.
- (61) Olins, A.L. and Warner, R.C. Physicochemical Studies on a Lipopolysaccharide From the Cell Wall of *Azotobacter vinelandii*. *J Biol Chem* **1967**, 242(21), 4994–5001.
- (62) Schromm, A.B. *et al.* The Charge of Endotoxin Molecules Influences their Conformation and IL-6-Inducing Capacity. *J Immunol* **1998**, 161(10), 5464–5471.
- (63) Bishop, R.E. Fundamentals of Endotoxin Structure and Function. *Concepts in Bacterial Virulence* **2005**, 12, 1–27.
- (64) Erridge, C. *et al.* Structure and Function of Lipopolysaccharides. *Microbes Infect* **2002**, 4 (8), 837–851.
- (65) Aurell, C.A. and Wistrom, A.O. Critical Aggregation Concentrations of Gram-Negative Bacterial Lipopolysaccharides (LPS). *Biochem Biophys Res Commun* **1998**, 253 (1), 119–123.
- (66) Amor, K. *et al.* Distribution of Core Oligosaccharide Types in Lipopolysaccharides From *Escherichia coli*. *Infect Immun* **2000**, 68(3), 1116–1124.
- (67) Plested, J.S. *et al.* Conservation and Accessibility of an Inner Core Lipopolysaccharide Epitope of *Neisseria meningitidis*. *Infect Immun* **1999**, 67(10), 5417–5426.
- (68) Silipo, A. and Molinaro, A. The Diversity of the Core Oligosaccharide in Lipopolysaccharides. *Subcell Biochem* **2010**, 53, 69–99.
- (69) Rietschel, E.T. *et al.* Bacterial Endotoxin: Molecular Relationships of Structure to Activity and Function. *FASEB* **1994**, 8(2), 217–225.
- (70) Nevola, J.J. *et al.* Colonization of the Mouse Intestine by an Avirulent *Salmonella typhimurium* Strain and Its Lipopolysaccharide-Defective Mutants. *Infect Immun* **1985**, 50(1), 152–159.
- (71) Murray, G.L. *et al.* Regulation of *Salmonella typhimurium* Lipopolysaccharide O Antigen Chain Length Is Required for Virulence; Identification of FepE as a Second Wzz. *Mol Microbiol* **2003**, 47(5), 1395–1406.
- (72) Raetz, C.R.H.; Whitfield, C. Lipopolysaccharide Endotoxins. *Annu. Rev. Biochem.* **2002**, 71, 635–700.
- (73) Jiménez de Bagüés, M.P. *et al.* Vaccination with *Brucella abortus* Rough Mutant RB51 Protects BALB/C Mice Against Virulent Strains of *Brucella abortus*, *Brucella melitensis*, and *Brucella ovis*. *Infect Immun* **1994**, 62 (11), 4990–4996.
- (74) Stenutz, R.; Weintraub, A.; Widmalm, G. R. The Structures of *Escherichia coli* O-Polysaccharide Antigens. *FEMS Microbiol Rev* **2006**, 30 (3), 382–403.
- (75) Whitfield, C. Biosynthesis of Lipopolysaccharide O Antigens. *Trends*

- Microbiol **1995**, 3(5), 178–185.
- (76) Goldman, R.C. and Leive, L. Heterogeneity of Antigenic-Side-Chain Length in Lipopolysaccharide From *Escherichia coli* O111 and *Salmonella typhimurium* LT2. Eur J Biochem **1980**, 107(1), 145–153.
- (77) Scheutz, F. *et al.* Designation of O174 and O175 to Temporary O Groups OX3 and OX7, and Six New *E. coli* O Groups That Include Verocytotoxin-Producing *E. coli* (VTEC): O176, O177, O178, O179, O180 and O181. Apmis **2004**, 112(9), 569-584.
- (78) Lerouge, I. and Vanderleyden, J. O-Antigen Structural Variation: Mechanisms and Possible Roles in Animal/Plant-Microbe Interactions. FEMS Microbiol Rev **2002**, 26 (1), 17–47.
- (79) Krüger, D. Assessing the Quality of Medicinal Products Containing Ingredients Obtained by Gene Technology; Drugs Made Germany, 1989; Vol. 32, pp 64–67.
- (80) Hirayama, C. and Sakata, M. Chromatographic Removal of Endotoxin From Protein Solutions by Polymer Particles. J Chromatog B **2002**, 781 (1-2), 419–432.
- (81) Bergstrand, A. *et al.* Aggregation Behavior and Size of Lipopolysaccharide From *Escherichia coli* O55:B5. Colloids Surf B Biointerfaces **2006**, 53 (1), 9–14.
- (82) Santos, N.C. *et al.* Evaluation of Lipopolysaccharide Aggregation by Light Scattering Spectroscopy. ChemBioChem **2003**, 4 (1), 96–100.
- (83) Israelachvili, J.N. Intermolecular and Surface Forces, 2nd ed.; Academic Press: London, 1991.
- (84) Ruckenstein, E. and Nagarajan, R. Critical Micelle Concentration. Transition Point for Micellar Size Distribution. J Phys Chem **1975**, 79 (24), 2622–2626.
- (85) Din, Z.Z. *et al.* Effect of pH on Solubility and Ionic State of Lipopolysaccharide Obtained From the Deep Rough Mutant of *Escherichia coli*. Biochemistry **1993**.
- (86) Sasaki, H. and White, S.H. Aggregation Behavior of an Ultra-Pure Lipopolysaccharide That Stimulates TLR-4 Receptors. Biophys J **2008**, 95(2), 986–993.
- (87) Moroi, Y. CMC Range Due to Polydispersity of Micelles. J Colloid Interface Sci **1991**, 141(2), 581-583.
- (88) Seydel, U. *et al.* Phase Behavior, Supramolecular Structure, and Molecular Conformation of Lipopolysaccharide. Immunobiol **1993**, 187(3-5), 191–211.
- (89) Brandenburg, K.; Wiese, A. Endotoxins: Relationships Between Structure, Function, and Activity. Curr Top Med Chem **2004**, 4(11), 1127–1146.
- (90) Gutschmann, T.; Schromm, A.; Brandenburg, K. The Physicochemistry of Endotoxins in Relation to Bioactivity. Intl J Med Microbiol **2007**, 297(5), 341–352.
- (91) Netea, M.G. *et al.* Does the Shape of Lipid A Determine the Interaction of LPS with Toll-Like Receptors? Trends Immunol. **2002**, 23(3), 135–139.
- (92) Seydel, U.; Schromm, A. B.; Blunck, R.; Brandenburg, K. Chemical Structure, Molecular Conformation, and Bioactivity of Endotoxins. Chem

- Immunol Allergy **2000**, 74, 5–24.
- (93) Rietschel, E.T. *et al.* Newer Aspects of the Chemical Structure and Biological Activity of Bacterial Endotoxins. *Prog Clin Biol Res.* **1985**, 189, 31051.
- (94) Nagarajan, R. Molecular Packing Parameter and Surfactant Self-Assembly: the Neglected Role of the Surfactant Tail †. *Langmuir* **2002**, 18(1), 31–38.
- (95) Jucker, B.A. *et al.* Polymer Interactions Between Five Gram-Negative Bacteria and Glass Investigated Using LPS Micelles and Vesicles as Model Systems. *Colloids Surf B: Biointerfaces* **1998**, 11(1), 33-45.
- (96) Petsch, D. and Anspach, F.B. Endotoxin Removal From Protein Solutions. *J Biotech* **2000**, 76(2), 97-119.
- (97) Seydel, U. *et al.* Chemical Structure, Molecular Conformation, and Bioactivity of Endotoxins. *Chem Immunol* **2000**, 74, 5–24.
- (98) Schromm, A.B. *et al.* Biological Activities of Lipopolysaccharides Are Determined by the Shape of Their LipidA Portion. *Eur J Biochem* **2000**, 267 (7), 2008–2013.
- (99) Mueller, M. *et al.* Aggregates Are the Biologically Active Units of Endotoxin. *J Biol Chem* **2004**, 279(25), 26307–26313.
- (100) Vasselon, T. *et al.* Internalization of Monomeric Lipopolysaccharide Occurs After Transfer Out of Cell Surface Cd14. *J Exp Med* **1999**, 190(4), 509–522.
- (101) Rietschel, E.T. *et al.* Biological Activities of Chemically Modified Endotoxins. *Eur J Biochem* **1971**, 22(2), 218–224.
- (102) Golenbock, D.T. *et al.* Lipid a-Like Molecules That Antagonize the Effects of Endotoxins on Human Monocytes. *J Biol Chem* **1991**, 266(29), 19490–19498.
- (103) Brandenburg, K. *et al.* Physicochemical Properties of Bacterial Glycopolymers in Relation to Bioactivity. *Carbohydr Res* **2003**, 338(23), 2477–2489.
- (104) Jerala, R. Structural Biology of the LPS Recognition. *Int J Med Microbiol* **2007**, 297(5), 353–363.
- (105) Stromberg, L.R. *et al.* Membrane Insertion for the Detection of Lipopolysaccharides: Exploring the Dynamics of Amphiphile-in-Lipid Assays. *PLoS ONE* **2016**, *In review*.
- (106) James, E. A. *et al.* Detection of Endotoxin Using an Evanescent Wave Fiber-Optic Biosensor. *Appl Biochem Biotech* **1996**, 60(3), 189-202.
- (107) Kannenberg, E.L. *et al.* Lipopolysaccharide Epitope Expression of Rhizobium Bacteroids as Revealed by in Situ Immunolabelling of Pea Root Nodule Sections. *J Bacteriol* **1994**, 176(7). 2021-2032.
- (108) Haselhorst, T. *et al.* NMR Experiments Reveal Distinct Antibody-Bound Conformations of a Synthetic Disaccharide Representing a General Structural Element of Bacterial Lipopolysaccharide Epitopes. *Biochemistry* **1999**, 38(20), 6449–6459.
- (109) Hershberger, C. and Binkley, S.B. Chemistry and Metabolism of 3-Deoxy-D-Mannooctulosonic Acid I. Stereochemical determination. *J Biol Chem* **1968**, 243(7), 1578–1584.

- (110) Aurell, C.A. *et al.* Direct Visualization of Gram-Negative Bacterial Lipopolysaccharide Self-Assembly. *Mol Cell Biol Res Commun* **1999**, 2(1), 42–46.
- (111) Adams, P.G. *et al.* Lipopolysaccharide-Induced Dynamic Lipid Membrane Reorganization: Tubules, Perforations, and Stacks. *Biophysical Journal* **2014**, 106(11), 2395–2407.
- (112) Van Alphen, L. *et al.* <sup>31</sup>P Nuclear Magnetic Resonance and Freeze-Fracture Electron Microscopy Studies on Escherichia Coli. II. Lipopolysaccharide and Lipopolysaccharide-Phospholipid Complexes. *BBA Biomembranes* **1980**, 597(3), 502–517.
- (113) Coughlin, R.T. *et al.* Physical Properties of Defined Lipopolysaccharide Salts. *Biochemistry* **1983**, 22(8), 2007–2013.
- (114) Coughlin, R.T. *et al.* Quantitation of Metal Cations Bound to Membranes and Extracted Lipopolysaccharide of *Escherichia coli*. *Biochemistry* **1983**, 22(8), 2002–2007.
- (115) Naumann, D. *et al.* New Insights Into the Phase Behaviour of a Complex Anionic Amphiphile: Architecture and Dynamics of Bacterial Deep Rough Lipopolysaccharide Membranes as Seen by FTIR, X-Ray, and Molecular Modelling Techniques. *J Mol Struct* **1989**, 214, 213–246.
- (116) Schindler, M. and Osborn, M. J. Interaction of Divalent Cations and Polymyxin B with Lipopolysaccharide. *Biochemistry* **1979**, 18(20), 4425–4430.
- (117) Hurley, J.C. Endotoxemia: Methods of Detection and Clinical Correlates. *Clin Microbiol Rev* **1995**, 8(2), 268–292.
- (118) Su, W. and Ding, X. Methods of Endotoxin Detection. *J Lab Autom* **2015**, 20(4), 354–364.
- (119) Kato, D. *et al.* Electrochemically Amplified Detection for Lipopolysaccharide Using Ferrocenylboronic Acid. *Biosens Bioelectron* **2007**, 22(7), 1527–1531.
- (120) McCabe, W.R. Endotoxin: Microbiological, Chemical, Pathophysiological and Clinical Correlations; Seminars in Infectious Diseases, 1980.
- (121) McClosky, W.T. *et al.* Results of First U. S. P. Collaborative Study of Pyrogens. *J. Pharm. Sci.* **2006**, 32(3), 69–73.
- (122) Cooper, J. F. *et al.* Quantitative Comparison of *in Vitro* and *in Vivo* Methods for the Detection of Endotoxin. *J Lab Clin Med* **1971**, 78 (1), 138–148.
- (123) Roberts, K. J. *et al.* Endotoxins: Pyrogens, LAL Testing and Depyrogenation; Williams, K. L., Ed.; CRC Press: Taylor & Francis Group LLC. **2007**, 167, 261–284.
- (124) Park, C.Y. *et al.* Comparison of the Rabbit Pyrogen Test and Limulus Amoebocyte Lysate (LAL) Assay for Endotoxin in Hepatitis B Vaccines and the Effect of Aluminum Hydroxide. *J Biol Std* **2005**, 33 (3), 145–151.
- (125) Bang, F.B. A Bacterial Disease of *Limulus Polyphemus*; Bulletin of the Johns Hopkins Hospital, **1956**, 98(5), 325-351.
- (126) Levin, J. and Bang, F.B. Clottable Protein in *Limulus*; Its Localization and Kinetics of Its Coagulation by Endotoxin. *Thromb Diath Haemorrh* **1968**, 19(1), 186-197.

- (127) Levin, J. *et al.* Detection of Endotoxin in the Blood of Patients with Sepsis Due to Gram-Negative Bacteria. *N Engl J Med* **1970**, 283(24), 1313–1316.
- (128) Convention, U. S. P. <85> Bacterial Endotoxins Test; 2011; Vol. USP 39 - NF 34, pp 1–5.
- (129) Center for Drug Evaluation and Research, Food and Drug Administration. Guideline on Validation of the Limulus Amebocyte Lysate Test as an End-Product Endotoxin Test for Human and Animal Parenteral Drugs, Biological Products. US Dept of Health and Human Services, 1987.
- (130) Wachtel, R.E. and Tsuji, K. Comparison of Limulus Amebocyte Lysates and Correlation with the United States Pharmacopeial Pyrogen Test. *Appl Environ Microbiol* **1977**, 33(6), 1265-1269.
- (131) Novitsky, T.J. and Roslansky, P. F. Quantification of Endotoxin Inhibition in Serum and Plasma Using a Turbidimetric LAL Assay. *Prog Clin Biol Res* **1984**, 189, 181–196.
- (132) Nachum, R. and Berzofsky, R. N. Chromogenic Limulus Amoebocyte Lysate Assay for Rapid Detection of Gram-Negative Bacteriuria. *J Clin Microbiol* **1985**, 21 (5), 759–763.
- (133) Sakti, S.P. *et al.* Disposable TSM-Biosensor Based on Viscosity Changes of the Contacting Medium. *Biosens Bioelectron* **2001**, 16 (9-12), 1101–1108.
- (134) Iwanaga, S. *et al.* Chromogenic Substrates for Horseshoe Crab Clotting Enzyme. *Pathophysiol Haemost Thromb* **1978**, 7(2-3), 183–188.
- (135) Levin, J. *et al.* Detection of Endotoxin in Human Blood and Demonstration of an Inhibitor; *J Lab Clin Med*, **1970**, 75(6), 903-911.
- (136) Harris, H. W. *et al.* Human Very Low Density Lipoproteins and Chylomicrons Can Protect Against Endotoxin-Induced Death in Mice. *J Clin Invest*, **1990**, 86(3), 696.
- (137) Cavaillon, J. M. *et al.* Cytokine Response by Monocytes and Macrophages to Free and Lipoprotein-Bound Lipopolysaccharide. *Infect Immun* **1990**, 58 (7), 2375–2382.
- (138) Hurley, J. C. *et al.* Quantitative Limulus Lysate Assay for Endotoxin and the Effect of Plasma. *J Clin Pathol* **1991**, 44(10), 849–854.
- (139) Cohen, J. and McConnell, J.S. Observations on the Measurement and Evaluation of Endotoxemia by a Quantitative Limulus Lysate Microassay. *J Infect Dis* **1984**, 150(6), 916–924.
- (140) Arditi, M. *et al.* Cerebrospinal Fluid Endotoxin Levels in Children with H. *Influenzae meningitis* Before and After Administration of Intravenous Ceftriaxone. *J Infect Dis* **1989**, 160(6), 1005–1011.
- (141) Nachum, R. and Shanbrom, E. Rapid Detection of Gram-Negative Bacteriuria by Limulus Amoebocyte Lysate Assay. *J Clin Microbiol* **1981**.
- (142) Sloyer, J.L. and Karr, L.J. Usefulness of a Kinetic Assay to Quantitate Endotoxin. *J Microbiol* **1985**, 36–38.
- (143) Tuazon, C.U. *et al.* Detection of Endotoxin in Cerebrospinal and Joint Fluids by Limulus Assay. *Arch Intern Med* **1977**, 137(1), 55–56.
- (144) Tarao, K. *et al.* Detection of Endotoxin in Plasma and Ascitic Fluid of Patients with Cirrhoissis: Its Clinical Significance. *Gastroenterology* **1977**,

- 73(3), 539–542.
- (145) Platz-Christensen, J.J. *et al.* Endotoxin and Interleukin-1 Alpha in the Cervical Mucus and Vaginal Fluid of Pregnant Women with Bacterial Vaginosis. *Am J Obstet Gynecol* **1993**, 169(5), 1161–1166.
- (146) Pugin, J. *et al.* Rapid Diagnosis of Gram Negative Pneumonia by Assay of Endotoxin in Bronchoalveolar Lavage Fluid. *Thorax* **1992**, 47(7), 547–549.
- (147) Svensson, A. and Hahn-Hägerdal, B. Comparison of a Gelation and a Chromogenic Limulus (LAL) Assay for the Detection of Gram-Negative Bacteria, and the Application of the Latter Assay to Milk. *J Dairy Res* **1987**, 54(2), 267–273.
- (148) Jay, J.M. *et al.* Determining Endotoxin Content of Ground Beef by the Limulus Amoebocyte Lysate Test as a Rapid Indicator of Microbial Quality. *Appl Environ Microbiol* **1979**, 38(5), 885–890.
- (149) Jay, J.M. Rapid Estimation of Microbial Numbers in Fresh Ground Beef by Use of the Limulus Test. *J Food Prot* **1981**, 44(4), 275–278.
- (150) Cooperstock, M. *et al.* Possible Pathogenic Role of Endotoxin in Reye's Syndrome. *Lancet* **1975**, 305(7919), 1272–1274.
- (151) Goto, H. and Nakamura, S. Dry Up Method as a Revised Limulus Test with a New Technique for Gelatin Inhibitor Removing. *Jpn J Exp Med* **1979**, 49(1), 19–25.
- (152) Hartman, I. *et al.* Application of the Limulus Amoebocyte Lysate Test to the Detection of Gram-Negative Bacterial Endotoxins in Normal and Mastitic Milk. *Res Vet Sci* **1976**, 20(3), 342–343.
- (153) Reinhold, R.B. and Fine, J.A. Technique for Quantitative Measurement of Endotoxin in Human Plasma; *Proc Soc Exp Biol Med* **1971**, 137(1), 334–340.
- (154) Maxie, M.G. and Valli, V.E. Studies with Radioactive Endotoxin. III. Localization of <sup>3</sup>H-Labelled Endotoxin in the Formed Elements of the Blood and Detection of Endotoxin in Calf Blood with the Limulus Amebocyte Lysate. *Can J Comp Med* **1974**, 38 (4), 383–390.
- (155) Yin, E.T. *et al.* Picogram-Sensitive Assay for Endotoxin: Gelation of Limulus Polyphemus Blood Cell Lysate Induced Lipopolysaccharides and Lipid a From Gram-Negative Bacteria. *Biochimica Biophysica Acta (BBA)* **1972**, 261(1), 284–289.
- (156) Takagi, K. *et al.* Quantitative Measurement of Endotoxin in Human Blood Using Synthetic Chromogenic Substrate for Horseshoe Crab Clotting Enzyme: a Comparison of Methods of Blood Sampling and Treatment. *Thromb Res* **1981**, 23(1-2), 51–57.
- (157) Niwa, M. *et al.* Proceedings: Quantitative Aspects of the Gelation Reaction of Horseshoe Crab Amoebocyte and Bacterial Endotoxin. *Jpn J Med Sci Biol.* **1975**, 28(1), 98–100.
- (158) Tsuji, K. *et al.* Recovery of Endotoxin From Human Plasma by Acid Oxidative Treatments as Monitored by an Automated Microtiter Plate-Chromogenic Substrate Limulus Amebocyte Lysate (LAL) Assay Method. *Prog Clin Biol Res* **1987**, 231, 443–457.
- (159) Harris, R.I. *et al.* An Improved Chromogenic Substrate Endotoxin Assay for

- Clinical Use. *J Clin Pathol* **1983**, 36(10), 1145–1149.
- (160) Kelly, N.M. *et al.* Differential Induction of Tumor Necrosis Factor by Bacteria Expressing Rough and Smooth Lipopolysaccharide Phenotypes. *Infect Immun* **1991**, 59 (12), 4491–4496.
- (161) Karibian, D. *et al.* Comparison of Lipids a of Several *Salmonella* and *Escherichia* Strains by 252Cf Plasma Desorption Mass Spectrometry. *J Bacteriol* **1993**, 175(10), 2988–2993
- (162) Roslansky, P.F. and Novitsky, T.J. Sensitivity of Limulus Amebocyte Lysate (LAL) to LAL-Reactive Glucans. *J Clin Microbiol* **1991**, 29(11), 2477–2483.
- (163) Seki, N. *et al.* Horseshoe Crab (1, 3)-Beta-D-Glucan-Sensitive Coagulation Factor G. a Serine Protease Zymogen Heterodimer with Similarities to Beta-Glucan-Binding Proteins. *J Biol Chem* **1994**, 269(2), 1370–1374.
- (164) Schletter, J. *et al.* Molecular Mechanisms of Endotoxin Activity. *Arch Microbiol* **1995**, 164(6), 383–389.
- (165) Engvall, E.; Perlmann, P. Enzyme-Linked Immunosorbent Assay (ELISA) Quantitative Assay of Immunoglobulin G. *Immunochemistry* **1971**, 8, 871–874.
- (166) Engvall, E. and Perlmann, P. Enzyme-Linked Immunosorbent Assay, Elisa; III. Quantitation of Specific Antibodies by Anti-Immunoglobulin in Antigen-Coated Tubes. *J Immunol* **1972**, 109(1), 129–135.
- (167) Van Weemen, B.K. and Schuurs, A. Immunoassay Using Antigen—Enzyme Conjugates. *FEBS Lett.* **1971**, 15(3), 232–236.
- (168) Carlsson, H.E. *et al.* Titration of Antibodies to Salmonella O Antigens by Enzyme-Linked Immunosorbent Assay. *Infect Immun* **1972**.
- (169) Nielsen, B. *et al.* The Serological Response to Salmonella Serovars Typhimurium and Infantis in Experimentally Infected Pigs. The Time Course Followed with an Indirect Anti-LPS ELISA and Bacteriological Examinations. *Vet Microbiol* **1995**, 47(3), 205–218.
- (170) Nalepka, J.L. and Greenfield, E.M. Detection of Bacterial Endotoxin in Human Tissues. *Biotechniques* **2004**, 37(3), 413–417.
- (171) Reither, K. *et al.* Low Sensitivity of a Urine LAM-ELISA in the Diagnosis of Pulmonary Tuberculosis. *BMC Infect Dis* **2009**, 9(1), 141.
- (172) Takahashi, K.K. *et al.* Detection of Lipopolysaccharide (LPS) and Identification of Its Serotype by an Enzyme-Linked Immunosorbent Assay (ELISA) Using Poly-L-Lysine. *J Immunol Methods* **1992**, 153(1-2), 67–71.
- (173) Scott, B.B. and Barclay, G.R. Endotoxin-Polymyxin Complexes in an Improved Enzyme-Linked Immunosorbent Assay for IgG Antibodies in Blood Donor Sera to Gram-Negative Endotoxin Core Glycolipids. *Vox Sang* **1987**, 52(4), 272–280.
- (174) Sternberger, L.A. The Unlabeled Antibody (PAP) Method, Introduction. *J of Histochem Cytochem* **1979**, 27(12), 1657–1657.
- (175) Hsu, S.M. *et al.* The Use of Antiavidin Antibody and Avidin-Biotin-Peroxidase Complex in Immunoperoxidase Technics. *Am J Clin Pathol* **1981**, 75(6), 816–821.
- (176) Mackenzie, A.M. *et al.* Sensitivities and Specificities of Premier *E. Coli* O157 and Premier EHEC Enzyme Immunoassays for Diagnosis of Infection

- with Verotoxin (Shiga-Like Toxin)-Producing *Escherichia coli*. J Clin Microbiol **1998**, 36(6), 1608–1611.
- (177) Poxton, I.R. Antibodies to Lipopolysaccharide. J Immunol Methods **1995**, 186(1), 1–15.
- (178) Kerr, P. *et al.* Development of a Monoclonal Sandwich ELISA for the Detection of Animal and Human *Escherichia coli* O157 Strains. J Appl Microbiol **2001**, 90(4), 543–549.
- (179) Choi, D. *et al.* Sandwich Capture ELISA by a Murine Monoclonal Antibody Against a Genus-Specific LPS Epitope for the Detection of Different Common Serotypes of *Salmonellas*. J Appl Bacteriol **1992**, 72(2), 134–138.
- (180) Miller, S. *et al.* Method for Detecting and Removing Endotoxin. US Patent Office. **2006**. US20090017445 A1.
- (181) Schütz, M. *et al.* Method for Identifying and for Extracting Endotoxin. US Patent Office. **2003**. US7585620 B2
- (182) Endotoxin Testing Solutions LLC. Entotoxin Detection in Human Plasma with ESP™ Sample Preparation Kit. Entotoxin Test Sample Preparation Kit.
- (183) Alberts, B. *et al.* Molecular Biology of the Cell, 5 ed.; Garland Science, 2008; pp 1539–1557.
- (184) Hyams, K.C. *et al.* Serum Antibody to Lipopolysaccharide Antigens of Shigella Species Among U.S. Military Personnel Deployed to Saudi Arabia and Kuwait During Operations Desert Shield and Desert Storm. Clin Diagn Lab Immunol **1995**, 2(6), 700–703.
- (185) Blatz, R. *et al.* Prevalence of Chlamydia Specific Antibodies Among Obstetric and Gynecological Outpatients in Gondar, North-West Ethiopia. Ethiop Med J **2001**, 39(4), 293–303.
- (186) House, D. *et al.* Serology of Typhoid Fever in an Area of Endemicity and Its Relevance to Diagnosis. J Clin Microbiol **2001**, 39(3), 1002–1007.
- (187) Freudenberg, M. A. *et al.* ELISA for Antibodies to Lipid A, Lipopolysaccharides and Other Hydrophobic Antigens. Infection **1989**, 17(5), 322–328.
- (188) Suthienkul, O. *et al.* ELISA for Seroepidemiological Study of Exposure to *Vibrio cholerae* of Population in Krabi Province, Thailand. Asian Pac J Allergy Immunol **1992**, 10(1), 55–60.
- (189) Chaicumpa, W. *et al.* Diagnosis of Typhoid Fever by Detection of *Salmonella typhi* Antigen in Urine. J Clin Microbiol **1992**, 30(9), 2513–2515.
- (190) Chaicumpa, W. *et al.* Monoclonal Antibody-Based Dot-Blot ELISA for the Detection of *Salmonella* in Foods. Asian Pac J Allergy Immunol **1995**, 13(2), 159–166.
- (191) Hegde, N. V. *et al.* Detection of the Top Six Non-O157 Shiga Toxin–Producing *Escherichia coli* O Groups by ELISA. Foodborne Pathog Dis **2012**, 9 (11), 1044–1048.
- (192) Covinsky, M. *et al.* An IgM Lambda Antibody to *Escherichia coli* Produces False-Positive Results in Multiple Immunometric Assays. Clin Chem **2000**, 46(8), 1157–1161.
- (193) Ben-Hur, H. *et al.* Transport of Maternal Immunoglobulins Through the Human Placental Barrier in Normal Pregnancy and During Inflammation.

- Intl J Mol Med **2005**, 16(3), 401-407.
- (194) Morrison, D.C. and Jacobs, D.M. Binding of Polymyxin B to the Lipid A Portion of Bacterial Lipopolysaccharides. *Immunochem* **1976**, 13(10), 813–818.
- (195) Mattsby-Baltzer, I. *et al.* Endotoxin Is Angiogenic. *Intl J Exp Pathol* **1994**, 75(3), 191.
- (196) Hardy, E. *et al.* Enhanced ELISA Sensitivity Using TCA for Efficient Coating of Biologically Active Lipopolysaccharides or Lipid A to the Solid Phase. *J Immunol Methods* **1994**, 176(1), 111-116.
- (197) Weintraub, A. *et al.* *Vibrio cholerae* O139 Bengal Possesses a Capsular Polysaccharide Which May Confer Increased Virulence. *Microb Pathog* **1994**, 16(3), 235-241.
- (198) Vreugdenhil, A.C. *et al.* LPS-Binding Protein Circulates in Association with apoB-Containing Lipoproteins and Enhances Endotoxin-LDL/VLDL Interaction. *J Clin Invest* **2001**, 107(2), 225–234.
- (199) Vreugdenhil, A. and Rousseau, C.H. Lipopolysaccharide (LPS)-Binding Protein Mediates LPS Detoxification by Chylomicrons. *J Exp Med* **2003**, 170(3), 1399-1405.
- (200) Tirola, T. *et al.* Novel Enzyme Immunoassay Utilizing Lipopolysaccharide-Binding Protein as a Capture Molecule for the Measurement of Chlamydial Lipopolysaccharide in Serum. *Diagn Microbiol Infect Dis* **2006**, 54(1), 7–12.
- (201) Fomsgaard, A. and Dinesen, B. Elisa for Human IgG and IpM Anti-Lipopolysaccharide Antibodies with Indirect Standardization. *J Immunoassay* **1987**, 8(4), 333–350.
- (202) Péterfi, Z. and Kocsis, B. Comparison of Blocking Agents for an Elisa for LPS. *J Immunoassay* **2000**, 21(4), 341–354.
- (203) Gorbet, M.B. and Sefton, M.V. Endotoxin: the Uninvited Guest. *Biomaterials* **2005**, 26(34), 6811–6817.
- (204) Westerman, R.R. *et al.* Production and Characterization of Monoclonal Antibodies Specific for the Lipopolysaccharide of *Escherichia coli* O157. *J Clin Microbiol* **1997**, 35(3), 679–684.
- (205) Mutharia, L.M. *et al.* Monoclonal Antibodies Specific for *Escherichia coli* J5 Lipopolysaccharide: Cross-Reaction with Other Gram-Negative Bacterial Species. *Infect Immun* **1984**, 45(3), 631-636.
- (206) Coughlin, R.T. and Bogard, W.C. Immunoprotective Murine Monoclonal Antibodies Specific for the Outer-Core Polysaccharide and for the O-Antigen of *Escherichia coli* O111: B4 Lipopolysaccharide (LPS). *J Immunol* **1987**, 139(2), 557–561.
- (207) Bogard, W.W. *et al.* Isolation and Characterization of Murine Monoclonal Antibodies Specific for Gram-Negative Bacterial Lipopolysaccharide: Association of Cross-Genus Reactivity with Lipid A Specificity. *Infect Immun* **1987**, 55(4), 899–908.
- (208) Rivera-Betancourt, M.M. and Keen, J. Murine Monoclonal Antibodies Against *Escherichia C]coli* O4 Lipopolysaccharide and H5 Flagellin. *J Clin Microbiol* **2001**, 39(9), 3409–3413.
- (209) de Jongh-Leuvenink, J. *et al.* Detection of Antibodies Against

- Lipopolysaccharides of *Escherichia coli* and *Salmonella* R and S Strains by Immunoblotting. *Infect Immun* **1985**, 50(3), 716–720.
- (210) Gibb, A.P. *et al.* Frequencies of Lipopolysaccharide Core Types Among Clinical Isolates of *Escherichia coli* Defined with Monoclonal Antibodies. *J Infect Dis* **1992**, 166(5), 1051–1057.
- (211) Porat, Y.B. *et al.* Quantitative Dot-Blot Assay for Low Titer Anti-Lipopolysaccharide Antibodies in Human Plasma. *J Immunol Methods* **1995**, 180(2), 213–218.
- (212) Evans, M.E. *et al.* Fluorescence-Activated Cell Sorter Analysis of Binding by Lipopolysaccharide-Specific Monoclonal Antibodies to Gram-Negative Bacteria. *J Infect Dis* **1990**, 162(1), 148–155.
- (213) Evans, M.E. *et al.* Lipopolysaccharide Heterogeneity in *Escherichia coli* J5 Variants: Analysis by Flow Cytometry. *J Infect Dis* **1992**, 166(4), 803–811.
- (214) Nelson, D. *et al.* Comparison of Immunoblotting, Flow Cytometry and ELISA to Monitor the Binding of Anti-Lipopolysaccharide Monoclonal Antibodies. *J Immunol Methods* **1990**, 133(2), 227–233.
- (215) Nelson, D. Flow Cytometry in Bacteriology. *Rev Med Microbiol* **1993**, 4(4), 215–221.
- (216) Kim, S.E. *et al.* Harnessing Aptamers for Electrochemical Detection of Endotoxin. *Analytical Biochemistry* **2012**, 424(1), 12–20.
- (217) Su, W. *et al.* Determination of Endotoxin Through an Aptamer-Based Impedance Biosensor. *Biosens Bioelectron* **2012**, 32 (1), 32–36.
- (218) Cho, M. *et al.* Sensitive Electrochemical Sensor for Detection of Lipopolysaccharide on Metal Complex Immobilized Gold Electrode. *Sensors Act B Chem* **2012**, 174, 490–494.
- (219) Ding, S.J. *et al.* A New Method for Detection of Endotoxin on Polymyxin B-Immobilized Gold Electrodes. *Electrochem Commun* **2007**, 9(5), 1206–1211.
- (220) Zuo, M.Y. *et al.* Detecting Endotoxin with a Flow Cytometry-Based Magnetic Aptasensor. *Analy Biochem* **2014**, 466, 38–43.
- (221) Lan, M. *et al.* Copolythiophene-Derived Colorimetric and Fluorometric Sensor for Visually Supersensitive Determination of Lipopolysaccharide. *J Am Chem Soc* **2012**, 134(15), 6685–6694.
- (222) Mohammed, A.H. *et al.* Development and Evaluation of an Enzyme-Linked Immunosorbent Assay for Endotoxin in Milk. *Vet Microbiol* **1988**, 18 (1), 27–39.
- (223) Demarco, D.R. and Lim, D.V. Detection of *Escherichia Coli* O157:H7 in 10- and 25-Gram Ground Beef Samples with an Evanescent-Wave Biosensor with Silica and Polystyrene Waveguides. *J Food Prot* **2002**, 65(4), 596–602.
- (224) Lamoureux, L.R. *et al.* An Optical Biosensor for Detection of Pathogen Biomarkers From Shiga Toxin-Producing *Escherichia coli* in Beef Lysates. In *SPIE Bios: Proc SPIE Int Soc Opt Eng* **2015**, 931004-931004.
- (225) Mukundan, H. *et al.* Understanding the Interaction of Lipoarabinomannan with Membrane Mimetic Architectures. *Tuberculosis* **2012**, 92(1), 38–47.
- (226) Bouafsoun, A. *et al.* Impedance Endothelial Cell Biosensor for

- Lipopolysaccharide Detection. *Mater Sci Eng C Mater Biol Appl* **2008**, 28(5-6), 653–661.
- (227) Inoue, K.Y. *et al.* Cell-Based Electrochemical Assay for Endotoxin Using a Secreted Alkaline Phosphatase Reporter System. *Electrochem* **2008**, 76(8), 525–528.
- (228) Unger, R.E. *et al.* Human Endothelial Cell-Based Assay for Endotoxin as Sensitive as the Conventional Limulus Amebocyte Lysate Assay. *Biomaterials* **2014**, 35(10), 3180–3187.
- (229) Schumann, R.R. *et al.* Structure and Function of Lipopolysaccharide Binding Protein. *Science* **1990**, 249(4975), 1429–1431.
- (230) Priano, G. *et al.* Endotoxin Detection in a Competitive Electrochemical Assay: Synthesis of a Suitable Endotoxin Conjugate. *Anal Biochem* **2007**, 362(1), 108–116.
- (231) Priano, G. and Battaglini, F. Use of an Antimicrobial Protein for Endotoxin Detection in a Competitive Electrochemical Assay. *Anal Chem* **2005**, 77(15), 4976–4984.
- (232) Rahman, M.A. *et al.* Detection of Bacterial Endotoxin in Food: New Planar Interdigital Sensors Based Approach. *J Food Eng* **2013**, 114(3), 346–360.
- (233) Beveridge, T.J. and Koval, S.F. Binding of Metals to Cell Envelopes of *Escherichia coli* K-12. *Appl Environ Microbiol* **1981**, 42(2), 325–335.
- (234) Langley, S. and Beveridge, T.J. Effect of O-Side-Chain-Lipopolysaccharide Chemistry on Metal Binding. *Appl Environ Microbiol* **1999**, 65(2), 489–498.
- (235) Ganesh, V. *et al.* Effective Binding and Sensing of Lipopolysaccharide: Combining Complementary Pattern Recognition Receptors. *Angew Chem Int Ed* **2009**, 48(2), 356–360.
- (236) Burkhardt, M. *et al.* A. Purification of Soluble CD14 Fusion Proteins and Use in an Electrochemiluminescent Assay for Lipopolysaccharide Binding. *Protein Expression and Purification* **2007**, 51(1), 96–101.
- (237) Wurfel, M.M. and Wright, S.D. Lipopolysaccharide-Binding Protein and Soluble CD14 Transfer Lipopolysaccharide to Phospholipid Bilayers: Preferential Interaction with Particular Classes of Lipid. *J Immunol* **1997**, 158(8), 3925–3934.
- (238) Fitzgerald, K.A. *et al.* Endotoxin Recognition and Signal Transduction by the TLR4/MD2-Complex. *Microbes Infect* **2004**, 6(15), 1361–1367.
- (239) Yu, B. *et al.* Lipopolysaccharide Binding Protein and Soluble CD14 Catalyze Exchange of Phospholipids. *J Clin Invest* **1997**, 99(2), 315–324.
- (240) Yeo, T.Y. *et al.* Electrochemical Endotoxin Sensors Based on TLR4/MD-2 Complexes Immobilized on Gold Electrodes. *Biosens Bioelectron* **2011**, 28(1), 139–145.
- (241) Limbut, W. *et al.* Capacitive Biosensor for Detection of Endotoxin. *Anal Bioanal Chem* **2007**, 389(2), 517–525.
- (242) Anderson, A.S. *et al.* Functional PEG-Modified Thin Films for Biological Detection. *Langmuir* **2008**, 24(5), 2240–2247.
- (243) Kwon, S.J. *et al.* An Electrochemical Immunosensor Using Ferrocenyl-Tethered Dendrimer. *Analyst* **2006**, 131(3), 402–406.
- (244) Senaratne, W. *et al.* Self-Assembled Monolayers and Polymer Brushes in

- Biotechnology: Current Applications and Future Perspectives. *Biomacromolecules* **2005**, 6(5), 2427–2448.
- (245) Inoue, K.Y. *et al.* A Screen-Printed Endotoxin Sensor Based on Amperometry Using a Novel P-Aminophenol Conjugated Substrate for a *Limulus* Amebocyte Lysate Protease Reaction. *Analyst* **2013**, 138(21), 6523–6531.
- (246) Takano, S. *et al.* Electrochemical Sensor with Substitutional Stripping Voltammetry for Highly Sensitive Endotoxin Assay. *Analyst* **2014**, 139(19), 5001–5006.
- (247) Inoue, K.Y. *et al.* Electrochemical Detection of Endotoxin Using Recombinant Factor C Zymogen. *Electrochemistry Communications* **2010**, 12(8), 1066–1069.
- (248) Iijima, S. *et al.* Enzymatically Amplified Electrochemical Detection for Lipopolysaccharide Using Ferrocene-Attached Polymyxin B and Its Analogue. *Biosens Bioelectron* **2011**, 26(5), 2080–2084.
- (249) Hreniak, A. *et al.* A Luminescence Endotoxin Biosensor Prepared by the Sol–Gel Method. *Optical Materials* **2004**, 26(2), 141–144.
- (250) da Silva, J.L. *et al.* Impedimetric Sensor of Bacterial Toxins Based on Mixed (Concanavalin a)/Polyaniline Films. *Colloids Surf B Biointerfaces* **2014**, 117, 549–554.
- (251) Oliveira, M.L. *et al.* Impedimetric Biosensor Based on Self-Assembled Hybrid Cystein-Gold Nanoparticles and CramoLL Lectin for Bacterial Lipopolysaccharide Recognition. *J Colloid Int Sci* **2011**, 362(1), 194–201.
- (252) Su, W. *et al.* Selective Detection of Endotoxin Using an Impedance Aptasensor with Electrochemically Deposited Gold Nanoparticles. *Innate Immun* **2013**, 19(4), 388–397.
- (253) Su, W. *et al.* Aptamer-Assisted Gold Nanoparticles/PEDOT Platform for Ultrasensitive Detection of LPS. *Electroanalysis* **2013**, 25(2), 380–386.
- (254) Bai, L. *et al.* A Signal-on Electrochemical Aptasensor for Ultrasensitive Detection of Endotoxin Using Three-Way DNA Junction-Aided Enzymatic Recycling and Graphene Nanohybrid for Amplification. *Nanoscale* **2014**, 6(5), 2902–2908.
- (255) Zuzuarregui, A. *et al.* Novel Integrated and Portable Endotoxin Detection System Based on an Electrochemical Biosensor. *Analyst* **2015**, 140(2), 654–660.
- (256) Nieradka, K. *et al.* Microcantilever Array Biosensors for Detection and Recognition of Gram-Negative Bacterial Endotoxins. *Sens Actuators B Chem* **2014**, 198, 114–124.
- (257) Wu, J. *et al.* Peptide Functionalized Polydiacetylene Liposomes Act as a Fluorescent Turn-on Sensor for Bacterial Lipopolysaccharide. *J Am Chem Soc* **2011**, 133(25), 9720–9723.
- (258) Rangin, M. and Basu, A. Lipopolysaccharide Identification with Functionalized Polydiacetylene Liposome Sensors. *J Am Chem Soc* **2004**, 126(16), 5038–5039.
- (259) Johnson, B.J. *et al.* Immobilized Proanthocyanidins for the Capture of Bacterial Lipopolysaccharides. *Anal Chem* **2008**, 80(6), 2113–2117.

- (260) Zeng, L. *et al.* Sensing of Bacterial Endotoxin in Aqueous Solution by Supramolecular Assembly of Pyrene Derivative. *Org Lett* **2010**, 12(18), 4014–4017.
- (261) Voss, S. *et al.* A Fluorescence-Based Synthetic LPS Sensor. *J Am Chem Soc* **2007**, 129(3), 554–561.
- (262) Lim, S.K. *et al.* Peptide-Assembled Graphene Oxide as a Fluorescent Turn-on Sensor for Lipopolysaccharide (Endotoxin) Detection. *Anal Chem* **2015**, 87(18), 9408–9412.
- (263) Thompson, M. *et al.* A True Theranostic Approach to Medicine\_ Towards Tandem Sensor Detection and Removal of Endotoxin in Blood. *Biosens Bioelectron* **2015**, 67 (C), 3–10.
- (264) Harmon, P.A. The Release and Detection of Endotoxin From Liposomes. *Analy Biochem* **1997**, 250(2), 139-146.
- (265) Sakamuri, R.M. *et al.* Novel Optical Strategies for Biodetection. *Proc SPIE Int Soc Opt Eng* **2013**, 8812, 881209-881209.
- (266) Mukundan, H. *et al.* Optimizing a Waveguide-Based Sandwich Immunoassay for Tumor Biomarkers: Evaluating Fluorescent Labels and Functional Surfaces. *Bioconj Chem* **2009**, 20(2), 222–230.
- (267) Veiseh, M. *et al.* Single-Cell-Based Sensors and Synchrotron FTIR Spectroscopy: a Hybrid System Towards Bacterial Detection. *Biosens Bioelectron* **2007**, 23(2), 253–260.
- (268) Shanmugam, A. *et al.* Synthetic Toll Like Receptor-4 (TLR-4) Agonist Peptides as a Novel Class of Adjuvants. *PLoS ONE* **2012**, 7(2), e30839.
- (269) Lamping, N. *et al.* LPS-Binding Protein Protects Mice From Septic Shock Caused by LPS or Gram-Negative Bacteria. *J Clin Invest* **1998**, 101(10), 2065–2071.
- (270) Chien, J.Y. *et al.* Low Serum Level of High-Density Lipoprotein Cholesterol Is a Poor Prognostic Factor for Severe Sepsis. *Crit Care Med.* **2005**, 33(8), 1688–1693.
- (271) Stromberg, Z.R. *et al.* Prevalence of Enterohemorrhagic *Escherichia coli* O26, O45, O103, O111, O121, O145, and O157 on Hides and Preintervention Carcass Surfaces of Feedlot Cattle at Harvest. *Foodborne Pathog Dis* **2015**, 12(7), 631–638.
- (272) Gould, L.H. *et al.* Emerging Infections Program Foodnet Working Group. Increased Recognition of Non-O157 Shiga Toxin-Producing *Escherichia coli* Infections in the United States During 2000-2010: Epidemiologic Features and Comparison with *E. coli* O157 Infections. *Foodborne Pathog Dis.* **2013**, 10(5), 453–460.
- (273) Levin, J. *et al.* Detection of Endotoxin in the Blood of Patients with Sepsis Due to Gram-Negative Bacteria. *N Engl J Med* **1970**, 283(24), 1313–1316.
- (274) Jay, J.M. The Limulus Lysate Endotoxin Assay as a Test of Microbial Quality of Ground Beef. *J Appl Bacteriol* **1977**, 43(1), 99–109.
- (275) Kimura, H. Measurement of Endotoxin. II. Comparison of Reactivities Measured by Radioimmunoassay and with the Limulus Test. *Acta Med Okayama* **1976**, 30(4), 257–270.
- (276) Ong, K.G. *et al.* A Rapid Highly-Sensitive Endotoxin Detection System.

- Biosens Bioelectron **2006**, 21(12), 2270–2274.
- (277) Grallert, H. *et al.* EndoLISA: a Novel and Reliable Method for Endotoxin Detection. Nat Meth **2011**, 8(10),iii-v.
- (278) Rangin, M. and Basu, A. Supporting Information for: Lipopolysaccharide Identification with Functionalized Polydiacetylene Liposome Sensors. J Am. Chem Soc **2004**, 126(16), S1–S

## **Chapter 2. Goals and Overview of this Work**

Shiga toxin-producing *Escherichia coli* (STEC) are food-borne pathogens that present as contaminants in beef, produce, and water. These bacteria are capable of causing serious infections in humans, often resulting in severe symptoms such as gastroenteritis and hemolytic uremic syndrome. Due to the severity of disease and increasing prevalence of STEC in the food chain, the United States Department of Agriculture currently mandates screening for several serotypes of STEC in raw beef products. Discriminative detection of STEC serotypes is critical for prevention and management of outbreaks, as well as for epidemiological modeling. However, the discrimination between types of bacteria is challenging due to similarities between strains and serotypes. LPS is a critical component for determining the serotype of a bacterial species. Therefore, the goal of this work is to develop, characterize, and optimize both assays and functional surfaces for detection of serogroup-specific STEC LPS in beef homogenates by using a signal transduction scheme specifically designed for amphiphiles, termed membrane insertion.

Historically, detection of LPS has relied on the presence of non-specific endotoxin contaminants. In this work, we propose the development of targeted methods for differential detection of LPS O-ag to facilitate serotyping of bacterial pathogens. This effort required special consideration of the amphiphilic biochemistry of LPS. Developing and implementing methods where LPS is presented in physiologically relevant conformations is critical, not only for the development of a universal amphiphile sensor, but also for understanding the conditions necessary for

*in vitro* immune studies. We established guidelines for the serogroup specific detection of LPS and for extension of these methods to other amphiphilic biomarkers.

To achieve these goals, several aspects of the problem had to be simultaneously considered. Development of these individual aspects, and their integration into a well-characterized discriminative assay for amphiphilic LPS from the seven major serotypes of STEC is the focus of this work. This comprehensive effort involved the purification and characterization of LPS from seven serotypes of STEC, as they are not commercially available, and evaluation of the efficiency of available antibodies for discriminative detection, as outlined in Chapter 3. This effort demonstrated the poor efficacy and extensive cross-reactivity of available antibodies, highlighting the need to generate specific antibodies, as is described in Chapter 4.

Once the antigens were prepared, we proceeded to develop membrane insertion assays for amphiphilic LPS, as outlined in Chapter 6. To optimize the assay, we characterized the LPS interactions with sLBAs using fluorescence and atomic force microscopy. These experiments revealed an effect of LPS interacting with supported lipid bilayers – hole formation and other deformities which is detailed in Chapter 5. These interactions with bilayers resulted in a driving question as to whether LPS-induced hole formation occurred under the same conditions as membrane insertion assays or even when incubated with cell membranes. To answer the former, we developed a flow-cell mimetic system as outlined in Chapter 6, and evaluated LPS-induced hole formation under the conditions of the membrane

insertion assays. With respect to the latter, we realized that two different factors may contribute to, or impede, hole formation in cells. The first factor being complexity of the membrane and the second being association of LPS with carrier molecules in host blood. We used complex sLBAs enriched with cholesterol and sphingomyelin to investigate the effect of membrane complexity on LPS-induced hole formation as shown in Chapter 7. To examine the latter question, we used murine cell lines, and explored the effect of LPS-induced cytokine induction when the antigen was presented with serum versus buffer, as outlined in Chapter 7.

While the details of work performed in each chapter are outlined below, taken together, the work provides a comprehensive insight into the different factors that should be considered while working with amphiphilic biomarkers. Biochemistry is significant, and has a purpose in biological systems. It should not be ignored in our design and execution of laboratory studies if true corroboration with the physiological systems is the ultimate goal. Our studies show that time, temperature, serogroup, membrane complexity, and association with carrier molecules, all affect the presentation and subsequent interaction of LPS with physiological systems. This plethora of dependencies may, in fact, explain some of the glaring discrepancies in LPS-research in the literature.

The work detailed in **Chapter 3**, was published as a research article in the *Journal of Microbiological Methods*. As the primary author of this article, the majority of this research was performed by me at several institutions (University of Nebraska-Lincoln (UNL), University of New Mexico (UNM), and Los Alamos National Laboratory (LANL)). Zachary Stromberg assisted with final steps in the purification of

LPS from bacteria, and Afsheen Banisadr assisted with protocol development for SDS-PAGE and western blotting. Investigators on this project, Steven Graves, Rodney Moxley, and Harshini Mukundan, provided experimental guidance and assistance with data interpretation. In this chapter, we describe the sourcing and characterization of LPS from various serotypes of STEC used in our research. Developing highly sensitive and discriminatory detection assays requires the use of equivalent grade reagents, and in many cases both the antigens and antibodies required were not commercially available when this work began, and thus, had to be created. Isolation of the whole LPS and its respective sub-component antigens allowed for characterization of specificity associated with commercial antibodies. Additionally, the antigens resulting from this work were used for development and screening of new monoclonal antibodies with higher specificity to the O-ags of six strains of STEC. These antigens can also be made available as a resource for other investigators interested in these serotypes of STEC. The format of this chapter is as appears in the original publication: abstract, introduction, materials and methods, results and discussion, acknowledgements, and references. Supporting information for each body of work is available in the corresponding appendix, where figure numbers are preceded by a letter 'A' followed by the appendix number (e.g. Figure A2.1 indicates Figure 1, located in Appendix 2). Subsequent chapters are formatted in a similar manner to maintain consistency for the reader.

**Chapter 4** details ongoing efforts to develop monoclonal antibodies against O-ag of LPS from six serogroups of STEC. This research is a collaborative effort between UNM, UNL, LANL, and The Dana Farber Cancer Institute-Monoclonal

Antibody Core Facility (DFCI-MACF). As the primary author of this work, my role was to design assays and perform screening of all mouse serum for antibody reactivity to LPS antigens. This effort involved using both ELISA and immunoblotting techniques to assess cross reactivity and response. I was also responsible for developing assays with which to test the specificity of the resulting antibodies, which included performing waveguide assays with the LPS antigens and their corresponding commercial antibodies. Heather Mendez, the second author, has recently begun assisting with these screenings and will be responsible for the continued effort. Heather has also begun development of serum lipoprotein capture assays, as an alternate method for screening antibody specificity. Supervision, facilities, and experimental input for this project were provided by Steven Graves, Rodney Moxley, and Harshini Mukundan, while mouse immunizations and antibody production were managed by collaborators at the DFCI-MACF.

The work within this **Chapter 4** pursues the development of antigen-antibody suites of superior sensitivity and specificity for use in research and diagnostic assays. We discuss the current techniques used for screening LPS monoclonal antibodies in an attempt to highlight the difficulties with developing antibodies against the sugar epitopes of amphiphilic molecules. To address these challenges, we demonstrate alternative methods of screening that will result in antibodies with high specificity towards the O-ag and minimal cross reactivity against the conserved epitopes of LPS. Additionally, we show the membrane insertion-based detection of these LPS groups using commercial antibodies to explore feasibility of the method, and to identify areas for further development when said monoclonal antibodies

become available. Future work will implement the established antibodies into current detection platforms for multiple serogroups of STEC.

The work in **Chapter 5**, published in *Biophysical Journal*, details the interactions of a model LPS subtype with supported lipid bilayers (sLBA). The primary author is Dr. Peter Adams, who performed the majority of the experiments in this chapter. As the second author of this article, my role was to assist in experiments and provide suggestions for experiments as well as troubleshooting and advice for handling LPS, while learning various techniques for future projects. This investigation was commenced to study the interactions of LPS with supported lipid bilayer architectures, in order to optimize and enhance the performance of membrane insertion assays. Together, Dr. Adams and myself investigated different substrates, cleaning methods, and handling methods of LPS. I provided several different LPS subtypes to use as controls or for additional experiments; the preparation of these is described in Chapter 3. I participated in every weekly meeting to specifically discuss this paper and the data. I created the cover artwork that we submitted alongside the paper, though it was not selected. I also provided references for citations and proofread and revised all manuscript drafts. I worked closely on this project with Dr. Adams for 1.5 years and the results we obtained were fundamental in establishing the goals for my research. Additional contributions to the work were made by Kirstie Swingle, who participated by performing replicate experiments and data analysis. Investigators Harshini Mukundan and Gabriel Montaña provided experimental direction, data analysis, and interpretation.

A thorough understanding of the biophysical interactions of amphiphilic biomarkers with membrane architectures is required for optimization of our membrane insertion assay approach. Based on previous work by our group with the amphiphile LAM, we hypothesized that LPS would insert into sLBA, and be detectable by fluorescence microscopy using labeled antibodies. Instead, these studies revealed that LPS forms holes or multi-lamellar structures upon interaction with sLBA under specific ionic conditions. This observation allowed for more precise control and understanding of how the molecule interacts with specific hydrophobic interfaces. It also raised the critical question of whether LPS forms holes in lipid bilayers inside of a flow cell, and how that affects detection using membrane insertion. Lastly, this discovery caused us to question whether LPS-induced deformation would extend beyond the simple sLBA architecture, into complex bilayers and cell systems. This chapter describes the biophysics of the interaction of LPS with simple lipid bilayers, whereas its impact on our detection assays and in cellular systems is covered in the Chapters 6 and 7 of this dissertation.

Membrane insertion assays for detection of STEC LPS are presented in **Chapter 6**, which is currently being revised for publication in *PLOS One*. As the primary author of this manuscript, my role was to perform the membrane insertion assays, and biophysical studies of LPS interactions with lipid bilayers. I also designed and built the flow cell mimetics for imaging. Nicolas Hengartner was responsible for statistical analysis and ensuring accuracy of reporting in the manuscript. Kirstie Swingle performed temperature dependent studies of LPS with lipid bilayers and assisted with atomic force microscopy, both of which were

originally included in the manuscript, but were later cut. Kirstie was also instrumental in document proofreading. Membrane insertion assays for amphiphile detection were developed by Harshini Mukundan and her collaborators at LANL. Additionally, Harshini Mukundan and Gabriel Montaña served as primary investigators by providing experimental oversight, troubleshooting, and data analysis. Other investigators on this project were Steven Graves and Rodney Moxley.

The purpose of this research was to develop tailored methods for the direct detection and identification of amphiphilic LPS moieties in complex samples. Using a waveguide biosensor platform, and membrane insertion, we demonstrated the detection of intact LPS in ground beef lysates, which has only previously been performed by detecting endotoxin in processed samples. Membrane insertion exploits the natural association of amphiphilic LPS into a lipid bilayer, leaving the O-ag exposed to facilitate specific detection using fluorescently labeled antibodies. This study examines the signal response, and exhaustively looks at the physical and statistical variability associated with detection of amphiphilic molecules in aqueous systems on sLBA. The outcome of this study has important implications for detection of other pathogens that display similar biochemical targets. We also investigate the implications of LPS-induced deformities under the context of the detection assays. To determine if hole formation occurred in the bilayers under conditions synonymous with the established detection assays, we designed an imaging compatible flow cell modeled after the one used in the waveguide assays. We also studied the interactions of various LPS serogroups to determine if LPS induced hole formation was a mechanism of virulence, and could potentially interfere with the detection

assays. This study validated membrane insertion as a reliable method for detection of LPS, and demonstrated broad scale applicability for membrane insertion-based detection of amphiphiles in complex matrices. It also led to critical questions about the virulence mechanisms of subtypes of LPS in association with membrane mimetic architectures.

The work in **Chapter 7** looks at the interactions of LPS with enriched lipid bilayer systems to interrogate the consequence of the findings from Chapters 5 and 6 in physiologically relevant systems. While this work is still in preparation for publication, the contributions to the work made by other individuals are indicated here. I performed the majority of the imaging studies as well as all of the work pertaining to the *in vitro* experiments. Kirstie Swingle assisted by performing temperature dependence studies of LPS interacting with lipid bilayers. Investigators, Harshini Mukundan, Gabriel Montaña, and Steven Graves provided project supervision, experimental oversight, and data interpretation.

Since hole formation was noted in simple bilayer systems in the presence of physiological buffers, we wanted to investigate the consequences of LPS-induced hole formation in bilayer/membrane systems of increasing complexity. By increasing the complexity of lipid bilayers with relevant components such as sphingomyelin and cholesterol, we sought to more closely resemble cell membranes, where the mechanism of LPS-induced hole formation should be inhibited. Investigating the LPS interaction in this model system provides information for creating a more stable interface for membrane insertion and detection of all amphiphiles. While complex bilayers provide a molecular insight into such interactions, they do not represent the

entire complexity of cell membranes. Therefore, we also studied LPS interaction with *in vitro* cell lines, specifically using various methods to present LPS to cells with different serum variants. Our hypothesis was that presentation of amphiphilic LPS with serum binding proteins would result in a differential cytokine profile when compared to the one generated when the antigen is presented in buffer. LPS is a known stimulator of inflammatory cytokines, however, serum lipoproteins can play a major role in tissue protection, although their precise functions are not completely defined. By characterizing the effects of LPS binding in the presence and absence of serum binding proteins, we not only seek to answer key questions about the physiological requirements for immune studies, but also those necessary to develop universal detection sensors. Further studies will continue to explore presentation of LPS to complex bilayer systems, and will graduate from murine to human cell lines.

While individual chapters presented herein look at highly specific interactions of LPS molecules in small systems, taken as a whole, this dissertation represents a comprehensive approach to developing and optimizing detection methods for amphiphilic pathogen biomarkers. We present a careful evaluation of antigen sourcing, antibody testing, and assay development. This work can be readily transitioned to other bacterial pathogens that secrete amphiphilic biomarkers, as well as to non-infectious disease biomarkers, which have similar amphipathic structures. Continuing research and future directions for this work are presented in **Chapter 8**. The need for developing rapid, accurate, specific, and sensitive pathogen sensing systems will continue as long as new pathogens emerge, reemerge, or continue to develop drug resistance.

**Chapter 3.**  
**Purification and characterization of lipopolysaccharides from six strains of non-O157 Shiga toxin-producing *Escherichia coli***

Loreen R. Stromberg<sup>[1,2,3]</sup>, Zachary R. Stromberg<sup>[4]</sup>, Afsheen Banisadr<sup>[2]</sup>, Steven W. Graves<sup>[1,3]</sup>, Rodney A. Moxley<sup>[4]</sup>, and Harshini Mukundan<sup>[2,3]\*</sup>

<sup>1</sup>The University of New Mexico: Center for Biomedical Engineering, MSC01 1141 1 University of New Mexico, Albuquerque, NM 87131

<sup>2</sup>Chemistry Division, Los Alamos National Laboratory, MS J567, C-PCS, Los Alamos, NM 87545, USA

<sup>3</sup>The New Mexico Consortium 4200 West Jemez Rd., Suite 301, Los Alamos, NM 87544

<sup>4</sup>University of Nebraska-Lincoln: School of Veterinary Medicine and Biomedical Sciences, P.O. Box 830905, East Campus Loop and Fair Street Lincoln, NE 68583

Published in *Journal of Microbiological Methods* 116, 1-7, 2015, reprinted with permission from Elsevier. <http://www.sciencedirect.com/science/article/pii/S0167701215001864>  
*Author contributions to this work are described in Chapter 2.*

### **3.1 Abstract**

Certain Shiga toxin-producing *Escherichia coli* (STEC) are virulent human pathogens that are most often acquired through contaminated food. The United States Department of Agriculture, Food Safety and Inspection Service has declared several serogroups of STEC as adulterants in non-intact raw beef products. Hence, sensitive and specific tests for the detection of these STEC are a necessity for implementation in food safety programs. *Escherichia coli* serogroups are identified by their respective O-antigen moiety on the lipopolysaccharide (LPS) macromolecule. We propose that the development of O-antigen-specific immunological assays can facilitate simple and rapid discriminatory detection of STEC in beef. However, the resources (antigens and antibodies) required for such development are not readily available. To overcome this, we extracted and characterized LPS and O-antigen from six STEC strains. Using hot phenol extraction, we isolated the LPS component from each strain and purified it using a series of steps to eliminate proteins, nucleic acids, and lipid A antigens. Antigens and crude LPS extracts were characterized using gel electrophoresis, immunoblotting, and modified Western blotting with commercially available antibodies, thus assessing the serogroup specificity and sensitivity of available ligands as well. The results indicate that, while many commercially available antibodies bind LPS, their activities and specificities are highly variable, and often not as specific as those required for serogroup discrimination. This variability could be minimized by the production of antibodies specific for the O-antigen. Additionally, the antigens generated from this study provide a source of characterized LPS and O-antigen standards for six serogroups of STEC.

### **3.2 Introduction**

Certain STEC are virulent human foodborne pathogens that are most often acquired through contaminated food. These organisms are the primary cause of hemolytic-uremic syndrome in children, and a leading cause of gastroenteritis worldwide.<sup>1</sup> In 2012, the United States Department of Agriculture, Food Safety and Inspection Service began testing beef manufacturing trimmings for six serogroups of

non-O157 STEC, in addition to STEC O157:H7. All seven serogroups have been declared adulterants in raw, non-intact beef,<sup>2</sup> and the six non-O157 serogroups include O26, O45, O103, O111, O121, and O145. Additionally, the newly emergent O104:H4 strain has raised concerns about additional STEC serogroups contaminating food.

The emergence of STEC O157:H7 in the 1980's led to the development of a number of commercially available reagents and detection methods for this organism and more recently, several have become available for non-O157 STEC as well. These include differential agar for isolation of bacteria;<sup>3,4</sup> latex agglutination for O-antigen (O-ag) group testing of isolates;<sup>5</sup> immunomagnetic separation for targeted enrichment in broth culture;<sup>6-8</sup> enzyme-linked immunosorbent assay (ELISA) for detection of target antigens;<sup>9-11</sup> and polymerase chain reaction (PCR) for detection of virulence factor genes, including targeted amplification of the O-antigen gene.<sup>8,12-14</sup> In general, the reagents and detection methods for STEC O157:H7 are relatively sensitive and specific, but in contrast, those for non-O157 STEC are not.<sup>11,15-17</sup> Cross-reactivity, batch-to-batch variability, excessive cost, limited shelf life, and lag time to available results are some of the immediate issues associated with such assays. PCR assays, while very sensitive, are laboratory intensive, may detect residual nucleic acid contaminants, and cannot discriminate whether target genes originated from one or more bacterial cells or types. All of the above are factors that can potentially lead to false positive results.

Historically, identification of serotype has been an important part of the *Escherichia coli* (*E. coli*) diagnostic repertoire, and is part of the requirement for identification of STEC as adulterants. Serotyping is performed by identifying the unique chemical structures of O-, capsular (K), and flagellar (H) antigens, and combinations thereof present on the bacterial cell surface.<sup>17,18</sup> Due to the frequent problems associated with their identification, K-antigen testing is now only infrequently done. Current procedures primarily focus on identification of the O- and H- antigens or their associated genes. The detection of adulterant STEC in food products and distinguishing them from non-pathogenic species is problematic. Further, the number of existing O-, H-, and K- antigens is estimated to be 180, 60,

and 80 respectively, resulting in hundreds of serotypes of *E. coli*,<sup>19-22</sup> more than 200 of which are known to possess Shiga toxin.<sup>23</sup>

Lipopolysaccharide (LPS) makes up approximately 70% of the outer membrane of Gram-negative bacteria.<sup>24-26</sup> It is a virulence factor produced by several bacteria including *E. coli*<sup>27,28</sup> and released by the bacterial cells during an infection. The LPS molecules of various pathogens are structurally different. The contribution of LPS to virulence, and the differences in this biomarker between bacterial species contributes, not only to pathogenesis, but also makes LPS an ideal target for pathogen detection<sup>29</sup> and serogroup identification. The biochemical differences in LPS between different bacteria are attributable to three major components of the LPS macromolecule.<sup>26</sup> Specifically, the molecule contains a highly conserved lipid A group attached to a core polysaccharide and a hypervariable O-antigen (O-ag) polysaccharide chain.<sup>25</sup>

Since many structural elements of LPS are largely conserved between strains of *E. coli*, antibodies directed against the intact macromolecule exhibit cross-reactivity between different serogroups of STEC. Serogroups of LPS primarily differ in the chemical nature of the O-ag, while the other components remain relatively conserved.<sup>26,30</sup> Thus, to ensure serogroup discrimination, it is important that antibodies are targeted against the variable O-ag of LPS, and not the conserved regions of the molecule. It naturally follows that some research groups have developed antibodies against the specific O-ag epitopes of LPS<sup>31,32</sup> to facilitate serogroup-specific detection of *E. coli*. However, in the absence of purified and well-characterized STEC LPS from different serogroups, the evaluation of these antibodies is difficult. To overcome this limitation, the objective of this work was to isolate and purify the O-ag from strains of non-O157 STEC. These antigens can also be used to develop targeted and specific monoclonal antibodies, and consequently discriminatory detection assays for specific serogroups of STEC LPS. Isolation and characterization of LPS and O-ag from non-O157 STEC, including a comprehensive evaluation of commercially available antibodies against the same is presented herein.

### 3.3 Materials and methods

#### 3.3.1 Materials

Unless otherwise stated, all chemicals and reagents were obtained from Thermo Fisher Scientific™ Inc (Rockford, IL). STEC strains DEC10B (O26:H11), B8227-C8 (O45:H2), MT#80 (O103:H2), 0201 9611 (O111:H11), and GS G5578620 (O145:NM) were obtained from Dr. Shannon Manning (STEC Center, Michigan State University, Lansing, MI). Serogroup was confirmed using latex agglutination kits (Abraxis Inc, Warminster, PA) and PCR according to Bai *et al.*<sup>12</sup> TY-2482 (O104:H4) was obtained from Dr. John Luchansky (USDA, Agricultural Research Service, Eastern Regional Research Center, Wyndmoor, PA) and serogroup was confirmed by PCR as previously described.<sup>33</sup> MDCH-4 (O113:H21) was obtained from the STEC Center at Michigan State University and serogroup was confirmed by PCR according to Bai *et al.*<sup>12</sup> and subsequently retyped at the *E. coli* Reference Center at Pennsylvania State University (University Park, PA).<sup>12,34</sup> Twelve separate antibodies were used for characterization studies, and the identifying numbers used throughout this paper, as well as supplier information are listed in **Table 3.1**. LPS O111:B4 phenol extract, cetyltrimethylammonium bromide (CTAB), phenol (purified by re-distillation), eosin B, acetic acid, and bovine serum albumin (BSA) were from Sigma-Aldrich (St. Louis, MO). Precision Plus Dual Xtra Protein™ Standards, 40% acrylamide solution (19:1), polyvinylidene difluoride (PVDF) membrane, and nitrocellulose 0.2 µm membrane, were from Bio-Rad® Laboratories (Hercules, CA). Regenerated cellulose dialysis tubing (molecular weight cutoff, 12-14000) was from VWR Scientific (Radnor, PA), LPS O157:H7 was obtained from List Biological Labs (Campbell, CA), and sheep blood agar plates were from Remel (Lenexa, KS). Nitro-blue tetrazolium/5-bromo-4-chloro-3'-indolyphosphate (NBT-BCIP) came from Pierce™ Thermo Fisher Scientific™ (Grand Island, NY), and Tryptic soy broth (TSB), amino methylpersulfate (APS), and tetramethylethylenediamine (TEMED) were from Thermo Fisher Scientific™ Inc. (Rockford, IL). FreeZone6® Freeze Dry System and accompanying freeze drying flasks and accessories were from LabConco® (Fort Scott, KS). Water unless specified otherwise was 18.2 MΩ-cm, filtered through a

0.22 µm membrane from a Barnstead™Nanopure™ system (Thermo Fisher Scientific Inc., Rockford, IL).

**Table 3.2. Commercial Antibodies.**

# <sup>a</sup>	Antibody	Animal/Description	Catalog #	Source
1	Lipid A - O157	goat polyclonal	PA1-73178	Thermo Scientific Pierce (Grand Island, NY)
2	LPS - O157	goat polyclonal	LS-C71709	LSBio (Seattle, WA)
3	<i>E. coli</i> 'O' & 'K'	rabbit polyclonal	NB200-579	Novus Biologicals (Littleton, CO)
4	<i>E. coli</i> LPS	rabbit polyclonal	BS-2351R	Bioss (Boston, MA)
5	O104	rabbit polyclonal	40120	Abraxis (Warminster, PA)
6	O26	mouse monoclonal	410000	Abraxis (Warminster, PA)
7	O45	mouse monoclonal	410010	Abraxis (Warminster, PA)
8	O103	mouse monoclonal	410020	Abraxis (Warminster, PA)
9	O111	mouse monoclonal	410030	Abraxis (Warminster, PA)
10	O145	mouse monoclonal	410050	Abraxis (Warminster, PA)
11	O157	mouse monoclonal	ab75244	AbCam (Cambridge, MA)
12	O121	mouse monoclonal	410040	Abraxis (Warminster, PA)
13	Anti-Goat AP	rabbit secondary	31300	Thermo Scientific Pierce (Grand Island, NY)
14	Anti-Rabbit AP	goat secondary	31340	Thermo Scientific Pierce (Grand Island, NY)
15	Anti-Mouse AP	goat secondary	D0486	Dako (Carpinteria, CA)

<sup>a</sup>Numbers 1-5 indicate polyclonal antibodies and numbers 6-12 indicate monoclonal antibodies. Numbers 13-15 are secondary antibodies labeled with alkaline phosphatase (AP).

### 3.3.2 Growth of STEC

Pure cultures from each STEC strain were streaked for isolation onto sheep blood agar plates. Isolated colonies were inoculated into 20 milliliters (mL) of TSB (125 mL flasks) and incubated on a shaking incubator at 220 revolutions per minute (rpm), 37 degrees Celsius (°C), overnight (approximately 18 hours (h)). Broth cultures were swabbed for confluency on 150 millimeter (mm) TSB with agar plates using sterile cotton swabs.<sup>32,35</sup> Plates were allowed to dry for 3 minutes (min), then incubated for 24 h at 37° C. Bacterial paste was harvested with a sterile cell scraper, and suspended in water at an estimated 100% weight to volume (w/v) ratio. Theoretical bacterial yields for 150 mm plates, based on data previously collected by our lab,<sup>31</sup> was used to approximate an equivalent w/v ratio of wet bacterial cultures to water.<sup>36</sup> Bacteria were dried under vacuum with -20° C acetone using a Büchner

funnel apparatus.<sup>35,36</sup> Repeat washes were applied, and the bacteria were continually stirred and crushed using a glass rod.

### 3.3.3 Phenol extraction

Hot phenol-water extraction, following a modified procedure for high molecular weight polysaccharides was performed as outlined by Jann *et al.*<sup>31,35,37,38</sup> Dried bacterial cultures were suspended in 68° C water (5% w/v) with stirring for 20 min. Equal volumes of 90% hot phenol, were prepared in water, heated to 68° C, added to the bacterial suspension, and stirred for 20 min at 68° C. The mixture was cooled on ice to 10° C, and centrifuged at 5,100 x gravity (*g*), 10° C for 45 min. The resulting upper aqueous layer was collected and set aside on ice. Remaining organic interphase and phenol layers with bacterial pellet were rewashed with water, using equal volume to volume (v/v) ratios. Heating, cooling and centrifugation were repeated and the aqueous layers collected and combined. Aqueous supernatant was dialyzed, in large volumes of water for 72 h,<sup>39</sup> with periodic water changes to ensure removal of low molecular weight compounds and phenol. The resulting solution was spun at 5,100 x *g* for 30 min to remove insoluble material. Material was lyophilized at -40° C and 0.133 mBar, until a dry crude extract was obtained.

### 3.3.4 Purification of LPS

Crude extract was dissolved in 50° C water (3% w/v) with stirring. Resulting opalescent solution was centrifuged at 109,000 x *g* for 4 h at 4° C. Supernatant was collected and lyophilized. The pellet was re-dissolved in warm water and the process repeated two more times until the supernatant was completely clear. Resulting purified extracts were lyophilized prior to CTAB precipitation.

### 3.3.5 Precipitation of nucleic acids from purified extracts

To remove nucleic acids, 4% w/v CTAB was dissolved at room temperature (RT, 25° C) into sterile 0.25 M sodium chloride (NaCl) solution as described by Jann *et al.*<sup>35</sup> Lyophilized extracts were dissolved separately in 0.25 M NaCl with stirring, and 25 mL CTAB/NaCl solution was added to precipitate the nucleic acid-CTAB

salt.<sup>35</sup> The solution was stirred for 15 min, RT, and centrifuged at 7,197 x *g* for 1 h, RT, to remove the precipitated pellet. Three equal volumes of water were added to the supernatant to form the LPS precipitate. The mixture was placed on ice for 2 h, then centrifuged at 7,197 x *g*, 4° C for 1 h and supernatant was removed. The white LPS pellet was dissolved in 5 mL of 1.0 M NaCl, and purified LPS was precipitated using 40 mL of 100% ethanol, and repeated cooling and centrifugation.<sup>35</sup> The NaCl and ethanol precipitation was repeated and the ethanol supernatant was discarded. The final pellet was dissolved in 30 mL water and dialyzed (molecular weight cutoff 12-14000) at 4° C for 24 h in 1.0 liter of water with stirring. The resulting solution was then freeze dried to give the final purified LPS product.

### 3.3.6 Hydrolysis of lipid A

Lyophilized LPS was dissolved in glass vials using 1.5% acetic acid.<sup>36,40</sup> Solution was heated to 100° C using an oil bath, (to adjust for the lower boiling point of water at altitude) for 5 h to separate core polysaccharide from lipid A. Samples were centrifuged for 20 min, 2000 x *g*.<sup>36,40,41</sup> The supernatant was collected, and lipid A precipitate was rewashed with acetic acid and centrifuged two more times.<sup>36</sup> Acetic acid was removed from samples by rotary evaporation under high vacuum. Evaporated samples were brought up in water,<sup>36,41</sup> lyophilized on a Schlenk line and then stored at -20° C until further use.

### 3.3.7 Sodium dodecyl sulfate – polyacrylamide gel electrophoresis

Large polyacrylamide gels (16 cm x 16 cm) were prepared using a 15% resolving gel.<sup>32,42-46</sup> Gel was prepared by mixing a ratio of 15:15:6:4, acrylamide, gel buffer (3.0 M Tris, 0.3% sodium dodecylsulfate (SDS), pH 8.45), water, and glycerol, respectively.<sup>44</sup> Polymerization was induced by adding 100 microliters (μL) of 10% APS, then 10 μL TEMED. Two milliliters of ethanol was added to level the air-gel interface, and the gel allowed to cure for 2 h at RT. Ethanol was removed by wicking and a 4% stacking gel was cast 8:1:1 (water, acrylamide, gel buffer) and allowed to cure for 1 h.<sup>44</sup> The apparatus was assembled and filled with anode buffer (0.2 M Tris-hydrochloride (Tris-HCl), pH 8.9) and cathode buffer (0.1 M Tris-HCl, 0.1 M

tricine, 0.1% SDS, pH 8.25). LPS extracts were prepared in phosphate buffered saline (PBS) at 5 mg/mL, then diluted to 2.5 mg/mL in Laemmli buffer<sup>47</sup>, and heated at 96° C for 5 min. Ten microliters of protein standard was loaded into several lanes to monitor potential distortion patterns across the gel. Twenty five micrograms of each LPS sample was loaded, and the gel was run for 1.5 h to allow samples to enter the resolving matrix.<sup>44,48</sup> Voltage was increased to 90 V, and optimized to a period of 15 h, after which the gel was removed from the apparatus.

### 3.3.8 *Inverse staining with eosin B*

Gels were removed and fixed with 3 rinses of 400 mL, 50% methanol for 7 min each.<sup>49</sup> A solution of 0.4% eosin B and 50% methanol<sup>49</sup> was prepared by first dissolving eosin in tap water and titrating with 1.0 M sodium hydroxide until all eosin was in solution. Gels were stained for 40 min, RT, with shaking. Four hundred milliliters of 5% acetic acid was used to develop the gels for 2 min. Gels were scanned at 800 dpi using an HP Scanjet 4890, and adjusted for brightness and contrast.<sup>49</sup>

### 3.3.9 *Antibodies and immunoblotting*

Several commercially available antibodies (**Table 3.1**) were tested against LPS antigens. Antibodies were evaluated for specificity to whole LPS extracts, O-ag, and lipid A subgroups. In each case, nitrocellulose membranes were blotted two times with 2 µL blots of 5 mg/mL LPS (20 µg), or concentrated solutions of O-ag, and lipid A. Standard commercial preps of LPS O111:B4 and LPS O157 were used as comparative standards for determining activity. PBS and 5% BSA blots were used as negative controls. Antigen and control blots were allowed to dry and the membrane was blocked with 5% BSA for 2 h, 37° C in a shaking incubator. Membranes were rinsed three times each, first with PBS/0.1% Tween 20 (PBS-T), then with PBS, for 5 min/each, RT, and shaking. Primary antibodies (1-12) were prepared 1:2000 in PBS and incubated with the membranes for 4 h, 37° C. Membranes were rinsed again as previously described. Appropriate secondary antibodies (13-15) were diluted 1:5000 in PBS and incubated for 1 h, RT with

shaking, and the membrane was again rinsed as described. NBT-BCIP substrate was added, incubated for 30 min with shaking and rinsed twice with water. Blots were photographed with a Nikon CoolPix P50 against a dark purple background to increase contrast in the photos.

### *3.3.10 Western-type blotting of lipopolysaccharides*

To further characterize the LPS extracts, we used a Western-type blotting method as an alternative to SDS-polyacrylamide gel electrophoresis (PAGE). Alternate lanes were loaded with 25 µg of LPS, and run as described above. Gels were removed from the electrophoresis apparatus, then equilibrated in Bjerrum Schafer-Nielson buffer (BSN) (48 mM Tris, 39 mM Glycine, pH = 9.2),<sup>48,50</sup> for 2 h on an orbital shaker, RT, prior to transfer. PVDF membrane was cut to width of 1.5 lanes and strips were aligned to match up with lanes on the gel. Gels were transferred to PVDF using a Trans-Blot® SD Semi-Dry electrophoretic transfer device (BioRad) in BSN buffer at 24 V for 30 min. PVDF was then rinsed twice in tris-buffered saline (TBS, pH 7.5) for 5 min each on an orbital shaker at RT. Membranes were blocked with 5% milk/TBS for 2 h at 37 °C,<sup>32</sup> then overnight at 4° C. Membranes were subjected to a rinse cycle of 3 times with TBS + 0.05% Tween 20 for 5 min, and then 3 times with TBS, 5 min. Each strip of PVDF was individually blotted with the respective primary antibody, diluted 1:2000 in 1% milk/TBS,<sup>32</sup> and incubated with membranes for 4 h at 37° C with shaking, then rinsed as described. Secondary antibodies were prepared 1:5000 in 1% milk/TBS, and incubated 1 h, RT with shaking. Again PVDF was rinsed 3 times each with TBS-Tween and TBS, then developed with NBT-BCIP substrate for 30 min, RT, shaking. Membranes were then rinsed with water two times for 5 min each and photographed.

### *3.3.11 Image processing*

Images of Western-type blots and immunoblots were processed using Adobe Photoshop CS5, and gels (**Figure A2.1**) were processed using ImageJ. All images were converted to black and white, then brightness and contrast were optimized and

compared to the original images. All attempts were made to conserve the integrity of the original images.

### 3.4 Results and Discussion

#### 3.4.1 Bacterial growth and purification of lipopolysaccharides

The resulting yields from harvest of bacterial strains (**Table A2.1**) spanned a range of 11.1 – 53.3 grams of dried bacteria. According to previous studies, LPS crude extract should make up 8-10% of dry bacterial weight.<sup>35,51</sup> The crude extracts of only two strains, DEC10B and GS G55078620, fell within the expected range, but the products of B8227-C8 and MDCH-4 exceeded theoretical yields. Calculated yields of extracts from ultracentrifugation were obtained by using a theoretical yield of 200-250 mg LPS per gram of dry bacteria.<sup>35,38</sup> However, yields of extracts isolated were significantly lower than this predicted range, as were the yields from CTAB precipitation.<sup>35</sup> This was attributed to the low initial low yields from the LPS crude extracts, and also from withholding 100 mg of LPS crude extracts for assay development and antigen characterization. Upon hydrolysis of lipid A, the resulting low amounts of O-ag and lipid A in each vial inhibited our ability to gravimetrically estimate the mass of isolated O-ag and lipid A subgroups.

#### 3.4.2 Gel electrophoresis

Gel electrophoresis was performed to characterize the relative size of isolated antigens and test for the presence of lipid A contamination in the sample preps. In **Figure A2.2**, lane 3 and 4 show the resulting ladder-like banding patterns of core polysaccharide LPS O157, indicated by black arrows 1 and 2.<sup>39,44,45</sup> Concentrations of LPS below 2.50 mg/mL were not visible in lanes 5 and 6, due to poor sensitivity of staining methods.<sup>49</sup> Additionally, O-ag and lipid A from LPS O157 were also not visible in lanes 7 and 8. Good visualization of the typical O-ag banding pattern<sup>45,52</sup> of LPS O111:B4 were visible in lanes 9-11, and very faintly in lane 12, as indicated by arrow 3. Also seen, were strong banding patterns in the core polysaccharide region, indicated by arrow 4. In lanes 9 and 10, there was also a faint band, as indicated by

arrow 5 that we identified as lipid A, as it has the lowest molecular weight of the subgroups, and should migrate the furthest on the gel.

### 3.4.3 Western-type and immunoblotting

Since we were unable to detect the presence of O-ag and lipid A in our LPS control groups with SDS-PAGE, we began investigating the specificity of antibodies to O-ag and whole LPS to confirm binding activity. Results of the immunoblots are summarized in **Table 3.2**, and original pictures of the blots, inclusive of lipid A antigen blots, are shown in the supporting files, **Figure A2.1** and **Table A2.2** of Appendix 2. As expected, polyclonal antibodies 1-4 were the most cross-reactive due to the presence of multiple antibody paratopes in polyclonal antibody preparations. These antibodies seemed to have the lowest affinity for antigens from the O104 and O145 groups. As TY-2482 O104:H4 is a newly emergent strain,<sup>53</sup> available polyclonal antibodies against conserved epitopes of LPS would be expected to bind lipid A, or core polysaccharide present in whole LPS O104. This raises the question of whether the molecular structures of LPS O104 are similar to other LPS serogroup counterparts.

The results of the monoclonal antibodies were highly varied in regards to binding response against the antigens. We note that in all these cases, surfaces developed and optimized for protein estimation (e.g. nitrocellulose, PVDF) are being utilized for the detection of a lipoglycan antigen, LPS. These methods are therefore, sub-optimal due to the lack of adsorption efficiency demonstrated with LPS.<sup>42,54</sup> Antibody 6 had the highest degree of non-specificity amongst all of the monoclonal antibodies tested, as it reacted with all groups of whole LPS, many groups of O-ag, and was faintly reactive to some groups of lipid A (**Table A2.2**). Of note, antibodies 8 and 10 were exclusively specific to whole LPS O103 and O145, respectively, with no cross-reactive binding to other serogroups. However, no response signal was seen with either O-ag or lipid A, indicating poor sensitivity at the concentration of antigens used here, or that the epitope for this antibody is only present on whole LPS. Additionally, reduced adsorption of the antigens to nitrocellulose as well as

conformational presentation to the antibody may negatively affect the binding of the antibody.<sup>42</sup>

**Table 3.3. Immunoblotting antibody activity against LPS antigens**

Antigen	ID #	Antibody	Antigen Serogroup								
			O111:B4	O157	O26	O45	O103	O104	O111	O113	O145
LPS O-ag	1	Lipid A - O157	+	+	+++	+	+++	+	++	++	+
	2	LPS - O157	++	++	+++	+	++	+	+++	+++	+
	3	<i>E. coli</i> 'O' & 'K'	+	+	+++	+	++	+	++	++	+
	4	<i>E. coli</i> LPS	+	+	+++	+	+++	+	++	++	+
	5	O104	-	-	++	-	++	-	+	+	-
	6	O26	+	-	+	+	+	+	+	+	+
	7	O45	-	-	-	++	-	-	+	-	-
	8	O103	-	-	-	-	-	-	-	-	-
	9	O111	-	-	-	-	-	-	+++	-	-
	10	O145	-	-	-	-	-	-	-	-	+
	11	O157	-	-	-	-	-	-	-	-	-
	12	O121	-	-	-	-	-	-	-	-	-
Whole LPS	1	Lipid A - O157	+++	+++	+++	++	++	+	++	-	-
	2	LPS - O157	+++	+++	+++	++	+++	++	+++	++	-
	3	<i>E. coli</i> 'O' & 'K'	+	++	+++	++	++	+	++	+	+
	4	<i>E. coli</i> LPS	+++	+++	+++	++	++	+	+++	+	+
	5	O104	-	+	++	+	+	+++	-	-	-
	6	O26	+++	+	++	+++	+	+++	+++	++	++
	7	O45	++	-	+	+++	-	+	+	-	-
	8	O103	-	-	-	-	+	-	-	-	-
	9	O111	++	-	-	-	-	-	+++	-	-
	10	O145	-	-	-	-	-	-	-	-	+++
	11	O157	-	++	-	-	-	-	-	-	-
	12	O121	-	-	-	-	-	-	-	-	-

+++ = intensely positive, ++ = moderately positive, + = weakly positive, - = negative result.

Antibody 9 was also highly specific to both O111 serogroups, and reactivity against the commercial O111:B4 whole LPS as well as the extracted O111 O-ag can be seen. Interestingly enough, this antibody did not bind the O-ag or lipid A components of commercial LPS, but did bind these targets when tested with the extracted LPS

O111 antigens. As shown in **Table 3.2**, Antibody 12 did not react with any of the serogroups, either in the immunoblots or the Western-type blots (data not shown). Originally, the O121:H21 strain tested negative for O121 by latex agglutination, but had an amplicon similar to that of the O121 serogroup by PCR.<sup>12</sup> As such, the strain was sent to be retested by the *E. coli* Reference Center (Pennsylvania State University) and subsequently identified as O113:H21; a result previously seen by Son *et al.*<sup>34</sup> Since antibody 12 was not directed against the LPS antigens tested in this study, we have used it as a negative antibody control. Overall most antibodies exhibited some cross-reactivity indicating the need for more specific reagents for targeting O-ag, in addition to optimized surfaces for LPS detection. To address these issues, our team has been working on the development of targeted assays specifically designed for the detection of amphiphilic moieties like LPS.<sup>55,56</sup>

Due to poor results of our control antigens obtained with eosin staining, we decided to investigate the regions that antibodies would bind to by using a method similar to Western blotting for proteins. Since coating the LPS molecule with SDS does not result in the same effect of charge per mass unit of protein, it does not migrate through the gel based exclusively on size as proteins do.<sup>42</sup> The molecule, however, has been characterized by many to separate into size discriminate regions when subjected to a high percentage of acrylamide and extended run times.<sup>32,43-46</sup> Interestingly, in contrast to SDS-PAGE, LPS O111:B4 was not well represented on the blot (**Figure 3.1**) when incubated with antibody 1 (**Figure 3.1, lane B**), indicating perhaps that transfer of the O-ag region of LPS to PVDF membrane was diminished.<sup>54</sup> However, antibody 1 did bind the antigen in the core polysaccharide region, suggesting that lipid A attached to core polysaccharide was most likely present. The strongest binding responses in the Western-type blot (lane C and G) were seen with antibodies 5 and 11. This contrasted with the immunoblots where a very poor response was recorded with antibody 11 against LPS O-ag, but it did bind specifically to whole LPS O157. Additionally, antibody 5 reacted with whole LPS O104, but not against LPS O-ag O104.

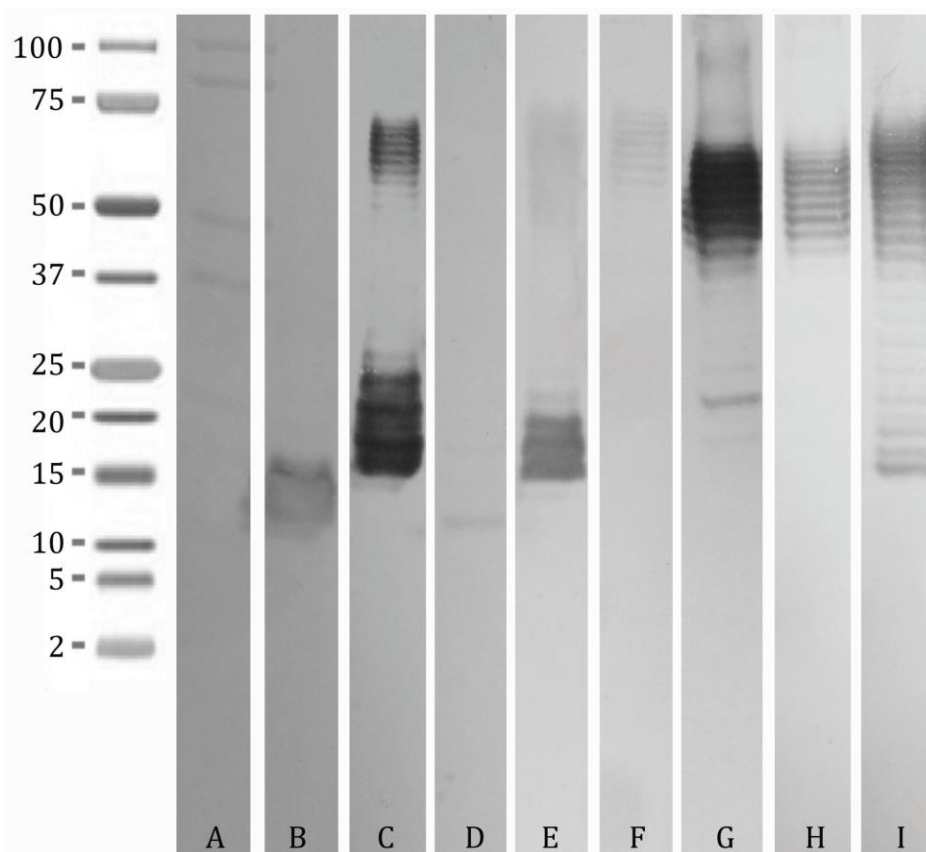


**Figure 3.1. Western-type blotting of LPS purified extracts.** Lane A is protein ladder to ensure even migration through the gel. (B). LPS O111:B4/antibody # 1 (C). LPS O157/# 11 (D). LPS O26/# 6 (E). LPS O45/# 7 (F). LPS O103/# 8. (G). LPS O104/# 5 (H). LPS O111/# 9 (I). LPS O145/# 10.

This discrepancy could be due to a variety of factors, the first being the choice of membrane (nitrocellulose in immunoblotting and PVDF in Western-type blotting) or blocking agent employed.<sup>42</sup> Additionally, the effect of electrophoretic charge separation on the conformation of LPS transferred to membranes should be considered when sensitivity of antibodies is evaluated.<sup>42,54</sup> Indeed, antibodies are known to exhibit differential performance in different assays (e.g. immunohistochemistry, ELISA, Western blot and others) as often indicated on their product information sheets. This may also explain the weak binding activity exhibited by antibody 6, (lane D) in Western-type assays, when compared to the indiscriminate binding seen in immunoblots.

Overall, we see that most antibodies appear to target the core polysaccharide region as demonstrated by bands in lanes, B-E, and arguably lanes G and I. We cannot, however, overrule the occurrence of trace O-ag in these preparations. Of all the antibodies tested, antibodies 8-10 have the most consistent results between

immunoblotting and Western-type blotting, with the exception that antibody 8 did not bind O-ag in the dot blots. These studies indicate that some commercial antibodies that are designed to be serogroup specific for different serogroups of STEC demonstrate significant cross-reactivity as evidenced with monoclonal antibodies 6 and 7, as well as polyclonals 1, 2, and 5.

### **3.5 Conclusions**

The overall goal of this work was to develop methods to contribute to the rapid and discriminatory detection among non-O157 STEC and non-pathogenic *E. coli* in beef products. Serotyping is often performed using antibodies that are not only expensive, but are also poorly effective as they cross-react between multiple serotypes of bacteria. However, this does not mean that antibody detection is a poor method for serotyping. Antibodies with high specificity and affinity for their epitopes can produce very rapid and discriminate results if the cognate antigens are available for screening the antibodies. Unfortunately, in the case of several non-O157 STEC, the O-ag for screening antibodies are not commercially available and must be prepared by extracting and purifying them from bacteria. We have extracted and chemically purified the LPS, lipid A, and O-ag from six non-O157 STEC strains and characterized them against 11 commercially available antibodies for cross-reactivity and specificity. These studies demonstrate that while some antibodies are specific and discriminatory, many of them are not, and there is still a need for improvement in monoclonal antibodies against STEC. As such, to our knowledge, this is the first time that these non-O157 STEC antigens have been prepared for the purposes of developing antibodies and detection tools against STEC. Future studies will involve screening monoclonal antibodies against O-ag, which we intend to implement into multiple detection schemes for more rapid and accurate serotyping of STEC.

### **3.6 Conflict of Interest**

No conflict of interest declared.

### **3.7 Acknowledgements**

The authors would like to thank Andrew Shreve, Douglas J. Perkins, Gabriel Montaña, Aaron Anderson, Basil Swanson, Carl Brown, and Priya Dighe for helpful discussions and critical review of data. Extra thanks goes to Gentry Lewis for her help with culture and bacterial harvest methods. This project was supported by Agriculture and Food Research Initiative Competitive Grant no. 2012-68003-30155 from the USDA National Institute of Food and Agriculture, Prevention, Detection and Control of Shiga Toxin-Producing *Escherichia coli* (STEC) from Pre-Harvest Through Consumption of Beef Products Program – A4101.

### 3.8 References

- (1) Quiñones, B. and Swimley, M. S. Use of a Vero Cell-Based Fluorescent Assay to Assess Relative Toxicities of Shiga Toxin 2 Subtypes From *Escherichia Coli*. *Methods Mol Biol* **2011**, 739, 61–71.
- (2) USDA-FSIS Rules and Regulations. Shiga Toxin-Producing *Escherichia coli* in Certain Raw Beef Products; 9 part 416, 417, 430, 2012; Vol. 77, pp 31975–31981.
- (3) Church, D. L. *et al.* Evaluation of BBL CHROMagar O157 Versus Sorbitol-MacConkey Medium for Routine Detection of *Escherichia coli* O157 in a Centralized Regional Clinical Microbiology Laboratory. *J Clin Microbiol* **2007**, 45 (9), 3098–3100.
- (4) March, S. B. and Ratnam, S. Sorbitol-MacConkey Medium for Detection of *Escherichia coli* O157:H7 Associated with Hemorrhagic Colitis. *J Clin Microbiol* **1986**, 23 (5), 869–872.
- (5) Karmali, M. A. *et al.* Evaluation of a Microplate Latex Agglutination Method (Verotox-F Assay) for Detecting and Characterizing Verotoxins (Shiga Toxins) in *Escherichia coli*. *J Clin Microbiol* **1999**, 37 (2), 396–399.
- (6) Drysdale, M. *et al.* The Detection of Non-O157 *E. coli* in Food by Immunomagnetic Separation. *J Appl Microbiol*. **2004**, 97 (1), 220–224.
- (7) Fu, Z. *et al.* Rapid Detection of *Escherichia coli* O157 : H7 by Immunomagnetic Separation and Real-Time PCR. *Int J Food Microbiol* **2005**, 99 (1), 47–57.
- (8) Varela-Hernandez, J. J. *et al.* Isolation and Characterization of Shiga Toxin-Producing *Escherichia coli* O157:H7 and Non-O157 From Beef Carcasses at a Slaughter Plant in Mexico. *Int J Food Microbiol* **2007**, 113 (2), 237–241.
- (9) Fach, P. *et al.* Comparison of Different PCR Tests for Detecting Shiga Toxin-Producing *Escherichia coli* O157 and Development of an ELISA-PCR Assay for Specific Identification of the Bacteria. *J Micro Meth* **2003**, 55 (2), 383–392.
- (10) Ge, B. L. *et al.* A PCR-ELISA for Detecting Shiga Toxin-Producing *Escherichia coli*. *Microbes and infection / Institut Pasteur* **2002**, 4 (3), 285–290.
- (11) Hegde, N. V. *et al.* Rapid Detection of the Top Six Non-O157 Shiga Toxin-Producing *Escherichia coli* O Groups in Ground Beef by Flow Cytometry. *J Clin Microbiol* **2012**, 50 (6), 2137–2139.
- (12) Bai, J. *et al.* Applicability of a Multiplex PCR to Detect the Seven Major Shiga Toxin-Producing *Escherichia coli* Based on Genes That Code for Serogroup-Specific O-Antigens and Major Virulence Factors in Cattle Feces. *Foodborne Pathog Dis* **2012**, 9 (6), 541–548.
- (13) Blanco, M. *et al.* Serotypes, Virulence Genes, and Intimin Types of Shiga Toxin (Verotoxin)-Producing *Escherichia coli* Isolates From Cattle in Spain and Identification of a New Intimin Variant Gene (Eae-). *J Clin Microbiol* **2004**, 42 (2), 645–651.
- (14) Settanni, L. and Corsetti, A. The Use of Multiplex PCR to Detect and

- Differentiate Food-and Beverage-Associated Microorganisms: a Review. *J Micro Meth* **2007**.
- (15) Carroll, K. C. *et al.* Comparison of a Commercial Reversed Passive Latex Agglutination Assay to an Enzyme Immunoassay for the Detection of Shiga Toxin-Producing *Escherichia coli*. *Eur J Clin Microbiol Infect Dis* **2003**, 22 (11), 689–692.
  - (16) Gerritzen, A. *et al.* Rapid and Sensitive Detection of Shiga Toxin-Producing *Escherichia coli* Directly From Stool Samples by Real-Time PCR in Comparison to Culture, Enzyme Immunoassay and Vero Cell Cytotoxicity Assay. *Clin Lab* **2011**, 57 (11-12), 993–998.
  - (17) Orskov, I. *et al.* Serology, Chemistry, and Genetics of O and K Antigens of *Escherichia coli*. *Bacteriol Rev* **1977**, 41 (3), 667.
  - (18) Wang, L. *et al.* The Variation of O Antigens in Gram-Negative Bacteria. *Subcell Biochem* **2010**, 53, 123–152.
  - (19) Eisenstein, B. and Zaleznik, D. *Mandell, Douglas and Bennett's Principles and Practice of Infectious Diseases*, 5 ed.; 2000; pp 2294–2310.
  - (20) Griffin, P. M. and Tauxe, R. V. The Epidemiology of Infections Caused by *Escherichia coli* O157:H7, Other Enterohemorrhagic *E. coli*, and the Associated Hemolytic Uremic Syndrome. *Epidemiol Rev* **1991**, 13, 60–98.
  - (21) Johnson, R. P. *et al.* Growing Concerns and Recent Outbreaks Involving Non-O157: H7 Serotypes of Verotoxigenic *Escherichia coli*. *J Food Protect* **1996**, 59(10), 1112-1122.
  - (22) Stenutz, R. *et al.* The Structures of *Escherichia coli* O-Polysaccharide Antigens. *FEMS Microbiol Rev* **2006**, 30 (3), 382–403.
  - (23) Kaper, J. B. *et al.* Pathogenic *Escherichia coli*. *Nat Rev Microbiol* **2004**, 2 (2), 123–140.
  - (24) Nikaido, H. Molecular Basis of Bacterial Outer Membrane Permeability Revisited. *Microbiol Mol Biol Rev* **2003**, 67 (4), 593-656.
  - (25) Raetz, C. R. H. *et al.* Discovery of New Biosynthetic Pathways: the Lipid a Story. *J Lipid Res* **2008**, 50 (Supplement), S103–S108.
  - (26) Whitfield, C. Biosynthesis of Lipopolysaccharide O Antigens. *Trends Microbiol* **1995**, 3 (5), 178–185.
  - (27) Alexander, C. and Rietschel, E. T. Invited Review: Bacterial Lipopolysaccharides and Innate Immunity. *J Endotoxin Res* **2001**, 7 (3), 167–202.
  - (28) Raetz, C. R. H. and Whitfield, C. Lipopolysaccharide Endotoxins. *Annu. Rev. Biochem.* **2002**, 71, 635–700.
  - (29) Bosshart, H. and Heinzelmann, M. Targeting Bacterial Endotoxin: Two Sides of a Coin. *Ann NY Acad Sci* **2007**, 1096 (1), 1–17.
  - (30) Meredith, T. C. *et al.* Redefining the Requisite Lipopolysaccharide Structure in *Escherichia coli*. *ACS Chem. Biol.* **2006**, 1 (1), 33–42.
  - (31) Clark, N. M. *et al.* Anti-Capsular Antibodies Activate Killing of *Escherichia coli* O8:K87 by the Alternate Complement Pathway in Porcine Serum. *Vet Immunol Immunopathol* **2006**, 114 (1-2), 185–191.
  - (32) Westerman, R. B. R. *et al.* Production and Characterization of Monoclonal Antibodies Specific for the Lipopolysaccharide of *Escherichia coli* O157. *J*

- Clin Microbiol* **1997**, 35 (3), 679–684.
- (33) Paddock, Z. D. *et al.* Detection of *Escherichia coli* O104 in the Feces of Feedlot Cattle by a Multiplex PCR Assay Designed to Target Major Genetic Traits of the Virulent Hybrid Strain Responsible for the 2011 German Outbreak. *App Environ Microbiol* **2013**, 79 (11), 3522–3525.
- (34) Son, I. *et al.* Detection of Five Shiga Toxin-Producing *Escherichia coli* Genes with Multiplex PCR. *Food Microbiology* **2014**, 40, 31–40.
- (35) Jann, K. and Westphal, O. *The Virulence Factors of Escherichia coli. Reviews and Methods.*, 13 ed.; Special Publications of the Society of General Microbiology, 1985; pp 365–379.
- (36) Limjuco, G. A. *et al.* Studies on the Chemical Composition of Lipopolysaccharide From *Neisseria meningitidis* Group B. *CORD Proc* **1978**, 104 (2), 187–191.
- (37) Darveau, R. P. and Hancock, R. E. Procedure for Isolation of Bacterial Lipopolysaccharides From Both Smooth and Rough *Pseudomonas aeruginosa* and *Salmonella typhimurium* Strains. *J Bacteriol* **1983**, 155 (2), 831–838.
- (38) Jann, B.; *et al.* Heterogeneity of Lipopolysaccharides. Analysis of Polysaccharide Chain Lengths by Sodium Dodecylsulfate-Polyacrylamide Gel Electrophoresis. *Eur. J. Biochem.* **1975**, 60 (1), 239–246.
- (39) Parolis, H. *et al.* Structural Studies on the Shigella-Like *Escherichia coli* O121 O-Specific Polysaccharide. *Carbohydr Res* **1997**, 303 (3), 319–325.
- (40) Altman, E. *et al.* Structure of the O-Chain of the Lipopolysaccharide of *Haemophilus pleuropneumoniae* Serotype 1. *Biochem Cell Biol* **1986**, 64 (12), 1317–1325.
- (41) Yi, E. C. and Hackett, M. Rapid Isolation Method for Lipopolysaccharide and Lipid a From Gram-Negative Bacteria. *Analyst* **2000**, 125 (4), 651–656.
- (42) Davies, R. L. *et al.* Evaluation of Different Methods for the Detection of Outer Membrane Proteins and Lipopolysaccharides of *Pasteurella haemolytica* by Immunoblotting. *J Immunol Methods* **1994**, 167 (1-2), 35–45.
- (43) Kim, J. S. *et al.* Separation of Bacterial Capsular and Lipopolysaccharides by Preparative Electrophoresis. *Glycobiology* **1996**, 6 (4), 433–437.
- (44) Lesse, A. J. *et al.* Increased Resolution of Lipopolysaccharides and Lipooligosaccharides Utilizing Tricine-Sodium Dodecyl Sulfate-Polyacrylamide Gel Electrophoresis. *J Immunol Methods* **1990**, 126(1),109
- (45) Palva, E. T. and Mäkelä, P. H. Lipopolysaccharide Heterogeneity in *Salmonella typhimurium* Analyzed by Sodium Dodecyl Sulfate / Polyacrylamide Gel Electrophoresis. *Eur J Biochem* **1980**, 107 (1), 137–143.
- (46) Sutcliffe, I. C. Characterisation of a Lipomannan Lipoglycan From the Mycolic Acid Containing Actinomycete *Dietzia maris*. *Antonie Van Leeuwenhoek* **2000**, 78 (2), 195–201.
- (47) Laemmli, U. K. U. Cleavage of Structural Proteins During the Assembly of the Head of Bacteriophage T4. *Nature* **1970**, 227 (5259), 680–685.
- (48) BioRad. *A Guide to Polyacrylamide Gel Electrophoresis and Detection Part I : Theory and Product Selection Part II : Methods Part III : Troubleshooting Part IV : Appendices*; Bio Rad Laboratories Incorporated.

- (49) Zhu, Z.-X. *et al.* Negative Staining of Lipopolysaccharides on Polyacrylamide Gels by Using Eosin B. *Anal Biochem* **2012**, 426 (1), 1–3.
- (50) Bjerrum, O. J. and Schafer-Nielsen, C. Buffer Systems and Transfer Parameters for Semidry Electroblothing with a Horizontal Apparatus. *Electrophoresis* **1986**, 86, 315–327.
- (51) Gamian, A. *et al.* Structure of the Sialic Acid-Containing *Escherichia coli* O104 O-Specific Polysaccharide and Its Linkage to the Core Region in Lipopolysaccharide. *Carbohydr Res* **1992**, 236, 195–208.
- (52) Rezaei, S. *et al.* Extraction, Purification and Characterization of Lipopolysaccharide From *Escherichia coli* and Salmonella Typhi. *Avicenna J Med Biotechnol* **2011**, 3 (1), 3–9.
- (53) Muniesa, M. *et al.* Shiga Toxin-Producing *Escherichia coli* O104: H4: a New Challenge for Microbiology. *App Environ Microbiol* **2012**, 78 (12), 4065-4073.
- (54) Pyle, S. W. and Schill, W. B. Rapid Serological Analysis of Bacterial Lipopolysaccharides by Electrotransfer to Nitrocellulose. *J Immunol Methods* **1985**, 85 (2), 371–382.
- (55) Mukundan, H. *et al.* Rapid Detection of Mycobacterium Tuberculosis Biomarkers in a Sandwich Immunoassay Format Using a Waveguide-Based Optical Biosensor. *Tuberculosis (Edinburgh, Scotland)* **2012**, 92 (5), 407–416.
- (56) Sakamuri, R. M. *et al.* Detection of Stealthy Small Amphiphilic Biomarkers. *J Microbiol Meth* **2014**, 103, 112–117.

**Chapter 4.**  
**O Antigen Monoclonal Antibodies For Shiga Toxin-Producing *Escherichia coli***  
**Serogroups O26, O45, O103, O111, O121, and O145**

Loreen R. Stromberg<sup>[1,2,3]</sup>, Heather M. Mendez<sup>[1,2,3]</sup>, Steven W. Graves<sup>[1,3]</sup>, Rodney A. Moxley<sup>[4]</sup>, Harshini Mukundan<sup>[1,2,3]\*</sup>

<sup>1</sup>Center for Biomedical Engineering, University of New Mexico, Albuquerque, New Mexico, United States, 87131

<sup>2</sup>Physical Chemistry and Applied Spectroscopy, Los Alamos National Laboratory, Los Alamos, New Mexico, United States 87545

<sup>3</sup>The New Mexico Consortium, Los Alamos, New Mexico, United States, 87544

<sup>4</sup>School of Veterinary Medicine and Biomedical Sciences, University of Nebraska-Lincoln, Lincoln, Nebraska, United States, 68583

\*Corresponding Author: Harshini Mukundan, 505-606-2122

*In preparation. Author contributions to this work are described in Chapter 2.*

#### **4.1 Abstract**

Shiga toxin-producing *Escherichia coli* (STEC) is an important human pathogen and foodborne contaminant. In recent years, there has been an increase in the occurrence of some serogroups of STEC, namely O26, O45, O103, O111, O121 and O145 in food products. Identification of the O antigens of bacterial lipopolysaccharides (LPS) is a critical part of serotype-specific detection, and an important element in disease control. However, many of the available antibodies for these O antigens are cross-reactive not only with other bacterial species, but also other serogroups. The goal of this work is to create highly specific antibodies that target STEC O-ag thereby allowing for discriminatory detection of serotypes. Using specific LPS extracts, O antigens and lipid A components, we have developed and characterized monoclonal antibodies. Immunized mice were used for pre-selection, followed by subsequent selection of hybridoma cell lines. We also present a new ELISA method for specifically screening LPS O antigens, and demonstrate serogroup specific detection of LPS using membrane insertion assays. The generation of a pool of highly specific antibodies against the O serogroups of non-O157 STEC is an important tool for developing detection assays for monitoring the health of the food chain. Herein we present the outcome of these screenings and assays for specific antibodies selected for STEC serogroups.

#### **4.2 Introduction**

Shiga toxin-producing *Escherichia coli* (STEC) are virulent strains of enterohemorrhagic *E. coli*. STEC are a major health concern, as they are foodborne pathogens, which upon infection can result in severe symptoms, such as diarrhea, hemorrhagic colitis, and hemolytic uremic syndrome.<sup>1</sup> One of the most frequent strains of STEC that causes disease from the serogroup O157.<sup>2</sup> However, in recent years the increasing emergence of several other pathogenic serotypes of STEC has been recognized as a threat to the food supply and human health.<sup>3,4</sup> As a result, the United States Department of Agriculture's Food Safety and Inspection Service (USDA-FSIS) declared mandatory screening for serogroups O26, O45, O103, O111, O121, and O145.<sup>5</sup>

Bacterial serotypes are determined by the chemical identity of the surface antigens, O polysaccharide (O-ag), capsular polysaccharide, and flagella.<sup>6,7</sup> Lipopolysaccharide (LPS) is the primary component of the outer leaflet on the outer membrane of Gram-negative pathogens.<sup>8-10</sup> The molecule itself is amphipathic in nature and consists of a hydrophobic lipid A group, a core polysaccharide, and the O-ag. The O-ag is considered hypervariable in nature, and is the component of LPS that is used to determine the serogroup of *E. coli* isolates.<sup>11,12</sup> Structurally, the O-ag is made up of subunit repeats of glycosyl residues, which are typically 1-7 oligosaccharide units in length. The variability of the O-ag stems from both the composition of the oligosaccharide subunits, and the degree of branching within the polysaccharide chain. Identity of the O-ag is important, as serogroup is a key indicator of virulence,<sup>13</sup> and STEC have a wide range of pathogenicity and virulence. To date, 187 unique O-ag have been identified for *E. coli*,<sup>14</sup> many of which have pathogenic phenotypes. The lipid A component of LPS is highly conserved within a species of bacteria<sup>8</sup> and several polyclonal antibodies have high affinity for the epitopes on lipid A, which results in many of the cross-reactivity issues seen in serotyping assays.<sup>15,16</sup> The core polysaccharide is also conserved in nature, but subject to variability due to substitutions of sugar groups and the possibility for chemical functionalization of those moieties.<sup>17,18</sup>

The development of antibodies against LPS, and its specific epitopes has proven a useful tool for investigating LPS structures, bacterial virulence, and in the development of detection assays.<sup>16</sup> Monoclonal antibodies in general have also been shown to be highly effective tools for disease treatment and detection,<sup>19</sup> but developing specific antibodies to the sugar epitopes of O-ag has unique challenges.<sup>16</sup> Antibodies for LPS are typically raised and screened against the whole antigen, resulting in a variety of clones. Another problem is the assays with which we screen resulting antibodies. Screening is performed using ELISAs, which historically have suffered from poor and inconsistent binding of the lipoglycan antigens to microtitre plates,<sup>20-24</sup> because the polystyrene is not optimized for the binding of amphiphiles and micelles. In fact, many researchers use the same methods for LPS as those used for proteins, which disregards the amphipathic

chemistry of LPS. For example, immunoblotting combined with sodium dodecyl sulfate (SDS) polyacrylamide gel electrophoresis, is used to determine the antigenicity of antibody clones.<sup>25</sup> While it is assumed that binding of the antibodies to the ladder pattern of the blots is indicative of specificity for the O-ag, LPS antigens are highly stable, and large intact antigens will remain higher in the gel in the O-ag region, which results in antibodies binding to that area. These issues can be circumvented by using functionalized ELISAs to facilitate physiological binding of LPS. Additionally, by implementing methods such as immunoblotting against all parts of LPS (whole antigen, O-ag, and lipid A), the resulting antibodies will have higher specificity towards the target antigen.

We have used a long-term immunization protocol with mice and whole heat-killed bacterial cells to develop O-ag specific monoclonal antibodies against six non-O157 STEC strains. To screen these antibodies, we have used standard sandwich ELISAs and immunoblotting against whole LPS, O-ag, and lipid A. Resulting clones will be tested in complex matrices to ensure assay performance. For additional screening and implementation into detection assays, we have tested multiple LPS antigens with membrane insertion assays and commercial antibodies. Lastly, we have developed protocols for functionalization of ELISA plates with serum proteins to facilitate physiological presentation of O-ag epitopes to antibodies. The development of these highly specific antibodies is a critical tool to facilitate detection and discrimination of non-O157 STEC pathogens in current detection platforms.

## **4.3 Materials and Methods**

### *4.3.1 Bacterial strains and serum screening*

Strains for antibody production, DEC10B [O26:H11], B8227-C8 [O45:H2], MT#80 [O103:H2], TY-2482 [O104:H4], 0201 9611 [O111:H11], MDCH-4 [O113:H21], DA-37 [O121:H21], and GS G5578620 [O145:NM] were grown in lysogeny broth (LB) for 24 h, then harvested and suspended in saline at a concentration of  $10^6$  CFU/mL. Cultures were heat inactivated for 2 hours at 100 °C on a heat block. Aliquots were centrifuged and the majority of the supernatant removed, then stored at -80 °C. To ensure inactivation of the dead cells, an aliquot

of the cells were inoculated into LB broth and fluid thiglycollate media and incubated at 37 °C, cultures were checked for any growth at 24 h and 48 h. LPS O157:H7 (List Biological Labs), and LPS O111:B4 (Sigma Aldrich) were purchased as control groups. LPS from the same strains of bacteria were prepared by hot phenol extraction, separated into their O-ag and lipid A portions, then tested for antigen activity as we have previously described.<sup>15</sup> Remaining strains not used for antibody development were used for assessing cross-reactivity of resulting antibodies.

Mice from strains BALB/c, Swiss Webster, and C57BL/6 were housed and inoculated at the Dana Farber Cancer Institute-Monoclonal Antibody Core Facility (DFCI-MACF) in accordance with the Institutional Animal Care and Use Committee guidelines. A mouse from each strain was bled prior to inoculation with heat-killed bacterial cells<sup>26,27</sup> and then bled again 35 days post-inoculum. Pre- and post-inoculated serum were shipped to The University of New Mexico, and screened using an indirect sandwich ELISA in which polyclonal anti-*E. coli* O157 antibody (pAb O157, LifeSpan Biosciences) was used as the capture antibody and goat anti-mouse horseradish peroxidase (HRP) labeled antibody (Pierce) was used as the reporter. Capture antibody was diluted 1:2000 in phosphate buffered saline (PBS, Sigma Aldrich) and incubated overnight, at 4 °C, in Nunc™ MaxiSorp™ 96-well plates. Wells were subsequently blocked for 1 h at room temperature (R/T) using 1x Tris-buffered saline (TBS, BioRad) + 0.05% Tween-20 (Sigma) + 0.5% bovine serum albumin (BSA, Sigma). LPS was prepared first by sonicating stock solutions (5 mg/mL in PBS) for 15 min in a water bath, then diluting to 50 µg/mL in blocking buffer, and sonicating an additional 15 min. LPS (whole antigen) solution was added to the microwells, covered, and incubated for 2 h at R/T. Wells were washed 3 times with 1x TBS/0.5% Tween-20. Pre- and post-inoculum mouse serum was diluted from 1:500 down to 1:64000 in blocking buffer, and then applied to the respective wells in triplicate, covered and incubated at R/T for 1.5 h. Wells were washed 3 times and then a 1:4000 solution of goat anti-mouse HRP diluted in 1x PBS, was applied to the wells and incubated for 1 h at R/T. Wells were washed 4 times, and 100 µL of 1-Step™ Ultra TMB-ELISA substrate (Pierce) was added to each well and incubated for 40 min at 37 °C to aid in color development. Development was stopped by adding

100  $\mu\text{L}$  of 2.0 M  $\text{H}_2\text{SO}_4$ , and the absorbance was measured at 450 nm on a SpectraMax M5 microplate reader (Molecular Devices). Data were averaged and plotted as absorbance for each value of serum dilution. The axes of the graphs are displayed on the same scale to facilitate the visual evaluation of response over time.

In addition to the evaluation discussed above, pre- and post-inoculated mouse serums were also screened using immunoblots to determine cross reactivity between O-ag and lipid A groups. Whole LPS, O-ag, and lipid A from control LPS groups O111:B4 and O157:H7 were blotted onto nitrocellulose (0.45  $\mu\text{m}$ , BioRad), 1  $\mu\text{L}$  at a time, allowed to dry, and an additional 1  $\mu\text{L}$  was reapplied to the same area. The target antigen for each LPS subtype was also blotted. Additional controls were 5% BSA, and 1x PBS. Membranes were blocked for 1 h at R/T using 2% BSA and then rinsed 3 times first with 0.1% Tween-20/PBS and then another 3 times with 1x PBS. Each rinse lasted for 5 min on an orbital shaker. Serum was diluted 1:500 in ELISA blocking buffer, and incubated with membranes for 4 h at R/T on an orbital shaker. Blots were rinsed again (3 times each with both buffers) and a 1:4000 dilution of goat-anti mouse alkaline phosphatase (AP, Pierce) in 1x PBS was applied and incubated for 1 h, R/T, on an orbital shaker. Nitrocellulose was again rinsed and 1-Step™ NBT-BCIP (Pierce) was applied to develop the blots. After development, blots were rinsed 2 times each with distilled water then laid on a paper towel and allowed to dry. Images, for the most part, were acquired using an HP Envy 100 scanner, and brightness and contrast were optimized. Immunoblot results were compared to ELISA results to determine if mice should be re-immunized or used to make hybridomas. In general, mice required 2-3 rounds of immunization before developing a strong response.

#### *4.3.2 Hybridoma production and screening*

Mice that developed a strong immune response to the LPS antigens were selected for hybridoma development. All hybridomas were developed and cultured at the DFCI-MACF using their previously established proprietary methods. Resulting clone supernatants were sent to us for screening. In general, culture supernatants were screened using the indirect ELISA method described in *Section 4.5.1*, with the

exception that undiluted culture supernatants were used in the place of mouse serum, and we also ran an additional background control of 1 mg/mL beef lysate (prepared as previously described<sup>28,29</sup>) to assess any cross reactivity that the resultant antibodies may have with the LPS subtypes present in beef lysates. Hybridomas were sub-cloned until a satisfactory activity response was obtained.

#### 4.3.3 Developing assays to test antibody specificity

To develop ELISAs capable of improved O-ag specific detection, we adapted protocols from Heumann *et al.*<sup>26</sup> and Vreugdenhil *et al.*<sup>30</sup> to complex LPS with serum lipoproteins to facilitate presentation of physiologically relevant LPS O-ag to antibodies. The surface of microtitre plates was functionalized with 50% mouse serum (Sigma Aldrich), in order to capture LPS with the serum lipoproteins. Mouse serum was diluted 1:2 with PBS, and incubated overnight (4 °C) in Nunc™ MaxiSorp™ 96-well plates. Wells were blocked for 1 hr, R/T, using 1x TBS/0.05% Tween/0.5% BSA. LPS O104, O26, and O45 (50 µg/mL) were prepared in blocking buffer as described in *Section 4.3.1*, and added to the microwells (R/T for 2 hr). Plates were washed (3 x) and then incubated with their respective pAb O104, mAb O26, or mAb O45 (Abraxis, 1:2000 in 1x PBS, R/T, 1.5 hrs). The assays were then carried out as described in *Section 4.3.1*. To further evaluate functionalization with serum proteins, and facilitate the use of anti-mouse reporter antibodies, we also repeated the experiment using donkey serum as the capture surface and goat anti-mouse HRP as the secondary antibody.

LPS membrane insertion assays were carried out as previously described,<sup>29</sup> to assess the performance of subtypes of LPS (O26, O45, O103, O111, O145) with pAb O157 and LPS O26 with its respective mAb O26 (Abraxis). Antibodies were labeled with Alexa Fluor® 647 labeling kits (af647, Molecular Probes) per manufacturer's instructions, and pre- and post-labeled antibodies were immunoblotted to ensure reactivity to the antigens. Waveguides were cleaned and bilayers prepared as previously described<sup>28,31-33</sup> using 1,2-Dioleoyl-*sn*-glycero-3-phosphocholine (DOPC, Avanti Polar Lipids) and 1,2-dioleoyl-*sn*-glycero-3-phosphoethanolamine-N-(cap biotinyl) (sodium salt) (cap-biotin, Avanti Polar Lipids).

Flow cells were blocked for 1 hr with 2% (w/v) BSA, then rinsed with 0.5% BSA/PBS prior to running an assay.

Incident light (635 nm) was coupled into the waveguide using a diffraction grating, and the response signal was adjusted for power and peak intensity using a spectrometer (USB2000, Ocean Optics) interfaced with the instrument and an optical power meter (Thor Labs).<sup>28,29,32,33</sup> The background signal of the lipid bilayer and BSA block was recorded after which the flow cell was incubated (90 min) with 25 nM of reporter antibody (either pAb O157-af647 or mAb O26-af647) to determine the amount of non-specific binding (NSB) between the antibody and the lipid bilayer. The flow cell was rinsed with wash buffer (0.5% BSA/PBS) after all incubations. After the NSB measurement, the flow cell was photobleached to the background signal level by opening the shutter.<sup>29</sup> This facilitates accurate measurement of the specific binding of the antibody to LPS. 25 µg/mL of LPS was incubated for 2 hr, and the signal recorded. Subsequently, reporter antibody was incubated for 90 min and rinsed, and the specific binding signal of the antibody was recorded. The average of the background spectra was subtracted from both the NSB and specific binding signals. Data was plotted as an average of the three replicates.

## **4.4 Results and discussion**

### *4.4.1 Serum screening and immunoblotting*

**STEC O45.** Three mice, one from each strain were immunized with dead bacterial cells. Serum was screened after each period of immunization to assess antibody response. In general ELISA responses were often poor, with high standard deviations, likely because of the configuration of antigen epitopes. The highest response for the O45 serogroup mice was recorded in the C57BL/6 mouse after two inoculations (**Figure 4.1**). This suggested that this mouse had developed better immunity over time. However, a comparison of the ELISA vs. immunoblot results between the two serum screens, (**Table 4.1**) showed significant discrepancy. Initially, the immunoblots showed an antibody response to at least one of the antigens from each of the serogroups in both the pre- and post-inoculated serum. However, this response diminished in the immunoblots by the next serum screen,

which was in sharp contrast to the ELISA. This is one of the main challenges in developing antibodies to sugar epitopes. The relative binding affinity of the antigens (whole LPS, O-ag, and lipid A) to nitrocellulose vs. polystyrene (ELISA plate) is unclear, and can affect the outcome of the assay. Further, antibodies were developed in an animal, wherein the presentation of LPS is in a distinctively different conformation, further affects the results of the assay. More importantly, this casts a question on the nature of the assay that should be used for antibody selection for amphiphilic antigens.

Initially we used an immunoblotting protocol, which required 4 h of incubation with the mouse serum at an elevated temperature (37 °C). After a few iterations of immunoblots, we discovered that the proteins in the mouse serum were competitively displacing the BSA block on the membranes, which resulted in high background staining of the membrane (**Figure A3.4**), making the blots difficult to interpret. To address this, the protocol was altered in two ways, first by performing the incubation at room temperature, and also by diluting the serum in the same blocking buffer used in the ELISA assays. The results of this modification are most evident when comparing the immunoblots in the O26 serogroups, which can be seen in the supplementary **Figure A3.8**.

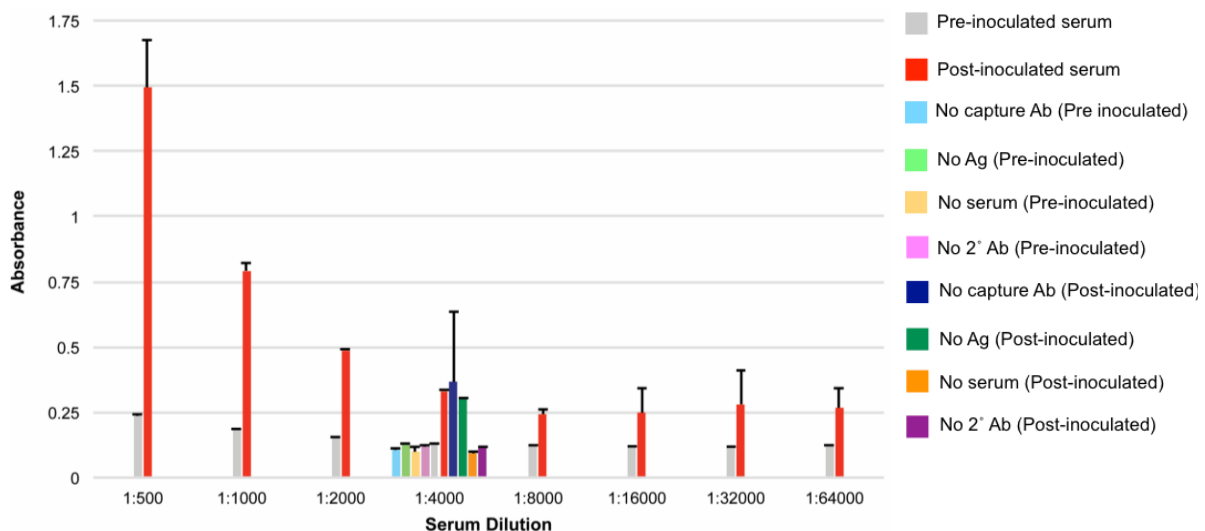


**Figure 4.1. ELISA results from a C57BL/6 mouse immunized with O45 bacterial antigens.** Due to the post immune response this mouse was selected for hybridoma development.

**Table 4.1. Immunoblot summary analysis of C57BL/6 mouse inoculated with O45 bacterial antigens.**

C57BL/6 mouse		Pre-Inoculated			Post-Inoculated		
LPS subtype		Whole LPS	O-ag	Lipid A	Whole LPS	O-ag	Lipid A
July 16, 2014	O111:B4	-	+	-	+	+	+
	O157	+	+	-	+	+	+
	O45	+	+	-	++	+	-
	1x PBS/5% BSA	-	-	-	-	-	-
September 04, 2014	O111:B4	-	-	-	-	-	-
	O157	-	-	-	-	++	++
	O45	+	-	-	-	-	-
	1x PBS/5% BSA	-	-	-	-	-	-

No response ' - ', Weak response ' + ', Moderate response ' ++ ', Intense response = ' +++ ', blue highlighted regions indicate the target serogroup.

The C57BL/6 mouse was selected for hybridoma development. The initial cell fusion resulted in 25 clones that were screened for activity. The signal to noise ratio for these clones is plotted in **Figure 4.2A**, where the signal is the activity of the antibody as a measure of absorbance in the ELISA assay, and the noise is the non-specific activity of the supernatant measured against a ground beef tissue lysate. Three clones (1C7, 2B2, and 1D5) were selected for subcloning from the first round of screening. After two procedures, (activity was monitored in between) we obtained a subclone (2BB.E10.D3) with higher activity than the others (**Figure 4.2B**).

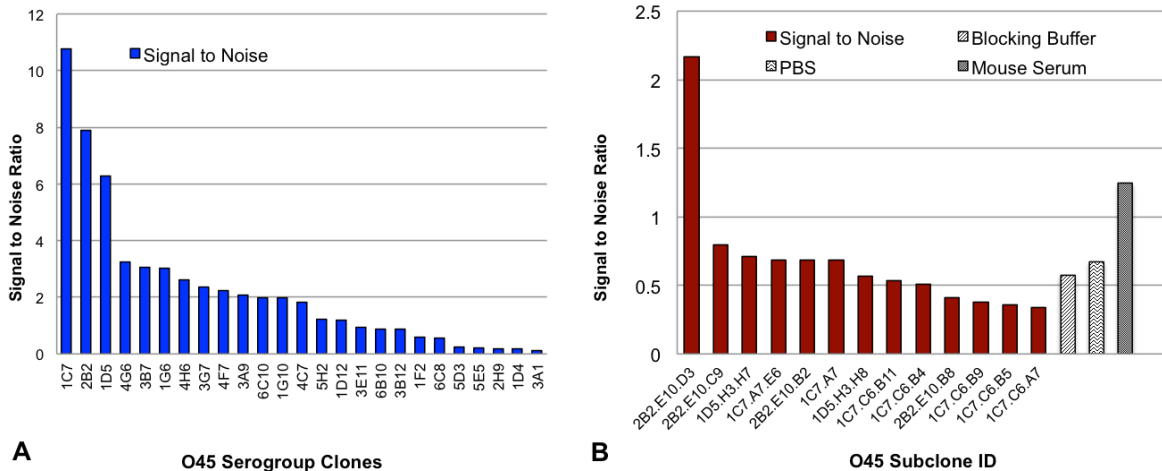


**Figure 4.2. Signal to noise ratios of O45 hybridomas.** A. First round of clone screening produced 25 clones. B. Activity of subclones produced from original O45 hybridomas.

Clone 2B2.E10.D3 was selected for antibody production, the line expanded, then frozen down in aliquots. 1.0 L of culture supernatant was purified with protein A purification techniques. However, when the purification resulted in less than 1.0 mg of antibody, the resulting product was tested and discovered to be an immunoglobulin M (IgM) instead of an immunoglobulin G (IgG). Clones that produce anti-LPS IgM's in response to a long term immunization protocol have been previously documented.<sup>34</sup> However, IgM's are difficult to purify due to their pH sensitivity, larger molecular weight (IgG ~ 150 kDa vs. pentameric IgM ~ 960 kDa), and tendency to denature during purification.<sup>35</sup> Another frozen stock of cells was expanded, and adapted to be grown in serum free media to facilitate size exclusion purification, without having to additionally purify the large proteins found in serum-supplemented media. Resulting antibodies will be tested for cross-reactivity using ELISAs and multiple strains of bacterial cells.

**STEC O26, O103, O111, O121 and O145.** For serogroups O26, O103, and O111, the mice were on the same immunization schedule. The BALB/c mice consistently exhibited the best immune response as compared to C57BL/6 and Swiss Webster mice in these serogroups (**Figure A3.9, A3.11, A3.15, A3.17, A3.21, and A3.23**). The results for the ELISA serum screens using the BALB/c mice in both the O26 and O111 serogroups is seen in **Figure 4.3**. After the second round of inoculation, these mice were sacrificed for hbridoma development. The BALB/c mouse in the O103 serogroup (**Figure 4.3B**) was immunized four times prior to being used for making antibodies. The immunoblots for these mice (**Table 4.2**) showed good correspondence with the ELISAs as all of the post-inoculated serums demonstrated moderate to intense response as compared to the pre-inoculated serums. We relied heavily on the immunoblot response for the both the O103 and O111 serogroups as the O-ag promptly developed within 1 minute of adding substrate, despite lower responses in the ELISAs. Although some of the mice showed good response to the antigens, no viable clones were produced from any of the mice. C57BL/6 and Swiss Webster mice are continuing the long term immunization protocol, and serum will be screened when available. Additionally, we have begun immunization of rats for each bacterial serogroup as the immune

response can be different between animals. For serogroups O121 and O145, all three mice have each been inoculated twice and screened. Mice in these groups have exhibited a low antibody response even after the second round, and were subjected to a third immunization. All ELISAs and immunoblot results to date for this ongoing effort are reported in **Appendix 3, Figures A3.25-A3.35**.

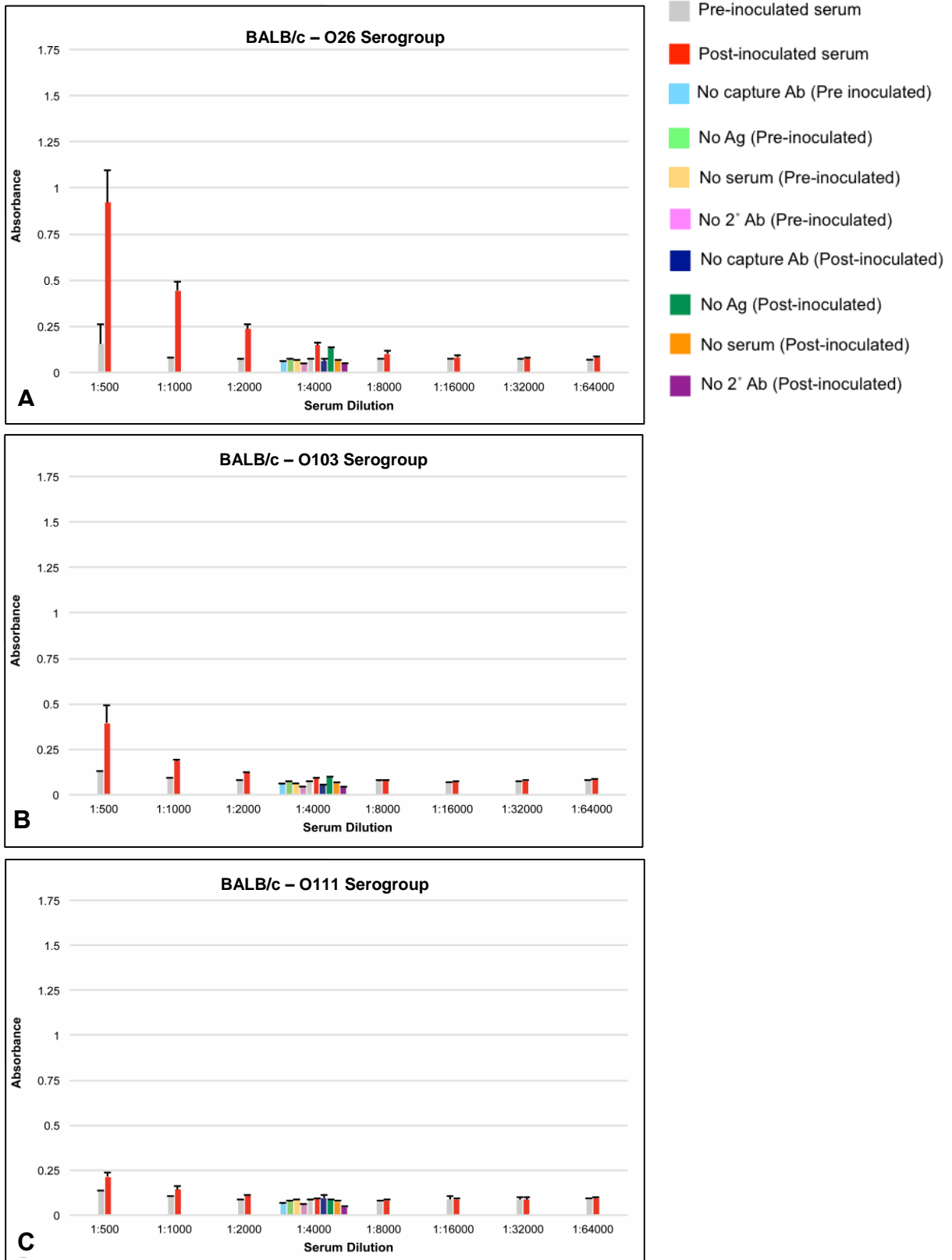


**Figure 4.3. ELISA results for serum screens from BALB/c mice. A-C. Screens for O26, O103, and O111 serogroups, respectively.**

**Table 4.2. Immunoblot summary analysis of BALB/c mice inoculated with O26, O103, and O111 bacterial antigens.**

BALB/c mouse		Pre-Inoculated			Post-Inoculated		
LPS subtype		Whole LPS	O-ag	Lipid A	Whole LPS	O-ag	Lipid A
Sept. 02, 2015	O111:B4	-	-	-	-	-	+
	O157	-	+	NA	+	+	NA
	O26	-	+	+	++	+++	++
	1x PBS/5% BSA	-	-	-	-	-	-
Sept. 02, 2015	O111:B4	-	-	NA	+	-	NA
	O157	-	-	NA	++	+	NA
	O103	-	+	-	++	+++	+
	1x PBS/5% BSA	-	-	-	-	-	-
Sept. 02, 2015	O111:B4	-	-	-	+	-	NA
	O157	-	-	NA	+	++	NA
	O111	-	+	+	+	++	+++
	1x PBS/5% BSA	-	-	-	-	-	-

No response ' - ', Weak response ' + ', Moderate response ' ++ ', Intense response = ' +++ ', NA = control antigens were not available for testing. Blue highlighted regions indicate the target serogroup.

#### 4.4.2 Assays for testing antibody specificity

We examined methods to improve upon the physiological presentation of LPS O-ag to detection antibodies in the ELISA format. By coating the surfaces of ELISA plates with serum lipoproteins, we were able to eliminate the need for costly capture antibodies. The lipid A group of LPS associates with serum lipoproteins<sup>30,36,37</sup> and therefore by using serum to coat ELISA plates we take advantage of better coating of the polystyrene surfaces with the serum proteins,<sup>26</sup> and the sequestering of the lipid A group into the hydrophobic pockets of serum proteins. In the serum screening assays we used a cross-reactive polyclonal antibody as a capture molecule. Using serum lipoproteins offers multiple advantages as compared to capture antibodies because serum is more cost effective, provides an additional blocking effect against nonspecific binding of reporter antibodies, and binds the lipid A molecule of LPS to present LPS O-ag in a conformationally relevant manner. By complexing LPS with lipoproteins, it also results in stability of LPS conformation by preventing disparate micelle formations in aqueous matrices. We saw excellent signal to noise ratios in the assays we tested with mouse serum and LPS O104 (**Figure 3.36 A**), but also saw decreased standard deviations when we used donkey serum instead of mouse

serum (**Figure 3.36 B**). Using donkey serum as compared to mouse serum provides a better detection platform for testing of murine monoclonal antibodies as the anti-mouse reporter antibody does not cross-react with the proteins in donkey serum. Additionally, serum serves a secondary role by providing an effective blocking step to the plate surface which minimizes background noise from the nonspecific binding of the secondary antibody.

Membrane insertion assays for LPS O157 have previously been developed and tested in beef lysates using a waveguide-based optical biosensor.<sup>29</sup> Membrane insertion uses a waveguide functionalized with lipid bilayers to facilitate the partitioning of the hydrophobic lipid A into the lipid bilayer, which leaves the O-ag exposed in the aqueous matrix. This method is advantageous as it facilitates detection of the O-ag while minimizing the availability of the lipid A epitopes. We tested multiple serogroups of LPS using membrane insertion and the same pAb O157 used in the ELISA capture assays. The average of the assay replicates for all serogroups, except LPS O111:B4, demonstrated signal to noise ratios from 2-10 (**Figure 4.4**). Despite these promising results, the signal responses for many of the LPS subtypes are quite close, therefore highlighting the need for more specific antibodies. Previously we have shown that implementing a specific polyclonal antibody in these assays can increase the signal by more than a factor of two,<sup>29</sup> and so we wanted to test a highly cross-reactive monoclonal antibody to see if we could increase the signal. Monoclonal anti-LPS O26 has been demonstrated to exhibit broad cross-reactivity to many of the LPS subtypes,<sup>15</sup> so we selected this as a test antigen. However, when we compared the signal of LPS O26 with the pAb O157 versus the mAb O26, (**Figure 4.5**) we saw absolutely no difference in signal between the nonspecific binding of the mAb O26 and the specific binding. This is a good indication that mAb O26 binds an epitope, such as lipid A, that does not present in membrane insertion. To confirm this result, we tested LPS O26 with the mAb O26 in the lipoprotein capture ELISA assays, and determined that the specific binding could not be discriminated from that of the no antigen control (**Figure A3.37**). This serves as further evidence that antibodies specific to the O-ag epitope are required to facilitate discriminatory detection of STEC antigens.

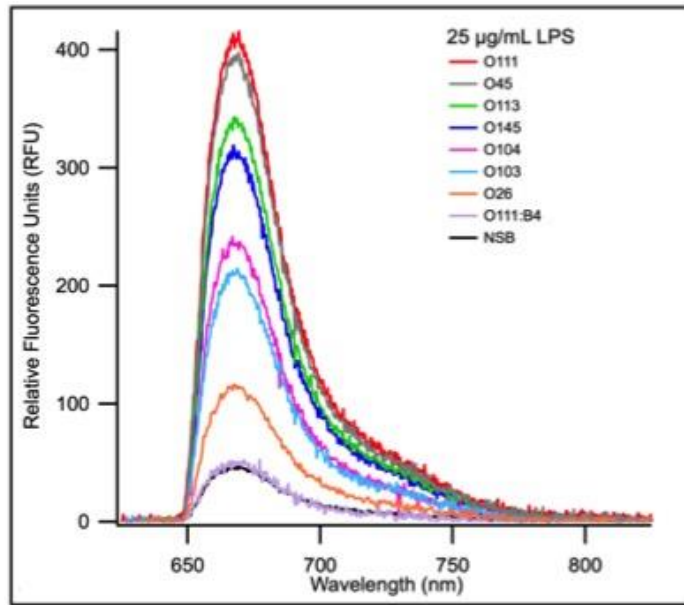


**Figure 4.4. Serogroup specific LPS membrane insertion assays.** A. Membrane insertion assays of multiple serogroups of LPS detected with the cross reactive pAb O157-af647. Serogroups are indicated by colored lines, and NSB (black line) is the nonspecific binding of the pAb O157-af647.

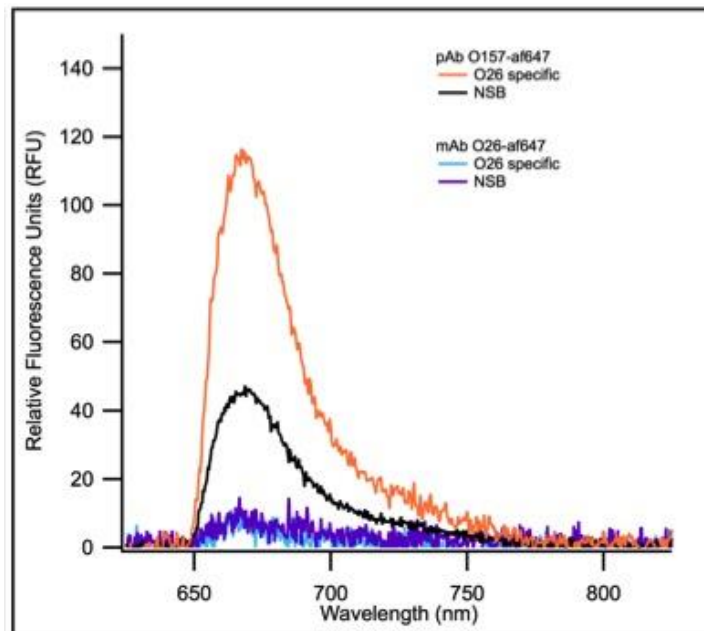


**Figure 4.5. Performance of mAb O26 for O-ag targeted detection.** Detection of LPS O26 with both pAb O157-af647 is also seen in (4.4), but here we demonstrate the lack of response using the 'specific' mAb O26-af647. Orange and black lines are the specific and NSB of the pAb O157-af647, while blue and purple represent the signals of the mAb O26-af647.

#### **4.5 Conclusion**

The importance of detecting and typing STEC pathogens in the food supply cannot be overstated. Currently, the primary method for serogroup identification relies on commercial antibodies. Many of the available antibodies for non-O157 STEC are highly cross-reactive and expensive. We have worked to develop monoclonal antibodies against the O-ag of six serogroups of STEC using ELISAs and immunoblotting to screen the clones. We have tested the detection of LPS serogroups using membrane insertion and commercial antibodies to demonstrate both assay feasibility and areas of improvement for existing monoclonal antibodies.

#### **4.6 Future directions**

Due to the lack of immune response to some of the antigens in mice, we have opted to begin immunization of a rat for each of the remaining antigens (O25, O103, O111, O121, and O145). This process is already underway. The inoculation and boosting of mice will continue, until a satisfactory antibody with desired specificity results for each LPS serogroup. The methods for implementation of this are already in place. Once antibodies have been purified, they will need to be tested for specificity in assay platforms using the established methods described in *Sections 4.3.3. and 4.2.2* Testing for cross reactivity also needs to be performed, both in complex matrices like beef lysate, and against multiple bacterial species and antigens. This will provide more information about antibody specificity, and validate performance in applicable assay platforms. An ideal application of these antibodies would be to affix them to latex beads to facilitate rapid identification of serogroup with latex agglutination tests. To address the cost associated problems with using antibodies, these antibodies should be made available to other STEC collaborators by depositing them in a repository, such as BEI Resources.

#### **4.7 Acknowledgments**

The authors would like to thank several people who helped further this research. Thank you to Heather Mendez for assistance with serum screens and ELISA development. Thank you to Dr. Zach Stromberg for growth of bacterial stains

and re-purification of LPS O121. Thank you to Drs Aneesa Noormohamed and Shailja Jakar for their technical assistance on days there was too much work for one person to do. Thank you to Dr. Mohan Brahmandam for assistance with protocol development. Thank you to the team of the Monoclonal Antibody Core Facility at the Dana Farber Cancer Institute (Drs Edward Greenfield and Craig Bencsics) for developing these antibodies. Thanks to Dr. Basil Swanson, Karen Grace and W. Kevin Grace, of LANL who developed the waveguide biosensor platform. Thanks to Drs. Swanson, Chaudhary, and Mukundan for conception, design, and testing of the membrane insertion assay. This work was supported by Agriculture and Food Research Initiative Competitive Grant No. 2012-68003-30155 from the United States Department of Agriculture's National Institute of Food and Agriculture.

#### 4.8 References

- (1) Griffin, P.M. and Tauxe, R.V. The Epidemiology of Infections Caused by *Escherichia coli* O157: H7, Other Enterohemorrhagic *E. coli*, and the Associated Hemolytic Uremic Syndrome. *Epidemiol Rev* **1991**, 13(1), 60–98.
- (2) Heiman, K.E. *et al.* *Escherichia coli* O157 Outbreaks in the United States, 2003–2012. *Emerg Infect Dis* **2015**, 21(8), 1293.
- (3) Gould, L. H. *et al.* Emerging Infections Program Foodnet Working Group. Increased Recognition of Non-O157 Shiga Toxin-Producing *Escherichia Coli* Infections in the United States During 2000-2010: Epidemiologic Features and Comparison with *E. Coli* O157 Infections. *Foodborne Pathog. Dis.* **2013**, 10 (5), 453–460.
- (4) Stromberg, Z. R. *et al.* Prevalence of Enterohemorrhagic *Escherichia Coli* O26, O45, O103, O111, O121, O145, and O157 on Hides and Preintervention Carcass Surfaces of Feedlot Cattle at Harvest. *Foodborne Pathog. Dis.* **2015**, 12 (7), 631–638.
- (5) United States Department of Agriculture. Rules and Regulations; Docket No. FSIS–2010–0023, FSIS, 2012; 77, 31975–31981.
- (6) Orskov, I. *et al.* Serology, Chemistry, and Genetics of O and K Antigens of *Escherichia Coli*. *Bacteriological reviews* **1977**, 41 (3), 667.
- (7) Wang, X. and Quinn, P. J. Endotoxins: Lipopolysaccharides of Gram-Negative Bacteria. In *Endotoxins: Structure, Function and Recognition; Subcellular Biochemistry*; Springer Netherlands: Dordrecht, 2010; Vol. 53, pp 3–25.
- (8) Raetz, C. R. H. *et al.* Discovery of New Biosynthetic Pathways: the Lipid a Story. *The Journal of Lipid Research* **2008**, 50 (Supplement), S103–S108.
- (9) Nikaido, H. Molecular Basis of Bacterial Outer Membrane Permeability Revisited. **2003**, 67 (4), 593–.
- (10) Whitfield, C. Biosynthesis of Lipopolysaccharide O Antigens. *Trends in Microbiology* **1995**, 3 (5), 178–185.
- (11) DebRoy, C. *et al.* Comparison of O-Antigen Gene Clusters of All O-Serogroups of *Escherichia Coli* and Proposal for Adopting a New Nomenclature for O-Typing. *PLoS ONE* **2016**, 11 (1), e0147434.
- (12) Brooks, J. T. *et al.* Non-O157 Shiga Toxin-Producing *Escherichia Coli* Infections in the United States, 1983-2002. *J Infect Dis* **2005**, 192 (8), 1422–1429.
- (13) Murray, G.L. *et al.* Regulation of Salmonella Typhimurium Lipopolysaccharide O Antigen Chain Length Is Required for Virulence; Identification of FepE as a Second Wzz. *Mol Microbiol* **2003**, 47(5), 1395–1406.
- (14) Scheutz, F. *et al.* Designation of O174 and O175 to Temporary O Groups OX3 and OX7, and Six New *E. Coli* O Groups That Include Verocytotoxin-Producing *E. Coli* (VTEC): O176, O177, O178, O179, O180 and O181. *Apmis* **2004**, 112(9) 569-84.
- (15) Stromberg, L. R. *et al.* Purification and Characterization of

- Lipopolysaccharides From Six Strains of Non-O157 Shiga Toxin-Producing *Escherichia coli*. *J Microbiol Methods* **2015**, 116, 1-7.
- (16) Poxton, I. R. Antibodies to Lipopolysaccharide. *J Immunol Methods* **1995**, 186(1), 1–15.
- (17) Silipo, A. and Molinaro, A. The Diversity of the Core Oligosaccharide in Lipopolysaccharides. *Subcell Biochem* **2010**, 53, 69–99.
- (18) Amor, K. *et al.* Distribution of Core Oligosaccharide Types in Lipopolysaccharides From *Escherichia coli*. *Infect Immun* **2000**, 68(3), 1116–1124.
- (19) Sommerfeld, S. and Strube, J. Challenges in Biotechnology Production—Generic Processes and Process Optimization for Monoclonal Antibodies. *Chemical Engineering and Processing: Process Intensification* **2005**, 44(10), 1123–1137.
- (20) Jauho, E.S. *et al.* New Technology for Regiospecific Covalent Coupling of Polysaccharide Antigens in ELISA for Serological Detection. *J Immunol Methods* **2000**, 242(1-2), 133–143.
- (21) Takahashi, K. *et al.* Detection of Lipopolysaccharide (LPS) and Identification of Its Serotype by an Enzyme-Linked Immunosorbent Assay (ELISA) Using Poly-L-Lysine. *J Immunol Methods* **1992**, 153(1-2), 67–71.
- (22) Nielsen, K.H. *et al.* Improved Competitive Enzyme Immunoassay for the Diagnosis of Bovine *Brucellosis*. *Vet Immunol Immunopathol* **1995**, 46(3-4), 285–291.
- (23) Nalepka, J.L. and Greenfield, E.M. Detection of Bacterial Endotoxin in Human Tissues. *Biotechniques* **2004**, 37(3), 413–417.
- (24) Reither, K. *et al.* Low Sensitivity of a Urine LAM-ELISA in the Diagnosis of Pulmonary Tuberculosis. *BMC Infect Dis* **2009**, 9(1), 141.
- (25) Brooks, B.W. *et al.* Monoclonal Antibodies to Lipopolysaccharide O Antigens of Enterohemorrhagic *Escherichia coli* Strains in Serogroups O26, O45, O103, O111, O121, and O145. *J Food Protect* **2015**, 78(7), 1252-1258.
- (26) Heumann, D. and Baumgartner, J.D. Antibodies to Core Lipopolysaccharide Determinants: Absence of Cross-Reactivity with Heterologous Lipopolysaccharides. *J Infect Dis* **1991**, 163(4), 762-768.
- (27) Sakulramrung, R. and Domingue, G.J. Cross-Reactive Immunoprotective Antibodies to *Escherichia coli* 0111 Rough Mutant J5. *J Infect Dis* **1985**, 151(6), 995–1004.
- (28) Lamoureux, L.R. *et al.* An Optical Biosensor for Detection of Pathogen Biomarkers From Shiga Toxin-Producing *Escherichia coli* in Beef Lysates. *SPIE BIOS: Proc SPIE Int Soc Opt Eng* 2015. 931004-931004.
- (29) Stromberg, L.R. *et al.* Membrane Insertion for the Detection of Lipopolysaccharides: Exploring the Dynamics of Amphiphile-in-Lipid Assays. *PLoS ONE* **2016**, *In Review*.
- (30) Vreugdenhil, A.C. *et al.* LPS-Binding Protein Circulates in Association with apoB-Containing Lipoproteins and Enhances Endotoxin-LDL/VLDL Interaction. *J Clin Invest* **2001**, 107(2), 225–234.
- (31) Mukundan, H. *et al.* Quantitative Multiplex Detection of Pathogen Biomarkers on Multichannel Waveguides. *Analytical Chemistry* **2010**, 82(1), 136–144.

- (32) Mukundan, H. *et al.* Planar Optical Waveguide-Based Biosensor for the Quantitative Detection of Tumor Markers. *Sens Actuators B Chem* **2009**, 138 (2), 8–8.
- (33) Mukundan, H. *et al.* Optimizing a Waveguide-Based Sandwich Immunoassay for Tumor Biomarkers: Evaluating Fluorescent Labels and Functional Surfaces. *Bioconj Chem* **2009**, 20(2), 222–230.
- (34) Appelmelk, B.J.*et al.* Monoclonal Antibodies Detecting Novel Structures in the Core Region of *Salmonella minnesota* Lipopolysaccharide. *FEMS Microbiol Lett* **1987**, 40(1), 71–74.
- (35) Gagnon, P. *et al.* Purification of IgM Monoclonal Antibodies; BioPharm International, Advanstar, 2008; pp 1–10.
- (36) Lamping, N. *et al.* LPS-Binding Protein Protects Mice From Septic Shock Caused by LPS or Gram-Negative Bacteria. *J Clin Invest* **1998**, 101(10), 2065–2071.
- (37) Harris, H.W. *et al.* Human Very Low Density Lipoproteins and Chylomicrons Can Protect Against Endotoxin-Induced Death in Mice. *J Clin Invest* **1990**, 86 (3), 696–702.

**Chapter 5**  
**Lipopolysaccharide-induced dynamic lipid membrane reorganization: tubules, perforations and stacks**

Peter G. Adams<sup>[1]</sup>, Loreen Lamoureux<sup>[2]</sup>, Kirstie L. Swingle<sup>[1,3]</sup>, Harshini Mukundan<sup>[4,5]</sup>, Gabriel A. Montaña<sup>[1]\*</sup>

<sup>1</sup> Center for Integrated Nanotechnologies, Los Alamos National Laboratory, Los Alamos, NM, 87545.

<sup>2</sup> Center for Biomedical Engineering, University of New Mexico, Albuquerque, NM, 87131.

<sup>3</sup> Department of Biology, University of New Mexico, Albuquerque, NM 87131.

<sup>4</sup> New Mexico Consortium, Los Alamos, NM, 87545.

<sup>5</sup> Physical Chemistry and Applied Spectroscopy, Los Alamos National Laboratory, Los Alamos, NM, 87545.

## 5.1 Abstract

Lipopolysaccharide (LPS) is a unique lipoglycan, with two major physiological roles: (i) as a major structural component of the outer membrane of Gram-negative bacteria and (ii) as a highly potent mammalian toxin when released from cells into solution (“endotoxin”). LPS is an amphiphile that spontaneously inserts into the outer leaflet of lipid bilayers to bury its hydrophobic lipidic domain, leaving the hydrophilic polysaccharide chain exposed to the exterior polar solvent. Divalent cations have long been known to neutralize and stabilize LPS in the outer membrane, whereas LPS in the presence of monovalent cations forms highly mobile negatively-charged aggregates. Yet, much of our understanding of LPS and its interactions with the cell membrane does not take into account its amphiphilic biochemistry and charge polarization. Herein, we report fluorescence microscopy and atomic force microscopy analysis of the interaction between LPS and fluid-phase supported lipid bilayer assemblies (sLBAs), as model membranes. Depending on cation availability, LPS induces three remarkably different effects on simple sLBAs. Net negative LPS- $\text{Na}^+$  leads to the formation of 100  $\mu\text{m}$ -long flexible lipid tubules from surface associated lipid vesicles and the destabilization of the sLBA resulting in micron-size hole formation. Neutral LPS- $\text{Ca}^{2+}$  gives rise to 100  $\mu\text{m}$ -wide single- or multi-lamellar planar sheets of lipid and LPS formed from surface associated lipid vesicles. Our findings have important implications about the physical interactions between LPS and lipids and demonstrate that sLBAs can be useful platforms to study the interactions of amphiphilic virulence factors with cell membranes. Additionally, our study supports the general phenomenon that lipids with highly charged or bulky headgroups can promote highly curved membrane architectures due to electrostatic and/or steric repulsions.

## 5.2 Introduction

Lipopolysaccharide (LPS) is of major medical importance, firstly, because it forms the outer surface of many pathogenic bacteria and, secondly, because LPS is a highly potent toxin when released from cells. The outer membrane of Gram-negative bacteria is a highly asymmetrical complex lipid bilayer, comprised of an

inner leaflet of various common phospholipids and the outer leaflet of the unique glycolipid, LPS.<sup>1-3</sup> An *Escherichia coli* (*E. coli*) cell contains several million LPS molecules, covering 75% of the outer membrane surface, with the remaining area being occupied by proteins.<sup>1</sup> LPS has several important functions for the bacteria including acting as a permeability barrier between the cell and the exterior, for structural stability of the membrane and for protecting against foreign particles (anti-microbial peptides, drugs, toxic heavy metals, salts and enzymes).<sup>4,5</sup> LPS is critical to many pathogens' ability to cause disease and is released from the outer membrane of the bacterium during infection. LPS, historically known as 'endotoxin', can cause over-activation of the immune system in toxic shock syndrome at  $\mu\text{g}/\text{kg}$  LPS/ body mass ratios.<sup>6,7</sup> Thus, LPS is an excellent target for diagnostics, vaccines and treatment strategies against these pathogens.<sup>3,7</sup>

The structure of LPS has been studied for many years.<sup>8</sup> LPS is an amphiphilic molecule comprised of a hydrophobic domain named 'lipid A', covalently linked to a hydrophilic polysaccharide chain that extends away from the cell. The lipid A component contains six saturated fatty acid chains linked to a phosphate-substituted disaccharide.<sup>2,9</sup> This is linked to the relatively conserved 'core-oligosaccharide' and the variable 'O-polysaccharide' of 0-50 oligosaccharide repeat units, dependent on the particular bacterial species and strain. LPS preparations are heterogeneous, and a mixture of LPS structures are found in each preparation with partial modifications depending on growth conditions.<sup>3</sup> Each LPS molecule has multiple negatively charged groups from phosphate and acid groups in the lipid A and core-polysaccharide. In the current study, we use LPS from *E. coli* serotype O111:B4, structure shown in **Figure 5.1**, details in refs.<sup>3,10-12</sup> There are at least 6 negatively charged groups per LPS and a range of 1–18 O-polysaccharide repeat units. In the bacterial outer membrane, divalent cations such as  $\text{Mg}^{2+}$  and  $\text{Ca}^{2+}$  are essential to neutralize this negative charge, allowing cross-linking between LPS molecules, which maintains an effective barrier to drugs and other damaging molecules.<sup>2,13-16</sup> Chelation of divalent cations leads to increased permeability to drugs, LPS release and rapid disintegration of the outer membrane.<sup>14,17</sup> In comparison to the common phospholipid 1,2-dioleoyl-*sn*-glycero-3-phosphocholine (DOPC), LPS contains a

much larger hydrophobic domain containing saturated fatty acids. In addition, LPS has a large hydrophilic, negatively-charged head-group, whereas DOPC has a small zwitterionic head-group (**Figure 5.1**).

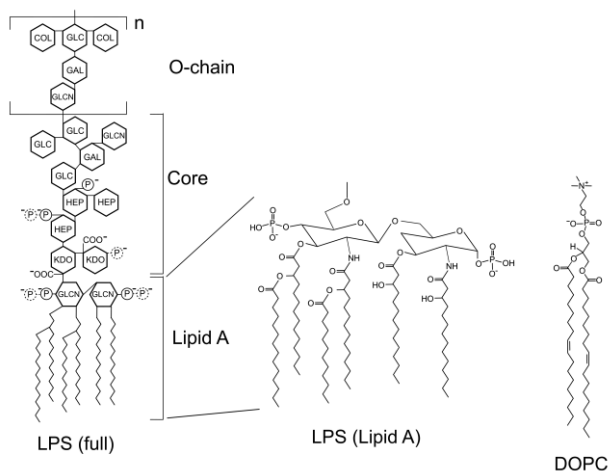


**Figure 5.1. Comparison of the chemical structure of lipopolysaccharide from *E. coli* serotype O111 and the phospholipid 1,2-dioleoyl-*sn*-glycero-3-phosphocholine (DOPC).** Partial covalent modifications, which may result in additional phosphate groups are shown with dotted lines (dependent on growth conditions and other factors). Number of repeat units in the O-chain,  $n$ , ranges from 1-18. COL, colitose (3,6-dideoxy-L-xylo-hexose); GAL, galactopyranose; GLC, glucopyranose; GLCN, 2-amino-2-deoxyglucopyranose; HEP, L-glycero-D-*manno*-heptopyranose; KDO, 3-deoxy-D-*manno*-oct-2-ulopyranosonic acid; P, phosphate.

LPS has previously been shown to form very different structures depending on its local ionic environment, observed in cell-free LPS extracts and reconstituted LPS-lipid membranes. LPS aggregates exposed to  $\text{Na}^+$  are not fully neutralized and have a net negative charge,<sup>16</sup> resulting in formation of long tubular structures which were converted into bilayers by exposure to  $\text{Ca}^{2+}$  ions.<sup>18</sup> Multiple studies have shown that divalent cations reduced the mobility of LPS aggregates and increased the rigidity of LPS bilayers, decreasing their permeability.<sup>18-24</sup> Additionally, divalent cations have led to formation of highly ordered, stacked multilamellar LPS structures.<sup>20,21</sup> The physiological activity of LPS also depends on its ion associations and LPS isolates rich in  $\text{Na}^+$  and  $\text{K}^+$  cations are significantly more active as an endotoxin than those with  $\text{Mg}^{2+}$  or  $\text{Ca}^{2+}$  ions.<sup>25</sup> The more rigid, multilamellar LPS

formations induced by divalent cations were determined to be inactive as opposed to more freely mobile aggregates in monovalent cation rich environments.<sup>26</sup> These studies together indicate that the effect of cations on LPS structure and aggregate formation is an important factor that should be considered when studying the manifestation of endotoxic shock.

In studies where hybrid membranes were prepared by combining LPS with different lipids, LPS distribution and incorporation<sup>27</sup> and the membrane fluidity<sup>28</sup> was found to depend on lipid composition. The structure of LPS from different strains or species can be dramatically different. Studies have observed that LPS structural changes, self-association, toxicity all depend on LPS subtype.<sup>8,22,29,30</sup> In the human body, LPS interacts with intermediary factors of the human immune system including LPS Binding Protein, which has been shown to affect LPS interaction with membranes.<sup>31-33</sup> Our current study focuses on the direct interaction of *E. coli* O111 LPS aggregates with fluid phase DOPC membranes as a model for LPS-membrane interactions.

While many studies have investigated the structures resulting from reconstitution of LPS-lipid membranes, the dynamic interaction of LPS with membrane architectures remains poorly characterized. In giant unilamellar vesicles (GUVs) formed from LPS and lipids, LPS was found to segregate into gel-like domains, showing that LPS lateral rearrangement and self-association of LPS molecules can occur within the lipid bilayer.<sup>29</sup> Soluble LPS has been shown to insert into preformed lipid GUVs and cause shape changes and vesicle fission.<sup>34</sup> Supported lipid bilayer assemblies (sLBAs) have been used for many years as models for biological phospholipid bilayers, as planar membrane systems with lateral lipid mobility.<sup>35-37</sup> To our knowledge, there has not been direct visualization of the dynamic effects of 'free' LPS aggregates on a sLBA, as a simple platform for evaluation of the interaction of amphiphilic toxins with membrane architectures. Herein, we evaluate the direct interaction of LPS with sLBAs using a combination of fluorescence microscopy and atomic force microscopy (AFM), powerful tools for investigating membrane organization.<sup>38-41</sup> Our experiments were performed with concentrations of LPS ranging from 5 to 500 µg/mL, highly comparable to the lethal

doses for various species ranging from 1 to 200 mg/ kg body weight.<sup>6</sup> Our findings could have significant ramifications on our understanding of the action of the important toxin LPS, and have general implications that should be considered for all amphiphilic pathogenic molecules.

### 5.3 Materials and Methods

#### 5.3.1 Materials

All materials were used as received without further purification. Organic solvents were HPLC grade (Fisher Scientific, Waltham, MA). Phosphate buffered saline (PBS), HEPES, EDTA, NaCl and CaCl<sub>2</sub> were purchased from Fisher Scientific. All aqueous buffers were prepared using 18 MΩ•cm H<sub>2</sub>O (Barnstead Nanopure filter) and then passed through 0.22 μm filter membranes (Millipore, Billerica, MA). All lipids and fluorescence dyes were purchased in dry powdered form. 1,2-dioleoyl-*sn*-glycero-3-phosphocholine (DOPC) was purchased from Avanti Polar Lipids (Alabaster, AL). Lipid-based dyes used for doping the lipid membranes were as follows: 2-(4,4-difluoro-5,7-dimethyl-4-bora-3a,4a-diaza-s-indacene-3-pentanoyl)-1-hexadecanoyl-*sn*-glycero-3-phosphocholine (C<sub>5</sub>-BODIPY FL HPC) or Texas Red 1,2-dihexadecanoyl-*sn*-glycero-3-phosphoethanolamine, triethylammonium salt (Texas Red DHPE) (Molecular Probes, Eugene, OR). The standard LPS used in this study unless otherwise mentioned was from *E. coli* serotype O111:B4 (phenol extract); a FITC-conjugate of LPS from *E. coli* serotype O111:B4 was used for direct tracking (Sigma-Aldrich, St. Louis, MO).

#### 5.3.2 Liposome and Supported Lipid Bilayer Formation

The standard DOPC liposome preparation contained 99.5% (mol/mol) DOPC and 0.5% C<sub>5</sub>-BODIPY-HPC or 0.5% Texas Red DHPE. Lipids and lipid dyes in chloroform were mixed in the desired molar ratios, dried overnight under vacuum and rehydrated in buffer solution. The lipid suspension was subjected to three freeze-thaw cycles followed by probe sonication for 10 min in an ice bath to form small liposomes.<sup>41</sup> Hydrophilic glass coverslips were used as substrates (cleaned with 'piranha' solution of 3:1 H<sub>2</sub>SO<sub>4</sub>/30% H<sub>2</sub>O<sub>2</sub>). Hydrophobic ultrathin adhesive 'imaging spacers' (0.12 mm depth, 9 mm diameter) were attached to substrates to

create small wells to confine a droplet of buffer (Electron Microscopy Sciences, Hatfield, PA), for an ‘open’ sample set-up to allow multiple buffer exchanges and top-down access for atomic force microscopy. sLBAs were formed by deposition of liposomes onto the substrate. After 20 min incubation at room temperature, the sLBA was washed by exchanging the buffer solution ten times to remove excess liposomes, although significant numbers of associated lipid vesicles evidently remain.

### *5.3.3 Treatment of surfaces with LPS*

LPS was handled as per manufacturer’s guidelines, dissolved into buffer at 5 mg/ mL, stored in silanized glass vials at 4 °C and, before each usage, stocks were vortexed and bath sonicated (15 min) at room temperature to homogenize immediately prior to sLBA treatment. sLBAs of DOPC were prepared and washed with buffer. The DOPC sLBA was then treated with LPS and analyzed with microscopy as described in the Results section. For experiments testing LPS in the presence of monovalent cations, the buffer used was PBS (137 mM NaCl, 2.7 mM KCl, 10 mM Na<sub>2</sub>HPO<sub>4</sub>, 10 mM KH<sub>2</sub>PO<sub>4</sub>, pH 7.4), whereas for testing LPS in the presence of divalent cations “Ca<sup>2+</sup> buffer” was used (150 mM CaCl<sub>2</sub> and 20 mM HEPES, pH 7.5). For experiments testing the effects of cation concentration, buffers containing 20 mM TRIS-HCl (pH 7.5) and 10–900 mM NaCl or 10–900 mM CaCl<sub>2</sub> were used. Control experiments confirmed that buffering with phosphates, HEPES and TRIS were equivalent for our studies (data not shown). Control experiments found that common small molecule contaminants had no observable effect on our sLBAs (RNA from baker’s yeast, bovine serum albumin, fetal bovine serum) (data not shown), compared to the effects of LPS under the same conditions.

### *5.3.4 Microscopy of LPS-treated sLBAs*

Lipid bilayers were imaged with laser scanning confocal fluorescence microscopy (LSCM), epifluorescence microscopy, total internal reflection fluorescence microscopy (TIRFM) and AFM. Samples were kept hydrated and never allowed to dry either during preparation or analysis.

LSCM used an FV-1000 inverted optical microscope (Olympus, Tokyo, Japan) equipped with multi-channel photomultiplier detectors, operated in 'photon-counting mode' (very low background noise, 0-2 counts), acquiring 512 x 512 pixel images unless otherwise stated. A 40 x air objective (NA = 0.95) was used for the majority of experiments and a 60 x water-immersion objective (NA = 1.20) was used for higher resolution confirmation. Excitation was provided by a multi line Ar laser (488 nm, for BODIPY), a HeNe laser (543 nm, for Texas Red), or a diode laser (635 nm, for AlexaFluor 647). Appropriate high performance band-pass emission filters were used (505-525 nm for BODIPY and FITC; 655-755 nm for Texas Red and AlexaFluor 647). Fluorescence recovery after photobleaching (FRAP) was performed using manufacturer's provided software.

Epifluorescence was performed using an IX-81 inverted optical microscope with a Hamamatsu model C11440-22C CCD camera. A 100 x oil-immersion objective (NA = 1.40) was used. Excitation was provided by a 200W metal-halide lamp and a FITC filter set and appropriate ND filters were used. Images and movies were acquired at 1024 x 1024 pixels using the software.

TIRFM was performed using an Olympus IX-71 inverted optical microscope equipped with a Hamamatsu model C7780-20C CCD camera (1344 X 1032 pixels). A 100 x oil-immersion TIRFM objective (NA = 1.45) was used. Excitation was provided by a 488 nm Ar ion laser and a green filter set and appropriate ND filters were used.

AFM was performed using an MFP-3D-SA system, equipped with a closed loop XY scanner and all-digital ARC2 Controller (Asylum Research, Santa Barbara, CA). All imaging was performed under fluid using Bruker SNL probes, sharpened Si tip on a triangular SiN cantilever ( $k \sim 0.12$  N/m). High quality topographs were generally acquired at 512 x 512 pixels and 1 Hz scan speed. Images were processed using the manufacturer's provided Igor Pro-based software.

## 5.4 Results

sLBAs were formed on glass substrates by deposition of small unilamellar vesicles comprised of 99.5% DOPC and 0.5% C<sub>5</sub>-BODIPY FL HPC.<sup>41</sup> AFM

confirmed that the bilayers are continuous and defect free over many microns with a few small protrusions (**Figure 5.2 A**). LSCM showed a relatively homogenous fluorescence with small numbers of higher intensity dots (**Figure 5.2 B before LPS**). The fluidity of DOPC sLBAs at room temperature was confirmed by fluorescence recovery after photobleaching (FRAP) (data not shown). The higher intensity fluorescence dots and protrusions in AFM data represent lipid vesicles that remain loosely associated with the surface even after rinsing with buffers. Lipid vesicles have an average size of ~50 nm in solution (**Figure A4.1**); the largest may be resolved as surface-associated vesicles in LSCM. Sequential images show that surface-associated vesicles are highly mobile and independent of the underlying sLBA (**Movie A4.1**).

#### *5.4.1 Lipid tubule formation is induced by LPS in PBS*

In order to test the effect of soluble LPS on our model lipid bilayer system, experiments were first performed in PBS, containing monovalent cations ( $\text{Na}^+$ ). LSCM fluorescence images (time lapse series) obtained after addition of 100  $\mu\text{g}/\text{mL}$  LPS in PBS to sLBA are shown in **Figure 5.2 B** and **Movie A4.2**. The surface-associated vesicles that originally exist were observed to split into multiple vesicles, leading to an increase in mobility and the formation of fluorescent strand-like structures. Initially disordered webs of strands stretch out over a few minutes into elongated strands that we term 'lipid tubules', analogous to the tubules characterized by other studies of membrane-perturbing molecules.<sup>42,43</sup> The lipid tubules retain a point of association to the membrane surface and often extend up to 100  $\mu\text{m}$  in length and span many microns above the surface, as shown by epifluorescence microscopy (**Figure 5.2 C**). Movies of sequential epifluorescence images confirmed the high degree of mobility of lipid tubules (**Movie A4.3**). The lipid tubules stretch away from the boundary of the substrate, to orient in a radial organization during the course of the experiment, suggesting that fluid flow plays a role in tubule extension (**Figure A4.2**).

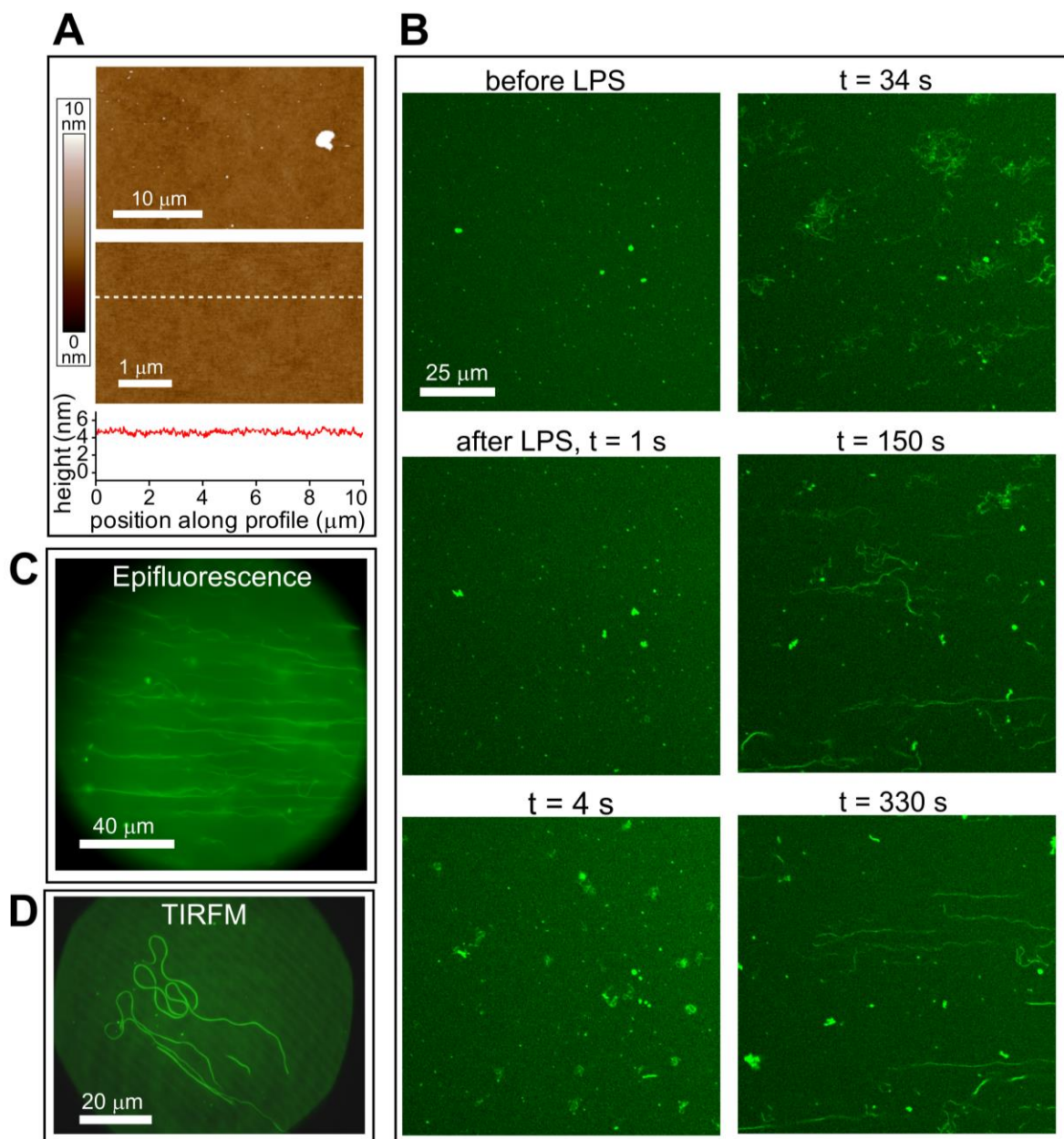


**Figure 5.2. Lipid tubule formation induced by LPS in PBS.** (A) AFM topographs showing a DOPC supported lipid bilayer assembly in PBS buffer at low and high magnification. A height profile across the lower image (*dashed white line*) shows a relatively flat surface. (B) LSCM of the DOPC sLBA (doped with 0.5% green fluorescent lipids) in PBS before and after addition of 100 µg/ mL LPS. Sequential images are shown at selected time periods after addition of the LPS. (C) Representative epifluorescence microscopy image of lipid tubules. (D) Representative TIRFM image showing long tubules. The background of green fluorescence suggested a homogenous lipid bilayer (note, 45° periodic noise is an optical artifact that should be ignored).

AFM imaging of LPS-treated sLBAs revealed a flat surface (data not shown) and no lipid tubules were observed, as may be expected because of the relatively

poor stability and high mobility of these formations. Membrane-inserted LPS was not detected by AFM, which could be due to the instability of the protruding polysaccharide chain that can be 'pushed aside' by the AFM probe<sup>44</sup> or due to the transient nature of LPS insertion into lipid bilayers, previously observed in GUVs<sup>34</sup>. TIRFM, which has higher signal/ noise and restricted penetration depth of excitation, was used in an attempt to observe any subtle height variations in the sLBA, such as bubbles, ripples or other perturbations that may not have been observed with other optical techniques. TIRFM images (**Figure 5.2 D**) did not show any evidence of disruptions to the underlying lipid bilayer, but both lipid tubules and surface-associated vesicles were prominent. The lack of any observable changes to the underlying lipid bilayer by both AFM and TIRFM indicate that it is either intact, or that any perturbations cannot be observed by these strategies.

#### *5.4.2 Hole formation in the sLBA after LPS treatment in PBS and washing*

After treatment of the sLBA with LPS in PBS, the DOPC bilayer was washed to remove any residual unassociated LPS. This resulted in the unexpected formation of voids lacking fluorescence of approximately 1-5  $\mu\text{m}$  in width (**Figure 5.3 A**). Intensity profiles from single photon counting (SPC) LSCM data shows that there is essentially zero fluorescence at the centre of these voids (**Figure 5.3 B**). The fluorescence intensity of membrane areas other than voids was roughly similar before and after LPS treatment, suggesting a continuous membrane interface. It should be noted that these voids were stable, with no detectable change in shape or size over the course of 80 min at the  $\sim 250$  nm resolution of our microscope (**Figure A4.3**). In order to test whether the voids of fluorescence were actually physical holes in the lipid bilayer, AFM was performed on an LPS-treated sample in PBS. The DOPC bilayer appeared as a relatively smooth film with many holes of  $\sim 5$  nm depth via AFM, consistent with expected height of a sLBA (**Figure 5.3 E**). The lateral size of holes varied from less than 1  $\mu\text{m}$  up to 5  $\mu\text{m}$  in width. High resolution topographs (**Figure 5.3 F**) demonstrated that holes are essentially empty with only small amounts of debris visible, which correlated with the SPC fluorescence data. TIRFM (**Figure 5.3 C**) images were likewise consistent with LSCM and AFM. FRAP showed

that lipids had lateral mobility within the remaining membrane, with holes unperturbed (**Figure 5.3 D**). These observations support the notion of static holes within an otherwise continuous fluid lipid bilayer.

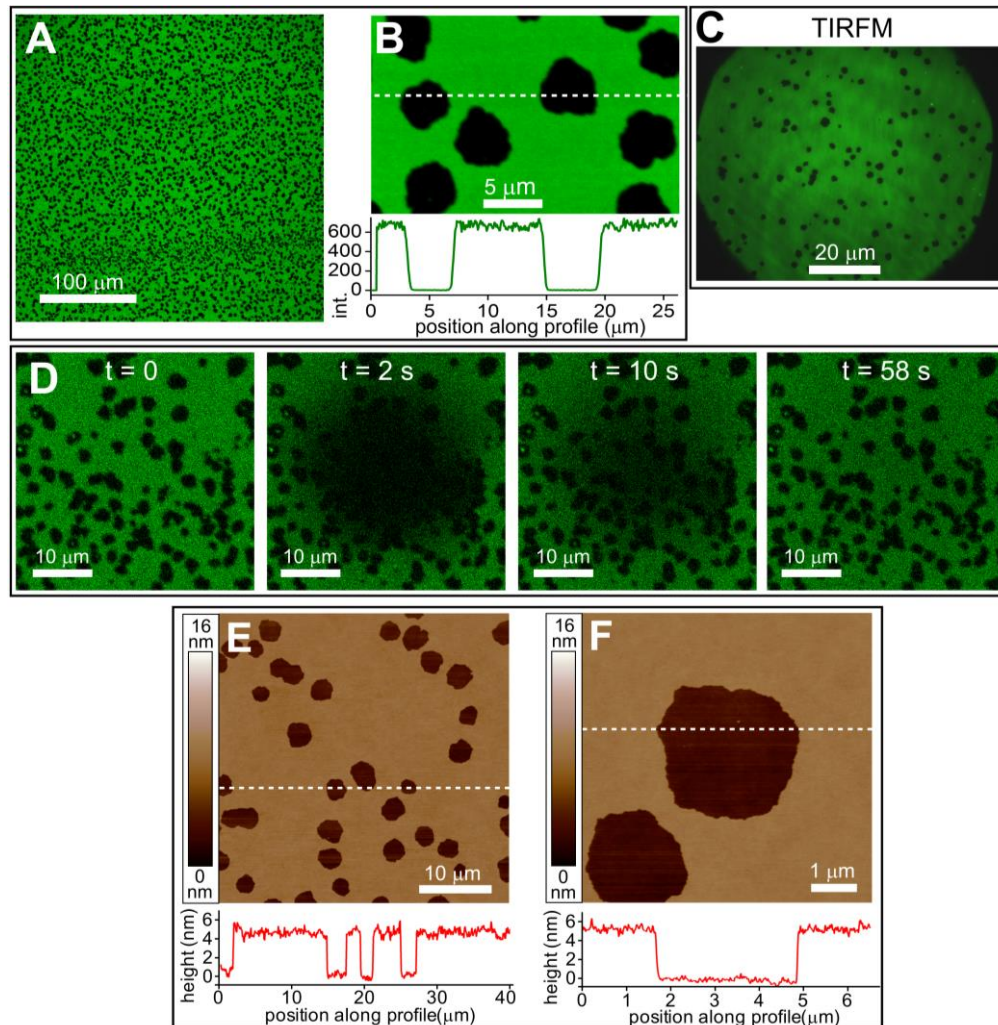


**Figure 5.3. Holes in sLBAs after LPS treatment and washing.** (A) LSCM fluorescence images showing DOPC sLBAs after treatment with 100  $\mu\text{g}/\text{mL}$  LPS in PBS followed by washing the surface (PBS, ten changes). (B) Higher magnification LSCM image. A profile of the fluorescence intensity (*below*) shows the SPC counts along a line drawn across the image (*white dashed line*). (C) A representative TIRFM image of a similar sample. (D) FRAP experiment from the sample in (A). A circular region was photobleached and then sequential images acquired to show the lateral diffusion of fluorescent lipids. (E) AFM topograph showing accurate width and depth of holes induced by LPS, similar sample to (A). Height profiles (*below, red lines*) show the height data across *white dashed lines* in the image, chosen to show the depth of holes in the lipid bilayer. (F) Higher magnification topograph from the field of holes in (E).

Hole formation was found to depend on both LPS concentration and incubation time. To test concentration effects, sLBAs were treated with different

concentrations of LPS for a standard 20 min and then rinsed. Above 20  $\mu\text{g}/\text{mL}$ , which is higher than the critical micelle concentration (CMC) of LPS (10-14  $\mu\text{g}/\text{mL}$ ),<sup>45,46</sup> hole formation increased with LPS concentration (**Figure 5.4 A-C**). Holes were not initially detected using LPS at concentrations  $\leq 20 \mu\text{g}/\text{mL}$ . To test incubation time effects, sLBAs were treated with a standard LPS concentration and then rinsed with buffer after different time periods (**Figure 5.4 D-F**). At sub-CMC concentration, (5  $\mu\text{g}/\text{mL}$ ), the number and size of holes increased with LPS incubation time from 20 to 180 min as the numbers of surface-associated vesicles decreased (related to their increased conversion to tubules and removal after rinsing). Thus, hole formation can occur above or below the CMC of LPS, however more time is necessary for hole formation at sub-CMC concentrations.

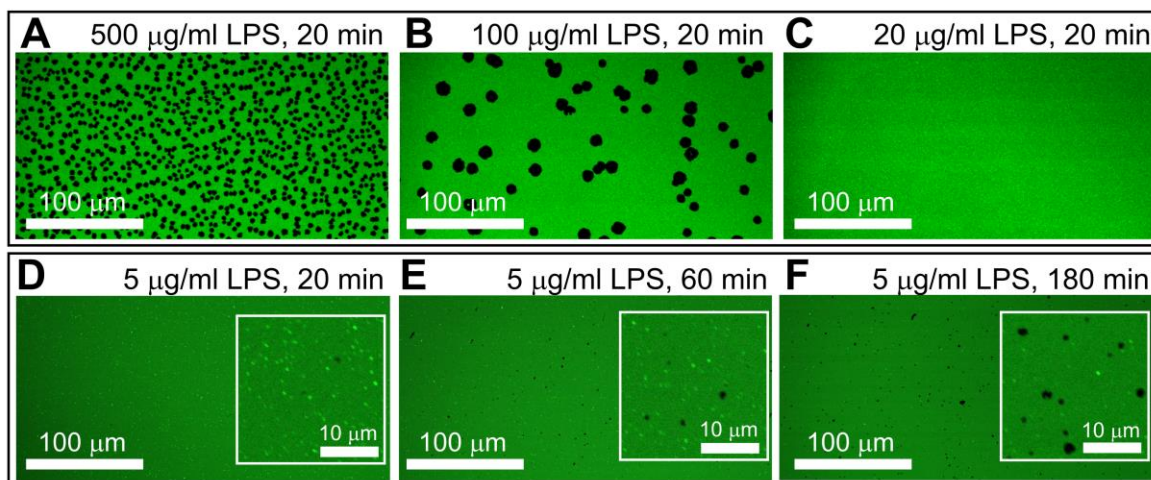


**Figure 5.4. LPS concentration and time dependence on hole formation.** LSCM fluorescence images of a DOPC sLBA treated for 20 min with LPS at varying concentrations of LPS in PBS, (A) 500  $\mu\text{g}/\text{mL}$ , (B) 100  $\mu\text{g}/\text{mL}$  or (C) 20  $\mu\text{g}/\text{mL}$ , and then washed with PBS, showing decreasing numbers of holes with LPS concentration. Parallel samples were treated with 5  $\mu\text{g}/\text{mL}$  LPS in PBS for (D) 20 min, (E) 60 min or (F) 180 min, and then washed and imaged immediately. More holes are observed with increased incubation time. These images were acquired at higher pixel density (4096 x 4096) in order to resolve small holes. *Inset* (D-F), digitally magnified areas of these images showing small holes more clearly.

Although AFM showed that holes in the DOPC bilayer were mostly empty, we could not rule out whether small amounts of LPS were present but undetected by AFM. To directly detect the presence of LPS, a FITC-labeled LPS was used with a DOPC sLBA doped with Texas Red DHPE lipid dye (**Figure A4.4**). A fluid lipid

bilayer was observed with low background in the FITC channel. Addition of FITC-LPS (100 to 500  $\mu\text{g}/\text{mL}$ ) resulted in a significant FITC signal increase.

Unfortunately, we were unable to discriminate FITC-LPS in solution (or in lipid tubules) from that interacting with the surface, due to the overwhelming signal. After surface rinsing holes were observed, with no enhanced FITC fluorescence in holes relative to background counts. This suggests that little or no LPS remained associated with the lipid bilayer or in solution after rinsing.

#### *5.4.3 LPS in $\text{Ca}^{2+}$ buffer induces lamellar sheet formation instead of lipid tubules*

The action of LPS on lipid membranes under different cation conditions was tested using LPS in “ $\text{Ca}^{2+}$  buffer” (divalent cations, see section 5.4). Time-lapse LSCM fluorescence images were acquired during treatment of DOPC sLBAs with 100  $\mu\text{g}/\text{mL}$  LPS in  $\text{Ca}^{2+}$  buffer (**Figure 5.5 A**, **Movie A4.4**). Within seconds, small patches of fluorescence were observed that slowly grew in size over the course of minutes. SPC fluorescence intensity profiles from LSCM data show that these LPS-induced membranes had fluorescence intensity of roughly double that of the normal lipid bilayers (**Figure 5.5 B**), suggesting a second lipid-containing bilayer stacked on top of the original sLBA. Overlapping sheets with fluorescence intensity at multiples of the original lipid bilayer were observed (**Figure 5.5 C**), indicating that LPS can induce formation of multiple lipid-LPS membranes stacked on top of each other, in the presence of  $\text{Ca}^{2+}$ . FRAP experiments revealed slightly reduced lateral lipid mobility in the newly-formed lamellar sheets and underlying sLBA compared to a DOPC sLBA before LPS- $\text{Ca}^{2+}$  treatment (**Figure A4.5 A-C**). Recovery of fluorescence indicative of multi-layers after almost complete photobleaching of stacked membranes suggests that lipids can exchange from the underlying sLBA into the lipid-LPS stacks (**Figure A4.5 D-E**). Multilamellar membranes were not observed by AFM, instead a smooth surface expected to represent the original lipid bilayer was found (data not shown), implying that these membranes were too unstable for AFM imaging. LSCM fluorescence images after washing the surface with fresh  $\text{Ca}^{2+}$  buffer showed the apparent removal of LPS-induced lamellar membranes (**Figure 5.5 D**), confirming their lack of stability.

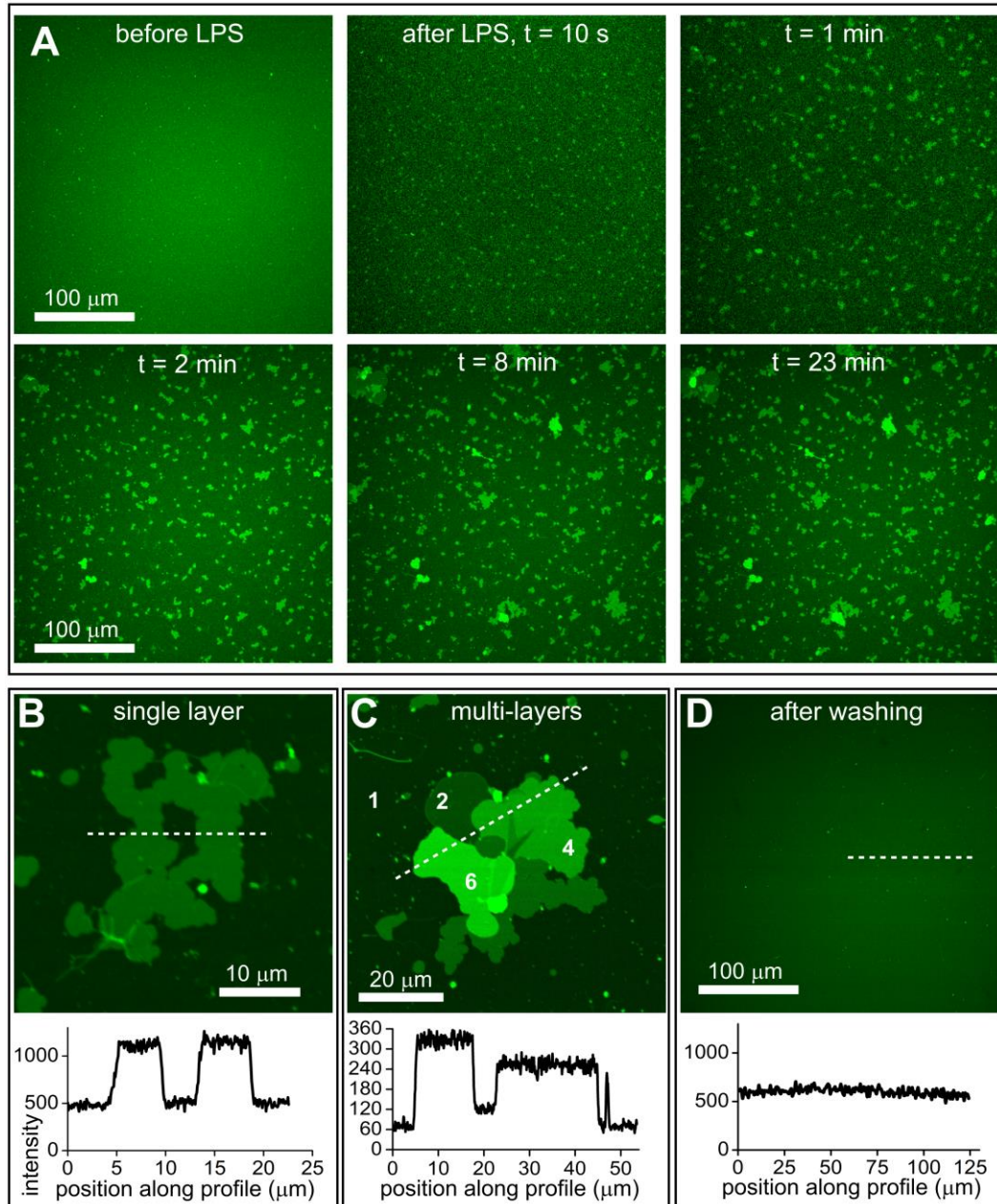


**Figure 5.5. LPS in Ca<sup>2+</sup> buffer causes formation and growth of multilamellar stacks.** (A) LSCM of the DOPC sLBA in Ca<sup>2+</sup> buffer before and after addition of 100 μg/ mL LPS in Ca<sup>2+</sup> buffer. Sequential images are shown from selected time points after addition of the LPS. Fluorescent patches are observed in images immediately after LPS addition (10 s) and continue to grow in size over the following minutes (1 min – 23 min). (B) Image at high magnification showing a patch of contiguous fluorescence of approximately double the intensity of the DOPC bilayer. (C) Image at a high magnification showing a fluorescent patch with multiple distinct step-changes in the intensity. Numbers (2), (4) and (6) indicate expected stacked bilayers with multiples of intensity of a single bilayer (1). (D) Fluorescence image after washing the LPS-Ca<sup>2+</sup>-treated surface with ten changes of Ca<sup>2+</sup> buffer. Note, images (C) acquired with lower exposure settings than (B) and (D), hence, lower fluorescence intensity.

Formation of lipid-LPS- $\text{Ca}^{2+}$  membranes was dependent on the concentration of LPS. Patches formed using  $5 \mu\text{g}/\text{mL}$  LPS in  $\text{Ca}^{2+}$  buffer were smaller, fewer in number and less stable, appearing to disintegrate over time (**Figure A4.6**), relative to the larger, more stable patches formed at higher concentrations. This LPS concentration dependence confirms the direct relationship between LPS ( $\text{Ca}^{2+}$ ) and sheet formation.

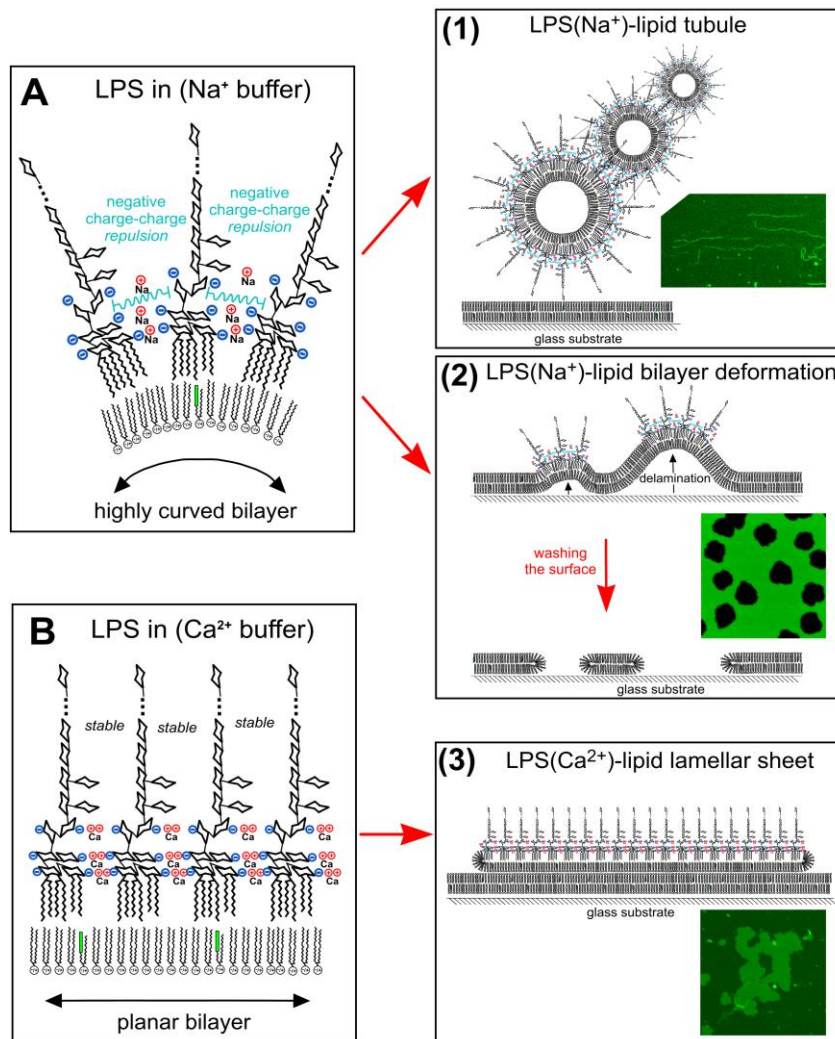


**Figure 5.6. Schematic of the mechanism of LPS-induced lipid bilayer deformation.** See text for description. LPS is represented by a simplified molecular structure showing the hydrophobic domain with six fatty acid tails linked to ‘core’ sugar units and the extended ‘O’ chain. Sugar units are represented by their cyclic rings. Note that for clarity side groups are not displayed and the polysaccharide chain is greatly shortened, represented by (...). ‘Normal’ phospholipids are represented by their two fatty acid tails linked to a head-group (*green* boxes represent BODIPY dye). Negatively charged groups of LPS are represented by *blue* (-) charge symbols. Cations that associate with LPS are represented by their elemental symbol and single or double charge, (+) or (+)(+) symbols in *red*. The *cyan* lines represent electrostatic repulsion.

Concentration of cations also modified the effect of LPS, as observed when sLBAs were treated with 100 µg/ mL LPS in buffers at a range of NaCl or CaCl<sub>2</sub> concentrations (**Figure A4.7**). Concentrations from 10 to 300 mM NaCl all produced lipid tubules, whereas at and above 450 mM NaCl both lipid tubules and potential lamellar sheets were observed (**Figure A4.7 A**). Holes were always observed with NaCl buffers after rinsing the surface. In contrast, all concentrations of CaCl<sub>2</sub> from 10 to 900 mM produced lipid sheets, which were removed without hole formation by rinsing the surface (**Figure A4.7 B**). Lipid sheet size increased with CaCl<sub>2</sub> concentration, and the largest sheets were over 100 µm in width (**Figure A4.7 C**).

## 5.5 Discussion

### 5.5.1 Considerations of the model membrane system

sLBAs are model membranes that are relatively stable, robust and relevant to biological systems. Previous studies have demonstrated the ability of a single component sLBA to form highly curved structures, including curved lipid caps and vesicle budding.<sup>41</sup> In the current study, we report that LPS, a biological toxin of significant concern, can cause three remarkably different deformations by insertion into the controlled environment of a model lipid membrane. LPS insertion into membranes, as observed in previous studies,<sup>34</sup> may be driven by LPS in aggregates in a polar solvent transferring into a more thermodynamically favorable environment as the large hydrophobic lipid A tail of LPS becomes buried in the hydrophobic core of lipid bilayer. LPS insertion occurs into both surface-associated vesicles and the solid-supported LBA. Once inserted, the effect of LPS varies due to differences in membrane curvature, interactions with the support and the local ionic environment.

The first two effects (lipid tubules and holes in the sLBA) were generated by exposure of DOPC sLBAs to LPS in the presence of (<450 mM) monovalent cations (LPS-Na<sup>+</sup>). The third effect (lamellar membranes) was observed by exposing the same DOPC system to LPS in the presence of divalent cations (LPS-Ca<sup>2+</sup>) or very high (≥450 mM) monovalent cation concentration. It is clear that ionic strength and valency influence both the structure of LPS, and its interaction with lipidic architectures. Hundreds of publications have investigated the nature of different membrane deformations induced by biological or synthetic nanoparticles, including

theoretical simulations.<sup>47,48</sup> We focus on how LPS could induce such changes, discussing examples of similar membrane rearrangements.

### *5.5.2 Membrane effects induced by LPS-Na<sup>+</sup>*

Treatment of sLBAs with Na<sup>+</sup>-LPS induced the formation of highly mobile, fluorescent lipid-based tubules (**Figure 5.2**; **Movie A4.2** and **A4.3**). Tubules are known to form when there is a high degree of local membrane curvature and an abundant supply of lipids.<sup>42,43</sup> sLBAs can have multiple ‘surface-associated liposomes’, observed as brighter spots in fluorescence images and protrusions in AFM topography, even after washing the surface. We established the presence of surface-associated lipid vesicles on our sLBAs in **Figure 5.2 A**, **A4.1**, and **Movie A4.1**. We conclude that the surface-associated lipid vesicles and any remaining solution-based vesicles are the source of lipids in formation of tubules, along with LPS, based on the following evidence. Firstly, in some images we can observe apparent tubule nucleation from surface-associated liposomes (**Figure 5.2 B**; **Movie A4.2**). Secondly, if multiple cycles of LPS treatment are performed, fewer tubules are formed each time as surface-associated vesicles are ‘used up’ (**Figure A4.8 A**). We can estimate the amount of lipids required for an average tubule by calculating the outer surface area of a tubule (modeling as a cylinder) and equating this to the surface area of multiple liposomes (modeling as a sphere). A tubule of 10 microns in length and 25 nm in diameter (as previously reported for LPS tubes<sup>18</sup>) would require ~100 vesicles of 50 nm diameter. This could represent, for example, 50 DOPC lipid vesicles and 50 LPS aggregates, a reasonable quantity considering that LSCM may resolve only the larger surface-associated vesicles. LPS appears to promote fusion of multiple lipid-LPS vesicles leading to the observed growth of tubular structures. We postulate that the destabilizing inserting/ excising effect of LPS<sup>34</sup> and its natural propensity to form tubules on its own,<sup>18</sup> could cause nanoscale membrane defects which increase the exposure of lipids to the external environment, promoting further lipid-lipid associations and vesicle fusion, however, further studies are needed to confirm this. Fluid flow due to convection currents within an open droplet, as described by studies of the “coffee-ring effect”,<sup>49-51</sup> may then direct the stretching out

of these tubules observed in LSCM (**Figure A4.2**). In contrast, tubules observed by TIRFM, where a closed-box sample enclosure was employed, appeared to rest onto the sLBA surface (**Figure 5.2 D**), possibly due to a reduction in fluid flow.

Upon rinsing the surface of LPS- $\text{Na}^+$ -treated sLBA with fresh buffer, holes devoid of lipids were observed in a concentration and time dependent manner (**Figure 5.3-5.4**). In addition to the removal of lipid tubules, these observations indicate that LPS accumulates in the sLBA over time. Apart from holes, the remaining lipid appeared to be in the form of a normal sLBA with high lateral mobility of lipids and flat, continuous membrane. This evidence, along with the fact that LPS is not found to be associated with the sLBA after hole formation (**Figure A4.4**), suggests that LPS clusters into large domains that are then dislodged from the surface during the rinsing process. If LPS induces membrane curvature in surface-associated liposomes resulting in tubules it is logical that LPS could insert and disrupt the sLBA, although the LPS-treated sLBA appears 'flat' by microscopy. The likely explanation is that LPS causes minor curvature in sLBAs below the detection limit of our instruments, and that we only observe the result of this destabilization when holes are formed after rinsing the surface. Subtle, LPS-induced membrane curvature could lead to separation of the lipid bilayer and the solid support by only a few nanometers, which would not be resolved by optical measurements. LPS insertion into lipid bilayers may be highly transient, as previously reported,<sup>34,44</sup> which would hinder detection of membrane deformations by AFM. The interaction of the sLBA and the solid support could also limit curvature and cause a strained system as compared to the relatively unrestricted surface-associated liposomes. Based on these arguments, we conclude that LPS induces subtle membrane curvature in sLBAs which leads to localized delamination sufficient to form holes upon washing the surface.

We expect that tubules and holes are different manifestations of similar effects of LPS- $\text{Na}^+$  acting on different starting material, either surface-associated liposomes or a sLBA. Both require: (i) LPS insertion into the outer leaflet of lipid membranes, (ii) LPS self-association or clustering and (iii) LPS induction of membrane curvature. We will briefly describe other studies in which one or more of

these effects are observed, supporting our conclusions. Spontaneous insertion of LPS from solution into the lipid membranes has been previously observed in GUVs whereupon it appeared to induce subtle, localized curvature resulting in shape changes from spherical to pear-shaped or pearls-on-a-string vesicles.<sup>34</sup> Other studies have shown that short-length LPS can self-associate to form gel-like domains.<sup>29</sup> While we are using full-length LPS, for which these authors did not observe phase segregation, self-association of LPS in our sLBA system may be transient or on smaller scales. LPS has been observed to form highly curved structures depending on its ionic environment. Exposure of native LPS to Na<sup>+</sup> resulted in formation of long tubular LPS-based structures of 9-18 nm diameter, as observed by electron microscopy.<sup>18</sup> These could be related to the membrane curvature and lipid tubules formed in our experiments with LPS in the Na<sup>+</sup>-containing buffer PBS. Each LPS molecule contains at least six negatively-charged groups, phosphate and carboxylate<sup>12</sup> (**Figure 5.1**), which typically cannot be fully neutralized by monovalent cations due to electrostatic repulsion of individual ions, resulting in LPS with a net negative charge.<sup>16</sup> The authors concluded that incomplete charge neutralization leads to electrostatic repulsion between LPS chains, causing a high degree of curvature and formation of LPS tubes. We extend these previous findings to show that not only does LPS-Na<sup>+</sup> form tubules in isolation but can also induce curvature in preformed sLBAs. In our sLBA system, attractive hydrophobic self-associations of saturated fatty acids in the lipid A domains of LPS in contrast to unsaturated DOPC lipids and size/shape mismatch may drive phase segregation of LPS away from DOPC lipids, outweighing the electrostatic repulsion that would otherwise drive negatively-charged LPS apart into a maximally separated configuration. Then, the negative charge-charge repulsion of the membrane extrinsic hydrophilic domains of nearby LPS would induce membrane curvature.

We may compare our findings of membrane curvature induced by proteins in both natural and artificial systems. In nature, lipid tubules and vesicle budding is found in multiple specific situations, e.g. endocytosis, exocytosis, phagocytosis, endoplasmic reticulum- and cytoskeleton- associated protein trafficking.<sup>52-54</sup> In each case, specific proteins are targeted to a local area of the membrane leading to either

the budding off of vesicles or the protrusion of long tubules from the membrane. Common mechanisms involve insertion of amphiphilic protein helices and wedge shaped proteins into the cellular lipid membranes,<sup>55-59</sup> which could be related to LPS insertion. Lipid tubules have been induced *in vitro* from lipid GUVs by promoting protein crowding at a localized point on the vesicle surface; tubule growth was observed to occur in real time from the point of protein binding.<sup>42,43</sup> Relevant to our study is the finding that any generic protein was sufficient to induce tubule formation so long as it leads to the build-up of a sufficient high density of protein packing. This lead to the conclusion that steric repulsion between any bulky particles packed at the surface has the potential to cause severe membrane bending. Crowding of LPS could have an analogous effect due to the bulky polysaccharide chain, however it seems that electrostatic rather than steric repulsive effects dominate in the case of LPS.

Perforation of lipid membranes by LPS was suggested by previous indirect evidence of electrical resistance of lipid membranes stretched across an aperture where treatment with LPS (110 to 720  $\mu\text{g}/\text{mL}$ ) led to a decreased resistance and eventual collapse.<sup>60</sup> Holes and other lesions can be formed in lipid bilayers by various small molecules, including pore-forming protein toxins (61), highly charged synthetic nanoparticles<sup>62-66</sup> and polycationic polymers.<sup>67-71</sup> Hole formation in each case is dependent on the specific interactions between the membrane and the disruptive molecule of interest. It appears that LPS belongs to this list of membrane-disruptive molecules.

### *5.5.3 Membrane effects induced by LPS-Ca<sup>2+</sup>*

LPS is known to change its structure, aggregation state and mobility depending on the availability and concentration of monovalent and divalent cations.<sup>18-24</sup> In our experiments, we conclude that LPS-Ca<sup>2+</sup> inserts into surface adsorbed liposomes and causes these LPS-lipid assemblies to fuse, resulting in very different structures in comparison to LPS-Na<sup>+</sup> of similar concentrations. Whereas LPS-Na<sup>+</sup> induces membrane curvature, LPS-Ca<sup>2+</sup> induces planar membrane formation (**Figure 5.5**). We find that surface-associated and solution-based vesicles

are the source of lipids along with LPS for planar sheet formation, analogous to lipid tubule formation, with evidence provided by multiple cycles of LPS ( $\text{Ca}^{2+}$ ) treatment (**Figure A4.8 B**). Furthermore, increasing  $\text{Ca}^{2+}$  concentration (10–900 mM) results in increasing the extent of multilamellar formation (**Figure A4.7 B**). In contrast, concentrations of  $\geq 450$  mM  $\text{Na}^+$  are required for LPS to induce even small lamellar sheets, which occur in addition to tubules and holes (**Figure A4.7 A**), suggesting that LPS induces planar membranes only at very high  $\text{Na}^+$  and even then not as extensive as those observed with  $\text{Ca}^{2+}$ . Although we were unable to verify the topography of these structures by AFM, due to their seemingly unstable nature, we are able to infer their multilamellar membrane-like nature from fluorescence data. The slight decreased lateral lipid mobility in planar lamellar membranes compared to a normal DOPC sLBA (**Figure A4.5**) suggests that LPS- $\text{Ca}^{2+}$  within the lipid bilayers impedes lipid diffusion or increases the rigidity of the membrane. While the precise structure of stacked membranes is uncertain, we found that they associated closely enough to the underlying sLBA for lipid exchange to occur. Previous spectroscopy and electron microscopy studies found that divalent cations reduce the molecular mobility of LPS within aggregates and cause LPS to reorganize into stacked multibilayers.<sup>18,20,21</sup> Our findings are congruent with these studies and suggest that not only does LPS change its own organization due to  $\text{Ca}^{2+}$  but induces lipids to rearrange with it.

It is instructive to look at the natural environment of LPS in the outer membrane of bacteria. LPS is found in the outer leaflet of a lipid bilayer forming a selectively permeable barrier between the cell and the exterior.<sup>4,5</sup> The outer membrane is relatively flat, when compared with small lipid vesicles, with a gentle curvature over many hundreds of nanometers to micrometers. Studies have shown that the outer membrane is enriched in divalent cations relative to the cytoplasmic membrane<sup>16,18</sup> and that divalent cations are essential for outer membrane stability.<sup>2,17</sup> The prevailing view from these studies is that  $\text{Mg}^{2+}$  or  $\text{Ca}^{2+}$  neutralize the negative charge of LPS where  $\text{Na}^+$  cannot at physiological concentrations. This allows the self-association of LPS where otherwise it would be electrostatically unfavorable, and LPS-LPS bridging and linkages to transmembrane proteins

stabilize the membrane.<sup>72</sup> Our current findings agree with this consensus and further demonstrate that LPS can spontaneously insert into lipid membranes and induce self-assembly into an outer-membrane-like structure in the presence of  $\text{Ca}^{2+}$  at low concentration (10 mM), whereas much higher  $\text{Na}^+$  (450 mM) is required for similar effects. Divalent ions are known to be significantly more effective at screening electrostatic interactions at lower concentrations when compared to similar solutions of simple monovalent ions<sup>73</sup> and our results confirm that this applies to the neutralization of LPS, visualizing the biological importance of divalent cations.

#### *5.5.4 Understanding LPS-sLBA interaction*

We have demonstrated three very different rearrangements of a simple, single component lipid system, all caused by one membrane-inserting amphiphile in different local environments. A schematic of LPS-induced rearrangements of lipid membranes dependent on monovalent or divalent cations is shown in **Figure 5.6**. The thermodynamically favorable insertion of LPS into the lipid membranes and clustering leads to a high density of LPS, at which point the net charge of the extrinsic polysaccharide portion of LPS appears to determine whether this causes curved or planar structures. The net-negative LPS- $\text{Na}^+$  leads to electrostatic charge repulsion between adjacent LPS and induces membrane curvature (**Figure 5.6 A**). Surface-associated lipid vesicles merge and the high membrane curvature drives formation and elongation of lipid tubules (**Figure 5.6, (1)**). In supported lipid bilayers, LPS-induced curvature disrupts the lipid bilayer's interaction with the surface support causing unstable delaminated regions which can be excised from the remainder of the lipid bilayer by washing the surface, leading to hole formation (**Figure 5.6, (2)**). In contrast, even low concentrations of  $\text{Ca}^{2+}$  promote planar self-associations of LPS (**Figure 5.6 B**). Fusion of surface-associated lipid vesicles in this case leads to growth of planar lamellar sheets of lipid and LPS on top of the sLBA surface (**Figure 5.6, (3)**). In order to form multi-layers, we postulate that mobile lipid-LPS particles deposit on top of the first lipid-LPS planar sheet, leading to growth of a second layer and potentially further layers, held together by inter-layer interactions between LPS. The ability of LPS to switch from curvature-inducing to planar-sheet formation simply

by changing its net charge by adjusting the buffering cations indicates that LPS-induced membrane curvature is due to electrostatic repulsion rather than steric repulsive effects.<sup>42,43</sup>

Previous studies with another amphiphilic pathogenic molecule, lipoarabinomannan, detected insertion into lipid membranes without any disruption.<sup>74</sup> Lipoarabinomannan and LPS are both amphiphilic virulence factors that each interact with similar factors when they infect a mammalian host (TLR2, TLR4, HDL).<sup>3</sup> Structurally, they share similarities, both with hydrophobic fatty acid tails and a membrane extrinsic domain, but they evidently interact very differently with sLBAs. Whereas lipoarabinomannan inserts passively without destabilizing the membrane,<sup>74</sup> LPS causes major disruptions, as shown by our current study. Thus, each membrane-inserting amphiphile may cause very different effects depending on their unique physical properties.

Finally, we consider three examples of other complex lipids that have been reported to induce membrane curvature. *Firstly*, studies on poly(ethylene glycol)-derivatized-lipids (PEG-lipids) at low concentration within fluid lipid bilayers in hydrogels<sup>75,76</sup> are informative because of similarities between LPS and PEG-lipids (negatively-charged headgroup, bulky hydrophilic domain). PEG-lipids were found to phase segregate into domains that stabilize regions of high curvature based on steric and electrostatic repulsions.<sup>76</sup> *Secondly*, gangliosides, lipids with a single negative charge and a bulky aromatic headgroup, have also been reported to induce formation of tubules and pearls in DOPC GUVs.<sup>77</sup> *Thirdly*, multivalent cationic lipids (MVLs) have been shown to cause formation of narrow tubules and ‘pearling instabilities’ in DOPC lipid vesicles.<sup>78-80</sup> In these studies, the authors hypothesized that increased membrane tension due to electrostatic repulsion between the highly-positively charged lipid headgroups leads to phase segregation whereby curved regions become enriched in and stabilized by MVLs. In common with our findings on LPS, screening of MVL charges by increased salt concentrations lead to a transition from tubular to multilamellar stacked membranes.<sup>79</sup> It is remarkable that both cationic (MVLs) and anionic lipids (gangliosides, PEG-lipids, LPS) can induce similar effects, bolstering suggestions of a general phenomenon<sup>78</sup> that lipids with highly-

charged (or very bulky) headgroups have the potential to cause dramatic membrane curvature and reorganizations, dependent on repulsive effects: electrostatic, steric, or a combination of both.

## **5.6 Conclusions**

We have demonstrated that LPS, a biologically important molecule, causes dynamic rearrangements of DOPC lipid bilayers dependent upon cation availability, indicating potential driving forces behind physiological effects. It was not the purpose of this study to investigate physiological effects of LPS, which are influenced by a myriad of immunological and other factors in the human body, however it is our hope that the work presented will facilitate the future design of experimental systems to investigate the role of this complex toxin on the host cells. The continuum of effects observed suggests an ability to tune the membrane deformation by adjusting conditions and components. Further variations may exist if one used different lipid mixtures (e.g. charged or gel-phase), LPS from different bacteria or alternative cations. Our study supports the general notion that highly curved membrane architectures can be generated by clustering of membrane amphiphiles that have an effectively conical shape, due to charged or bulky headgroups, causing electrostatic and/or steric repulsions.

## **5.7 Acknowledgements**

The authors thank Dr. Nathan F Boussein (Sandia National Laboratory) and Aaron Collins (Los Alamos National Laboratory) for helpful discussions. This work was performed, in part, at the Center for Integrated Nanotechnologies, an Office of Science User Facility operated for the U.S. Department of Energy (DOE) Office of Science. Los Alamos National Laboratory, an affirmative action equal opportunity employer, is operated by Los Alamos National Security, LLC, for the National Nuclear Security Administration of the U.S. Department of Energy under contract DE-AC52-06NA25396. Work by P.G.A. and K.L.S. was supported by Photosynthetic Antenna Research Center (PARC), *an Energy Frontier Research Center funded by the U.S. Department of Energy, Office of Science, Basic Energy Sciences under*

*Award # DE-SC0001035. H.M. and L.L. were supported by the Agriculture and Food Research Initiative Competitive Grant no. 2012-68003-30155 from the USDA National Institute of Food and Agriculture.*

## 5.8 References

- (1) Nikaido, H., and M. Vaara. Molecular basis of bacterial outer membrane permeability. *Microbiol Rev* **1985**, 49:1–32.
- (2) Raetz, C. R. H. Bacterial endotoxins: extraordinary lipids that activate eucaryotic signal transduction. *J Bacteriol* **1993**, 175:5745–5753.
- (3) Raetz, C. R. H., and C. Whitfield. Lipopolysaccharide endotoxins. *Annu Rev Biochem* **2002**, 71:635–700.
- (4) Nikaido, H. Molecular basis of bacterial outer membrane permeability revisited. *Microbiol Mol Biol Rev* **2003**, 67:593–656.
- (5) Delcour, A. H. Outer membrane permeability and antibiotic resistance. *Biochim. Biophys. Acta, Proteins Proteomics* **2009**, 1794:808–816.
- (6) Berczi, I. *et al.* Comparative studies on the toxicity of *Escherichia coli* lipopolysaccharide endotoxin in various animal species. *Can J Microbiol* **1966**, 12:1070–1071.
- (7) Cohen, J. The immunopathogenesis of sepsis. *Nature* **2002**, 420:885–891.
- (8) Erridge, C. *et al.* Structure and function of lipopolysaccharides. *Microbes Infect* **2002**, 4:837–851.
- (9) Rietschel, E. T. *et al.* Bacterial endotoxin: molecular relationships of structure to activity and function. *FASEB J* **1994**, 8:217–225.
- (10) Amor, K. *et al.* Distribution of Core Oligosaccharide Types in Lipopolysaccharides from *Escherichia coli*. *Infect Immun* **2000**, 68:1116–1124.
- (11) Kenne, L. *et al.* Structural studies of the O-antigens from *Salmonella greenside* and *Salmonella adelaide*. *Carbohydr Res* **1983**, 111:289–296.
- (12) Peterson, A. A. *et al.* Physical properties of short- and long-O-antigen-containing fractions of lipopolysaccharide from *Escherichia coli* 0111:B4. *J Bacteriol* **1986**, 165:116–122.
- (13) Shroll, R. M., and T. P. Straatsma. Molecular structure of the outer bacterial membrane of *Pseudomonas aeruginosa* via classical simulation. *Biopolymers* **2002**, 65:395–407.
- (14) Hancock, R. E. W. The bacterial outer membrane as a drug barrier. *Trends Microbiol* **1997**, 5:37–42.
- (15) Kotra, L. P. *et al.* Dynamics of the lipopolysaccharide assembly on the surface of *Escherichia coli*. *J Am Chem Soc* **1999**, 121:8707–8711.
- (16) Coughlin, R. T. *et al.* Quantitation of metal cations bound to membranes and extracted lipopolysaccharide of *Escherichia coli*. *Biochemistry* **1983**, 22:2002–2007.
- (17) Amro, N. A. *et al.* High-resolution atomic force microscopy studies of the *Escherichia coli* outer membrane: Structural basis for permeability. *Langmuir* **2000**, 16:2789–2796.
- (18) Coughlin, R. T. *et al.* Physical properties of defined lipopolysaccharide salts. *Biochemistry* **1983**, 22:2007–2013.
- (19) Brandenburg, K. *et al.* Phase diagram of lipid A from *Salmonella minnesota* and *Escherichia coli* rough mutant lipopolysaccharide. *J Struct Biol* **1990**, 105:11–21.

- (20) Naumann, D. *et al.* New insights into the phase behaviour of a complex anionic amphiphile: architecture and dynamics of bacterial deep rough lipopolysaccharide membranes as seen by FTIR, X-ray, and molecular modelling techniques. *J Mol Struct* **1989**, 214:213–246.
- (21) Van Alphen, L. *et al.*  $^{31}\text{P}$  Nuclear magnetic resonance and freeze-fracture electron microscopy studies on *Escherichia coli*. II. Lipopolysaccharide and lipopolysaccharide-phospholipid complexes. *Biochim Biophys Acta, Biomembr* **1980**, 597:502–517.
- (22) Snyder, D. S., and T. J. McIntosh. The lipopolysaccharide barrier: correlation of antibiotic susceptibility with antibiotic permeability and fluorescent probe binding kinetics. *Biochemistry* **2000**, 39:11777–11787.
- (23) Kučerka, N. *et al.* Effect of cations on the structure of bilayers formed by lipopolysaccharides isolated from *Pseudomonas aeruginosa* PAO1. *J Phys Chem B* **2008**, 112:8057–8062.
- (24) Jeworrek, C. *et al.* Effects of specific versus nonspecific ionic interactions on the structure and lateral organization of lipopolysaccharides. *Biophys J* **2011**, 100:2169–2177.
- (25) Garidel, P. *et al.* Divalent cations affect chain mobility and aggregate structure of lipopolysaccharide from *Salmonella minnesota* reflected in a decrease of its biological activity. *Biochim Biophys Acta, Biomembr* **2005**, 1715:122–131.
- (26) Schromm, A. B. *et al.* Biological activities of lipopolysaccharides are determined by the shape of their lipid A portion. *Eur J Biochem* **2000**, 267:2008–2013.
- (27) Nomura, K. *et al.* Interaction of lipopolysaccharide and phospholipid in mixed membranes: Solid-state  $^{31}\text{P}$ -NMR spectroscopic and microscopic investigations. *Biophys J* **2008**, 95:1226–1238.
- (28) Cañadas, O. *et al.* Bacterial lipopolysaccharide promotes destabilization of lung surfactant-like films. *Biophys J* **2011**, 100:108–116.
- (29) Kubiak, J., *et al.* Lipid lateral organization on giant unilamellar vesicles containing lipopolysaccharides. *Biophys J* **2011**, 100:978–986.
- (30) Tong, J., and T. J. McIntosh. Structure of supported bilayers composed of lipopolysaccharides and bacterial phospholipids: Raft formation and implications for bacterial resistance. *Biophys J* **2004**, 86:3759–3771.
- (31) Roes, S., *et al.* Localization of the lipopolysaccharide-binding protein in phospholipid membranes by atomic force microscopy. *J Biol Chem* **2006**, 281:2757–2763.
- (32) Schromm, A. B. *et al.* The charge of endotoxin molecules influences their conformation and IL-6-inducing capacity. *J Immunol* **1998**, 161:5464–5471.
- (33) Gutschmann, T. *et al.* Dual role of Lipopolysaccharide (LPS)-Binding Protein in neutralization of LPS and enhancement of LPS-induced activation of mononuclear cells. *Infect Immun* **2001**, 69:6942–6950.
- (34) Alam, J. M., and M. Yamazaki. Spontaneous insertion of lipopolysaccharide into lipid membranes from aqueous solution. *Chem Phys Lipids* **2011**, 164:166–174.
- (35) Castellana, E. T., and P. S. Cremer. Solid supported lipid bilayers: From biophysical studies to sensor design. *Surf Sci Rep* **2006**, 61:429–444.

- (36) Johnson, S. J. *et al.* Structure of an adsorbed dimyristoylphosphatidylcholine bilayer measured with specular reflection of neutrons. *Biophys J* **1991**, 59:289–294.
- (37) Tamm, L. K., and H. M. McConnell. Supported phospholipid bilayers. *Biophys J* **1985**, 47:105–113.
- (38) Adams, P. G., and C. N. Hunter. Adaptation of intracytoplasmic membranes to altered light intensity in *Rhodobacter sphaeroides*. *Biochim Biophys Acta, Bioenerg* **2012**, 1817:1616–1627.
- (39) Adams, P. G. *et al.* Monomeric RC–LH1 core complexes retard LH2 assembly and intracytoplasmic membrane formation in PufX-minus mutants of *Rhodobacter sphaeroides*. *Biochim Biophys Acta, Bioenerg* **2011**, 1807:1044–1055.
- (40) Montañó, G. A. *et al.* Scanning probe microscopy of nanocomposite membranes and dynamic organization. *Adv Funct Mater* **2013**, 23:2576–2591.
- (41) Goertz, M. P. *et al.* Lipid bilayer reorganization under extreme pH conditions. *Langmuir* **2011**, 27:5481–5491.
- (42) Stachowiak, J. C. *et al.* Membrane bending by protein–protein crowding. *Nat Cell Biol* **2012**, 14:944–949.
- (43) Stachowiak, J. C. *et al.* Steric confinement of proteins on lipid membranes can drive curvature and tubulation. *Proc Natl Acad Sci USA*. **2010**, 107:7781–7786.
- (44) Stoica, O., A. *et al.* Elasticity of membrane vesicles isolated from *Pseudomonas aeruginosa*. *Langmuir* **2003**, 19:10916–10924.
- (45) Bergstrand, A. *et al.* Aggregation behavior and size of lipopolysaccharide from *Escherichia coli* O55:B5. *Colloids Surf B* **2006**, 53:9–14.
- (46) Santos, N. C. *et al.* Evaluation of lipopolysaccharide aggregation by light scattering spectroscopy. *ChemBioChem* **2003**, 4:96–100.
- (47) Van Lehn, R. C., and A. Alexander-Katz. Penetration of lipid bilayers by nanoparticles with environmentally-responsive surfaces: simulations and theory. *Soft Matter* **2011**, 7:11392–11404.
- (48) Makarucha, A. J. *et al.* Nanomaterials in biological environment: a review of computer modelling studies. *Eur Biophys J* **2011**, 40:103–115.
- (49) Weon, B. M., and J. H. Je. Capillary force repels coffee-ring effect. *Phys Rev* **2010**, E 82:015305.
- (50) Fang, X., *et al.* Drying of DNA droplets. *Langmuir* **2006**, 22:6308–6312.
- (51) Deegan, R. D. *et al.* Capillary flow as the cause of ring stains from dried liquid drops. *Nature* **1997**, 389:827–829.
- (52) Aderem, A., and D. M. Underhill. Mechanisms of phagocytosis in macrophages. *Annu Rev Immunol* **1999**, 17:593–623.
- (53) Conner, S. D., and S. L. Schmid. Regulated portals of entry into the cell. *Nature* **2003**, 422:37–44.
- (54) Brownhill, K., *et al.* Molecular motors and the Golgi complex: Staying put and moving through. *Semin Cell Dev Biol* **2009**, 20:784–792.
- (55) Antony, B. Membrane deformation by protein coats. *Curr Opin Cell Biol* **2006**, 18:386–394.

- (56) Farsad, K., and P. D. Camilli. Mechanisms of membrane deformation. *Curr Opin Cell Biol* **2003**, 15:372–381.
- (57) Campelo, F. *et al.* The hydrophobic insertion mechanism of membrane curvature generation by proteins. *Biophys J* **2008**, 95:2325–2339.
- (58) Doherty, G. J., and H. T. McMahon. Mechanisms of endocytosis. *Annu Rev Biochem* **2009**, 78:857–902.
- (59) Shibata, Y. *et al.* Rough sheets and smooth tubules. *Cell* **2006**, 126:435–439.
- (60) Schuster, B. G. *et al.* The effect of endotoxin on thin lipid bilayer membranes. *J Membrane Biol* **1970**, 3:67–72.
- (61) Czajkowsky, D. M. *et al.* The vacuolating toxin from *Helicobacter pylori* forms hexameric pores in lipid bilayers at low pH. *Proc Natl Acad Sci USA*. **1999**, 96:2001–2006.
- (62) Goodman, C. M. *et al.* Toxicity of gold nanoparticles functionalized with cationic and anionic side chains. *Bioconjugate Chem* **2004**, 15:897–900.
- (63) Xiao, X. *et al.* Lipid bilayer templated gold nanoparticles nanoring formation using zirconium ion coordination chemistry. *Langmuir* **2011**, 27:9484–9489.
- (64) Xiao, X. *et al.* Surface charge dependent nanoparticle disruption and deposition of lipid bilayer assemblies. *Langmuir* **2012**, 28:17396–17403.
- (65) Arvizo, R. R. *et al.* Effect of nanoparticle surface charge at the plasma membrane and beyond. *Nano Lett* **2010**, 10:2543–2548.
- (66) Chen, J. *et al.* Cationic nanoparticles induce nanoscale disruption in living cell plasma membranes. *J Phys Chem B* **2009**, 113:11179–11185.
- (67) Hong, S. *et al.* Interaction of poly(amidoamine) dendrimers with supported lipid bilayers and cells: hole formation and the relation to transport. *Bioconjugate Chem* **2004**, 15:774–782.
- (68) Hong, S. *et al.* Interaction of polycationic polymers with supported lipid bilayers and cells: Nanoscale hole formation and enhanced membrane permeability. *Bioconjugate Chem* **2006**, 17:728–734.
- (69) Leroueil, P. R. *et al.* Wide varieties of cationic nanoparticles induce defects in supported lipid bilayers. *Nano Lett* **2008**, 8:420–424.
- (70) Leroueil, P. R. *et al.* Nanoparticle interaction with biological membranes: Does nanotechnology present a janus face? *Acc Chem Res* **2007**, 40:335–342.
- (71) Mecke, A. *et al.* Lipid bilayer disruption by polycationic polymers: The roles of size and chemical functional group. *Langmuir* **2005**, 21:10348–10354.
- (72) Van Alphen, L. *et al.* Architecture of the outer membrane of *Escherichia coli* III. Protein-lipopolysaccharide complexes in intramembraneous particles. *J Bacteriol* **1978**, 134:1089–1098.
- (73) Israelachvili, J. *Intermolecular and surface forces*. Academic Press, **1991**. New York.
- (74) Mukundan, H. *et al.* Understanding the interaction of Lipoarabinomannan with membrane mimetic architectures. *Tuberculosis (Edinb)* **2012**, 92:38–47.
- (75) Needham, D. *et al.* Repulsive interactions and mechanical stability of polymer-grafted lipid membranes. *Biochim Biophys Acta, Biomembr* **1992**, 1108:40–48.

- (76) Warriner, H. E. *et al.* Lamellar biogels: fluid-membrane-based hydrogels containing polymer lipids. *Science* **1996**, 271:969–973.
- (77) Akiyoshi, K. *et al.* Induction of neuron-like tubes and liposome networks by cooperative effect of gangliosides and phospholipids. *FEBS Lett* **2003**, 534:33–38.
- (78) Zidovska, A. *et al.* Block liposome and nanotube formation is a general phenomenon of two-component membranes containing multivalent lipids. *Soft Matter* **2011**, 7:8363–8369.
- (79) Zidovska, A. *et al.* The effect of salt and pH on block liposomes studied by cryogenic transmission electron microscopy. *Biochim Biophys Acta, Biomembr* **2009**, 1788:1869–1876.
- (80) Zidovska, A. *et al.* Block Liposomes from curvature-stabilizing lipids: connected nanotubes, -rods, or -spheres. *Langmuir* **2009**, 25:2979–2985.

**Chapter 6.**  
**Membrane Insertion for the Detection of Lipopolysaccharides: Exploring the Dynamics of Amphiphile-in-Lipid Assays**

Loreen R. Stromberg<sup>1,2,3,¶</sup>, Nicolas W. Hengartner<sup>4</sup>, Kirstie L. Swingle<sup>5</sup>, Rodney A. Moxley<sup>6</sup>, Steven W. Graves<sup>1,3</sup>, Gabriel A. Montañó<sup>5¶</sup>, Harshini Mukundan<sup>1,2,3¶\*</sup>

<sup>1</sup> Center for Biomedical Engineering, University of New Mexico, Albuquerque, New Mexico, United States

<sup>2</sup> Physical Chemistry and Applied Spectroscopy, Los Alamos National Laboratory, Los Alamos, New Mexico, United States

<sup>3</sup> The New Mexico Consortium, Los Alamos, New Mexico, United States

<sup>4</sup> Theoretical Biology and Biophysics, Los Alamos National Laboratory, Los Alamos, New Mexico, United States

<sup>5</sup> Center for Integrated Nanotechnologies, Los Alamos National Laboratory, Los Alamos, New Mexico, United States

<sup>6</sup> School of Veterinary Medicine and Biomedical Sciences, University of Nebraska-Lincoln, Lincoln, Nebraska, United States

¶These authors contributed equally to this work.

In revision, for publication in *PLoS One*. Author contributions are described in Chapter 2.

## 6.1 Abstract

Shiga toxin-producing *Escherichia coli* is an important cause of foodborne illness, with cases attributable to beef, fresh produce and other sources. Many serotypes of the pathogen cause disease, and differentiating one serotype from another relies on the specific identification of the O antigen, which consists of sugar repeats on the distal end of the amphiphilic biomarker, lipopolysaccharide (LPS). The structure of LPS, which includes large carbohydrate groups and lipid tails, poses a challenge when using classical detection methods not optimized for lipoglycans. However, it is this structure that allows LPS to partition into a lipid bilayer, leaving the hydrophilic O antigen extended into the aqueous environment. The association of LPS with a lipid bilayer allows for a reliable, qualitative detection approach, called membrane insertion, where the exposed antigen can be targeted for detection. Here, we demonstrate the use of membrane insertion assays on a waveguide-based optical biosensor platform for the detection of LPS from *E coli* O157:H7 in ground beef. Also demonstrated is the serogroup-specific detection of LPS by targeting the exposed O antigen group. Membrane insertion allows for qualitative and reliable detection of amphiphilic LPS in complex samples like beef homogenates with minimal sample preparation. Additionally, we report on the biophysical interactions of LPS with lipid bilayers inside a flow cell environment to evaluate endotoxin-induced hole formation under the conditions of our detection assay. These results demonstrate that hole formation does not occur under the conditions of the membrane insertion assay, and further evaluate hole-formation between different LPS subgroups, which may have future ramifications on the understanding of endotoxin activity. Together, these findings describe the sensitive and serotype-specific detection of amphiphilic biomarkers like LPS in complex samples using a membrane insertion assay.

## 6.2 Introduction

Shiga toxin-producing *Escherichia coli* (STEC) is an important cause of foodborne illness with cases attributable to beef and fresh produce, among other sources.<sup>1</sup> There are many serotypes of STEC with a wide range of virulence, which

are capable of infecting humans. Identification in part has relied upon detection of serotype, which in turn, relies on the identification of external biomarkers on the bacterial cell.

Lipopolysaccharide (LPS) is the primary component of the outer membrane of Gram-negative bacteria, and a key stimulator of the mammalian innate immune system.<sup>2-4</sup> LPS is among a class of molecules called pathogen-associated molecular patterns (PAMPs). PAMPs are bacterial products, often with redundant molecular structure, that are recognized by many host immune receptors, e.g., Toll-like receptors.<sup>5,6</sup> The bacterial membrane of an *Escherichia coli* (*E. coli*) cell is comprised of approximately  $10^6$  LPS molecules, or about 75% of the outer membrane.<sup>7-9</sup> LPS, and more specifically the lipid A moiety is also known as endotoxin, and can induce septic shock in a variety of mammalian hosts through the activation of monocytes and macrophages that release a series of inflammatory cytokines<sup>10-15</sup> in response to invading pathogens.

The structure and signaling mechanism of LPS has been well studied.<sup>16</sup> LPS is a negatively charged amphiphilic molecule that consists of three primary components (**Figure 6.1**). The hydrophobic lipid A tail is a highly conserved molecule consisting of 6-7 fatty acid tails.<sup>8</sup> The endotoxic effects of lipid A<sup>9,16,17</sup> are initiated by the binding of this component to host receptors and serum binding proteins *in vivo*.<sup>13,18,19</sup> Lipid A is covalently attached to the less conserved core polysaccharide region, which in turn extends to the hypervariable O polysaccharide antigen (O-ag).<sup>16,17,20,21</sup> Typically, the O-ag consists of 1-50 subunits made of 1-7 glycosyl residues.<sup>20,21</sup> Among different serotypes and species, the O-ag can vary greatly in both identity and degree of branching of the glycosyl residues.<sup>21</sup> This variability is therefore used for classifying a bacterial serotype. Interestingly, many of the PAMPs that stimulate host innate immune recognition, such as lipoarabinomannan from *Mycobacterium tuberculosis*, share a similar amphipathic structure.<sup>22,23</sup> Beyond LPS, detection of such amphiphilic signatures is critical to the understanding of host-pathogen biology.

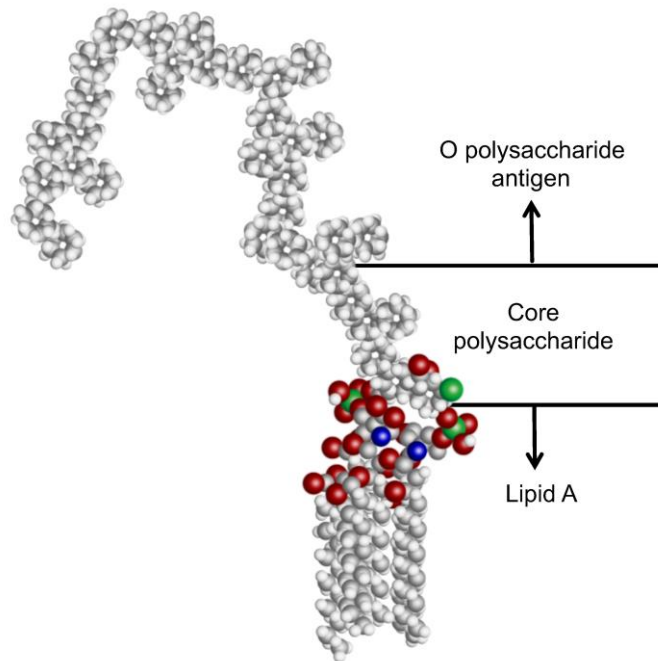


**Figure 6.1. Representative structure of the molecular components of LPS.** The conserved, hydrophobic lipid A group, core polysaccharide, and hypervariable O polysaccharide antigen. The lipid A group of most *E. coli* strains has 6 fatty acid tails which anchors LPS into the bacterial cell membrane, and is recognized by host receptor proteins.

Detection of LPS and identification of the O-ag is not always straightforward because of the variability in structure, and the possibility for conserved epitopes to present on multiple serogroups of LPS.<sup>16,21,24</sup> Additionally, many immunoassay techniques used for detection of protein antigens are not optimized for the amphiphilic biochemistry of LPS, resulting in low sensitivity of detection.<sup>25,26</sup> Factors such as conserved fatty acids, micelle aggregation, and poor binding affinity make lipoglycans difficult targets for detection using conventional immunoassay methods designed for detection of protein antigens.<sup>25,27</sup> Detection of the O-ag with classical methods such as latex agglutination or immunomagnetic separation utilizes polyclonal antibodies, which leads to cross reactivity and misidentification of the serogroup.<sup>28-32</sup> Enzyme-linked immunosorbent assays for detection of both LPS and O-ag serogroup identification have also been developed, but require extensive sample preparation and multiple antibodies, and yet suffer from non-specific interactions of the antibodies.<sup>33-37</sup> Polymerase chain reaction is also a method for detecting the specific LPS transport and polysaccharide biosynthesis genes. However, cross reactivity between specific genes of particular serotypes has been

noted,<sup>38-40</sup> leading to misidentification of those serotypes. Additionally, residual nucleic acids can indicate false positive results due to the presence of non-viable bacteria in samples.<sup>41</sup>

Thus there is a need to improve current detection methods for identification of both LPS and STEC. It has been well documented that amphiphiles, like LPS, interact both with lipid components of artificial membranes, as well as host serum-binding proteins.<sup>13,19,42-46</sup> Our team has explored the amphiphilic biochemistry of biomarkers such as LPS and lipoarabinomannan, and developed a tailored method, membrane insertion, for their detection.<sup>43,44,47</sup> Previously, we have reported on the detection of lipoarabinomannan using membrane insertion and sandwich immunoassays, and characterized the interaction of the amphiphile with lipid bilayers by atomic force microscopy (AFM).<sup>43,44,47-49</sup> Our approach utilized a waveguide-based optical biosensor platform that was developed specifically for the ultra-sensitive detection of biomarkers.<sup>29,49,50</sup> This platform uses single mode planar optical waveguides functionalized with a lipid bilayer inside a flow cell to facilitate detection through the use of evanescent sensing and a fluorescently conjugated antibody.<sup>50-54</sup> This technique is based on the principle of exponential decay of the evanescent wave away from the surface of the waveguide material, which results in an excitation field that extends only 200 nm from the surface of the waveguide. Therefore, only samples and fluorophores within the evanescent field are illuminated by incident light. This minimizes background signal, thereby increasing the signal-to-noise (s:n) ratio of excited antibody-fluorophore conjugates bound to antigen at or near the surface of the waveguide. Waveguides are functionalized with supported lipid bilayer assemblies. Upon exposure to the amphipathic biomarker, the hydrocarbon tails (e.g. lipid A) passively diffuse through the aqueous matrix, and associate with the lipid bilayer, eliminating the need for capture antibodies.<sup>44,47</sup> In this manuscript, we show waveguide-based membrane insertion assays for detection of LPS O157 in ground beef lysate. Also presented are membrane insertion assays for detection of LPS from other serogroups, demonstrating broad applicability of this platform. Due to the heterogeneous nature of LPS, the inability to determine an accurate molecular weight or conformation of the antigens restricts the

quantitative capability of these membrane insertion assays. Yet, they offer a reliable and direct strategy for the detection of amphiphilic targets in complex backgrounds with minimal sample preparation at a high s:n levels and low ( $\mu\text{g/mL}$ ) limits of detection.

To identify, describe, and delineate assay parameters, we have used biophysical methods to characterize the interaction of LPS with lipid bilayers. Lipid bilayers have been previously used to study the interactions of LPS in simple biomimetic systems.<sup>42,55</sup> Recent work from our team demonstrated LPS-induced deformations in 1,2-dioleoyl-sn-glycero-3-phosphocholine (DOPC) lipid bilayers based on ionic conditions.<sup>10</sup> These findings raised questions on the dynamics of the interaction of amphiphilic LPS with bilayers in membrane insertion assays. Since the detection antibodies would bind to the open glass substrate caused by hole formation, a high signal would result, which in the given scenario could be an artifact of hole formation. In this manuscript, we address that question by devising a flow cell mimetic chamber to explore the interactions of LPS with lipid bilayers at conditions synonymous with our detection assays. Finally, we examine LPS-lipid bilayer dynamics using multiple serogroups of LPS to determine if the variable O-ag structure of the molecule affects the interactions with lipid bilayers, and explore the relevance to detection assays and the study of host-pathogen biology.

## **6.3 Materials and Methods**

### *6.3.1 Materials*

Lipopolysaccharides from six strains of non-O157 STEC (DEC10B [O26:H11], B8227-C8 [O45:H2], MT#80 [O103:H2], 0201 9611 [O111:H11], MDCH-4 [O113:H21], DA-37 [O121:H21], GS G5578620 [O145:NM], and TY-2482 [O104:H4]) were selected and prepared by hot phenol extraction and tested for antigen activity as we have previously described.<sup>32</sup> LPS O157:H7 was purchased from List Biological Labs (Campbell, CA), and LPS O111:B4, bovine serum albumin (BSA), Dulbecco's phosphate buffered saline (PBS), Ethylenediaminetetraacetic acid (EDTA), and potassium chloride were from Sigma Aldrich (St. Louis, MO). Polyclonal antibody (pAb) anti-*E. coli* O157 (pAb O157) was from LifeSpan Biosciences

(Seattle, WA). pAb *E. coli* O104, as well as monoclonal antibody (mAb) for *E. coli* O111 were from Abraxis Inc. (Warminster, PA). 1,2-Dioleoyl-*sn*-glycero-3-phosphocholine (DOPC) and 1,2-dioleoyl-*sn*-glycero-3-phosphoethanolamine-N-(cap biotinyl) (sodium salt) (cap-Biotin) were obtained from Avanti® Polar Lipids (Alabaster, AL). C5-BODIPY® FL HPC (2-(4,4-difluoro-5,7-dimethyl-4-bora-3a,4a-diaza-s-indacene-3-pentanoyl)-1-hexadecanoyl-*sn*-glycero-3-phosphocholine) was purchased from Molecular Probes® (Eugene, OR). Sylgard® silicone elastomer kit (Dow Corning, Midland, MI) was used to pour a 90/10 mix of polydimethylsiloxane (PDMS). Alexa Fluor® 647 labeling kits, UltraPure™ Glycerol, and HEPES were all from Life Technologies (Thermo Fisher Scientific, Grand Island, NY). Silicon oxynitride waveguides were purchased from nGimat (Norcross, GA) and the functional surface of silicon dioxide was maintained by Spectrum Thin Films (Hauppauge, NY). Silicone gaskets for waveguide assembly were from Grace Bio-Labs (Bend, OR) and Secure seal spacers (9 mm diameter x 0.12 mm deep) were from Electron Microscopy Sciences (Hatfield, PA). Glass microscope slides, Gold Seal™ cover glass, and sucrose were purchased from Thermo Fisher Scientific (Rockford, IL). Epoxy was from Gorilla Glue, Inc., (Cincinnati, OH), and Simple Truth® organic ground beef was purchased from the local Kroger Stores (Los Alamos, NM). All reagents were of the highest quality for their intended purpose.

### 6.3.2 Waveguide preparation

Single mode planar optical waveguides were cleaned and prepared as previously described.<sup>29,50,51,53,56,57</sup> In brief, the waveguides and coverslips were cleaned by bath sonication for 5 min each in chloroform, ethanol, then water. Waveguides and coverslips were dried under an argon stream and exposed to UV-ozone (UVOCS Inc., Montgomeryville, PA) for 40 min. Flow cells for immunoassays were immediately assembled using cleaned waveguides and coverslips which were bonded together by a silicone gasket with a laser cut channel in the center. Following assembly, the flow cells were injected with a preparation of lipid micelles, then incubated overnight at room temperature (RT), to facilitate vesicle fusion.<sup>53</sup>

### 6.3.3 *Micelle preparation*

Micelles for waveguide membrane insertion experiments were prepared by probe sonication as previously described.<sup>29,50,51,57</sup> 2 mM DOPC and 1% (mol/mol) cap-Biotin were prepared by deposition of chloroform-dissolved lipids into glass tubes, and evaporation of solvent under an argon stream. Biotin incorporation allows for the evaluation of bilayer integrity at the conclusion of assays.<sup>47,53</sup> Lipids were rehydrated in phosphate buffered saline (PBS), stirred for 2 hours (hr) at RT, 120 revolutions per minute (rpm) on an orbital shaker, followed by 10 freeze-thaw cycles. Finally lipids were probe sonicated for 6 min (1.0 s pulse on/off, 15% amplitude) using a Branson ultrasonic generator.

Micelles for fluorescent imaging were prepared in a similar fashion as those for waveguide experiments with the addition of 0.5-1% (mol/mol) of C<sub>5</sub>-BODIPY FL HPC to serve as a fluorescent marker for imaging. Lipids in chloroform were vacuum dessicated overnight and subsequently prepared in PBS, followed by 6 freeze-thaw cycles and 10 minutes of continuous probe sonication (tip dia. = 3 cm, 12 watts) (Sonicator 3000, Misonix, Farmingdale, NY)

### 6.3.4 *Lipopolysaccharides, beef samples, and antibodies*

Except in the cases of concentration dependence assays, LPS stocks (5 mg/mL) were thawed and bath sonicated for 15 min, diluted to the working concentration in PBS and sonication was repeated prior to injection in the flow cell. For the benchmark assays on concentration dependence of LPS, the stocks were sonicated for 5 min, diluted to working concentration in PBS and re-sonicated for an additional 5 min prior to injection.

Ground beef was flash frozen in liquid nitrogen, and freeze-dried on a Schlenk line for 48 hr. Dried material was crushed using a mortar and pestle, then homogenized in lysis buffer (0.5 M sucrose, 10 mM HEPES, 25 mM KCl, 1 mM EDTA, 10% v/v glycerol, 5 mg/mL concentration).<sup>29</sup> The suspension was alternately vortexed (30 sec) and bath sonicated (30 s) until large protein aggregates were eliminated. Samples were diluted to 1 mg/mL in PBS immediately before use. The beef homogenate was used as a negative control, in order to evaluate background

fluorescence and assess antibody cross-reactivity with a crude matrix that simulates an actual test sample. Additionally we also spiked LPS directly into homogenates to determine detection capabilities in a beef sample.<sup>29</sup>

Reporter antibodies for LPS were pAb anti-*E. coli* LPS O157 (pAb O157), pAb anti-*E. coli* LPS O104:H4 (pAb O104) and mAb anti-*E. coli* O111:H11 (mAb O111). All reporter antibodies were fluorescently labeled with Alexa Fluor® 647 (af647) per kit instructions. Molar ratio of dye to protein was measured using a NanoDrop™ 1000 (Thermo Scientific) and calculated (3.68 for LPS concentration assays, and 7.37 for beef lysate assays) per Alexa Fluor® kit instructions. Degree of labeling for pAb O104-af647 was 3.17 and that for mAb O111-af647 was 7. After labeling, antibodies were checked for activity using immunoblotting of 5 mg/mL LPS antigens onto nitrocellulose, and compared with immunoblotting results for antibodies prior to labeling.

#### *6.3.5 LPS membrane insertion assays*

Concentration dependent LPS insertion assays were repeated at least three times using LPS O157 and 25 nM pAb O157-af647 as the reporter antibody. Flow cells were prepared as described and blocked for 1 hr with 2% (w/v) BSA, then rinsed with 0.5% BSA/PBS. Incident light from a 635 nm laser, (power 440-443  $\mu$ W) was coupled into the waveguide using a diffraction grating. The response signal was adjusted for maximum peak intensity using a spectrometer (USB2000, Ocean Optics, Winter Park, FL) interfaced with the instrument and an optical power meter (Thor Labs, Newton, NJ).<sup>29,50,51,54</sup> The background signal associated with the lipid bilayer and protein block was recorded after which the flow cell was incubated (90 min) with pAb O157-af647 to determine NSB between the antibody and the lipid bilayer. The flow cell was rinsed with 2 mL of wash buffer (0.5% BSA/PBS) after all incubations. Incubation times for LPS were optimized to 2 hr to allow maximal association with the supported lipid bilayer. Excess LPS micelles were removed by washing and the signal recorded. Subsequently, reporter antibody was incubated for 90 min and rinsed, and the specific signal associated with antibody bound to LPS captured on the bilayer was recorded.

Membrane insertion assays for serogroups of LPS were performed in triplicate at a concentration of 25  $\mu\text{g}/\text{mL}$ , using pAb O157-af647 as the reporter antibody. This approach exploits the cross-reactivity of a polyclonal antibody to the conserved regions of different serogroups of LPS.<sup>32</sup> However, we raised the hypothesis that by use of antibodies specific for a particular LPS serogroup, we could potentially enhance the sensitivity and selectivity of detection by targeting the variable O-ag region. To evaluate this, LPS O104 was tested under identical conditions using 25 nM pAb O104-af647 as the reporter, and then compared to the signal using the non-specific pAb O157-af647. Additionally we also tested whether using mAb specific to the O-ag would increase the specific signal and tested LPS O111:H11 with its respective mAbs.

To determine NSB of the detection antibody with the beef lysate, a 1 mg/mL beef homogenate sample was prepared by diluting in PBS and incubating with the bilayer for 2 hr. NSB of the reporter antibody was assessed against the beef lysate after a 90 min incubation, and then LPS (6.25, 25, or 50  $\mu\text{g}/\text{mL}$ ) was spiked into beef lysate and incubated for 2 hr. Specific signal was recorded after 90 min incubation with the reporter antibody.

#### 6.3.6 *Imaging inside of a flow cell*

We established a flow cell mimic to investigate the interactions of LPS with DOPC bilayers inside a flow cell of identical dimensions and functionalized surfaces as our waveguide biosensor (**Figure 6.5 A-B**). For this, two holes were drilled into a glass slide and a 24x50 mm cover glass was used in place of the waveguide piece to allow imaging. Glass was cleaned in 30:10 sulfuric oxides for 40 min then rinsed repeatedly and bath sonicated 3 times (5 min/each) in deionized water. The flow cell model was constructed from the two glass pieces with the addition of an attached outflow tube and a rubber septum to allow buffer exchange. PDMS (90:10 elastomer:curing agent) was poured into plastic petri dishes to a final height of  $\sim 4$  mm, allowed to cure, and then cut into a square ( $\sim 1$  cm x 1 cm). To create an injection port, a rubber septum was inserted into the PDMS when it was approximately halfway cured. For the fluid outflow port, a 2 mm hole was made in a

1 cm<sup>2</sup> of self-adhesive silicone using a biopsy punch and tubing was inserted through the hole. PDMS and flow cell assembly was then exposed to UV-Ozone for 2 min after which PDMS/septum assembly and silicone were stuck to the glass slide and seams were sealed using epoxy. Epoxy was allowed to cure for 1 hr prior to deposition of 2 mM DOPC + 1% biotin + BODIPY® labeled lipid micelles. Lipids were deposited into the flow cell, the outflow tube was clamped shut, and the apparatus was incubated O/N at 4° C in the dark. Flow cell was rinsed with 10 mL PBS and imaged on an Olympus IX-81 motorized inverted microscope with excitation provided by a 488 nm Argon ion laser and green filter set. Fluorescence recovery after photobleaching (FRAP) was used to confirm lateral fluidity of lipid bilayers. LPS membrane insertion assays were then performed in the same manner as the waveguide assays, with images recorded to determine hole formation (or lack thereof) under these conditions. In most cases, images were recorded at 1024 x 1024 pixels at a scan rate of 12.5 µs/pixel. FRAP was performed on 512 x 512 pixel frames, using 5x zoom, at a scan rate of 10 µs/pixel.

### *6.3.7 Imaging LPS on glass slides*

To determine differential interactions of various LPS serogroups on DOPC lipid bilayers, 9 mm secure seal spacers were adhered to clean glass cover slides and 2 mM DOPC + BODIPY® micelles were deposited and incubated for 20 min as previously described.<sup>10</sup> Free lipid vesicles were rinsed away using 10 exchanges of PBS buffer (1 mL total volume) and then LPS was prepared and incubated with the bilayers for 20 min at RT, after which free LPS was rinsed away with 10 exchanges of buffer. FRAP and fluorescence imaging was used to determine the effect of the LPS groups on the fluidity and conformation of the bilayers. Data was optimized for contrast and brightness using ImageJ 1.48.

### *6.3.8 Data processing*

Resulting spectra from the waveguide biosensor were processed and graphed using Igor Pro 6.37. Due to NSB signals that were nearly equivalent to background values, the data for the membrane insertion assays of LPS O104:H4

and O111:H11 were not background corrected, and were integrated as raw spectral curves between 550 and 850 nm and then averaged. In all other cases, individual spectra replicates were integrated between the wavelengths of 550 – 850 nm, where the significant signal appears for detection with af647 and a long pass 647 nm filter, and then corrected for background noise levels. Integrated values were then averaged and used to calculate a s:n ratio. LoD were obtained by taking the average integrated NSB for all replicates in a set, determining the standard deviation ( $\sigma$ ) of the replicates, adding  $3\sigma$ , then multiplying by the sample concentration ( $\mu\text{g/mL}$ ), and dividing by the integrated average specific signal for that concentration (**see Equation 6.1**).

$$LoD = \frac{(NSB + 3S)[Sample]}{Specific} \quad \text{Equation 6.1}$$

### 6.3.9 Statistical Analysis

Linear regression was used to relate the logarithm of the raw integrated intensities according to LPS concentration (LPSc), waveguide ID (wg#), power coupled (power), and type of measurement (background (mBG), non-specific (mNSB), specific, and specific (mSP)). Analysis of variance (ANOVA) was then used to determine the significance of the variables at the 5% level, (**Table A5.1**). Subsequently, to explain the observed heteroscedasticity, we regressed the absolute value of the residuals from the previous regression analysis onto the same set of explanatory variables (**Table A5.2**). Model selection was performed using Akaike information criterion to determine the significance of the variables. Absolute values of the residuals of the means for LPSc, wg#, and power were processed with regression analysis (**Table A5.3**) using the type of measurement as a covariate.

## 6.4 Results and Discussion

### 6.4.1 Detection of LPS with membrane insertion

To determine the concentration range over which LPS can be reliably detected by membrane insertion, assays of LPS O157 were performed a minimum of three times over a concentration range of 6.25 – 200  $\mu\text{g/mL}$  LPS (**Figure 6.2 A**), using polyclonal antibody (pAb) anti-*E. coli* O157 (O157) labeled with Alexa Fluor®

647 (af647) as the detection antibody (pAb O157-af647). The limits of detection (LoD) for LPS O157 were calculated to be 4.80 µg/mL using **Equation 6.1** with the specific signal intensity values from the lowest concentration. The results indicated that membrane insertion consistently detects a broad concentration range of LPS with low non-specific binding (NSB) of the reporter antibody. However, the detection trend is non-linear (**Figure 6.2 B**) with larger variability at higher concentrations. This lack of linearity is expected, and can be explained by the biochemical properties of amphiphilic LPS which significantly affect the size and conformational presentation of the molecule. For one, LPS will present in a micellar conformation in aqueous solutions.<sup>17,58-60</sup> Beyond the critical micelle concentration (CMC) of LPS O157, the amphiphile would exist both as monomers and aggregates,<sup>61,62</sup> making repeatable quantitation challenging.<sup>61</sup> LPS micelles can further vary based on the size of the O-ag chains, which can be full-length, truncated, or absent entirely, depending on bacterial strain and growth phase.<sup>17,58,63</sup> Furthermore, LPS can also present in different shapes of micelles, such as lamellar, cubic, and hexagonal inverted structures,<sup>64-67</sup> which are dependent on antigen structure, pH, ion concentration, solution composition, and temperature.<sup>10,17,65,68</sup> All of the above factors contribute to the size or shape of the micelles, and influence the binding availability of epitopes for detection, which in turn affects the inter-assay variability (**Figure 6.2 B**). While reasonable efforts to control for the size of micelles in the preparations was taken (e.g. extended bath sonication<sup>66</sup> during testing of serogroup and beef lysate assays), we cannot be certain that LPS micelles in our assay systems are homogenous. This biochemical variability has limited the quantitative measurement of amphiphilic biomarkers in general.<sup>47,67</sup> Lastly, due to the stability of endotoxin<sup>69,70</sup> we cannot entirely discount the potential of endogenous endotoxin that may have been present on glassware, either from previous assays or other environmental bacteria, even though rigorous cleaning procedures were employed. This is also a relevant concern in beef lysates. We therefore only demonstrate the concentration range over which LPS can be reliably and repeatedly detected using membrane insertion. Membrane insertion is not intended to provide a quantitative measurement of concentration, but to accurately detect LPS with minimal sample processing in complex samples such

as beef lysates. To determine that the variability between assays was caused by the variable nature of LPS, we employed rigorous statistical analysis of the data. Statistical regression analysis of the uncorrected data sets and the residuals (**Tables A5.1-5.3**) from multiple experiments demonstrate that factors such as antigen (LPS) concentration, choice of waveguide, power coupled into the waveguide, non-specific interaction of the antibodies with the lipid bilayer, and other systematic parameters do not account for the large deviations seen in detecting specific concentrations of LPS. The only significant factor resulting from the analysis is the antigen itself, though we also saw some significance associated with a single waveguide (**Table A5.3**). This suggests that variations in the CMC of the amphiphile, due to the heterogeneous nature and other biophysical properties, affect the interaction of LPS with the lipid bilayer and the detection antibody. This is further substantiated by measurements of protein binding on the same instrumentation in this and previous studies that do not present with such variability. Therefore, we conclude that the variability in signal at specific concentrations is primarily dependent on the conformation of the LPS antigens, and not variability associated with the detection platform, methods, or other reagents.

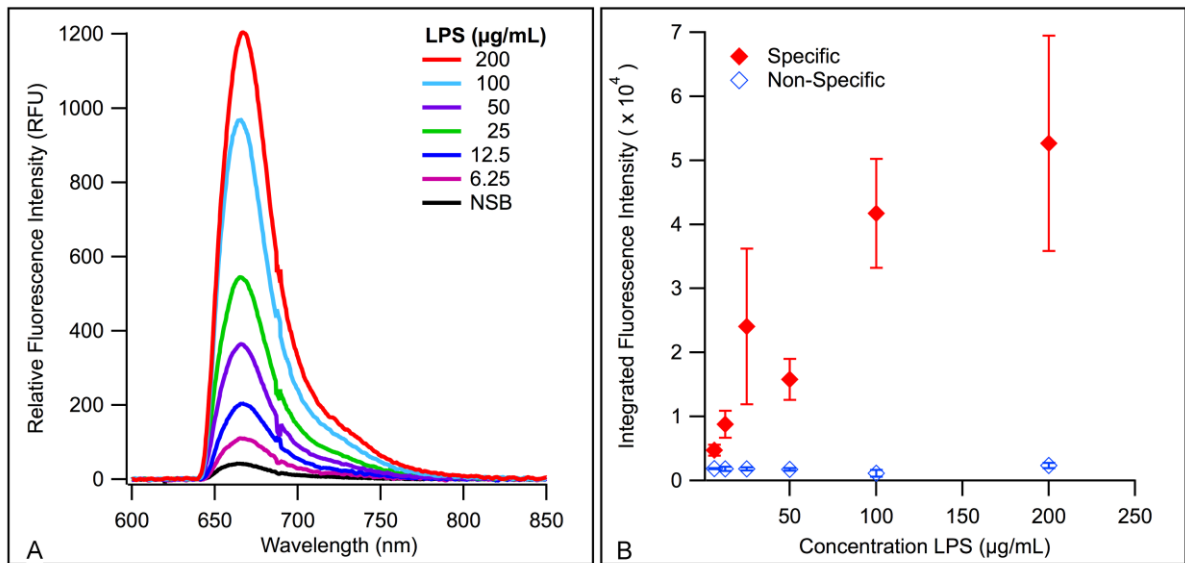


**Figure 6.2. Membrane insertion for detection of LPS O157.** (A) Spectral curves demonstrating detection of various concentrations of LPS O157. (B) Integrated values of spectral curves plotted as single points with standard error of the mean. Closed diamonds indicate averaged integrated signal intensity, and open diamonds are integrated NSB.

To assess application for detecting contamination in food products, assays were performed in a complex sample matrix (e.g. beef lysate). Membrane insertion assays were performed in 1 mg/mL ground beef lysate at three concentrations over the range of 6.25 – 50 µg/mL LPS O157 (**Figure 6.3**). LoD for this assay was calculated to be 4.2 µg/mL LPS O157. The ratios between specific signal and NSB (s:n) at 6.25 µg/mL (~4), and at 50 µg/mL (~27) are comparable, albeit slightly higher, to the those seen in the benchmark assay (**Table 6.1**). However, the ratio at 25 µg/mL (s:n~10) was lower than that observed in the benchmark assay (**Table 6.1**). The changes in the presentation and micellar properties of the antigen in complex physiological backgrounds can account for both observations. We attribute the increased signal at 6.25 and 50 µg/mL to the possibility that LPS is known to associate with lipoproteins,<sup>13,19,43,47,49</sup> such as low-density and high-density lipoproteins (LDL and HDL respectively), in serum and muscle tissue.<sup>71</sup> Since these lipoproteins carry amphiphiles and can insert them into cell membranes,<sup>45,72</sup> it is possible that HDL and LDL are serving to insert monomeric LPS or LPS-lipoprotein complexes into the DOPC lipid bilayer. HDL is a critical factor for both treatment and prognosis of septic patients,<sup>73,74</sup> because of its ability to shuttle amphiphilic LPS in hosts. No data is readily available on the CMC of LPS O157, however, it is reasonable to assume it to be somewhat similar to the CMC of LPS O111:B4 (22 µg/mL).<sup>17</sup> This means that at 6.25 µg/mL, LPS would be present mostly as a monomer, and above 25 µg/mL, aggregates would be the primary conformation. At 25 µg/mL mL the change in the s:n ratio between the two assays could also be caused by the difference in solution composition between the beef lysate and benchmark (PBS) assays, which could affect micelle conformation. It is tempting to speculate about the conformation of LPS at this specific concentration. This is especially important to consider when detecting multiple subtypes of LPS in complex matrices. Since conformation will vary slightly between different LPS antigens, the enhanced s:n ratios we see in the beef lysate will aid in the detection of multiple serogroups of LPS associated with STEC or other Gram-negative species. While we have begun preliminary biophysical characterization of this specific concentration of LPS O157 using AFM, there are still numerous unanswered questions about the

conformations LPS adapts while interacting with lipids, which could be affecting quantitative detection capabilities. Further, we used much milder sonication conditions for these assays, compared to subsequent measurements of different serotypes of STEC LPS, which may contribute to some of the variability. Finally, the epitopes recognized by the detection antibodies, and their presentation can change significantly depending on the micellar conformation of LPS, which may contribute to the variability. Thus, several factors can affect variation in measured detection signals of intact amphiphilic biomarkers such as LPS, and should be taken into account for the design and evaluation of diagnostic assays as well as the understanding of host-pathogen biology.

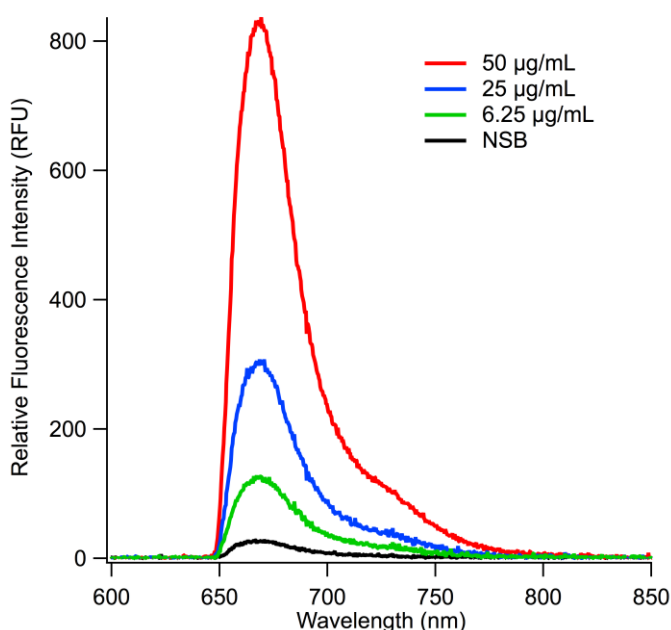


**Table 6.1. Signal to Noise Ratios of LPS Membrane Insertion Assays**

LPS µg/mL	Signal:Noise Ratios	
	benchmark	beef lysate*
6.25	2.6	4.1
12.5	5.2	-----
25	13.4	9.8
50	8.8	26.9
100	23.3	-----
200	29.5	-----

\*LPS O157 was tested at 3 concentrations in beef lysates

**Figure 6.3. Concentration dependent detection of LPS O157 in 1 mg/mL beef lysates.**

Detection of LPS in beef lysates shows an increase in signal to noise ratios (Table 6.1) as compared to those seen in the benchmark assay.

To demonstrate the broad applicability of membrane insertion assays, we tested LPS from other pathogenic *E. coli* (LPS O104:H4 and LPS O111:H11) using af647 labeled detection antibodies targeted against the specific O-ag (**Figure 6.4**), Sensitive detection is demonstrated in both cases with LPS O104 demonstrating a significantly higher (s:n~39) response than LPS O111 (s:n~6). This difference can largely be attributed to the sensitivity of the respective antibodies.<sup>32</sup> Due to the large

difference in s:n ratios in these assays, the limits of detection also demonstrate the same pattern (0.77 and 7.36  $\mu\text{g}/\text{mL}$  respectively). This is due in part to the low NSB of both antibodies, but also the specificity of the antibodies for their specific epitopes. Both LoDs fall within the reported range for physiologically relevant concentrations of LPS.<sup>72</sup> We observed a much lower variability between the assay replicates (**Figure A5.1**) as compared to the benchmark assay at 25  $\mu\text{g}/\text{mL}$  LPS. We attribute this primarily to the increased sonication time during antigen preparation that was implemented here, but also acknowledge that the O-ag of these LPS subtypes are much different from O157 and therefore may be more homogenous at this concentration.

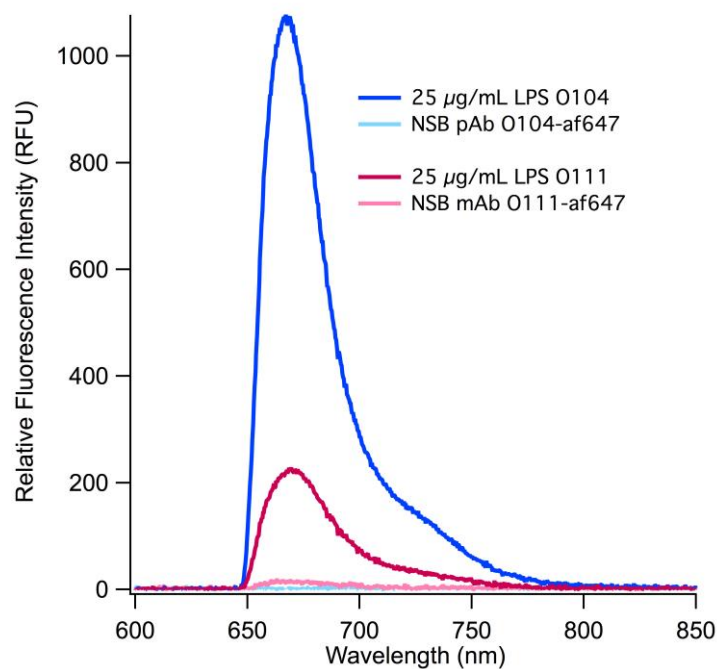


**Figure 6.4. O-ag targeted detection of LPS.** Using membrane insertion, two types of LPS were detected using their complement antibodies, polyclonal anti-*E. coli* O104 (pAb O104) and monoclonal anti-*E. coli* O111 (mAb O111) labeled with af647.

A key factor that affects performance of any antibody-based assay is the sensitivity and specificity of the antibody being used. In membrane insertion, the amphiphilic antigen is presented partitioned into a lipid bilayer, which mimics the physiological presentation of such antigens *in vivo*. The antibody targeting LPS O104 is a polyclonal, extracted from an animal immunized with whole bacteria, and likely is more suitable for recognizing LPS when presented in a lipid carrier interface.

In contrast, the antibody against LPS O111:H11, is monoclonal, and was raised *in vitro*. Also, pAb have multiple paratopes that can bind several different epitopes on the antigen, as compared to mAbs that target a single epitope. The source animal for antibodies may also play a large role in antibody affinity and specificity, since it has been demonstrated that different animal types exhibit varied levels of sensitivity to LPS,<sup>11,75</sup> which would affect antibody expression. The above factors in antibody specificity and sensitivity are not unique to the two that are discussed here or to the membrane insertion approach, but indeed should be considered in the development of all assays involving detection antibodies.

#### 6.4.2 Imaging LPS-lipid bilayer interactions inside a flow cell

We have used fluorescence microscopy<sup>10</sup> as a tool to characterize amphiphile-lipid interactions, thereby building more robust membrane insertion assays for these difficult antigens. Previously, we have shown that LPS O111:B4 can form holes in supported lipid bilayers<sup>10,76</sup> using fluorescence microscopy. It therefore became imperative to determine whether LPS forms holes in a supported bilayer under the conditions of the membrane insertion assay. To investigate this, we developed an imaging compatible flow cell model (**Figure 6.5 A**) that replicated the internal dimensions and functional surfaces of the flow cell used in our waveguide-based assays (**Figure 6.5 B**). This model enabled direct imaging of lipid bilayers, as well as the specific binding of the fluorescent antibodies to LPS (**Figure 6.5 C-F**). We investigated the effects of LPS O111:B4 (**Figure 6.5 C-D**) and LPS O157 at 100 µg/mL, 50 µg/mL, and 25 µg/mL (**Figure 6.5 E-F**), under the same conditions as the waveguide assays. We found that with LPS O157, the lipids maintained excellent lateral fluidity (**Figure A5.3**) and there was no hole formation in the bilayers at any of the tested concentrations, thereby eliminating our concerns. LPS O111:B4, on the other hand, formed holes in lipid bilayers (**Figure 6.5 C**) within the flow cell, but only at higher concentrations of antigen (>50 µg/mL) (**Figure 6.5 D**). No hole formation was observed at lower, more physiologically relevant concentrations of LPS (**Figure 6.5 D**). We were also able to generate composite images of the fluorescent lipids and the specific binding of pAb O157-af647 (**Figure 6.5 E-F**) at localized spots

within the flow cell for LPS O157. As demonstrated by the lack of overall red fluorescence (**Figure A5.4**) in the images, the NSB of the antibody is quite low, while the specific binding intensity is saturated at localized positions. This data supports the low NSB signals seen in the membrane insertion assays.

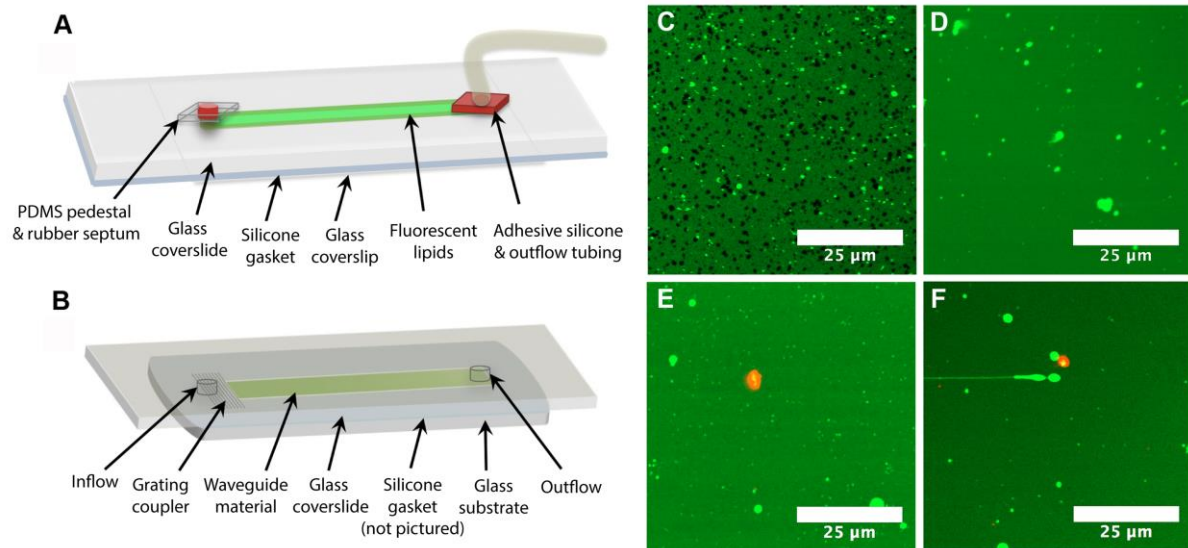


**Figure 6.5. Assay performance inside flow cells.** Schematics of (A) imaging flow cell and (B) waveguide flow cell. Major differences between these two flow cells include replacement of the waveguide glass substrate with a thin glass coverslip for imaging, and the addition of PDMS and silicone pedestals to create an airtight environment to preserve lipid integrity throughout an assay. (C) 100 µg/mL and (D) 50 µg/mL LPS O111:B4 incubated with BODIPY labeled DOPC lipids. Composite images of (E) 50 µg/mL and (F) 25 µg/mL LPS O157 bound by fluorescently labeled pAb O157-af647.

#### 6.4.3 Imaging LPS subtypes on glass slides

We evaluated the effect of 50 µg/mL LPS from various serogroups (O26, O45, O103, O104, O111, O113, O121, and O145) on open cover slides to observe membrane dynamics. LPS is an indicator of bacterial virulence, which in turn varies significantly between serotypes. Thus, our simplistic model may provide some insight into bacterial virulence. Surprisingly, no membrane deformation was observed in any of the LPS serogroups (**Figures 6.6 and A5.5**), except LPS O111:B4 (**Figure A5.5**), as anticipated.<sup>10</sup> The variability between these sub-types of LPS, and the difference in interactions with a simple lipid bilayer, are intriguing. Since the structure of the O-ag chain affects the CMC of LPS,<sup>17</sup> the size and shape of the micelle produced in an aqueous medium can be different between serotypes. Additionally, differences in O-ag structure combined with possible chemical

signature differences in the core polysaccharide of LPS<sup>77</sup> between strains could contribute to a variable charge distribution in the LPS.<sup>78,79</sup> This, in turn, could affect the delamination of the lipid bilayer by LPS micelles. Lastly, there is the potential for capsular K polysaccharide antigens to be co-expressed in these different preparations of LPS,<sup>80</sup> which we are working to confirm with nuclear magnetic resonance spectroscopy. In addition, we are exploring the effect of factors such as complex lipids, temperature, and pH on hole formation with different serogroups of LPS, to be reported in future studies.

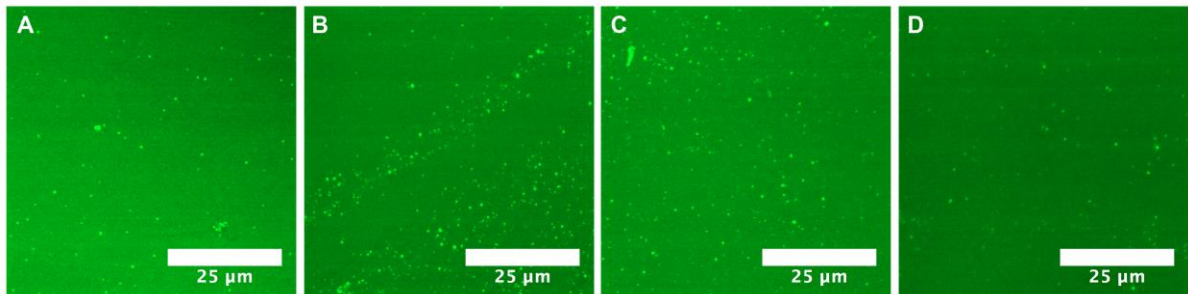


**Figure 6.6. Imaging LPS O157 with lipid bilayers.** (A) Bilayer prior to incubating with LPS O157. 50 µg/mL LPS (B) O157, (C) O104, and (D) O111:H11.

## 6.5 Conclusion

In conclusion, we have shown that LPS can be sensitively detected in complex beef lysate samples using membrane insertion with higher s:n ratios than those seen in the benchmark assays. The micellar properties of LPS in aqueous media, be it buffer or complex samples, affect the interaction at high concentrations, causing the assay to be non-linear. However, we can consistently and reliably measure LPS in complex samples using this method, making this an effective tool for detection of amphipathic biomarkers in complex backgrounds.

We have also shown that LPS from multiple serotypes do not induce membrane deformation in supported lipid bilayers at concentrations less than 50 µg/mL at room temperature. The imaging of amphiphilic interactions with supported lipid bilayers in a closed system (a.k.a. a flow cell) is a useful experimental tool that can be utilized for many similar studies. Since LPS is globally used as an immune stimulant and a key indicator of bacterial infection, the continued study of this

molecule is critical for understanding host-pathogen interactions and developing better amphiphilic detection platforms.

These studies demonstrate the challenges associated with the measurement of amphiphilic biomarkers such as LPS. Previous studies reporting the poor sensitivity of assays for the direct detection of LPS and other biomarkers in aqueous milieu, such as blood, have ignored their amphipathic biochemistry. With this manuscript and others, we hope to unravel the challenges associated with the detection of such biomarkers in clinically relevant samples, and develop strategies to overcome them effectively in the future.

## **6.6 Acknowledgments**

The authors would like to thank several people who dedicated time towards helping with the ideas and development of this paper. Many thanks to Dr. Andrew Shreve, Dr. Peter Adams, Dr. Aaron Collins, Dr. Pearlson Prashanth, and Dr. Rama Sakamuri for method development, data analysis, imaging troubleshooting, and training. Additionally we would like to thank Mr. Aaron Anderson and Mr. Matthew Rush for their technical help and suggestions. Thank you to Dr. Zach Stromberg for re-purification of LPS O121. Thanks to Dr. Basil Swanson, Karen Grace and W. Kevin Grace, of LANL who developed the waveguide biosensor platform. Thanks to Drs. Swanson, Chaudhary, and Mukundan for conception, design, and testing of the membrane insertion assay. We also thank the STEC Center at Michigan State University, and Dr. John Luchansky for providing the STEC strains.

This work was performed, in part, at the Center for Integrated Nanotechnologies, an Office of Science User Facility operated for the United States Department of Energy's Office of Science. Los Alamos National Laboratory, an affirmative action equal opportunity employer, is operated by Los Alamos National Security, LLC, for the National Nuclear Security Administration of the United States Department of Energy under contract No. DE-AC52-06NA25396. Work by G. A. M and K.L.S. was supported by Photosynthetic Antenna Research Center, an Energy Frontier Research Center funded by the United States Department of Energy, Office of Science, Basic Energy Sciences under Award No. DE-SC0001035. H.M., R.A.M,

S.W.G and L.R. S. were supported by Agriculture and Food Research Initiative Competitive Grant No. 2012-68003-30155 from the United States Department of Agriculture's National Institute of Food and Agriculture. N.H was supported by Los Alamos National Laboratory Directed Research Award, Integrative Biosurveillance (Mukundan and McMahon).

## 6.7 References

- (1) Gyles C.L. Shiga toxin-producing *Escherichia coli*: An overview. J Anim Sci. **2007**, 85(13\_suppl): E45-E62.
- (2) Aderem A. and Ulevitch R.J. Toll-like receptors in the induction of the innate immune response. Nature. **2000**, 406(6797), 782–787.
- (3) Dobrovolskaia M.A. and Vogel S.N. Toll receptors, CD14, and macrophage activation and deactivation by LPS. Microbes Infect. **2002**, 4(9), 903-914.
- (4) Nikaido H. and Vaara M. Molecular basis of bacterial outer membrane permeability. Microbiol Rev. **1985**, 49(1), 1-32.
- (5) Akira S. and Hemmi H. Recognition of pathogen-associated molecular patterns by TLR family. Immunol Lett. **2003**, 85(2), 85-95
- (6) Takeda K. and Akira S. Toll-like receptors in innate immunity. Int Immunol. **2005**, 17(1), 1–14.
- (7) Galloway S.M. and Raetz C.R. A mutant of *Escherichia coli* defective in the first step of endotoxin biosynthesis. J Biol Chem. **1990**, 265(11), 6394–6402.
- (8) Meredith T.C. *et al.* Redefining the requisite lipopolysaccharide structure in *Escherichia coli*. ACS Chem Biol. **2006**, 1(1), 33–42.
- (9) Raetz C.R.H. *et al.* Discovery of new biosynthetic pathways: the lipid A story. J Lipid Res. **2009**, 50(Suppl), S103–8.
- (10) Adams P.G. *et al.* Lipopolysaccharide-Induced Dynamic Lipid Membrane Reorganization: Tubules, Perforations, and Stacks. Biophys J. **2014**, 106(11), 2395–2407.
- (11) Berczi I. *et al.* Comparative studies on the toxicity of *Escherichia coli* lipopolysaccharide endotoxin in various animal species. Can J Micro. **1966**, 12(5), 1070-1071.
- (12) Cohen J. The immunopathogenesis of sepsis. Nature. **2002**, 420(6917), 885-891.
- (13) Levine D.M. *et al.* In vivo protection against endotoxin by plasma high density lipoprotein. Proc Natl Acad Sci USA. **1993**, 90(24), 12040-12044.
- (14) Raetz C.R. Bacterial endotoxins: extraordinary lipids that activate eucaryotic signal transduction. J Bacteriol. **1993**, 175(18), 5745.
- (15) Takada H. and Kotani S. Structural requirements of lipid A for endotoxicity and other biological activities. Crit Rev Microbiol. **1989**, 16(6), 477-523.
- (16) Erridge C. *et al.* Structure and function of lipopolysaccharides. Microbes Infect. **2002**, 4(8), 837–851.
- (17) Aurell C.A. and Wistrom A.O. Critical aggregation concentrations of gram-negative bacterial lipopolysaccharides (LPS). Biochem Biophys Res Commun. **1998**, 253(1), 119–123.
- (18) Schumann R.R. *et al.* Structure and function of lipopolysaccharide binding protein. Science. **1990**, 249(4975), 1429–1431.
- (19) Vreugdenhil A.C. *et al.* LPS-binding protein circulates in association with apoB-containing lipoproteins and enhances endotoxin-LDL/VLDL interaction. J Clin Invest. **2001**, 107(2), 225–234.
- (20) Nikaido H. Molecular basis of bacterial outer membrane permeability revisited. Microbiol Mol Biol Rev. **2003**, 67(4), 593–656.
- (21) Stenutz R. *et al.* The structures of *Escherichia coli* O-polysaccharide antigens.

- FEMS Microbiol Rev. **2006**, 30(3), 382–403.
- (22) Nigou J. *et al.* Lipoarabinomannans: from structure to biosynthesis. *Biochimie*. **2003**, 85(1-2), 153-166.
  - (23) Sutcliffe I. Lipoarabinomannans—structurally diverse and functionally enigmatic macroamphiphiles of mycobacteria and related actinomycetes. *Tuberculosis (Edinb)*. **2005**, 54(4), 205-6
  - (24) Samuel G. *et al.* Relationships of the *Escherichia coli* O157, O111, and O55 O-antigen gene clusters with those of *Salmonella enterica* and *Citrobacter Freundii*, which express identical O antigens. **2004**, 186(19), 6536-43.
  - (25) Sada E. *et al.* Detection of lipoarabinomannan as a diagnostic test for tuberculosis. *J Clin Microbiol*. **1992**, 30(9), 2415-2418.
  - (26) Boehme C. *et al.* Detection of mycobacterial lipoarabinomannan with an antigen-capture ELISA in unprocessed urine of Tanzanian patients with suspected tuberculosis. *Trans R Soc Trop Med Hyg*. **2005**, 99(12), 893-900.
  - (27) Takahashi K. *et al.* Detection of lipopolysaccharide (LPS) and identification of its serotype by an enzyme-linked immunosorbent assay (ELISA) using poly-L-lysine. *J Immunol Methods*. **1992**, 153(1-2), 67–71.
  - (28) Karch H. *et al.* Epidemiology and diagnosis of Shiga toxin-producing *Escherichia coli* infections. *Diagn Microbiol Infect Dis*. **1999**, 34(3), 229-243.
  - (29) Lamoureux L. *et al.* An optical biosensor for detection of pathogen biomarkers from Shiga toxin-producing *Escherichia coli* in ground beef samples. *Proc SPIE Int Soc Opt Eng BiOS*. **2015**, 9310, 931004-931004.
  - (30) Šafaříková M, and Šafařík I. Immunomagnetic separation of *Escherichia coli* O26, O111 and O157 from vegetables. *Lett Appl Microbiol*. **2001**, 33(1), 36-39.
  - (31) Sowers E.G. *et al.* Evaluation of commercial latex reagents for identification of O157 and H7 antigens of *Escherichia coli*. *J Clin Microbiol*. **1996**, 34(5), 1286-1289.
  - (32) Stromberg L.R. *et al.* Purification and characterization of lipopolysaccharides from six strains of non-O157 Shiga toxin-producing *Escherichia coli*. *J Microbiol Methods*. **2015**, 116, 1-7.
  - (33) Brooks B.W. *et al.* Evaluation of a monoclonal antibody-based enzyme-linked immunosorbent assay for detection of *Campylobacter fetus* in bovine preputial washing and vaginal mucus samples. *Vet Microbiol*. **2004**, 103(1-2), 77-84.
  - (34) Hegde N.V. *et al.* Detection of the top six non-O157 Shiga toxin-producing *Escherichia coli* O groups by ELISA. *Foodborne Pathog Dis*. **2012**, 9(11), 1044–1048.
  - (35) Mohammed A.H. *et al.* Development and evaluation of an enzyme-linked immunosorbent assay for endotoxin in milk. *Vet Microbiol*. **1988**, 18(1), 27–39.
  - (36) Gall D. and Nielsen K. Improvements to the competitive ELISA for detection of antibodies to *Brucella abortus* in cattle sera. *J Immunoassay*. **1994**, 15(3), 277-291.
  - (37) Alonso-Urmeneta B, *et al.* Evaluation of lipopolysaccharides and polysaccharides of different epitopic structures in the indirect enzyme-linked immunosorbent assay for diagnosis of brucellosis in small ruminants and cattle. *Clin Diagn Lab Immunol*. **1998**, 5(6), 749-754.
  - (38) Bai J. *et al.* Applicability of a multiplex PCR to detect the seven major Shiga

- toxin-producing *Escherichia coli* based on genes that code for serogroup-specific O-antigens and major virulence factors in cattle feces. *Foodborne Pathog Dis.* **2012**, 9(6), 541–548.
- (39) Perelle S. Detection by 5'-nuclease PCR of Shiga-toxin producing *Escherichia coli* O26, O55, O91, O103, O111, O113, O145 and O157:H7, associated with the world's most frequent clinical cases. *Mol Cell Probes.* **2004**, 18(3), 185–192.
  - (40) Son I. *et al.* Detection of five Shiga toxin-producing *Escherichia coli* genes with multiplex PCR. *Food Microbiol.* 2014, 40, 31–40.
  - (41) Fode-Vaughan K.A. *et al.* Direct PCR detection of *Escherichia coli* O157:H7. *Lett Appl Microbiol.* **2003**, 37(3), 239–243.
  - (42) Alam J.M. and Yamazaki M. Spontaneous insertion of lipopolysaccharide into lipid membranes from aqueous solution. *Chem Phys Lipids.* **2011**, 164(2), 166–174.
  - (43) Mukundan H. *et al.* Understanding the interaction of Lipoarabinomannan with membrane mimetic architectures. *Tuberculosis (Edinb).* **2012**, 92(1), 38–47.
  - (44) Sakamuri R.M. *et al.* Novel optical strategies for biodetection. *Proc SPIE Int Soc Opt Eng NanoScience* **2013**, 8812, 881209-8812-09.
  - (45) Wurfel M.M. and Wright SD. Lipopolysaccharide-binding protein and soluble CD14 transfer lipopolysaccharide to phospholipid bilayers: preferential interaction with particular classes of lipid. *J Immunol.* **1997**, 158(8), 3925–3934.
  - (46) Wurfel M.M. *et al.* Lipopolysaccharide (LPS)-binding protein is carried on lipoproteins and acts as a cofactor in the neutralization of LPS. *J Exp Med.* **1994**, 180(3), 1025–1035.
  - (47) Sakamuri R.M. *et al.* Detection of stealthy small amphiphilic biomarkers. *J Microbiol Methods.* **2014**, 103, 112-117.
  - (48) Mukundan H. *et al.* Rapid detection of *Mycobacterium tuberculosis* biomarkers in a sandwich immunoassay format using a waveguide-based optical biosensor. *Tuberculosis (Edinb).* **2012**, 92, 407–416.
  - (49) Sakamuri R.M. *et al.* Association of lipoarabinomannan with high density lipoprotein in blood: Implications for diagnostics. *Tuberculosis (Edinb).* **2013**, 93(3), 301–307.
  - (50) Mukundan H. *et al.* Optimizing a waveguide-based sandwich immunoassay for tumor biomarkers: evaluating fluorescent labels and functional surfaces. *Bioconjug Chem.* **2009**, 20(2), 222–230.
  - (51) Mukundan H. *et al.* Planar optical waveguide-based biosensor for the quantitative detection of tumor markers. *Sens Actuators B Chem.* **2009**, 138(2), 453-460.
  - (52) Kale R.R. *et al.* Detection of Intact Influenza Viruses using Biotinylated Biantennary S-Sialosides. *J Am Chem Soc.* **2008**, 130(26), 8169–8171.
  - (53) Martinez J.S. *et al.* Pathogen detection using single mode planar optical waveguides. *J Mater Chem.* 2005, 15, 4639-4647.
  - (54) Mukundan H. *et al.* Waveguide-Based Biosensors for Pathogen Detection. *Sensors (Basel).* **2009**, 9(7), 5783–5809.
  - (55) McIntosh T.J. Short-range interactions between lipid bilayers measured by X-

- ray diffraction. *Curr Opin Struct Biol.* **2000**, 10(4), 481–485.  
doi:10.1016/S0959-440X(00)00118-4
- (56) Mukundan H. *et al.* Quantitative multiplex detection of pathogen biomarkers on multichannel waveguides. *Anal Chem.* **2010**, 82(1), 136–144.
  - (57) Mukundan H. *et al.* Toward photostable multiplex analyte detection on a single mode planar optical waveguide. *Proc SPIE Int Soc Opt Eng BiOS.* **2009**, 7553, 71670A-71670A.
  - (58) Bergstrand A. *et al.* Aggregation behavior and size of lipopolysaccharide from *Escherichia coli* O55:B5. *Colloids Surf B Biointerfaces.* **2006**, 53(1), 9–14.
  - (59) Santos N.C. *et al.* Evaluation of lipopolysaccharide aggregation by light scattering spectroscopy. *ChemBioChem.* **2003**, 4(1), 96-100
  - (60) Shnyra A. Role of the physical state of Salmonella lipopolysaccharide in expression of biological and endotoxic properties. *Infect Immun.* **1993**, 61(12), 5351-5360.
  - (61) James E.A. *et al.* Detection of endotoxin using an evanescent wave fiber-optic biosensor. *Appl Biochem Biotechnol.* **1996**, 60(3), 189-202.
  - (62) Ruckenstein E. and Nagarajan R. Critical micelle concentration. Transition point for micellar size distribution. *J Phys Chem.* **1975**, 79(24), 2622–2626.
  - (63) Nowotny A. Heterogeneity of endotoxins. *Handbook of endotoxin;* **1984**, 1, 308-338.
  - (64) Jucker B.A. *et al.* Polymer interactions between five gram-negative bacteria and glass investigated using LPS micelles and vesicles as model systems. *Colloids Surf B Biointerfaces.* **1998**, 11(1), 33-45.
  - (65) Moroi Y. CMC range due to polydispersity of micelles. *J Colloid Interface Sci.* **1991**, 141(2), 581-583.
  - (66) Borovikova L.V. *et al.* Vagus nerve stimulation attenuates the systemic inflammatory response to endotoxin. *Nature.* **2000**, 405(6785), 458-462.
  - (67) Reinhold R.B and Fine J. A technique for quantitative measurement of endotoxin in human plasma. *Proc Soc Exp Biol Med.* **1971**, 137(1), 334-340.
  - (68) Din Z.Z. *et al.* Effect of pH on solubility and ionic state of lipopolysaccharide obtained from the deep rough mutant of *Escherichia coli*. *Biochemistry.* **1993**, 32(17), 4579-4586.
  - (69) Petsch D. *et al.* Anspach FB. Endotoxin removal from protein solutions. *J Biotechnol.* **2000**, 76(2-3), 97-119.
  - (70) Sharma S.K. Endotoxin detection and elimination in biotechnology. *Biotechnol Appl biochem.* **1986**, 8(1), 5-22.
  - (71) Harrison M. *et al.* Lipoprotein particle distribution and skeletal muscle lipoprotein lipase activity after acute exercise. *Lipids Health Dis.* **2012**, 11, 64.
  - (72) Viktorov A.V. and Yurkiv V.A. Binding of lipopolysaccharide and complexes of lipopolysaccharide to serum low density lipoproteins to liver macrophages. *Biomed Khim.* **2007**, 52(1), 36–43.
  - (73) Chien J.Y. *et al.* Low serum level of high-density lipoprotein cholesterol is a poor prognostic factor for severe sepsis. *Crit Care Med.* **2005**, 33(8), 1688–1693.
  - (74) Opal S.M. and Yu R.L. Antiendotoxin strategies for the prevention and treatment of septic shock. *New approaches and future directions. Drugs.* **1998**,

- 55, 497–508.
- (75) Redl H. *et al.* Clinical detection of LPS and animal models of endotoxemia. *Immunobiology*. **1993**, 187(3-5), 330-345.
  - (76) Adams P.G. *et al.* Exploiting lipopolysaccharide-induced deformation of lipid bilayers to modify membrane composition and generate two-dimensional geometric membrane array patterns. *Sci Rep*. **2015**, 5, 10331.
  - (77) Silipo, A. and Molinaro, A. The Diversity of the Core Oligosaccharide in Lipopolysaccharides. *Subcell Biochem* **2010**, 53, 69–99.
  - (78) Seydel U. *et al.* Chemical structure, molecular conformation, and bioactivity of endotoxins. *Chem Immunol*. **2000**, 74, 5–24.
  - (79) Schromm A.B. *et al.* Biological activities of lipopolysaccharides are determined by the shape of their lipid A portion. *Eur J Biochem*. **2000**, 267(7), 2008–2013.
  - (80) Whitfield C. Biosynthesis and Assembly of Capsular Polysaccharides in *Escherichia coli*. *Annu Rev Biochem*. **2006**, 75, 39–68.

## Chapter 7. Understanding the *in vitro* effects of differential LPS presentation

### 7.1 Introduction

In bacteria, LPS serves to protect cells by reducing membrane permeability against foreign materials, such as antibiotics, peptides, enzymes, and protecting from changes in pH.<sup>1,2</sup> LPS also defines pathogen serogroup and is a key indicator of virulence.<sup>3-5</sup> In mammals, LPS falls into a special category of bacterial antigens called pathogen associated molecular patterns (PAMPs). PAMPs are evolutionarily conserved molecules which bind innate immune receptors in the host to facilitate the initial and adaptive immune response.<sup>6-10</sup> Low concentrations of LPS serve as an early indicator of infection through stimulation of Toll-like receptor 4 (TLR4) to induce immune response.<sup>11-13</sup> Because of this function, derivatives of LPS have also been tested as vaccine adjuvants,<sup>14</sup> and often LPS is used to study the pathways of immune diseases.<sup>15-17</sup> The continued study of LPS interactions with biomimetic systems is critical for advancing our understanding of this complex molecule and its physiological interactions.

Structurally, LPS is an amphiphilic molecule made up of three primary components, the hydrophobic lipid A, also called endotoxin, the core polysaccharide, and the O polysaccharide antigen<sup>18,19</sup>. The amphipathic nature of LPS is not to be trivialized. This unique biochemistry allows association of the molecule with several structures, such as; the outer membrane of Gram-negative pathogens,<sup>20</sup> membranes of eukaryotic cells,<sup>21</sup> liposomes,<sup>22,23</sup> lipid bilayers,<sup>24</sup> giant unilamellar vesicles,<sup>25</sup> serum binding proteins,<sup>26,27</sup> antibiotics,<sup>28</sup> and a host of other molecules which specifically bind the lipid A component.<sup>29-34</sup> In addition to this, LPS is often found as a micelle in aqueous systems,<sup>35-37</sup> as the hydrophobic lipid A group sequesters away from the hydrophilic media to lower the free energy of the structures. In physiological *in vivo* systems, the hydrophobic portion of LPS allows it to be taken up by serum carrier proteins such as high- and low- density lipoproteins (HDL, LDL)<sup>27,38-40</sup> as well as LPS Binding protein (LBP).<sup>26,41,42</sup> HDL and LDL are known to specifically sequester lipid A into the lipoprotein nanodisc structure, composed of cholesterol and triacylglycerides.<sup>43,44</sup> LBP has a hydrophobic binding pocket where it binds lipid A,

but has also been demonstrated to transfer other phospholipids as well.<sup>23,45-47</sup> Together, these lipoproteins facilitate clearance of LPS through the liver,<sup>42,48,49</sup> or transfer LPS to receptors on immune cells.<sup>23,50</sup> It is also through the mechanisms of these carrier proteins by which protective or inflammatory outcomes can result,<sup>51</sup> depending on the circumstances by which LPS is introduced to the host.<sup>52,53</sup> While it is well known that these serum carriers bind and are responsible for presenting LPS to cells,<sup>51</sup> many studies present LPS to cells in an aqueous buffer system rather than with its physiological protein carriers, which can attenuate cytokine response.<sup>51</sup> Upon presentation and subsequent activation of TLR4, LPS induces a pro-inflammatory cascade of cytokines, which serve many functions. However, over stimulation of the immune system by LPS, can result in a severe condition known as sepsis, in which tissues and organs start to degrade.<sup>54</sup> The cytokines typically associated with an LPS induced response are IL-1, TNF $\alpha$ , and IL-6, but other cytokines such as IL-12, IP-10, and MIP-2 have also been demonstrated to be expressed in macrophages.<sup>52</sup>

A simplified version of LPS-induced cytokine expression begins with activation of the TLR4 receptor. This activation results in the *de novo* synthesis of IL-1 $\alpha$  in macrophages. IL-1 $\alpha$  is often referred to as a damage associated molecular pattern (DAMP). The primary function of DAMPs is to signal to immune cells the presence of danger signals, which cause the cell to undergo a form of programmed cell death. When IL-1 $\alpha$  binds its receptor, it causes recruitment of proteins that leads to the activation of nuclear factor kappa beta (NF- $\kappa$ B). NF- $\kappa$ B then binds to receptors on the nucleus to initiate transcription and translation of other cytokines, such as IL-1 $\beta$ , TNF $\alpha$ , IL-6, and IL-12. Together with a host of other chemokines, these signals work to recruit other cells to deal with infection and build an adaptive immune response.<sup>55,56</sup> However, there are many conflicting reports on LPS-mediated induction of cytokines and chemokines, which makes it difficult to interpret the biological significance of these findings.

There is mounting evidence that a direct mechanism of LPS interacting with cell membranes may exist. The interaction of LPS with simple biomimetic systems, such as supported lipid bilayer assemblies (sLBAs), has been shown to cause dynamic deformation of these membranes.<sup>24,57</sup> Other researchers have documented

the presence of fluorescent LPS micelles inside cells,<sup>21</sup> indicating possibility of passive diffusion. Schromm *et al.*<sup>58</sup> demonstrated a CD14 independent mechanism by which LPS was transferred directly into a phospholipid membrane. Another amphiphilic lipopeptide called surfactin has been demonstrated to induce leakage in phospholipid vesicles.<sup>59</sup> Thus, it can be speculated that direct interaction of LPS with phospholipids can cause cell membrane damage and altered cytokine response.

With all the inherent variability, it is clear that the choice of model system dramatically impacts the outcome of any study that uses LPS. Addressing all these potential variations is beyond the scope of this research. *Our goal is to simply demonstrate the significance of the choice of model system for amphiphilic LPS.* For the purposes of this dissertation, we asked two simple questions and designed experimental systems to specifically answer them.

- 1) Does the complexity of cell membranes inhibit LPS induced deformation? To address this, we created sLBAs with increasing complexity and studied the effect of this modification on LPS-induced hole formation.
- 2) Does presentation of LPS in physiological systems affect its interaction with membranes and associated innate immune receptors? To address this, we chose to compare LPS-mediated cytokine and chemokine induction in cell lines with/without TLR4 when the antigen was presented in serum vs. buffer.

### 7.1.1 Model sLBAs

sLBAs are simple systems, which do not accurately represent the complexity of the surface of a cell. Model membranes often combine different lipids of varying fluid transition temperatures, or membrane proteins to simulate a more complex membrane surface.<sup>60,61</sup> Such membranes have been used to study the effects of direct incorporation of LPS, and its effects on membrane fluidity.<sup>62,63</sup> LBP has also been used to study the interaction of LPS with lipids and membranes.<sup>64,65</sup> To the best of our knowledge, no one has investigated whether LPS forms holes or other deformities in model sLBAs. We began with simple sLBAs and gradually increased their complexity by enriching with biomimetic lipids, such as sphingomyelin and cholesterol. This approach evaluated whether the degree of membrane complexity

can prevent or affect the mechanism of LPS-induced hole formation, and provides us with information about developing biomimetic sensors for LPS, as well as the *in vivo* mechanisms of inflammation.

#### 7.1.2 Cell lines with and without TLR4

We analyzed the LPS-induced inflammatory cytokines in both TLR4(+) and TLR4(-) cell lines in the presence of murine serum, delipidated serum, and no serum (buffer control). Since LPS is associated with serum proteins in physiological systems, we wanted to explore the impact of this association and its ability to stimulate innate immune response. Also, we asked the question if LPS in buffer can induce deformities in cells, irrespective of the presence of TLRs. Cytokines or chemokines expressed by a TLR4 deficient cell line could be one potential indicator of direct cell membrane damage. Taken together, these findings could have significant impact on our understanding of the mechanisms of LPS signaling, thereby effecting bacterial targeting, immunology, and vaccine research. These experiments not only address the specific questions outlined above, but also provide valuable information for the future design of amphiphilic detection assays.

## 7.2 Materials and Methods

### 7.2.1 Materials

Lipids and fluorescence dyes were purchased in powdered form and reconstituted per manufacturer's instructions. 1,2-dioleoyl-*sn*-glycero-3-phosphocholine (DOPC), 5-cholesten-3 $\beta$ -ol 12-[(7-nitro-2-1,3-benzoxadiazol-4-yl)amino]dodecanoate (NBD-Cholesterol), egg sphingomyelin (SM), and cholesterol from ovine wool were all purchased from Avanti<sup>®</sup> Polar Lipids. Fluorescent dyes for doping the lipids were as follows: 2-(4,4-difluoro-5,7-dimethyl-4-bora-3a,4a-diaza-s-indacene-3-pentanoyl)-1-hexadecanoyl-*sn*-glycero-3-phosphocholine (BODIPY) or Texas Red 1,2-dihexadecanoyl-*sn*-glycero-3-phosphoethanolamine, triethylammonium salt (Texas Red DHPE) (Molecular Probes). An AlexaFluor 488-conjugate of LPS from *E. coli* serotype O111:B4 was used to assess LPS uptake into bilayers (Molecular Probes). Studies with lipid bilayers and *in vitro* 12-plex

cytokine assays used LPS O111:B4 (phenol extract, Sigma Aldrich). For *in vitro* 25-plex cytokine assays, ULTRA PURE LPS O111:B4 (List Labs) was used to minimize the potential for protein contamination. All other forms of LPS used were purified by us as previously described.<sup>66</sup> Antibodies used for immunodepletion; polyclonal anti-apolipoprotein A-I (pAb ApoAI), polyclonal anti-apolipoprotein B (pAb ApoB), and polyclonal anti-lipopolysaccharide binding protein (pAb LBP) were from Antibodies-Online. Monoclonal anti-LBP (clone U54.R.mLBP.2, immunoglobulin M, rat) was from BEI Resources NIAID NIH. SPHERO™ carboxyl cross-linked magnetic particles (dia. 1.22 μm, Spherotech™) were used for immunomagnetic separation (IMS). Chemicals for preparation of IMS beads were: N-hydroxysulfosuccinimide (Sulfo-NHS), sodium azide, sodium tetraborate (all from ThermoFisher Scientific); and phosphate buffered saline (PBS), 1-ethyl-3-(3-dimethylaminopropyl) carbodiimide hydrochloride (WSC), Boric acid, glycine, and (3-(*N*-morpholino)propanesulfonic acid) (MOPS) (all from Sigma Aldrich).

### 7.2.2 Lipid and bilayer preparations

DOPC liposome preparations were prepared as 99.5% (mol/mol) DOPC to 0.5% BODIPY or 0.5% TR-DHPE. Lipids and dyes were mixed to the desired ratio, then dried overnight under vacuum and prepared to a final concentration of 2 mM DOPC in PBS. Liposomes containing (5%-15%) sphingomyelin, (25-50%) cholesterol, or (25-50%) NBD-cholesterol were prepared in a similar manner. When calculating the molar ratio of NBD-cholesterol we excluded the molecular weight of the NBD head group to obtain a more accurate ratio of cholesterol:DOPC. We also prepared liposomes with mixtures of sphingomyelin and cholesterol. The lipid suspensions were subjected to six freeze-thaw cycles followed by probe sonication for 10 min in an ice bath to form small liposomes. Glass coverslips were cleaned with a 3:1 solution of H<sub>2</sub>SO<sub>4</sub>/30% H<sub>2</sub>O<sub>2</sub> for 40 min and then rinsed three times with deionized water. Hydrophobic imaging spacers (0.12 mm x 9 mm, Electron Microscopy Sciences) were placed on substrates to confine the lipid bilayers. Lipids were deposited into the wells created by the spaces, and incubated for 20 min, R/T.

To remove excess liposomes, sLBAs were washed by pipetting 1x PBS, ten times over the lipids.

### *7.2.3 LPS interactions with sLBAs*

Prior to treatment of sLBAs with LPS, the LPS stocks (5 mg/mL) were bath sonicated for 15 min, diluted with PBS to a working concentration and then sonicated an additional 15 min. The sLBAs were then treated with LPS, for 20 min at R/T, unless otherwise specified. To perform experiments at elevated temperatures, substrates with LPS were covered in glass petri dishes and a droplet of water was added every 30 min to account for evaporated water and maintain the LPS concentration. After incubation with LPS, the sLBAs were rinsed with 6 exchanges of PBS and then assessed for fluidity using Fluorescence Recovery After Photobleaching (FRAP).

### *7.2.4 Microscopy*

Lipid bilayers were imaged with laser scanning confocal fluorescence microscopy (LSCM) and fluorescence microscopy. Samples were kept hydrated and never allowed to dry either during preparation or analysis. LSCM was performed with an FV-1000 inverted optical microscope (Olympus) equipped with photomultiplier detectors, and operated in 'photon-counting mode'. Images were acquired using a 40x objective, at 1024 x 1024 or 2048 x 2048 pixels using a 12.5  $\mu\text{m}/\text{sec}$  scan rate. FRAP movies were obtained at 512 x 512, 10  $\mu\text{m}/\text{sec}$ , using the manufacturer's provided software. Excitation was provided by a multi line Ar laser (488 nm, for BODIPY), a HeNe laser (543 nm, for TR-DHPE), or a diode laser (635 nm, for AlexaFluor 647). Band-pass emission filters were used (505-525 nm for BODIPY and FITC; 655-755 nm for TR-DHPE and AlexaFluor 647). Images were processed using ImageJ 1.48v.

### *7.2.5 Preparation of IMS beads*

SPHERO™ carboxyl cross-linked magnetic particles were prepared for covalent antibody coupling first by rinsing the beads in sterile PBS, and then

washing twice in activation buffer (MOPS, pH 4.5). Beads were suspended (10 mg/mL) in fresh MOPS buffer, and 10 mg/mL of water-soluble carbodiimide, and 2.50 mg/mL of NHS-Sulfo was added to the solution and allowed to spin on a tube rotisserie for 30 min, at 25 °C (R/T). Particles were washed twice in coupling buffer (borate buffer, pH 7.2) and then re-suspended in fresh buffer. Required protein concentration for particle coating was determined by assuming a smooth particle surface, and a mean particle diameter of 1.22 µm. We used ten times the amount of protein necessary to obtain a monolayer protein coat on the particles. Antibodies were added to the bead suspension and mixed for 3 h at R/T. For anti-LBP particles we used a 2:1 mix of pAb LBP to mAb LBP due to the low concentration of the mAb LBP. The reaction was quenched for 1 h at R/T using a solution of 100 mM glycine + 0.05% BSA. The beads were rinsed with sterile PBS and then stored in 0.05% BSA + 0.02% sodium azide. Prior to use, beads were rinsed three times with PBS. To test the activity of the beads, they were immunoblotted with mouse serum, using a 1:1000 dilution of beads in PBS as the primary antibody.

#### *7.2.6 Immunodepletion of serum proteins from mouse serum*

To explore how the lipoprotein composition of serum affects cell lines we chose to immunodeplete the serum of the respective proteins ApoAI, ApoB, and LBP. To do this 5 mL of mouse serum (Sigma Aldrich) was mixed with 70 mg of the appropriate IMS beads. Beads were incubated with serum for 24 h at 4 °C on a rotisserie, and the serum poured off and retained. Beads were rinsed two times with PBS, and then the protein was eluted two times using 500 mM glycine buffer, and 30 min incubations at R/T. The separation process was repeated two more times for each aliquot of mouse serum, until enough serum was obtained. This was repeated for other lipoproteins using previously depleted serum (e.g. serum depleted of ApoAI, was then used for depletion of LBP to obtain ApoAI (-) LBP (-) serum). Serum was then assessed on SDS-PAGE gels and immunoblots to determine whether lipoproteins remained in the preparations. Serum aliquots were syringe filtered (0.2 µm) under laminar flow conditions prior to use in the cytokine assays.

We also assayed the serum preparations for cholesterol levels using an HDL/LDL/VLDL cholesterol assay kit (Abcam).

### 7.2.7 Cell lines

The IC-21 (TLR4 (+)) cell line was selected for the comparative study based on the *Mus musculus* strain from which the TLR4(-) cell line was originally derived, C57BL. Many studies use a similar murine macrophage, RAW 264.7, which is derived from BALB/c mice, but the IC-21 cells are specifically described as displaying normal macrophage behavior and antigens. TLR4(+) murine macrophages were grown in Dulbecco's modification of Eagle's medium (DMEM, Corning Cellgro®) supplemented with 10% fetal bovine serum (FBS, Sigma). Cells were cultured to 90% confluence and then harvested using a silicone cell scraper and split 1:4 as needed. LADMAC murine macrophages were grown in eagle's minimum essential medium (MEM, Corning Cellgro®) supplemented with 10% FBS and spun down every 4 days to harvest the media supernatant. Harvested media was sterile filtered using Autofil 0.1 µm vacuum flasks (USA Scientific) to eliminate the possibility of mycoplasma contamination. Media for the 23ScCr, TLR4(-), murine macrophages was made with DMEM + 10% FBS + 20% LADMAC media. No antibiotics or antimycotics were used at any time for any of the cell lines. 23ScCr's cells were split 1:4 as needed. 23ScCr and IC-21 cells were harvested after the seventh pass and then plated  $1.0 \times 10^6$  cells per well in 12-well plates (Costar®). Cells were incubated overnight at 37°C, 5% CO<sub>2</sub>, and then rinsed two times with serum free media prior to LPS exposure. All experimental groups for cytokine assays were performed in triplicate.

### 7.2.8 LPS induced cytokine expression in TLR4(+) and TLR4(-) cell lines

For 12-plex cytokine assays, LPS stocks were sonicated for 15 min, diluted to 100 ng/mL in serum free media, resonicated and then applied to wells. To use a serum supplemented system, sonicated LPS was spiked into mouse serum, vortexed intermittently for 2 min, then incubated overnight at 4°C to allow for association of LPS with lipoproteins. Cells were rinsed two times with serum free

media before application of media supplemented with 50% mouse serum + LPS. Negative control cells received DMEM + 50% mouse serum, but no LPS.

For the experiments using the 25-plex assays, the ULTRA PURE LPS was prepared as described above and added to the serum variants (experimental conditions defined in **Table 7.1**) immediately prior to dosing the cells. This was based on the low response we saw when using LPS that was allowed to incubate overnight with serum (**Figure A6.9**). Delipidated serum (d.serum, MP Biomedicals) was applied with the same method as whole serum, and was used as an additional control.

**Table 7.1 Experimental groups for cytokine studies.**

<u>Serum variants</u>	<u>Abbreviation</u>
50% mouse serum + 100 ng/mL LPS	serum + LPS
50% mouse serum (no LPS)	serum
50% delipidated mouse serum + 100 ng/mL LPS	d.serum + LPS
50% delipidated mouse serum (no LPS)	d.serum
no serum + LPS (buffer control)	'no serum' + LPS
no serum (no LPS) (buffer control)	'no serum'

Except for the time course assays (**Figure A6.8 A**), cells were incubated (37°, 5% CO<sub>2</sub>) for 8 h, after which media supernatant was collected and assayed for cytokine levels using either a 12-plex mouse inflammatory cytokines multi-analyte ELISArray™ kit (Qiagen®), or a 25-plex Milliplex® MAP mouse cytokine/chemokine Magnetic Kit (EMD Millipore). ELISA results were measured on a SpectraMax M5 (Molecular Devices) and plotted as the mean absorbance values with standard deviations of the replicates. 25-plex cytokine results were obtained using a MAGPIX® (Luminex), and standards were processed per manufacturer's instructions using a 5 parameter logistic function (5PL) on myassays.com. The resulting functions were used to calculate the concentration of expressed cytokines in pg/mL.

We also wanted to investigate the effect of FBS on murine cells, as previous studies we did demonstrated that 50% murine serum caused the adherent IC-21 cell line to detach from the substrate. Thus, by simply adding FBS we hoped to establish a new method for detaching the cells. We assayed these simultaneously with the 25-

plex cytokine kit to determine if there was an unforeseen effect caused by increasing the FBS serum concentration to 50%.

## **7.3 Results and discussion**

### *7.3.1 Model sLBAs: Increasing the complexity of sLBAs*

We investigated the effects of LPS-induced hole formation using three different compositions of complex bilayers: 25-50% cholesterol, 5-15% sphingomyelin, and combinations of the two. We evaluated a physiologically relevant (25%) to a high (50%) cholesterol concentration, to investigate the parameters under which hole formation may be affected. The average concentration of sphingomyelin in cell membranes is between 2-15%.<sup>67</sup> While these two components alone do not create a membrane mimetic bilayer, they are both essential to the formation of lipid rafts and TLR4 signaling,<sup>67,68</sup> and thus were the first choice of materials to use for increasing bilayer complexity. Cholesterol is especially important in LPS trafficking. Membrane cholesterol facilitates formation of lipid rafts, without which CD14-dependent, LPS signal transduction could not occur.<sup>68</sup> Presence of free cholesterol in membranes has been linked to increased TLR4 induced inflammation,<sup>69-71</sup> and less cholesterol led to attenuated expression of NF $\kappa$ B and inflammation.<sup>72-75</sup> Sphingomyelin also has special roles in mediating signaling of LPS through formation of cholesterol and sphingomyelin rich lipid rafts.<sup>74</sup> It has been demonstrated that a deficiency in sphingomyelin synthase caused reduced recruitment of TLR4 and its co-receptors, also resulting in less expression of NF $\kappa$ B.<sup>76-79</sup> There is also another mechanism by which sphingomyelin regulates TLR4 mediated inflammation. When LPS activates the TLR4 receptor, the release of the cytokine TNF $\alpha$ , causes activation of the sphingomyelinase enzyme. This enzyme works to break down the membrane sphingomyelin into simple ceramides. Ceramides have been demonstrated to have an anti-inflammatory effect,<sup>80,81</sup> which may be due to the overall reduction in the total concentration of sphingomyelin within the membrane; thereby inhibiting the formation of lipid rafts and continued TLR4 signaling.<sup>68,82</sup>

### 7.3.2 Cholesterol model bilayers

In our experiments, lipid bilayers enriched with 25% (**Figure 7.1**) and 50% cholesterol (**Figure A6.2**) incubated with LPS exhibited hole formation at most concentrations. However, at the lowest concentration of LPS (25  $\mu\text{g}/\text{mL}$ , **Figure 7.1 D**, and **Figure A6.2 D**), hole formation was completely inhibited in bilayers with both 25 or 50% cholesterol. 25  $\mu\text{g}/\text{mL}$  LPS formed holes in the uniform DOPC control lipid bilayers (**Figure A6.1**) under identical conditions, in the absence of cholesterol. This study, validated in multiple repeats, clearly indicates that cholesterol can inhibit hole formation even in this simplistic system under certain conditions. Cholesterol itself also appears to be resistant to removal by LPS (**Figure A6.3 A-C**), as it remains on the periphery of the LPS-induced holes in the sLBAs, though at this point we are unable to quantitate the remaining cholesterol. Cholesterol could be functioning to increase membrane rigidity and stabilize regions of the bilayers,<sup>83</sup> so that at lower concentrations of LPS, the mechanism of hole formation is inhibited.

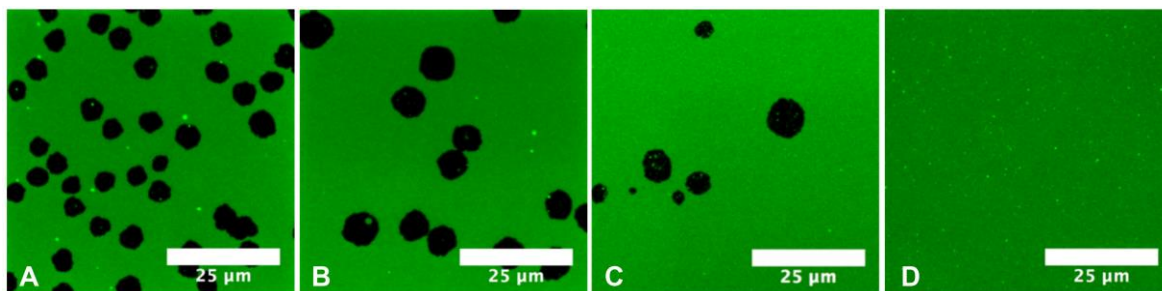


**Figure 7.1** DOPC lipid bilayers with 25% cholesterol. Bilayers (A-D) were incubated with 200, 100, 50, and 25  $\mu\text{g}/\text{mL}$  (respectively) LPS O111:B4 for 20 min at R/T and then rinsed and imaged.

### 7.3.3 Spingomyelin model bilayers

The presence of sphingomyelin alone did not impede hole formation under any of the concentrations tested. We observed hole formation under all concentrations of LPS when incubated with model sLBAs enriched with 15% (**Figure 7.2**) and 5% sphingomyelin (**Figure A6.4**). From this we conclude that the presence of sphingomyelin alone does not inhibit the formation of LPS-induced holes under our experimental conditions. The structures of sphingomyelin and cholesterol are very different. Cholesterol is a small rigid sterol with a polar group, while

sphingomyelin has a chemical structure much more similar to DOPC.<sup>67</sup> The hydrophobic cylindrical shaped tails allow it to form bilayers, however the transition temperature is comparatively high to DOPC. So at room temperature it may present in a liquid-ordered phase.<sup>67</sup> Our research has demonstrated that LPS interacts with fluid phase bilayers with high lateral mobility. As sphingomyelin is likely to be unevenly distributed through the bilayer due to its higher melting temperature, it is likely that LPS is just interacting with the regions of DOPC to form holes.

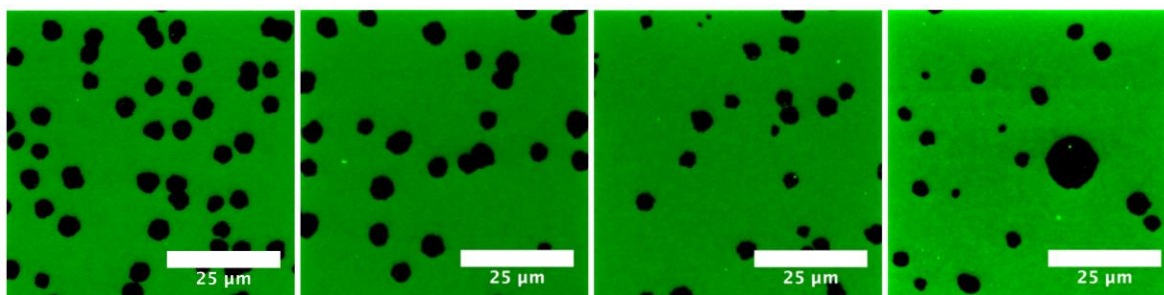


**Figure 7.2 DOPC lipid bilayers with 15% sphingomyelin.** Bilayers (A-D) were incubated with 200, 100, 50, and 25 µg/mL (respectively) LPS O111:B4 for 20 min at R/T and then rinsed and imaged.

#### 7.3.4 Mixed sphingomyelin and cholesterol model bilayers

We prepared sLBAs with varying combinations of sphingomyelin and cholesterol and studied LPS induced hole formation under these conditions. Interestingly enough, when we prepared sLBAs with 5% sphingomyelin and 50% cholesterol (**Figure 7.3**), we noted that there were infrequent small holes formed at both 50 and 25 µg/mL LPS (**Figure 7.3 C-D**). The appearance of these holes could indicate a region where LPS interacted with a DOPC/sphingomyelin area, but this needs further investigation. The borders of the holes were also not as sharp as those that occurred in the cholesterol bilayers. While the infrequent appearance of these holes (**Figure A6.5 C-D**) was consistent between repeat experiments, we cannot be entirely certain that these are not an artifact which occurs due to washing of the bilayers with the pipette. We have previously noted issues with the formation of these holes in relation to the direction of fluid flow associated with the washing mechanism.<sup>24</sup> These results demonstrate that the pattern of hole formation changes depending on the complexity of the lipid bilayer architecture employed.

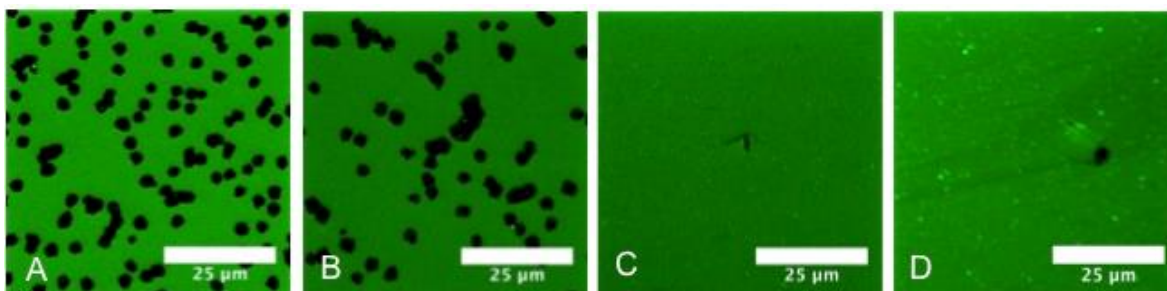


**Figure 7.3. DOPC lipid bilayers with 5% sphingomyelin and 50% cholesterol.** Bilayers (A-D) were incubated with 200, 100, 50, and 25  $\mu\text{g}/\text{mL}$  (respectively) LPS O111:B4 for 20 min at R/T and then rinsed and imaged.

### 7.3.5 Effect of temperature and LPS serogroup on hole formation in DOPC bilayers

Historically, we have performed all of our characterization studies at R/T (25  $^{\circ}\text{C}$ ), when DOPC is in a disordered fluid phase (transition temperature = -20  $^{\circ}\text{C}$ ). We investigated the ability of multiple types of LPS (from pathogenic *E. coli* isolates) to form holes in sLBAs at room temperature, and discovered that there was no induced hole formation (**Figure A5.5**) in any LPS subgroup except O111:B4.<sup>84</sup> We speculated that using physiologically relevant temperatures (37  $^{\circ}\text{C}$  = humans, ~40  $^{\circ}\text{C}$  = ruminants) may change the behavior of LPS micelles with these bilayers. The positive control, LPS O111:B4, formed holes at all temperatures (**Figure 7.4 A and 7.4 E**), though frequency of hole formation actually appeared to decrease at 40  $^{\circ}\text{C}$ . In the experimental groups, we found that 25  $\mu\text{g}/\text{mL}$  LPS, isolated from pathogenic *E. coli* serotypes (O104:H4, O111:H11, O157:H7), had absolutely no effect on the bilayers at R/T or at 37  $^{\circ}\text{C}$  after two hours of exposure (**Figure 7.4**). This data is in agreement with our previous results with nine different LPS types at R/T for 20 minutes each, where we found no defects in the bilayers, or decreases in bilayer fluidity (**Figure A5.5**).<sup>84</sup> However, when temperature was increased to 40  $^{\circ}\text{C}$ , all of the pathogenic LPS types induced hole formation. The hole formation of LPS O111:H11 most matched that of O111:B4 at 37  $^{\circ}\text{C}$  (**Figure 7.4 A,E,G**), while the frequency and size of the holes in LPS O104:H4 and O157:H7 sLBA systems were more closely matched (**Figure 7.4 F and H**).

Our findings demonstrate a temperature-dependence in hole formation induced by LPS, which differs between LPS subtypes. Even though these

experiments were performed in the homogenous DOPC bilayers, the results may have physiological relevance. Our results raise many interesting questions about the mechanisms of bacterial virulence, ruminant physiology, as well as immune studies. This is especially significant in the context of ruminant physiology, as cattle are natural hosts for this pathogen. The temperature of the rumen in cattle is 39 °C. Cattle get the majority of their protein from digesting bacteria in one of their stomachs. The specific LPS subtypes we are examining are from virulent, acid resistant pathogens, which are not digested, but instead get passed through the digestive system of cattle. It would be interesting to determine if the same mechanism of hole formation occurs at this temperature (39 °C) as well. If the difference of a single degree Celsius made the difference between hole formation vs. no hole formation, it could reveal a new mechanism by which these pathogens evade digestion. This is also important since many studies use the LPS O111:B4 as an immune stimulant.<sup>17</sup> Thus, the temperature dependence of LPS action, and its physiological relevance need further investigation. These results, show for the first time, the differential activity of LPS with sLBAs at increasing temperatures.

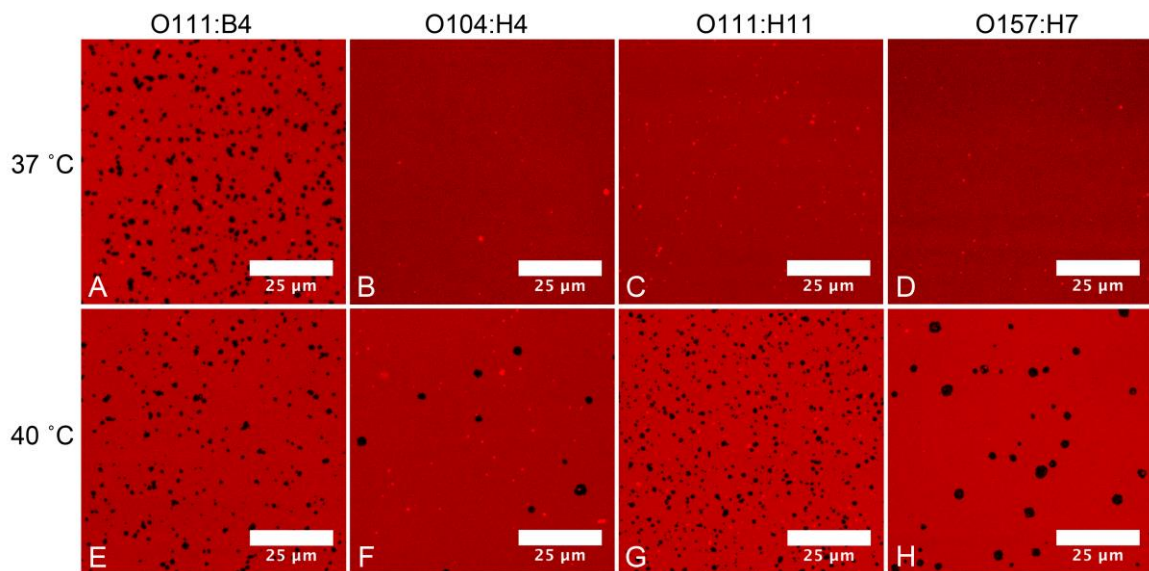


**Figure 7.4. The effect of temperature and serogroup on LPS-induced hole formation in sLBAs.** TR doped DOPC bilayers were incubated with 25 μg/mL of LPS for two hours at room temperature (not shown), 37 °C (A-D), and 40 °C (E-H). *data courtesy of K. Swingle & G. Montañó*

### 7.3.6 Cell studies: effect of murine serum on LPS-induced cytokine expression

Model bilayers are an effective tool for studying molecular interactions and lipid rafts.<sup>85</sup> However, they are limited in their capacity to assess the physiological response. To further investigate the question of LPS induced hole formation and how it may affect living systems, we advanced to cells in order to study these mechanisms. All of our investigations with sLBAs have been in buffer to date, but this is not representative of the complex milieu *in vivo*. LPS is not presented to cells as micelles, but is instead delivered to the receptors by serum carrier proteins.<sup>26,31,86-88</sup> Therefore we wanted to determine if the manner in which LPS is presented affects the outcome in cells.

To determine this we picked two murine macrophage cell lines to perform our experiments in. One line is capable of normal inflammatory response (TLR4+) and the other is a knockout cell line (TLR4-) which has been demonstrated to not respond to LPS stimulation.<sup>89</sup> Using these cell lines, we then looked at LPS presented under three conditions: buffer, serum, and delipidated serum (conditions in **Table 7.1**). Our first steps to assess TLR4 independent LPS signaling were to optimize the exposure time and LPS concentration. There is a broad array of conditions by which researchers expose LPS to cells from the picogram-microgram range, anywhere from 2-24 hours.<sup>17,41,90,91</sup> We did our initial experiments with LPS diluted in buffer, over a time course, and determined that 100 ng/mL LPS, for eight hours (**Figure A6.8 B**) would be sufficient for examining differential presentation methods of LPS. At this time, we saw the hallmark cytokines, TNF $\alpha$  and IL-6, of an LPS-induced inflammatory response.<sup>92</sup>

Using these optimized parameters, we performed further experiments to compare LPS presentation in the different serum conditions. To examine if there was a different response when LPS was presented in serum we pre-incubated LPS with serum overnight and then exposed cells to the mixture. We discovered that cytokine induction was almost completely inhibited when LPS was 'presented' to the cells in mouse serum, as there was very little difference in the cytokine profile between the 50% mouse serum with LPS and serum with no LPS (**Figure A6.9**). This data is in agreement with those published by Flegel *et al.*<sup>93</sup> when they performed a similar

experiment on human monocytes, and pre-incubated their LPS with serum. They saw a reduced expression of cytokines in their experimental group as compared to their control with no lipoproteins. Thus, presentation of LPS in serum negatively impacts cytokine production, and the amount of time that LPS is allowed to incubate with serum prior to dosing cells also impacts this mechanism.<sup>93</sup> The investigators concluded that LPS association with serum lipoproteins (specifically LDL and HDL) was responsible for this attenuated cytokine expression. This association with HDL is confirmed by data which shows that LPS injected into rats or mice, localizes to the liver within 5-10 minutes of injection.<sup>48,49</sup> This result is due to the association of LPS with serum lipoproteins such as HDL, LDL, and LBP. However, the role of these serum carrier proteins is not always protective. These proteins are also responsible for carrying LPS to TLR4 receptors and inducing the innate immune response.<sup>94</sup>

#### *7.3.6.1 No serum (buffer control) group*

There is a dramatic pattern in the increase of TLR4(+) cytokine expression when LPS is added to the 'no serum' group and incubated with the cells (**Figure 7.5**). Since the protective mechanism of lipoproteins is absent from this group, this is the response we would expect to see. The pro-inflammatory cytokines TNF $\alpha$ , IL-1 $\alpha$ , and IL-6 are all consistently upregulated in response to the LPS stimulation (**Figure 7.6 A,B**) in this group. We also noted minor increases in the levels of IL-12 and IFN $\gamma$ , which probably just demonstrates the beginning of upregulation for these cytokines.<sup>94</sup> This pattern of expression compared similarly to our previous experiments using a buffer control to deliver LPS (**Figure A6.8 B**). Some differences in expression profiles are expected between our initial experiment in buffer and these results because we used a different assay kit for each of these studies, and also used ultra pure LPS for the comparative experiments. LPS is often purified with phenol and the resulting product is found to be contaminated with proteins or other PAMPs,<sup>95,96</sup> which may attenuate or induce the cytokine expression, and we chose to avoid any effects associated with such contamination for these experiments.

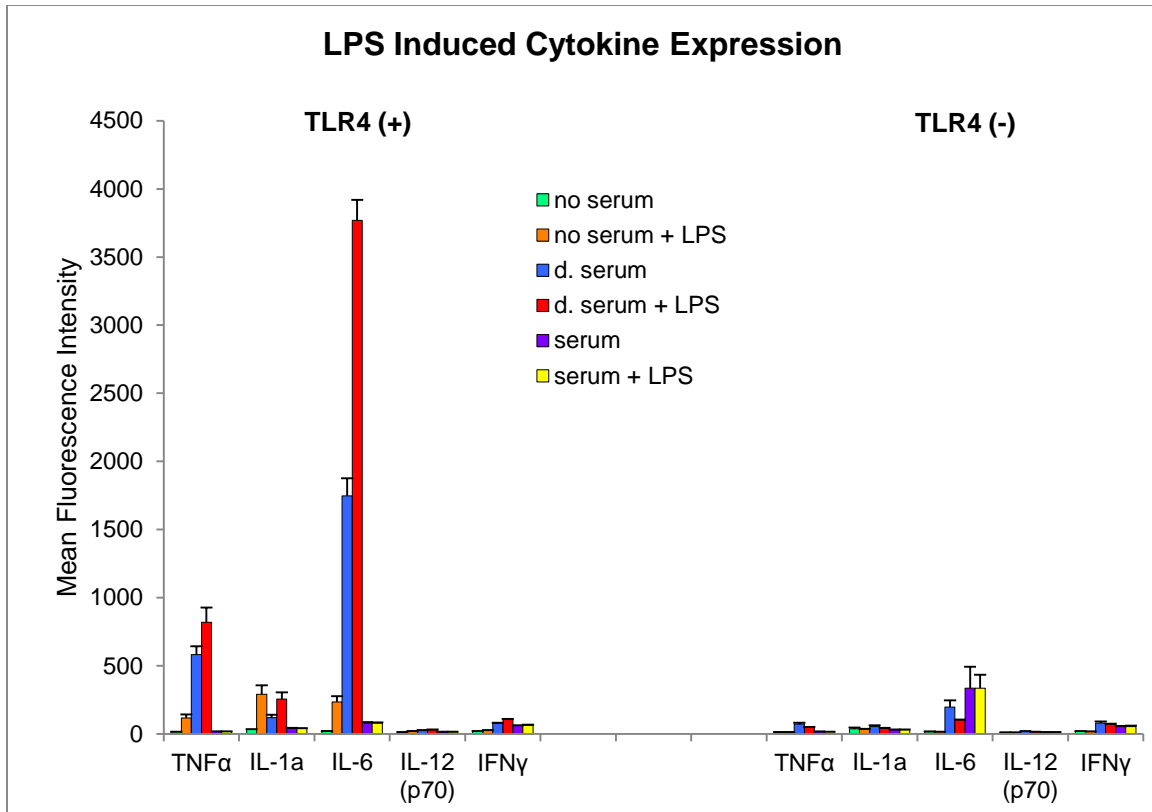


**Figure 7.5. The effect of serum on LPS induced cytokine expression.** ‘no serum’ indicates that only DMEM + buffer was used as a negative control or to deliver LPS. Delipidated serum (d.serum) was also investigated both with and without LPS. The final condition was 50% mouse serum (serum). Results are plotted as the MFI with standard deviations of three replicates.

### 7.3.3.2 Delipidated serum group

In the TLR4(+) cells we saw the highest level of cytokines expressed in the d.serum groups (**Figure 7.6 C,D**). Interestingly, d.serum with no LPS was able to induce expression of TNF $\alpha$ , IL-1 $\alpha$ , and IL-6, with some induction also seen in IL-12 and IFN $\gamma$  (as compared to the no serum control, **Figure 7.6 A**). When LPS was prepared in d.serum, the concentration of TNF $\alpha$  increased by a magnitude of 1.5x. IL-1 $\alpha$  increased by 2x, and IL-6 increased 2.4x. So overall, we saw a significant increase in cytokine levels (approximately 2x) that of the negative LPS control (**Figure 7.6 D**). There are a couple possible explanations of this data. (1) LBP is not actually a lipoprotein and so the effect of delipidating the serum would not inhibit the function of this protein. In fact, the serum concentration of LBP in mouse serum is quite high,<sup>41</sup> and when LBP was added to buffer, it was demonstrated to enhance

the stimulation of CD14 cells as much as 100-1000x.<sup>41,97,98</sup> (2) The inflammatory cytokine levels in the no LPS group are also high, especially in comparison to the 'no serum' and serum control groups (**Figure 7.6 A,F**). We have previously demonstrated that the serum of mice can exhibit an immune response to LPS antigens (**Appendix 3, Tables A3.1-A3.13**, pre-inoculated immunoblots), thus indicating some level of exposure to endogenous endotoxin in their controlled environment. It has also been documented that commercial preparations of fetal bovine serum can be contaminated with endotoxin.<sup>99</sup> From this, it does not seem unreasonable to assume that mouse serum could also be contaminated with LPS. Therefore, the addition of more LPS to the system would effectively increase the cytokine expression as we saw in the d.serum + LPS group. Endotoxin contamination is often a problem in the laboratory setting.<sup>100,101</sup> While we find this to be a likely reason for the elevated cytokine levels, we have not confirmed this with an endotoxin test. This is another consideration that should be taken into account when designing *in vitro* studies to assess cytokine expression.

#### 7.3.3.3 Whole serum group

As predicted, we saw very minor, if any, cytokine induction between the LPS group and the negative serum control group (**Figure 7.6 F,G**), when the antigen was presented in serum. There was no difference in the trend between either of the groups with or without LPS, irrespective of cell type. Together these results imply that there is a difference in critical cytokine expression depending on how amphiphilic LPS is presented. This is especially true when comparing the results between the LPS groups with 'no serum' and serum, as there is a clear attenuation of cytokine induction in the serum + LPS group as compared to the 'no serum' + LPS groups and the negative controls. Beyond any argument of which is the correct methodology or choice of cell line, this result iterates a simple yet salient fact: association of amphiphilic PAMPs with carrier proteins in aqueous serum has a major impact on innate immunity.

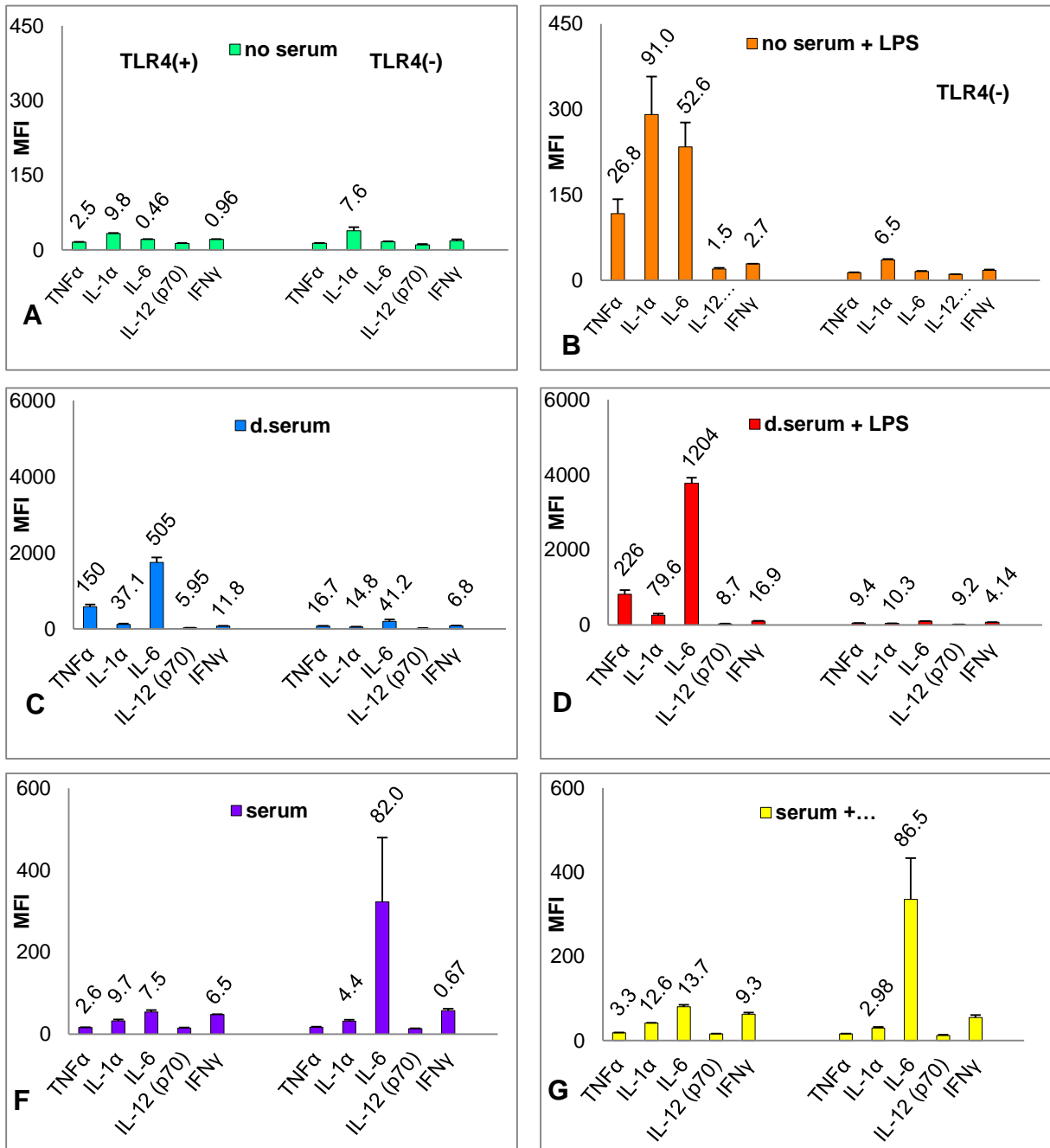


**Figure 7.6 Subset graphs of LPS-induced cytokine expression.** Y-axis is the mean fluorescence intensity (MFI). Results are plotted as the MFI with standard deviations of three replicates. Numbers above each bar correlate to the calculated concentration of cytokine expressed in pg/mL Bars without numbers above them fall outside of the range of the 5PL curve and the concentration cannot be directly calculated. TLR4(+) response is on the left side of the graph and TLR4(-) response is on the right side. Graphs A,C,F (left side) are the variations of serum with no LPS, while graphs B,D,G are the same corresponding variations of serum with LPS exposure.

This conclusion is supported by similar studies in the literature that have looked at expression of cytokines in murine macrophages (**Table 7.2**). For instance,

Lamping *et al.*<sup>41</sup> added merely 1% serum to their LPS preparations and noticed a 2-fold reduction in expression of TNF $\alpha$ . Cavaillon *et al.*<sup>102</sup> investigated the effect of lipoproteins on cytokine expression and determined supplementing with lipoproteins could reduce the levels of expressed TNF $\alpha$  and IL-6 by more than a factor of 10.

One of the more interesting things we did see was induction of IL-6 in the TLR4(-) cells. The levels of expression between the negative control, and the LPS group were not significantly different. The exact reasons for this induction are not known, but warrant investigation in future studies. Our closest available parallel to this is a study performed in buffer by Zughaier *et al.*<sup>103</sup> In their assessment of myeloid differentiation factor 88 (MyD88, a requisite cofactor for TLR4 signaling) they determined that no MyD88-dependent or independent signaling occurred in the same TLR4(-) murine cell line when they stimulated with LPS.

**Table 7.2 Murine macrophage cytokine responses seen as a result of *E. coli* LPS**

Reference	Our research		Shanmugam <i>et al.</i> , 2012	Lamping <i>et al.</i> , 1998	Cavaillon <i>et al.</i> , 1990		
	Cell Type: IC-21		Cell Type: RAW 264.7	Cell Type: RAW 264.7	Cell Type: Primary murine macrophages		
Cytokines and Chemokines	Serum + LPS	Free LPS	Unknown	1% serum + LPS	Free LPS	LP + LPS	Free LPS
	(pg/mL)		IDV	ng/mL		U/mL (activity)	
IL-1 $\alpha$	12.62	90.96	6000	*	*	*	*
TNF- $\alpha$	3.26	26.81	8500	2	4	84	1460
IL-6	13.71	52.63	15000	*	*	120	120
IL-12 (p70)	-	1.45	7000	*	*	*	*
IFN- $\gamma$	9.32	2.70	*	*	*	*	*
RANTES	-	0.36	13000				
MIP-2	11.31	553	*				
MIP-1b	3.56	934	22000				
MIP-1a	-	1002	20000				
KC	7.83	5.12	*				
MCP-1	16.94	65.94	20000				
IP-10	99.90	-	*				
IL-9	-	54.49	*				
G-CSF	258	137	10000				
GM-CSF	-	16.31	0				

LP = lipoproteins, - = does not fall within the calculable assay range, \* = not measured, IDV = defined as the density of spots compared to the density of positive controls

#### 7.3.3.4. Comparison of chemokine expression

Since we are investigating the potential for alternative signaling mechanisms of LPS in serum free systems, we also measured the profiles of several chemokines in our serum groups (**Table 7.1**) and compared them to what was available in the literature (**Table 7.2**, Shanmugam *et al.*<sup>104</sup>). Shanmugam *et al.*<sup>104</sup> represents one of the few studies that measured chemokine profiles in murine cells, however the exact conditions (serum or 'no serum') of this experiment were not described. By comparing the outcomes of this study with our own results (a subset shown in **Table 7.2**) it appears that Shanmugam *et al.*<sup>104</sup> were most likely using a serum free system. Under the "Free LPS", *aka* ('no serum') conditions, the results of this study and ours are very consistent and the only disparity is in the measurement of GM-CSF (16.31 pg/mL in our assay vs. zero in theirs). Since the cell lines are different and the sensitivity of each assay kit and associated antibodies is different, this may simply be an experimental limitation rather than observed difference.

When we look at the response of these chemokines in the TLR4(+) vs TLR4(-) cell lines, a different expression profile is revealed. We saw no calculable levels of RANTES, GM-CSF, or macrophage inflammatory proteins (MIP), MIP-2, MIP-1b, and MIP-1a in the TLR4(-) cells (**Table 7.3**). These chemokines serve primarily as signaling molecules to recruit neutrophils and granulocytes to the site of infection *in vivo*. When looking at KC, MCP-1, and IL-9 there are significantly higher levels expressed as compared to the TLR4(+) cells. KC and MCP-1 also both function as chemo-attractants to induce chemotaxis in neutrophils to the site of inflammation. IL-9 functions as a mediator of apoptosis, and when comparing the 'no serum' to the serum groups in the table, the protective effect of serum in both cell lines becomes more clear.

**Table 7.3. Calculated cytokine/chemokine expression (pg/mL) in IC-21 and 23ScCr serum/'no serum' LPS groups.**

<b>TLR4 (+)</b>	RANTES	MIP-2	MIP-1b	MIP-1a	KC	MCP-1	IP-10	IL-9	G-CSF	GM-CSF
'no serum' + LPS	0.3553	553.16	934.5	1002	5.12	65.94	-	54.49	137.1	16.31
serum + LPS	-	11.31	3.563	-	7.83	16.94	99.89	-	257.9	-

<b>TLR4 (-)</b>	RANTES	MIP-2	MIP-1b	MIP-1a	KC	MCP-1	IP-10	IL-9	G-CSF	GM-CSF
'no serum' + LPS	-	-	-	-	73.4	195.5	-	164.1	124.0	-
serum + LPS	-	-	-	-	54.3	35.28	64.12	-	324.6	-

## 7.4 Conclusion

The overarching theme in this work is that LPS can have differential interactions with systems when presented with its physiological serum carrier proteins. We have demonstrated that LPS micelles in buffer can cause hole formation in cholesterol and sphingomyelin enriched lipid bilayers. This supports our theory that LPS may be having a similar dynamic effect when presented in buffer to *in vitro* systems. The protective effect of serum lipoproteins on LPS induced inflammation is well documented within the literature, but presenting LPS in buffer to prime immune cells is still a common theme. We have shown here through the use of TLR4(+) and TLR4(-) cells, that there is a distinct difference between presenting LPS to cells in buffer versus serum, where native lipoproteins offer a protective effect. We additionally see high expression when we use d.serum, but it was much higher than the no serum control, which we concluded was primarily due to the presence of LBP transferring LPS to CD14. Thus, TLR4 signaling depends on the composition of serum used. The implications of this should be considered when designing *in vitro* studies which utilize LPS.

## 7.5 Future Directions

Our results clearly demonstrate that 1) increasing complexity of lipid bilayers affects formation of LPS-induced membrane deformations and 2) presentation of LPS dramatically modifies the cytokine/chemokine expression in murine cells with TLRs. These results also raise several questions, warranting further investigation in each of these experimental models.

While it is clear that LPS interacts with enriched sLBA systems, we would like to further examine this mechanism using several methods. First, it is necessary to evaluate the incorporation of sphingomyelin into the bilayers to assess the distribution seen in the bilayers. This is especially important for addressing the asymmetrical hole formation we saw in **Figure A6.6**. This could be easily performed using an NBD-labeled sphingomyelin, which we previously demonstrated with cholesterol (**Figure A6.3**). We have also previously used AFM as a tool to characterize DOPC bilayers. By performing topographical analysis of the enriched bilayers, more information about their composition and distribution of the lipid components within, both before and after incubation with LPS, would be available. While AFM should prove efficient enough to characterize the holes, the addition of a fluorescently labeled protein after rinsing away LPS would also help to determine whether any unlabeled cholesterol or sphingomyelin remained in the holes.

A systematic approach for characterizing the size and statistical distribution of the holes formed in the bilayers should also be developed and implemented. A recommended platform for this would be Matlab, as the software is readily available, and the image analysis tools could easily facilitate this. This tool would serve to provide necessary information about LPS micelles and the interactions they have with a variety of lipid compositions. Implementation of this would allow us to further analyze the differences that we saw in the temperature- and serogroup- dependent formation of holes (**Figure 7.4**).

A direct link between the interaction of LPS with complex lipid bilayers, and cell membrane damage has already been implied by us. However, a system to record whether membrane damage actually happens as a result of LPS incubation would serve to complement the data seen in both the biophysical and cytokine studies. A relatively simple experiment has been previously performed by Cervantes *et al*<sup>105</sup> to investigate the membrane damage induced by *Listeria monocytogenes*. This experiment could easily be applied to our TLR4(-) cell system to determine whether LPS forms holes in cell membranes. First, the cytosol of macrophages is stained with calcein-am, and free dye is rinsed away. Then cells are incubated with LPS and propidium iodide. Calcein leakage and propidium iodide uptake could be

measured via flow cytometry, and confirmation could be obtained with fluorescence microscopy. This experiment would be crucial to providing evidence of LPS-induced membrane damage.

A comprehensive review of the literature should be performed and published to document the recorded cytokine and chemokine expression profiles under specific conditions. Though it is well documented that experimental conditions have a direct effect on expressed cytokines, the conditions that researchers use to introduce LPS to cell systems, is often not made clear. Thus it can be difficult to make direct comparisons between results. To further elucidate the results we have documented, analysis of the serum lipoproteins components should be performed to help explain some of the differences in expression profiles. While this work has already begun, more development is necessary in order to completely evaluate the results seen in the cytokine expression profiles of the mouse serum variants, which were depleted of specific lipoproteins.

Finally, this work needs to be brought full circle to facilitate better detection methods for LPS and amphiphiles in general. PAMPs are key indicators of early infection, and the ability to detect infections and diseases earlier will lead to better outcomes for patient treatment. By characterizing the way PAMPs interact with membranes, be it direct or indirect, we can develop better surfaces to facilitate their detection.

## 7.6 References

- (1) Nikaido, H. Molecular basis of bacterial outer membrane permeability revisited. *Microbiol Mol Biol Rev*, 2003, 67(4), 593-656.
- (2) Delcour, A.H. Outer Membrane Permeability and Antibiotic Resistance. *Biochim Biophys Acta* **2009**, 1794(5), 808–816.
- (3) Orskov, F. *et al.* *Escherichia coli* Serotyping and Disease in Man and Animals. *Can. J. Microbiol.* **1992**, 38 (7), 699–704.
- (4) Orskov, I. *et al.* Serology, Chemistry, and Genetics of O and K Antigens of *Escherichia coli*. *Bacteriol Rev* **1977**, 41(3), 667.
- (5) Wang, X. and Quinn, P.J. Endotoxins: Lipopolysaccharides of Gram-Negative Bacteria. In *Endotoxins: Structure, Function and Recognition*; Subcellular Biochemistry; Springer Netherlands: Dordrecht, **2010**, 53, 3–25.
- (6) Takeuchi, O. and Akira, S. Pattern recognition receptors and inflammation. *Cell*, **2010** 140(6), 805-820.
- (7) Kumagai, Y. *et al.* Pathogen Recognition by Innate Receptors. *J. Infect. Chemother.* **2008**, 14 (2), 86–92.
- (8) Akira, S. *et al.* Pathogen Recognition and Innate Immunity. *Cell* **2006**, 124 (4), 783–801.
- (9) Kumar, H. *et al.* Toll-Like Receptors and Innate Immunity. *Biochem Biophys Res Commun* **2009**, 388 (4), 621–625.
- (10) Beutler, B.B., Tlr4: Central Component of the Sole Mammalian LPS Sensor. *Curr Opin Immunol* **2000**, 12 (1), 20–26.
- (11) Kawai, T.; Akira, S. TLR Signaling. *Sem Immunol* **2007**, 19 (1), 24–32.
- (12) Akira, S. and Takeda, K. Toll-like receptor signalling. *Nat Rev Immunol* **2004** 4(7), 499-511
- (13) Beutler, B. and Rietschel, E.T. Innate Immune Sensing and Its Roots: the Story of Endotoxin. *Nat Rev Immunol* **2003**, 3 (2), 169–176.
- (14) Aguilar, J. C.; Rodríguez, E. G. Vaccine Adjuvants Revisited. *Vaccine* **2007**, 25 (19), 3752–3762.
- (15) Björkqvist, M. *et al.* A Novel Pathogenic Pathway of Immune Activation Detectable Before Clinical Onset in Huntington's Disease. *J Exp Med* **2008**, 205(8), 1869–1877.
- (16) Bao, R. *et al.* Lipopolysaccharide Induces Immune Activation and SIV Replication in Rhesus Macaques of Chinese Origin. *PLoS ONE* **2014**, 9(2), e98636.
- (17) Le Feuvre, R.A. *et al.* Priming of Macrophages with Lipopolysaccharide Potentiates P2X7-Mediated Cell Death via a Caspase-1-Dependent Mechanism, Independently of Cytokine Production. *J Biol Chem* **2002**, 277 (5), 3210–3218.
- (18) Erridge, C. *et al.* Structure and Function of Lipopolysaccharides. *Microbes Infect* **2002**, 4 (8), 837–851.
- (19) Raetz, C.R.H.; Whitfield, C. Lipopolysaccharide Endotoxins. *Annu Rev Biochem* **2002**, 71, 635–700.
- (20) Beveridge, T.J. Structures of Gram-Negative Cell Walls and Their Derived Membrane Vesicles. *J Bacteriol* **1999**, 181(16), 4725–4733.
- (21) Kang, Y. H. *et al.* Ultrastructural and Immunocytochemical Study of the

- Uptake and Distribution of Bacterial Lipopolysaccharide in Human Monocytes. *J Leuk Biol* **1990**, *48* (4), 316–332.
- (22) Alam, J. M. and Yamazaki, M. Spontaneous Insertion of Lipopolysaccharide Into Lipid Membranes From Aqueous Solution. *Chem Phys Lipids* **2011**, *164* (2), 166–174.
- (23) Wurfel, M. M. and Wright, S. D. Lipopolysaccharide-Binding Protein and Soluble CD14 Transfer Lipopolysaccharide to Phospholipid Bilayers: Preferential Interaction with Particular Classes of Lipid. *J Immunol* **1997**, *158* (8), 3925–3934.
- (24) Adams, P. G. *et al.* Lipopolysaccharide-Induced Dynamic Lipid Membrane Reorganization: Tubules, Perforations, and Stacks. *Biophys J* **2014**, *106* (11), 2395–2407.
- (25) Kubiak, J. *et al.* Lipid Lateral Organization on Giant Unilamellar Vesicles Containing Lipopolysaccharides. *Biophys J* **2011**, *100* (3), 341a.
- (26) Vreugdenhil, A. C. *et al.* LPS-Binding Protein Circulates in Association with apoB-Containing Lipoproteins and Enhances Endotoxin-LDL/VLDL Interaction. *J Clin Invest* **2001**, *107* (2), 225–234.
- (27) Levine, D. M., *et al.* In vivo protection against endotoxin by plasma high density lipoprotein. *PNAS* **1993**, *90*(24), 12040-12044.
- (28) Morrison, D.C. and Jacobs, D.M. Binding of Polymyxin B to the Lipid a Portion of Bacterial Lipopolysaccharides. *Immunochemistry* **1976**, *13*(10), 813–818.
- (29) Inamori, K. I. *et al.* A Newly Identified Horseshoe Crab Lectin with Specificity for Blood Group a Antigen Recognizes Specific O-Antigens of Bacterial Lipopolysaccharides. *J Biol Chem* **1999**, *274* (6), 3272–3278.
- (30) Shimazu, R. *et al.* MD-2, a Molecule That Confers Lipopolysaccharide Responsiveness on Toll-Like Receptor 4. *J Exp Med* **1999**, *189*(11), 1777–1782.
- (31) Triantafilou, M. and Triantafilou, K. Lipopolysaccharide Recognition: CD14, TLRs and the LPS-Activation Cluster. *Trends Immunol* **2002**, *23*(6), 301–304.
- (32) Rangin, M. and Basu, A. Lipopolysaccharide Identification with Functionalized Polydiacetylene Liposome Sensors. *J Am Chem Soc* **2004**, *126*(16), 5038–5039.
- (33) da Silva, J.L. *et al.* Impedimetric Sensor of Bacterial Toxins Based on Mixed (Concanavalin a)/Polyaniline Films. *Colloids Surf B Biointerfaces* **2014**, *117*, 549–554.
- (34) Lan, M. *et al.* Copolythiophene-Derived Colorimetric and Fluorometric Sensor for Visually Supersensitive Determination of Lipopolysaccharide. *J Am Chem Soc* **2012**, *134*(15), 6685–6694.
- (35) Aurell, C.A. and Wistrom, A. O. Critical Aggregation Concentrations of Gram-Negative Bacterial Lipopolysaccharides (LPS). *Biochem Biophys Res Commun* **1998**, *253* (1), 119–123.
- (36) Santos, N. C. *et al.* Evaluation of Lipopolysaccharide Aggregation by Light Scattering Spectroscopy. *ChemBioChem* **2003**, *4*(1), 96–100.
- (37) Seydel, U. *et al.* Phase Behavior, Supramolecular Structure, and Molecular

- Conformation of Lipopolysaccharide. *Immunobiology* **1993**, 187(3-5), 191–211.
- (38) Sakamuri, R.M. *et al.* Association of Lipoarabinomannan with High Density Lipoprotein in Blood: Implications for Diagnostics. *Tuberculosis* **2013**, 93 (3), 301–307.
- (39) Kitchens, R.L., *et al.* Plasma CD14 Decreases Monocyte Responses to LPS by Transferring Cell-Bound LPS to Plasma Lipoproteins. *J Clin Invest* **2001**, 108 (3), 485–493.
- (40) Wright, S. D. Catalytic Properties of Lipopolysaccharide (LPS) Binding Protein. *J Biol Chem* **1996**, 271(8), 4100–4105.
- (41) Lamping, N. *et al.* LPS-Binding Protein Protects Mice From Septic Shock Caused by LPS or Gram-Negative Bacteria. *J Clin Invest* **1998**, 101(10), 2065–2071.
- (42) Gegner, J.A. *et al.* Lipopolysaccharide (LPS) Signal Transduction and Clearance. Dual Roles for LPS Binding Protein and Membrane CD14. *J Biol Chem* **1995**, 270 (10), 5320–5325.
- (43) Harris, R. I. *et al.* An Improved Chromogenic Substrate Endotoxin Assay for Clinical Use. *J Clin Pathol* **1983**, 36(10), 1145–1149.
- (44) Nath, A.; Atkins, W. M.; Sligar, S. G. Applications of Phospholipid Bilayer Nanodiscs in the Study of Membranes and Membrane Proteins †. *Biochemistry* **2007**, 46 (8), 2059–2069.
- (45) Yu, B. *et al.* Lipopolysaccharide Binding Protein and Soluble CD14 Catalyze Exchange of Phospholipids. *J Clin Invest* **1997**, 99 (2), 315–324.
- (46) Gutschmann, T. *et al.* Dual Role of Lipopolysaccharide (LPS)-Binding Protein in Neutralization of LPS and Enhancement of LPS-Induced Activation of Mononuclear Cells. *Infect Immun* **2001**, 69(11), 6942–6950.
- (47) Wurfel, M.M. Lipopolysaccharide (LPS)-Binding Protein Is Carried on Lipoproteins and Acts as a Cofactor in the Neutralization of LPS. *J Exp Med* **1994**, 180(3), 1025–1035.
- (48) Hampton, R.Y. *et al.* Recognition and Plasma Clearance of Endotoxin by Scavenger Receptors. *Nature* **1991**, 352(6333), 342–344.
- (49) Mimura, Y. *et al.* Role of Hepatocytes in Direct Clearance of Lipopolysaccharide in Rats. *Gastroenterology* **1995**, 109(6), 1969–1976.
- (50) Fitzgerald, K. A. *et al.* Endotoxin Recognition and Signal Transduction by the TLR4/MD2-Complex. *Microbes Infect* **2004**, 6(15), 1361–1367.
- (51) Murch O. *et al.* Lipoproteins in inflammation and sepsis. I. Basic science. *Intensive Care Med*. **2006** 33(1), 13–24.
- (52) Dobrovolskaia, M.A. and Vogel, S.N. Toll Receptors, CD14, and Macrophage Activation and Deactivation by LPS. *Microbes Infect* **2002**, 49(9), 903-914.
- (53) Fujihara, M. *et al.* Molecular Mechanisms of Macrophage Activation and Deactivation by Lipopolysaccharide: Roles of the Receptor Complex. *Pharmacol Ther* **2003**, 100(2), 171–194.
- (54) Cohen, J. The Immunopathogenesis of Sepsis. *Nature* **2002**, 4250(6917), 885-891.
- (55) Berczi, I., and Szentivanyi, A. Cytokines and chemokines. *NeuroImmun*

- Biol, **2003**, 3, 191-220.
- (56) Borish, L., and Steinke, J., Cytokines and chemokines. *J Allergy Clin Immunol* **2003**, 111(2), S460-S475.
- (57) Adams, P.G. *et al.* Exploiting Lipopolysaccharide-Induced Deformation of Lipid Bilayers to Modify Membrane Composition and Generate Two-Dimensional Geometric Membrane Array Patterns. *Sci Rep* **2015**, 5, 10331.
- (58) Schromm, A.B. *et al.* Lipopolysaccharide-Binding Protein Mediates CD14-Independent Intercalation of Lipopolysaccharide Into Phospholipid Membranes. *FEBS Lett.* **1996**, 399(3), 267–271.
- (59) Heerklotz, H. and Seelig, J. Leakage and Lysis of Lipid Membranes Induced by the Lipopeptide Surfactin. *Eur Biophys J.* **2007**, 36(4-5), 305–314.
- (60) Knoll, W. *et al.* Solid Supported Lipid Membranes: New Concepts for the Biomimetic Functionalization of Solid Surfaces. *Biointerphases* **2008**, 3(2), FA125.
- (61) Nielsen, C. H. Biomimetic Membranes for Sensor and Separation Applications. *Anal Bioanal Chem* **2009**, 395(3), 697–718.
- (62) Nomura, K. *etal.* Interaction of Lipopolysaccharide and Phospholipid in Mixed Membranes: Solid-State <sup>31</sup>P-NMR Spectroscopic and Microscopic Investigations. *Biophys J* **2008**, 95(3), 1226-1238.
- (63) Nomura, K. *et al.* Lipopolysaccharide Induces Raft Domain Expansion in Membrane Composed of a Phospholipid-Cholesterol-Sphingomyelin Ternary System. *Innate Immun* **2011**, 17(3), 256–268.
- (64) Tong, J. and McIntosh, T.J. Structure of Supported Bilayers Composed of Lipopolysaccharides and Bacterial Phospholipids: Raft Formation and Implications for Bacterial Resistance. *Biophys J* **2004**, 86(6), 3759–3771.
- (65) Roes, S. *et al.* Localization of the Lipopolysaccharide-Binding Protein in Phospholipid Membranes by Atomic Force Microscopy. *J.Biol Chem.* **2006**, 281(5), 2757–2763.
- (66) Stromberg, L.R., *et al.* Purification and Characterization of Lipopolysaccharides From Six Strains of Non-O157 Shiga Toxin-Producing *Escherichia coli*. *J Microbiol Methods* **2015**, 116, 1-7.
- (67) Ramstedt, B. and Slotte, J.P. Membrane Properties of Sphingomyelins. *FEBS Lett.* **2002**, 531(1), 33–37.
- (68) Olsson, S. and Sundler, R. The Role of Lipid Rafts in LPS-Induced Signaling in a Macrophage Cell Line. *Mol Immunol* **2006**, 43(6), 607–612.
- (69) Zhu, X. *et al.* Increased Cellular Free Cholesterol in Macrophage-Specific Abca1 Knock-Out Mice Enhances Pro-Inflammatory Response of Macrophages. *J Biol Chem* **2008**, 283(34), 22930–22941.
- (70) Zhu, X. *et al.* Macrophage ABCA1 Reduces MyD88-Dependent Toll-Like Receptor Trafficking to Lipid Rafts by Reduction of Lipid Raft Cholesterol. *J Lipid Res.* **2010**, 51(11), 3196–3206.
- (71) Sun, M. *et al.* Free cholesterol accumulation in macrophagemembranes activates Toll-like receptors and p38 mitogen-activated protein kinase and induces cathepsin K, *Circ Res* **2009**, 10(4), 455–465.
- (72) Arima, H., *et al.* Inhibitory effects of novel hydrophilic cyclodextrin

- derivatives on nitric oxide production in macrophages stimulated with lipopolysaccharide, *Pharm Res* **2001**, 18, 1167–1173.
- (73) Ruyschaert, J.M. and Loney, C. Role of lipid microdomains in TLR-mediated signalling. *Biochim Biophys Acta Biomembranes*, 2015, *1848*(9), 1860-1867.
- (74) Triantafilou, M., *et al.* Mediators of innate immune recognition of bacteria concentrate in lipid rafts and facilitate lipopolysaccharide induced cell activation, *J. Cell Sci.* 115 (2002) 2603–2611.
- (75) Cuschieri, J., Implications of lipid raft disintegration: enhanced anti-inflammatory macrophage phenotype, *Surgery* **2004**, 136, 169–175.
- (76) Hailemariam, T.K. *et al.* Sphingomyelin Synthase 2 Deficiency Attenuates NFkappaB Activation. *Arterioscler Thromb Vasc Biol* **2008**, 28(8), 1519–1526.
- (77) Gowda, S., *et al.* Sphingomyelin synthase 2 (SMS2) deficiency attenuates LPS-induced lung injury, *Am J Physiol Lung Cell Mol Physiol* **2011**, 300, L430–L440.
- (78) Li, Z., *et al.* Impact of sphingomyelin synthase 1 deficiency on sphingolipid metabolism and atherosclerosis in mice, *Arterioscler Thromb Vasc Biol* **2012**, 32(7), 1577–1584.
- (79) Chakraborty, M., *et al.* Myeloid cellspecific serine palmitoyltransferase subunit 2 haploinsufficiency reduces murine atherosclerosis, *J Clin Invest* **2013**, 123(4), 1784–1797.
- (80) Walton, K. A. *et al.* A Role for Neutral Sphingomyelinase Activation in the Inhibition of LPS Action by Phospholipid Oxidation Products. *J Lipid Res* **2006**, 47 (9), 1967–1974.
- (81) Zeidan, Y.H. and Hannun, Y.A. The Acid Sphingomyelinase/Ceramide Pathway: Biomedical Significance and Mechanisms of Regulation. *Curr Mol Med* **2010**, 10 (5), 454–466.
- (82) Jung, J.S. *et al.* Anti-Inflammatory Mechanism of Exogenous C2 Ceramide in Lipopolysaccharide-Stimulated Microglia. *Biochim Biophys Acta* **2013**, 1831(6), 1016–1026.
- (83) Petrache, H.I. *et al.* Alteration of lipid membrane rigidity by cholesterol and its metabolic precursors. In *Macromol Sym*, **2005**, 219(1), 39-50
- (84) Stromberg, L.R. *et al.* Membrane Insertion for the Detection of Lipopolysaccharides: Exploring the Dynamics of Amphiphile-in-Lipid Assays. *PLoS ONE* **2016**, *In Review*.
- (85) Edidin, M. The State of Lipid Rafts: From Model Membranes to Cells. *Annu Rev Biophys Biomol Struct* **2003**, 32 (1), 257–283.
- (86) Hailman, E. *et al.* Lipopolysaccharide (LPS)-Binding Protein Accelerates the Binding of LPS to CD14. *J Exp Med* **1994**, 179(1), 269–277.
- (87) Murch, O. *et al.* Lipoproteins in Inflammation and Sepsis. I. Basic Science. *Intensive Care Med* **2007**, 33 (1), 13–24.
- (88) Chien, J.Y. *et al.* Low Serum Level of High-Density Lipoprotein Cholesterol Is a Poor Prognostic Factor for Severe Sepsis. *Crit Care Med* **2005**, 33(8), 1688–1693.
- (89) Lorenz, E. *et al.* Toll-Like Receptor 4 (TLR4)-Deficient Murine Macrophage

- Cell Line as an in Vitro Assay System to Show TLR4-Independent Signaling of *Bacteroides Fragilis* Lipopolysaccharide. *Infect Immun* **2002**, 70(9), 4892–4896.
- (90) Vreugdenhil, A. and Rousseau, C.H. Lipopolysaccharide (LPS)-Binding Protein Mediates LPS Detoxification by Chylomicrons. *J Exp Med* **2003**.
- (91) Golde, L.M., *et al.* Resistance of macrophages from C3H/HeJ mice to the in vitro cytotoxic effects of endotoxins. *J Immunol* **1977**, 119, 162-166.
- (92) Lu, Y.C. *et al.* LPS/TLR4 Signal Transduction Pathway. *Cytokine* **2008**, 42(2), 145–151.
- (93) Flegel, W. A. *et al.* Prevention of Endotoxin-Induced Monokine Release by Human Low- and High-Density Lipoproteins and by Apolipoprotein a-I. *Infect Immun* **1993**, 61(12), 5140–5146.
- (94) Jerala, R. Structural Biology of the LPS Recognition. *Int J Med Microbiol.* **2007**, 297(5), 353–363.
- (95) Watanabe, J. *et al.* Endotoxin Contamination of Ovalbumin Suppresses Murine Immunologic Responses and Development of Airway Hyper-Reactivity. *J Biol Chem* **2003**, 278 (43), 42361–42368.
- (96) Lee, H.K. *et al.* Two Lipoproteins Extracted From *Escherichia coli* K-12 LCD25 Lipopolysaccharide Are the Major Components Responsible for Toll-Like Receptor 2-Mediated Signaling. *J Immunol* **2002**, 168(8), 4012–4017.
- (97) Mathison, J.C. *et al.* Plasma Lipopolysaccharide (LPS)-Binding Protein. a Key Component in Macrophage Recognition of Gram-Negative LPS. *J Exp Med* **1992**, 149(1), 200-206.
- (98) Schumann, R.R. *et al.* Structure and Function of Lipopolysaccharide Binding Protein. *Science* **1990**, 249(4975), 1429–1431.
- (99) Kirikae, T. *et al.* Endotoxin Contamination in Fetal Bovine Serum and Its Influence on Tumor Necrosis Factor Production by Macrophage-Like Cells J774.1 Cultured in the Presence of the Serum. *Int J Immunopharmacol* **1997**, 19(5), 255–262.
- (100) Gorbet, M. B.; Sefton, M. V. Endotoxin: the Uninvited Guest. *Biomaterials* **2005**, 26(34), 6811–6817.
- (101) Sharma, S. K. Endotoxin Detection and Elimination in Biotechnology. *Biotechnol Appl Biochem* **1986**, 8(1), 5-22.
- (102) Cavaillon, J.M. *et al.* Cytokine Response by Monocytes and Macrophages to Free and Lipoprotein-Bound Lipopolysaccharide. *Infect Immun* **1990**, 58(7), 2375–2382.
- (103) Zughailer, S.M. *et al.* Differential Induction of the Toll-Like Receptor 4-MyD88-Dependent and-Independent Signaling Pathways by Endotoxins. *Infect Immun* **2005**, 73(5), 2940-2959.
- (104) Shanmugam, A. *et al.* Synthetic Toll Like Receptor-4 (TLR-4) Agonist Peptides as a Novel Class of Adjuvants. *PLoS ONE* **2012**, 7(2), e30839.
- (105) Cervantes, J. *et al.* Intracytosolic *Listeria Monocytogenes* Induces Cell Death Through Caspase-1 Activation in Murine Macrophages. *Cell Microbiol* **2007**, 10(1), 41-52.

## **Chapter 8.** **Conclusions and Future Directions**

### **8.1 Conclusions**

#### *8.1.1 Development of antibodies and antigens for assay development*

As discussed in chapter 3, we have developed a suite of purified antigens (LPS, O-ag and lipid A) from six serotypes of STEC for the purpose of generating highly specific O-ag monoclonal antibodies. Currently available antibodies demonstrate high levels of cross reactivity between the conserved regions of LPS. We are working with the Dana Farber Cancer Institute and the University of Nebraska-Lincoln to develop a suite of targeted monoclonal antibodies that target the O-Ag of these serogroups of STEC and can therefore facilitate discriminative detection in our assay platform. During development it is important to consider the biochemical nature of the antigenic target. As the case of LPS has demonstrated, the antigen deposits in different configurations depending on the substrate used during testing. This has implications for the resulting antibodies, which may prefer conformational epitopes found in LPS antigens.<sup>1,2</sup> Thus, the use of physiologically relevant testing schemes, which expose only the O-ag maximizes the chances of obtaining specific antibodies and ensuring their success in physiological assays. The resulting antibodies will be implemented into our membrane insertion assays to increase detection signals and facilitate discriminative detection. Additionally, our collaborators would like to adhere the antibodies to the surface of latex agglutination beads to use in their lab. It is our intent to deposit both the methods for antigen development and the resulting hybridomas into a repository where other groups interested in STEC research can have low cost access to them.

#### *8.1.2 Implication of LPS-induced hole formation in sLBAs*

The discovery that LPS could reorganize sLBAs was highlighted the importance of characterizing the interactions of target antigens with the environment in the detection platforms. Additionally, it gave us new tools for membrane patterning, which can be used to develop better detection surfaces for both amphiphiles and proteins alike. The rearrangements induced in sLBA systems by

LPS under various conditions has demonstrated that biological molecules can behave in unpredictable ways, and thus it is critical to characterize their behavior to ensure assay performance. The implications that this discovery has left us with are far reaching into the fields of biological materials, microbiology, immunology, and assay development. The knowledge that hole formation is dependent on time, concentration, temperature, ionic conditions, and LPS subtype raises extremely interesting points about the mechanisms of bacterial virulence. Additionally, behavior of multiple subtypes of LPS at different temperatures or under varying conditions begs the question of how this molecule responds *in vivo* during infection. This information not only influences detection strategies but also has an impact on the development of vaccine adjuvants and *in vitro* immune studies.

### 8.1.3 Membrane insertion of LPS

Membrane insertion has demonstrated our ability to discriminatively detect LPS. The hydrophobic association of lipid A with the lipid bilayer during membrane insertion implies that the O-ag can be presented more effectively to detection antibodies. Additionally, by implementing an O-ag specific antibody we can increase the sensitivity of detection, validating the need for better reagents. This amphiphilic nature of the molecule demonstrates to be an advantage for discriminative detection, but a hurdle to quantitative measurements. The amphipathic properties of LPS need to be accounted for during sample preparation in order to maximize the homogeneity of the micelles to ensure statistically significant results. Using these techniques, we have demonstrated that membrane insertion of LPS works in minimally prepared, highly complex samples like beef lysates. Lastly, we developed a model system to further characterize and visualize the interactions of amphiphiles in enclosed lipid systems. The experiments done within the flow-cell model provide an opportunity for cross-talk between fluorescence-based detection assays and imaging systems. This can be used as an external method to validate assay performance, characterize antibody-binding behavior, and investigate new functional surfaces within the context of membrane insertion assays.

#### 8.1.4 Differential presentation LPS *in vitro*

The inflammatory effects of LPS both *in vitro* and *in vivo* are presented in the existing literature. *In vivo*, the primary response is that LPS is immediately taken up by serum binding proteins, such as HDL, and carried to the liver for clearance or presented to TLRs for innate immune induction. LPS being amphiphilic cannot exist in monomeric form in blood. Yet, this biochemistry and the physiological association with carrier proteins are conveniently ignored in the design and execution of cell studies. Using TLR4(+) and TLR(-) cells, we have successfully demonstrated that the expression profiles of cytokines and chemokines generated in response to LPS induction vary significantly depending on the serum solution LPS is presented in. Additionally, the expression level of cytokines can be impacted simply by altering the amount time of time LPS is allowed to pre-incubate with serum, as it determines the level of association with serum proteins prior to exposure. These results indicate that there are many interactions between LPS amphiphiles and cells that are still not well characterized. This is especially important to consider when designing studies aimed at being translational to *in vivo* models, as the observations we witness *in vitro* can be drastically altered based on experimental conditions.

## 8.2 Future directions

Taken as a whole, this work describes from beginning to end, the process and considerations for developing discriminative targeted assays against the O-ag of LPS from STEC. The principles we have established here can be transitioned to other amphiphiles. Summarized below are some suggested advancements and applications for this technology. Some of these new ideas are already being tested, while others are just concepts.

### 8.2.1 Advancements for screening antibody clones

In Chapter 4, we presented a new method specifically designed to screen mouse serum or hybridoma culture supernatants for specific antibodies against LPS O-ag. There have been many attempts in the literature to address this, but in general using purified proteins<sup>3</sup> or special functionalization techniques<sup>4,5</sup> is going to be costly

and time consuming. We simplified the functionalization strategy using the principle of lipoprotein capture of LPS.<sup>6,7</sup> When ELISA plates were coated with 50% serum we were able to demonstrate O-ag specific detection of LPS using monoclonal antibodies. The preliminary results have shown comparatively lower standard deviations between the replicates indicating that LPS binds the serum in a set ratio. The serum lipoproteins bind and effectively sequester the lipid A antigen, which minimizes cross reactive binding during the screening. Serum is also plentiful, easy to obtain, relatively inexpensive, and serves as an additional blocking reagent to minimize nonspecific interactions of the detection antibody. Using physiological methods to present the O-ag to the antibodies will maximize the likelihood that isolated antibodies will be specific to the target antigen. The results of this new method are promising, but the technique is still in its infancy. Eventually, we hope to be able to implement this as a new method to improve specificity of antibodies against the O-ag.

### *8.2.2 Improved membrane insertion methods for LPS detection*

Currently, membrane insertion of LPS is presented as a reliable, qualitative method for detection. There are a few techniques that could be implemented to achieve faster, and more repeatable results. Treating the LPS standards with a weak solution of surfactant or solvent prior to running the assay is a relatively simple option. This treatment could serve to homogenize the size distribution of LPS micelles. We have previously performed other assays with weak solutions of buffered Tween, DMSO and ethanol<sup>8,9</sup> and have not seen any disturbance of the lipid bilayers. In fact, the addition of Tween during the sonication of LPS samples helped improve the consistency and reproducibility of our LPS ELISA screening assays.

Passive diffusion of the LPS into the lipid bilayer is an inherently slow process, and strategies to enhance this association may help decrease time per assay. We have observed that using a mixture of fluid-gel phase lipids will cause LPS to migrate to the interface of those lipids in a rapid manner.<sup>10</sup> While the process still technically relies on diffusion, there is likely an exposed hydrophobic region in

the effectively 'taller' lipids, which acts as a driving force to attract LPS. This process could easily be imaged using the flow cell model that we have established and then implemented into the waveguide platform if it is effective. Increasing the speed of these assays would facilitate higher throughput, testing of more samples, and faster implementation of preventative strategies for food safety,

### *8.2.3 Membrane insertion for detection of Shiga toxin*

The virulence of pathogens is co-dependent on other biomarkers and toxins as well. In the case of the STEC, the primary virulence biomarkers are Shiga toxins, more specifically, Shiga toxin 1 (stx1) and Shiga toxin 2 (stx2). Shiga toxins are pentameric protein toxins, which bind an amphiphilic receptor called globotriosylceramide 3 (Gb3) on the surface of host cells.<sup>11</sup> To date, methods for direct and discriminative detection of stx1 from stx2 has been limited by the availability of specific antibodies against both variants of the proteins. To facilitate waveguide-based discriminative detection of stx1 and stx2, our original approach was to use a synthetic variant of Gb3, but there was no commercial source for it. Instead, we performed detection of Shiga toxin by using biotin-avidin chemistry to link antibodies to the surface of the lipid bilayer, to create a capture site. To date, the limitation of available antibodies has only allowed for non-specific capture. It has been demonstrated that LPS from *E. coli* serogroup O107 and O117 will selectively bind stx2, but not stx1.<sup>12</sup> Isolating this LPS and incorporating it into a membrane insertion assay for capture of stx2 is a natural path forward for our work. A capture antibody could be incorporated for stx1, and specific mAb's could be used to facilitate discriminative detection. This also highlights the advantage of using a platform, the waveguide biosensor that is amenable to various transduction schemes in parallel. This assay still pairs well with membrane insertion for detection of LPS, provided that O-ag specific antibodies are used. This approach takes advantage of the natural association of LPS with bilayers both to facilitate specific detection of LPS and create a discriminate ligand-binding site for stx2. Since individual capture methods are used for stx1, stx2, and LPS, the assay would be easy to multiplex using different fluorescent labels or quantum dots. The prevalence of virulent strains

of LPS O107 and O117 is low,<sup>13</sup> but should they be present in a sample, a drawback to this system is that it could not be tuned for the detection of these two serogroups. However, the positive identification of Shiga toxin is enough to determine the pathogenicity of bacterial isolates.

### 8.3 References

- (1) Brooks, C.L. *et al.* Exploration of Specificity in Germline Monoclonal Antibody Recognition of a Range of Natural and Synthetic Epitopes. *J Mol Struct* **2008**, 377(2), 450-568.
- (2) Nguyen, H.P. *et al.* Germline Antibody Recognition of Distinct Carbohydrate Epitopes. *Nat Struct Mol Biol* **2003**, 10(12), 1019–1025.
- (3) Tiirola, T. *et al.* Novel Enzyme Immunoassay Utilizing Lipopolysaccharide-Binding Protein as a Capture Molecule for the Measurement of Chlamydial Lipopolysaccharide in Serum. *Diagn Microbiol Infect Dis* **2006**, 54 (1), 7–12.
- (4) Takahashi, K. *et al.* Detection of Lipopolysaccharide (LPS) and Identification of Its Serotype by an Enzyme-Linked Immunosorbent Assay (ELISA) Using Poly-L-Lysine. *J Immunol Methods* **1992**, 153 (1-2), 67–71.
- (5) Jauho, E.S. *et al.* New Technology for Regiospecific Covalent Coupling of Polysaccharide Antigens in ELISA for Serological Detection. *J Immunol Methods* **2000**, 242 (1-2), 133–143.
- (6) Heumann, D. and Baumgartner, J.D. Antibodies to Core Lipopolysaccharide Determinants: Absence of Cross-Reactivity with Heterologous Lipopolysaccharides. *J Infect Dis* **1991**, 163(4), 763-768.
- (7) Vreugdenhil, A.C. *et al.* LPS-Binding Protein Circulates in Association with apoB-Containing Lipoproteins and Enhances Endotoxin-LDL/VLDL Interaction. *J Clin Invest* **2001**, 107 (2), 225–234.
- (8) Sakamuri, R.M. *et al.* Novel Optical Strategies for Biodetection. *Proc SPIE Int Soc Opt Eng*, **2013**, 8812, 881209-881209.
- (9) Sakamuri, R.M. *et al.* Detection of Stealthy Small Amphiphilic Biomarkers. *Journal of Microbiological Methods* **2014**, 103, 112–117.
- (10) Adams, P.G. *et al.* Exploiting Lipopolysaccharide-Induced Deformation of Lipid Bilayers to Modify Membrane Composition and Generate Two-Dimensional Geometric Membrane Array Patterns. *Sci Rep* **2015**, 5, 10331.
- (11) Sandvig, K. Shiga toxins. *Toxicon*, **2001**. 39(11), 1629-1635.
- (12) Gamage, S.D. *et al.* *Escherichia Coli* Serogroup O107/O117 Lipopolysaccharide Binds and Neutralizes Shiga Toxin 2. *J Bacteriol* **2004**, 186 (16), 5506–5512.
- (13) Tennant, S.M. *et al.* Characterisation of Atypical Enteropathogenic *E. Coli* Strains of Clinical Origin. *BMC Microbiol.* **2009**, 9 (1), 117.

## Appendix 1

### Section A1.1 Additional information for Chapter 1

<p><i>E. coli</i> lipid A</p>	<p><i>S. minnesota</i> lipid A</p>	<p><i>N. meningitidis</i> lipid A</p>	<p><i>H. influenzae</i> lipid A</p>
Endotoxic Activity: +++	Endotoxic Activity: +++	Endotoxic Activity: +++	Endotoxic Activity: +++
<p><i>K. pneumoniae</i> lipid A</p>	<p><i>C. jejuni</i> lipid A</p>	<p><i>Y. pestis</i> lipid A</p>	<p><i>H. pylori</i> lipid A</p>
Endotoxic Activity: +++	Endotoxic Activity: ++	Endotoxic Activity: ++(?)	Endotoxic Activity: ++
<p><i>P. aeruginosa</i> lipid A</p>	<p><i>C. trachomatis</i> lipid A</p>	<p><i>B. fragilis</i> lipid A</p>	<p><i>B. pertussis</i> lipid A</p>
Endotoxic Activity: +	Endotoxic Activity: +	Endotoxic Activity: +	Endotoxic Activity: + (?)
<p><i>R. sphaeroides</i> lipid A</p>	<p><i>P. gingivalis</i> lipid A</p>	<p>Compound 406 (Ia)</p>	<p>Lipid X</p>
Endotoxic Activity: - (LPS antagonist)	Endotoxic Activity: + (TLR-2 agonist)	Endotoxic Activity: - (LPS antagonist)	Endotoxic Activity: - (Very weak antagonist)

**Figure A1.1** Structures of Gram-negative lipid A molecules. Common substitutions are indicated by grey lines. Endotoxic activities is indicated by '+++' for strongest activity and '-' for no activity and is intended only as a qualitative guide only. Reprinted from Erridge et al. 2002 with permission from Elsevier.

## Appendix 2

### Section A2.1 Chapter 3 supplementary tables and figures

**Table A2.1. Extracted and purified amounts of LPS from dried bacteria.**

Strain	O-group	Dry Bacteria (g)	Crude Extract (g)	Starting Product (g)	Final Product (g)
DEC10B	O26	11.1	1.10	0.40	0.067
B8227-C8	O45	22.2	3.55	0.54	0.025
MT#80	O103	22.4	1.30	0.48	0.078
TY-2482	O104	38.9	1.07	2.45	0.028
O201 9611	O111	28.9	1.81	1.45	0.121
MDCH-4	O113	36.5	5.88	4.31	0.021
GS G5578620	O145	53.3	4.90	3.98	0.013

Crude extract has been phenol extracted from dried bacteria, dialyzed, and freeze dried. Starting product is the amount of purified extract post-ultracentrifugation that went into CTAB/ethanol precipitation and the resulting final dry product weights after removal of nucleic acids.

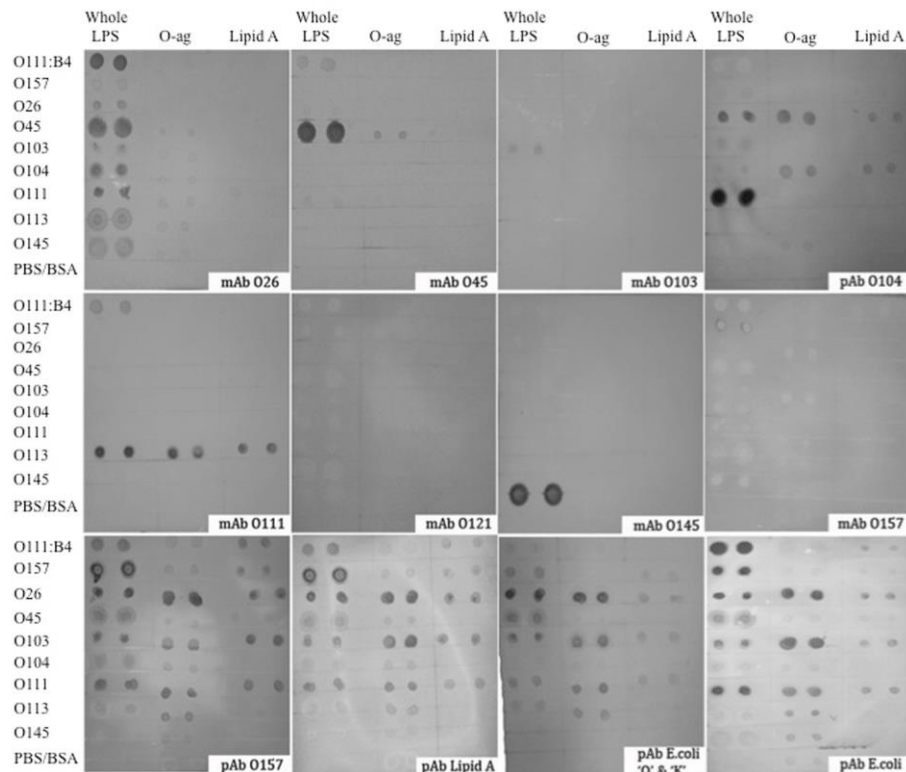


**Figure A2.1. Immunoblots of LPS antigens.** Results for O-ag and whole LPS are summarized in Table 3.2, and lipid A results are summarized in Table A1.2. Rows are the serogroup of LPS and columns are the antigenic portion being tested against the designated antibody.

**Table A2.2. Immunoblotting antibody activity against isolated lipid A fractions from LPS antigens.**

Antigen	ID #	Antibody	Antigen Serogroup								
			O111:B	O157	O26	O45	O103	O104	O111	O113	O145
LPS lipid A	1	Lipid A - O157	++	++	+++	-	+++	-	++	+	-
	2	LPS - O157	++	++	+++	+	+++	-	+++	+	-
	3	<i>E. coli</i> 'O' & 'K'	+	+	++	+	++	-	++	+	-
	4	<i>E. coli</i> LPS	+	+	++	+	++	-	+	+	+
	5	O104	-	+	++	-	++	-	-	-	-
	6	O26	+	+	+	-	+	+	-	-	-
	7	O45	-	-	-	+	-	-	-	-	-
	8	O103	-	-	-	-	-	-	-	-	-
	9	O111	-	-	-	-	-	-	+++	-	-
	10	O145	-	-	-	-	-	-	-	-	-
	11	O157	-	-	-	-	-	-	-	-	-
	12	O121	-	-	-	-	-	-	-	-	-

+++ = intensely positive, ++ = moderately positive, + = weakly positive, - = negative result.

1

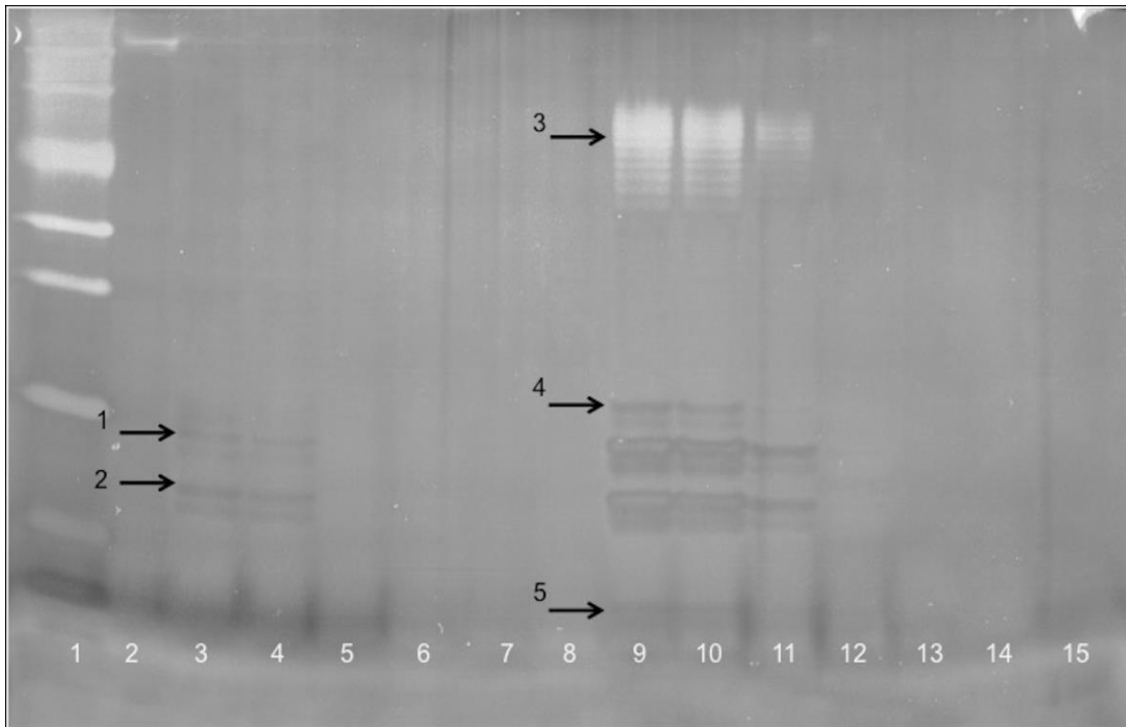


**Figure A2.2. Eosin stained SDS-PAGE of LPS extracts.** Lane (1) protein standard (2) 94µM BSA, lanes 3-6 LPS O157: (3) 3.33mg/mL, (4) 2.5mg/mL, (5) 500µg/mL, (6) 250µg/mL, (7) 1:1 dilution of O157 O-ag prep, (8) 1:1 dilution of O157 lipid A prep. Lanes 9-12 LPS O111:B4: (9) 3.33mg/mL, (10) 2.5mg/mL, (11) 500µg/mL, (12) 250µg/mL, (13) 1:1 dilution of O111:B4 O-ag prep, (14) 1:1 dilution of O111:B4 lipid A prep. Black arrows indicate the location of bands. 1 and 2 are the predicted core polysaccharide of LPS O157, 3 is the O-ag ladder pattern of LPS O111:B4, 4 is core polysaccharide and 5 is the lipid A.

## Appendix 3

### Section A3.1 Longitudinal results for mouse serum screens

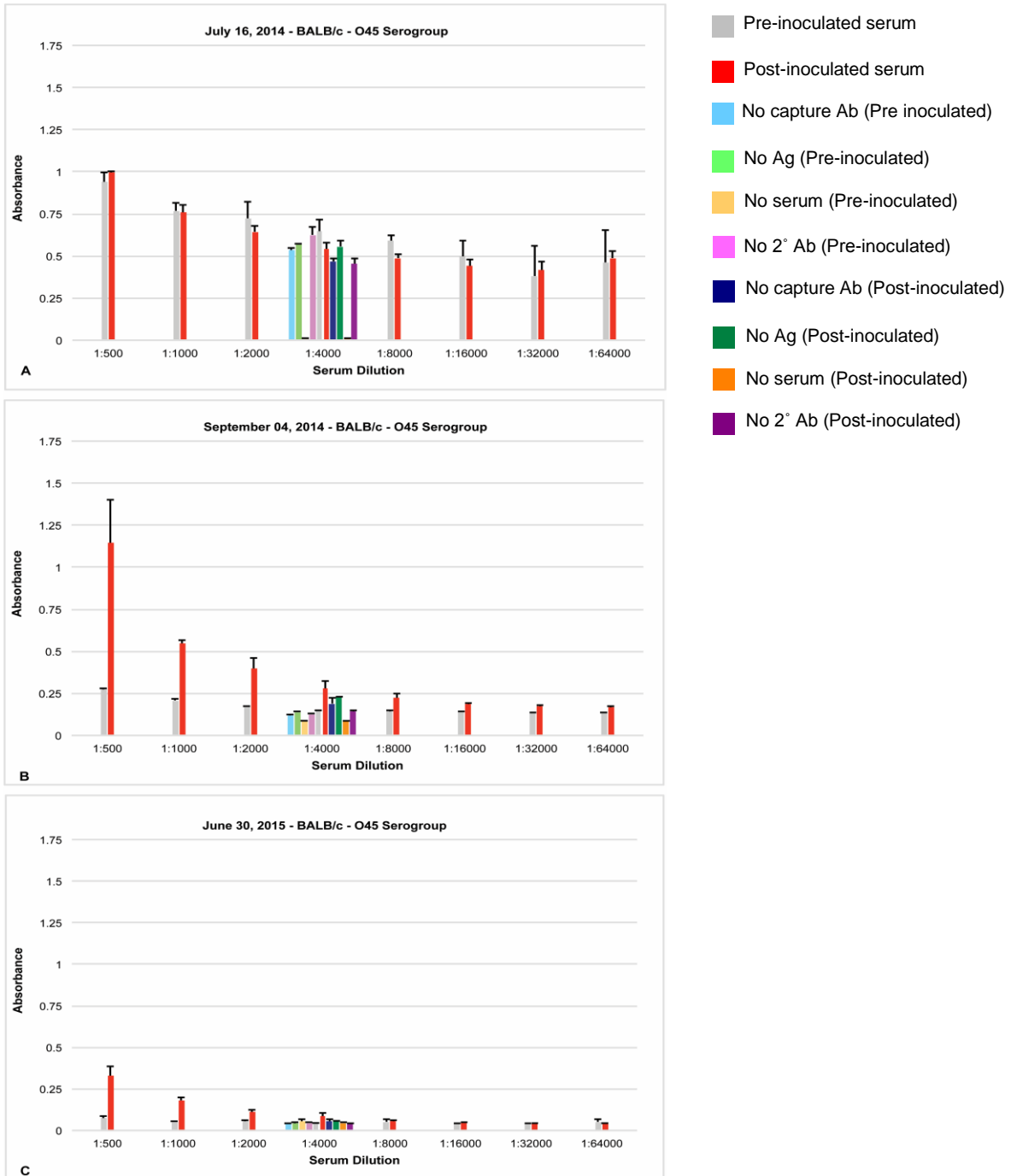


**Figure A3.1. ELISA results for a BALB/C mouse in O45 serogroup.** Three serum screens were performed over time on a BALB/c mouse that was repeatedly immunized with serogroup O45 bacterial antigens. ELISA results performed on June 30, 2015 were performed to analyze mouse immune response after an extended period. No immunoblot was performed for this mouse.

**Table A3.1 Immunoblot summary analysis of BALB/c mouse inoculated with O45 bacterial antigens.**

BALB/c mouse		Pre-Inoculated			Post-Inoculated		
		Whole LPS	O-ag	Lipid A	Whole LPS	O-ag	Lipid A
July 16, 2014	O111:B4	-	+	+	+	+	+
	O157	-	-	+	+	+	+
	O45	+	+	-	++	+	+
	1x PBS/5% BSA	-	-	-	-	-	-
Sept. 04, 2014	O111:B4	-	-	-	-	-	-
	O157	+	+	-	-	++	++
	O45	+	+	-	+	+	-
	1x PBS/5% BSA	-	-	-	-	-	-

No response ' - ', Weak response ' + ', Moderate response ' ++ ', Intense response = ' +++ ' Blue highlighted regions indicates the targeted antigen.

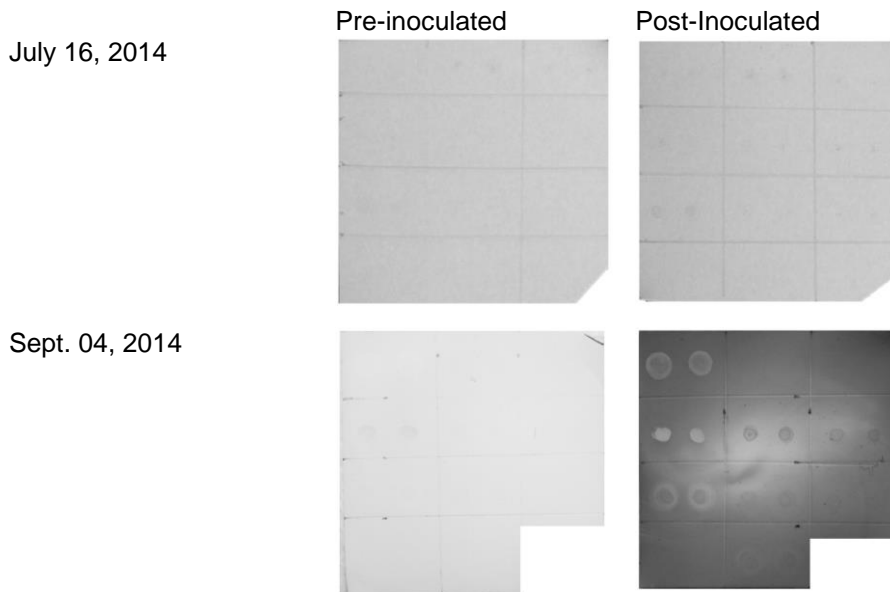


**Figure A3.2. Images of longitudinal dot blots for a BALB/c mouse in O45 serogroup.**  
A summary analysis of these images is presented in Table A3.1.

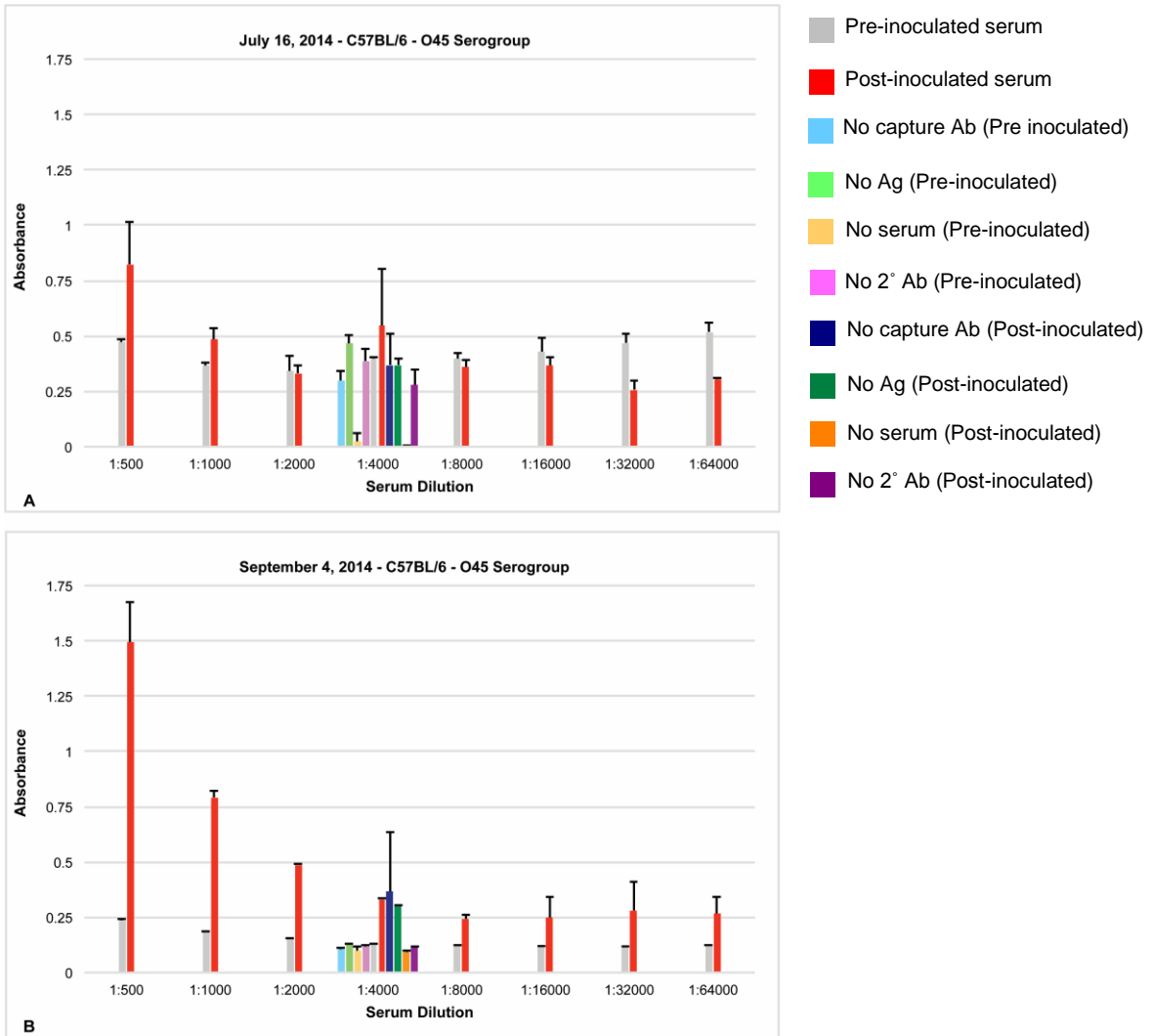


**Figure A3.3. ELISA results for a C57BL/6 mouse in O45 serogroup.** Two serum screens were performed over time on a C57BL/6 mouse that was repeatedly immunized with serogroup O45 bacterial antigens.

**Table A3.2 Immunoblot summary analysis of C57BL/6 mouse inoculated with O45 bacterial antigens.**

		C57BL/6 mouse					
		Pre-Inoculated			Post-Inoculated		
	LPS subtype	Whole LPS	O-ag	Lipid A	Whole LPS	O-ag	Lipid A
July 16, 2014	O111:B4	-	+	-	+	+	+
	O157	+	+	-	+	+	+
	O45	+	+	-	++	+	-
	1x PBS/5% BSA	-	-	-	-	-	-
Sept. 04, 2014	O111:B4	-	-	-	-	-	-
	O157	-	-	-	-	++	++
	O45	+	-	-	-	-	-
	1x PBS/5% BSA	-	-	-	-	-	-

No response ' - ', Weak response ' + ', Moderate response ' ++ ', Intense response = ' +++ ' Blue highlighted regions indicates the targeted antigen.

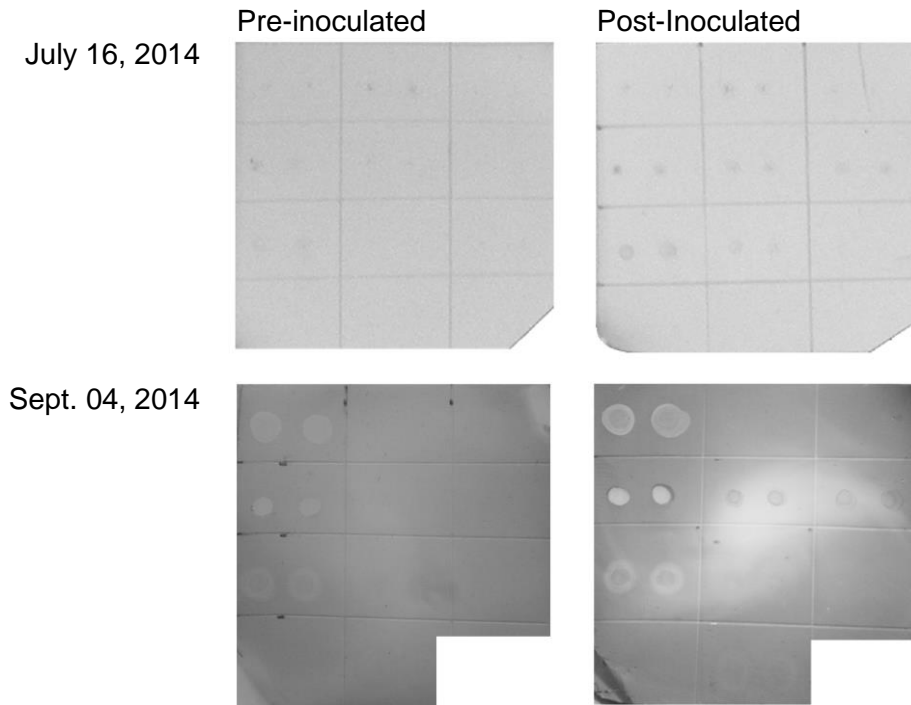


**Figure A3.4 Images of longitudinal dot blots for a C57BL/6 mouse in O45 serogroup.**

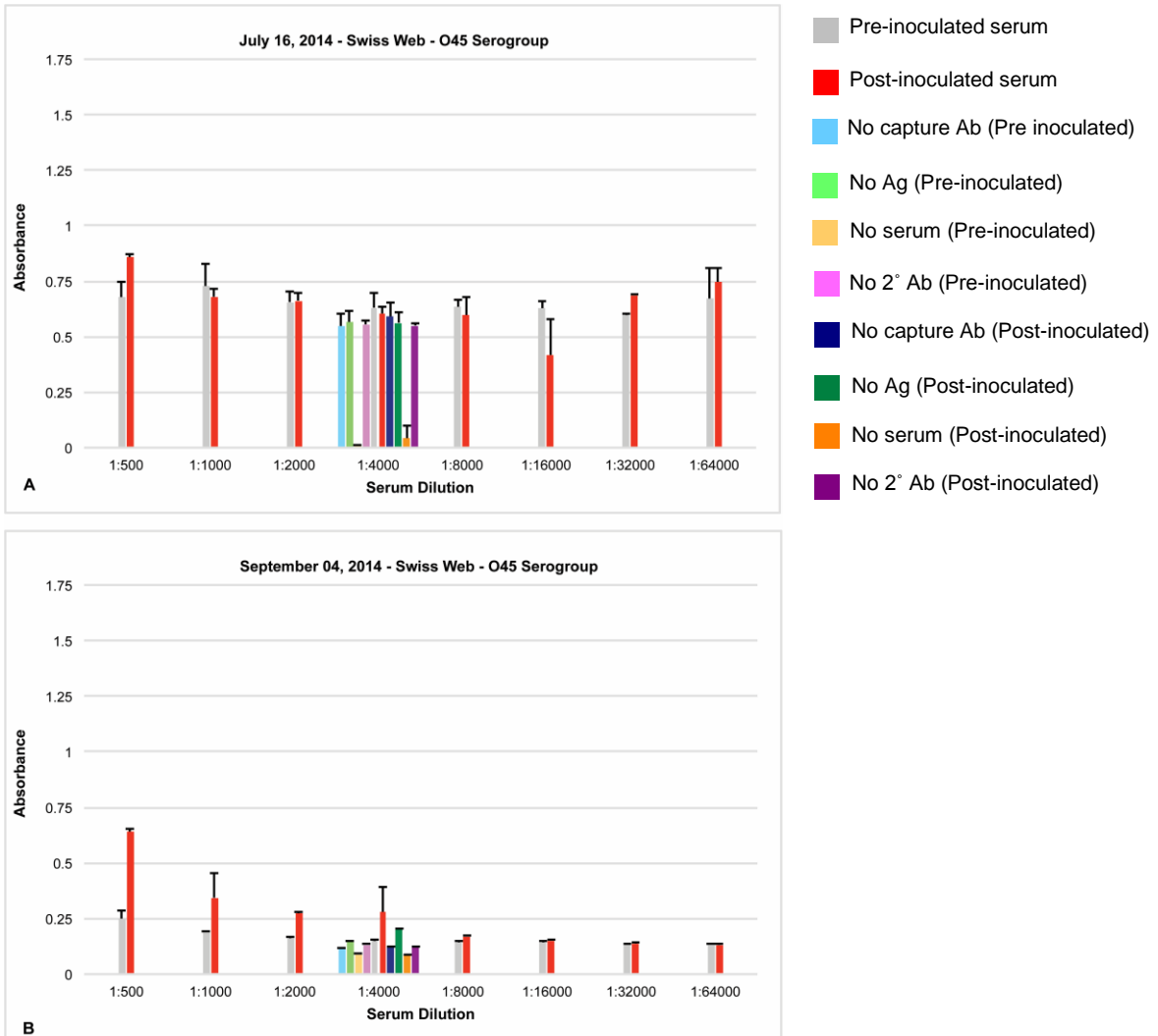


**Figure A3.5. ELISA results for a Swiss Webster mouse in O45 serogroup.** Two serum screens were performed over time on a Swiss Webster mouse that was repeatedly immunized with serogroup O45 bacterial antigens.

**Table A3.3 Immunoblot summary of Swiss Webster mouse inoculated with O45 bacterial antigens.**

		Swiss Webster mouse					
		Pre-Inoculated			Post-Inoculated		
LPS subtype		Whole LPS	O-ag	Lipid A	Whole LPS	O-ag	Lipid A
July 16, 2014	O111:B4	-	+	+	-	+	-
	O157	-	+	-	-	+	-
	O45	+	+	-	+	+	-
	1x PBS/5% BSA	-	-	-	-	-	-
Sept. 04, 2014	O111:B4	-	-	-	+	-	-
	O157	+++	-	-	-	-	+
	O45	+	-	-	-	-	-
	1x PBS/5% BSA	-	-	-	-	-	-

No response ' - ', Weak response ' + ', Moderate response ' ++ ', Intense response = ' +++ ' Blue highlighted regions indicates the targeted antigen.

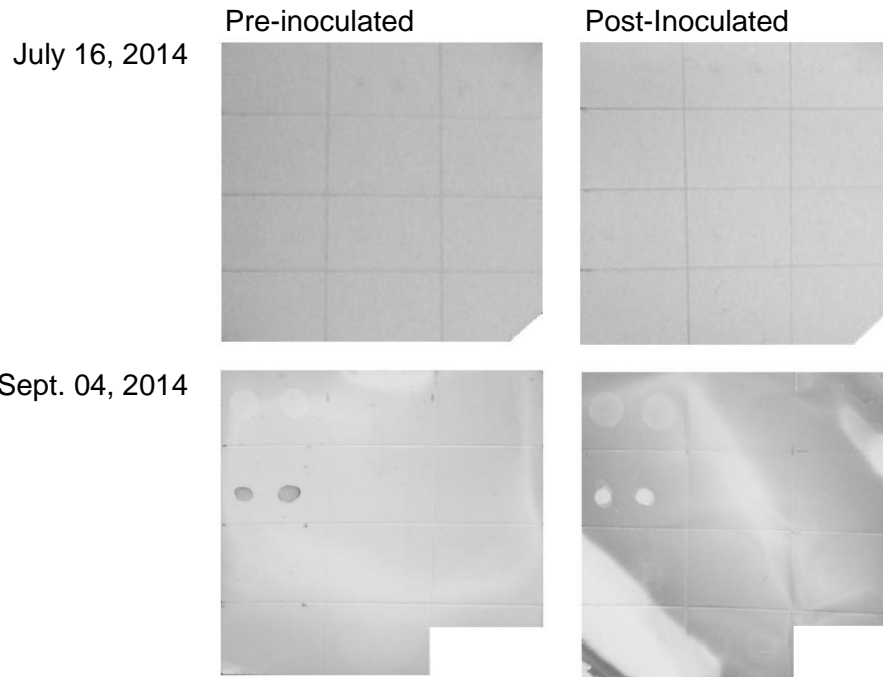


**Figure A3.6 Images of longitudinal dot blots for a Swiss Webster mouse in O45 serogroup.**

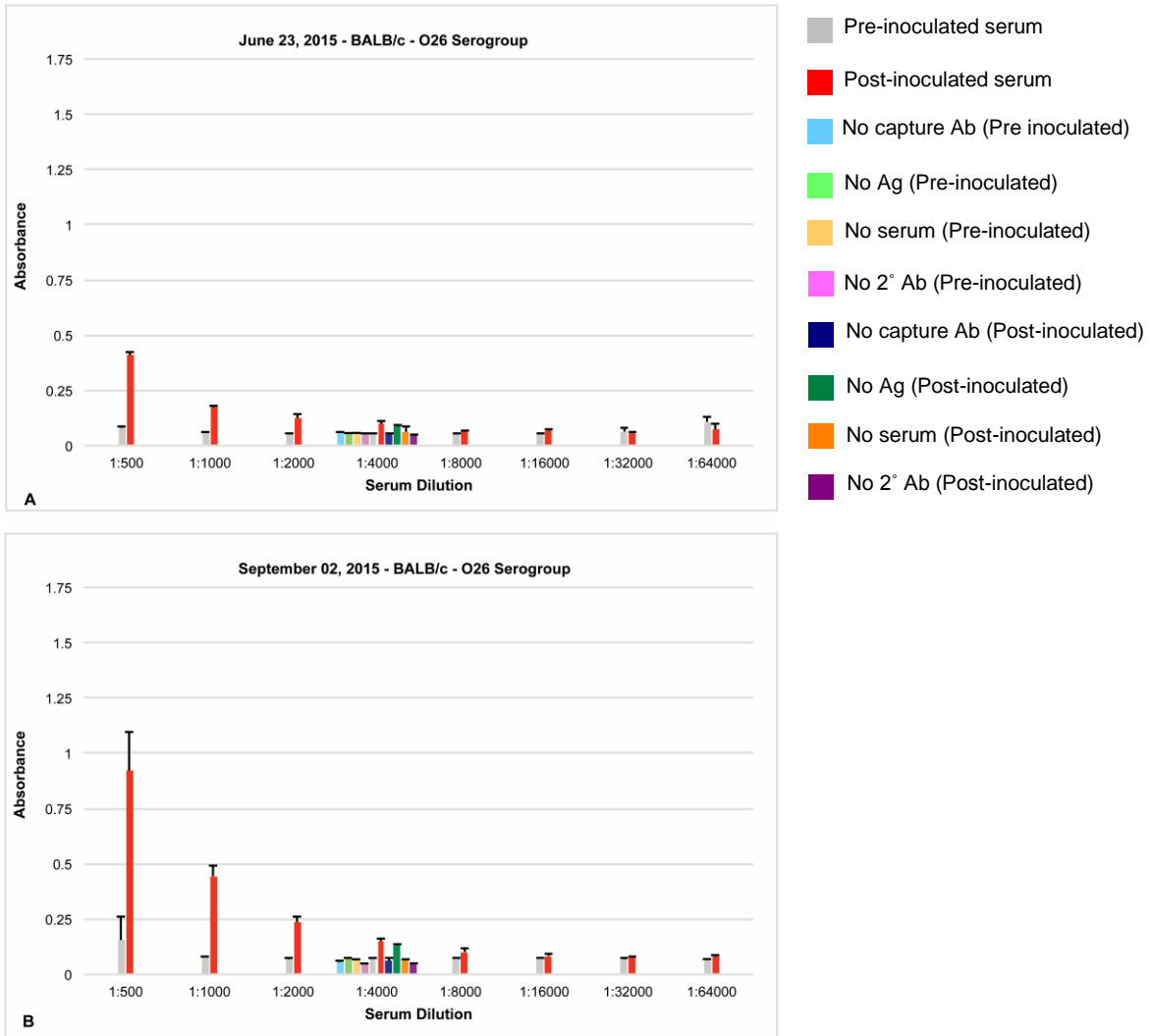


**Figure A3.7. ELISA results for a BALB/C mouse in O26 serogroup.** Two serum screens were performed over time on a BALB/c mouse that was repeatedly immunized with serogroup O26 bacterial antigens. This mouse was selected for hybridoma fusion after the second screening was completed.

**Table A3.4 Immunoblot summary of a BALB/c mouse inoculated with O26 bacterial antigens.**

BALB/c mouse		Pre-Inoculated			Post-Inoculated		
LPS subtype	Whole LPS	O-ag	Lipid A	Whole LPS	O-ag	Lipid A	
June 23, 2015	O111:B4	-	-	-	-	-	-
	O157	-	+	-	-	+	+
	O26	+	+	-	+	+	+
	1x PBS/5% BSA	-	-	-	-	-	-
Sept. 02, 2015	O111:B4	-	-	-	-	-	+
	O157	-	+	NA	+	+	NA
	O26	-	+	+	++	+++	++
	1x PBS/5% BSA	-	-	-	-	-	-

No response ' - ', Weak response ' + ', Moderate response ' ++ ', Intense response = ' +++ ', NA = control antigens were not available for testing. Blue highlighted regions indicates the targeted antigen.

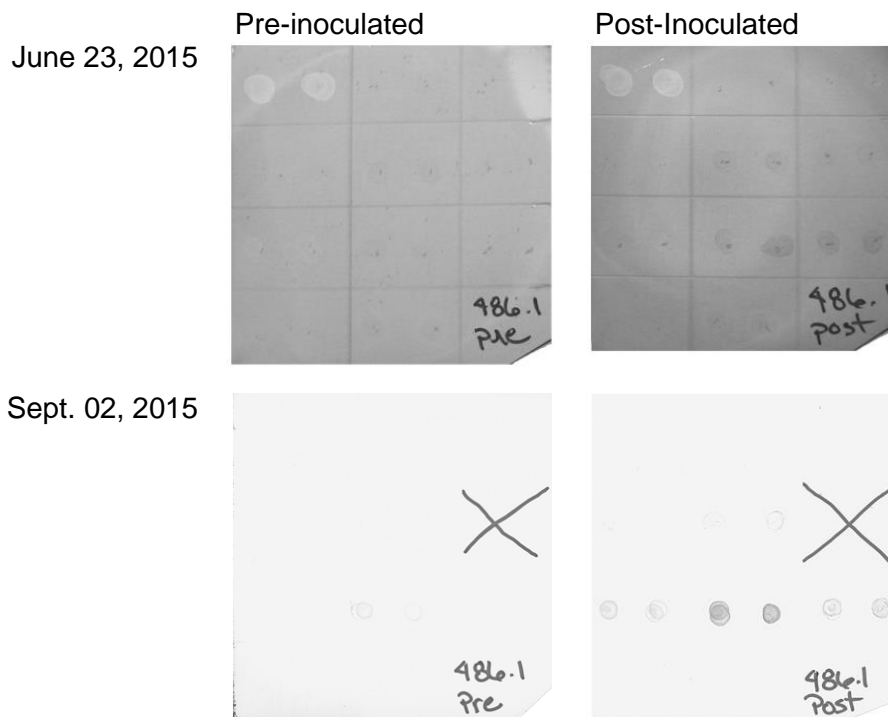


**Figure A3.8 Images of longitudinal dot blots for a BALB/c mouse in the O26 serogroup.** A new immunoblotting protocol was implemented on September 2, 2015, which resulted in much lower background staining of the nitrocellulose membranes. X's indicate the absence of an antigen blot in that square.

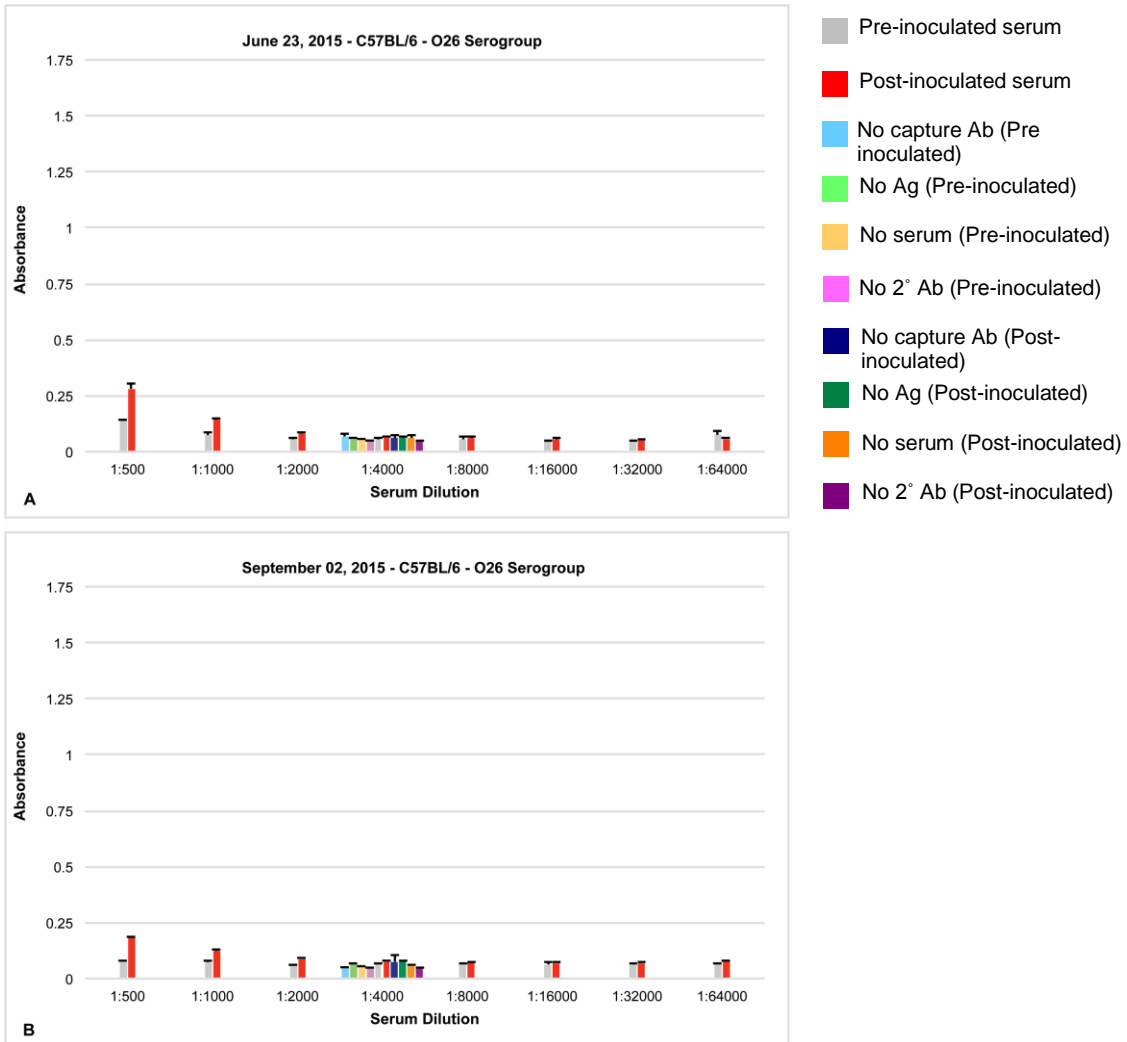


**Figure A3.9 (A-B). ELISA results for a C57BL/6 mouse in O26 serogroup.** A-B. First set of two graphs for serum screens performed over time on a C57BL/6 mouse that was repeatedly immunized with serogroup O26 bacterial antigens. C-D. Second set of 2 graphs in the longitudinal serum screen. Graphs C-D appear on the following page.

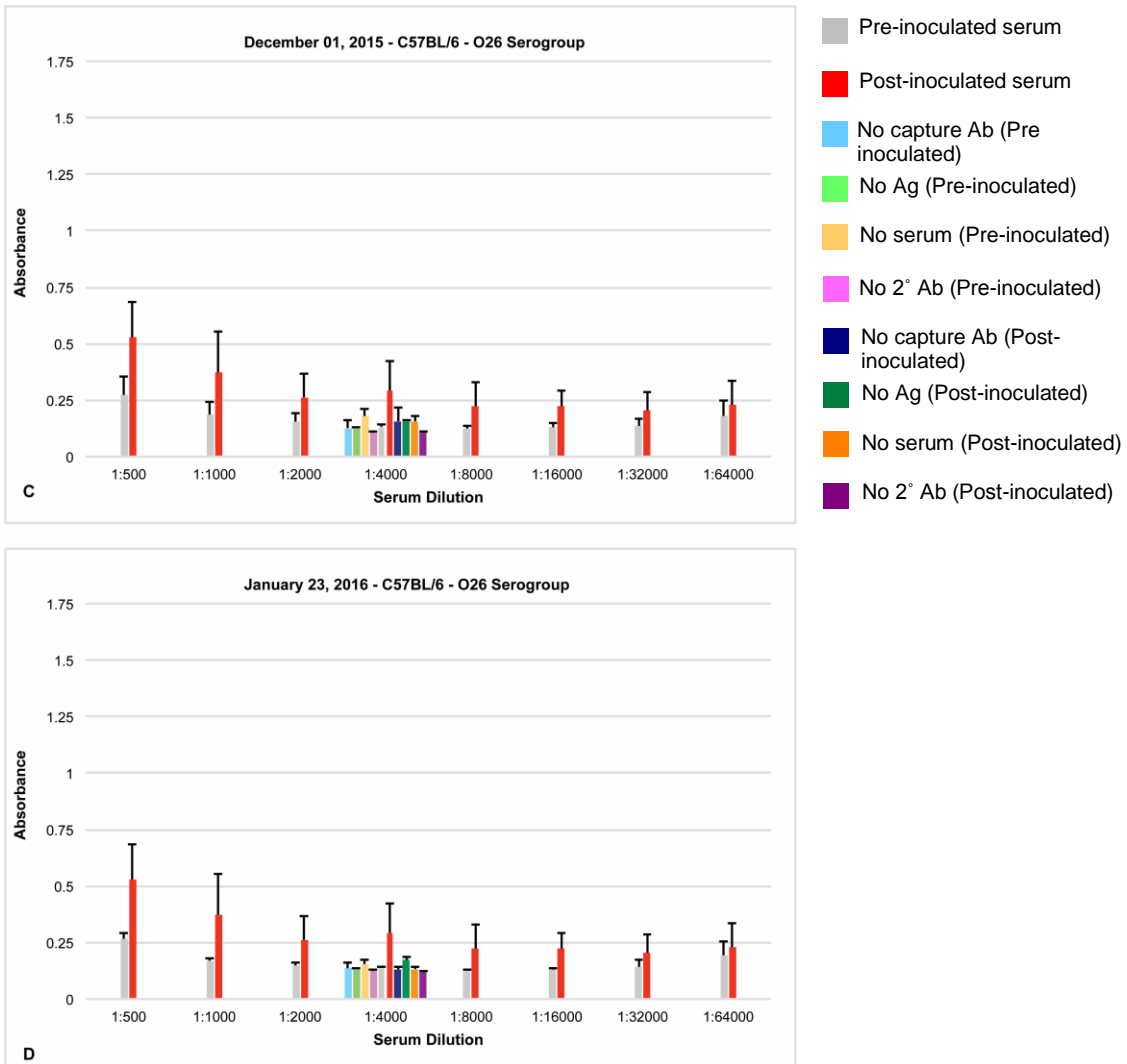


**Figure A3.9 (C-D). ELISA results for a C57BL/6 mouse in O26 serogroup.** A-B. First set of four graphs for serum screens performed over time on a C57BL/6 mouse that was repeatedly immunized with serogroup O26 bacterial antigens. Graphs A-B appear on the previous page. C-D. Second set of 2 graphs in the longitudinal serum screen.

**Table A3.5 Immunoblot summary analysis of C57BL/6 mouse inoculated with O26 bacterial antigens.**

		C57BL/6 mouse					
		Pre-Inoculated			Post-Inoculated		
	LPS subtype	Whole LPS	O-ag	Lipid A	Whole LPS	O-ag	Lipid A
June 23, 2015	O111:B4	-	-	-	-	-	-
	O157	-	-	-	+	+	+
	O26	+	+	-	+	+	+
	1x PBS/5% BSA	-	-	-	-	-	-
Sept. 02, 2015	O111:B4	-	-	NA	+	-	NA
	O157	-	-	NA	+	++	NA
	O26	+	+	+	++	+++	++
	1x PBS/5% BSA	-	-	-	-	-	-
Dec. 01, 2015	O111:B4	-	-	NA	-	-	NA
	O157	+	+	NA	+	++	NA
	O26	++	++	-	++	+++	++
	1x PBS/5% BSA	-	-	-	-	-	-
Jan. 23, 2016	O111:B4	-	-	NA	-	-	NA
	O157	-	-	NA	-	++	NA
	O26	++	+	-	-	++	+
	1x PBS/5% BSA	+++	-	-	++	-	-

No response '-'; Weak response '+'; Moderate response '++'; Intense response = '+++'; NA = control antigens were not available for testing. PBS control on January 23, 2016 became contaminated during the blotting procedure. Blue highlighted regions indicates the targeted antigen.

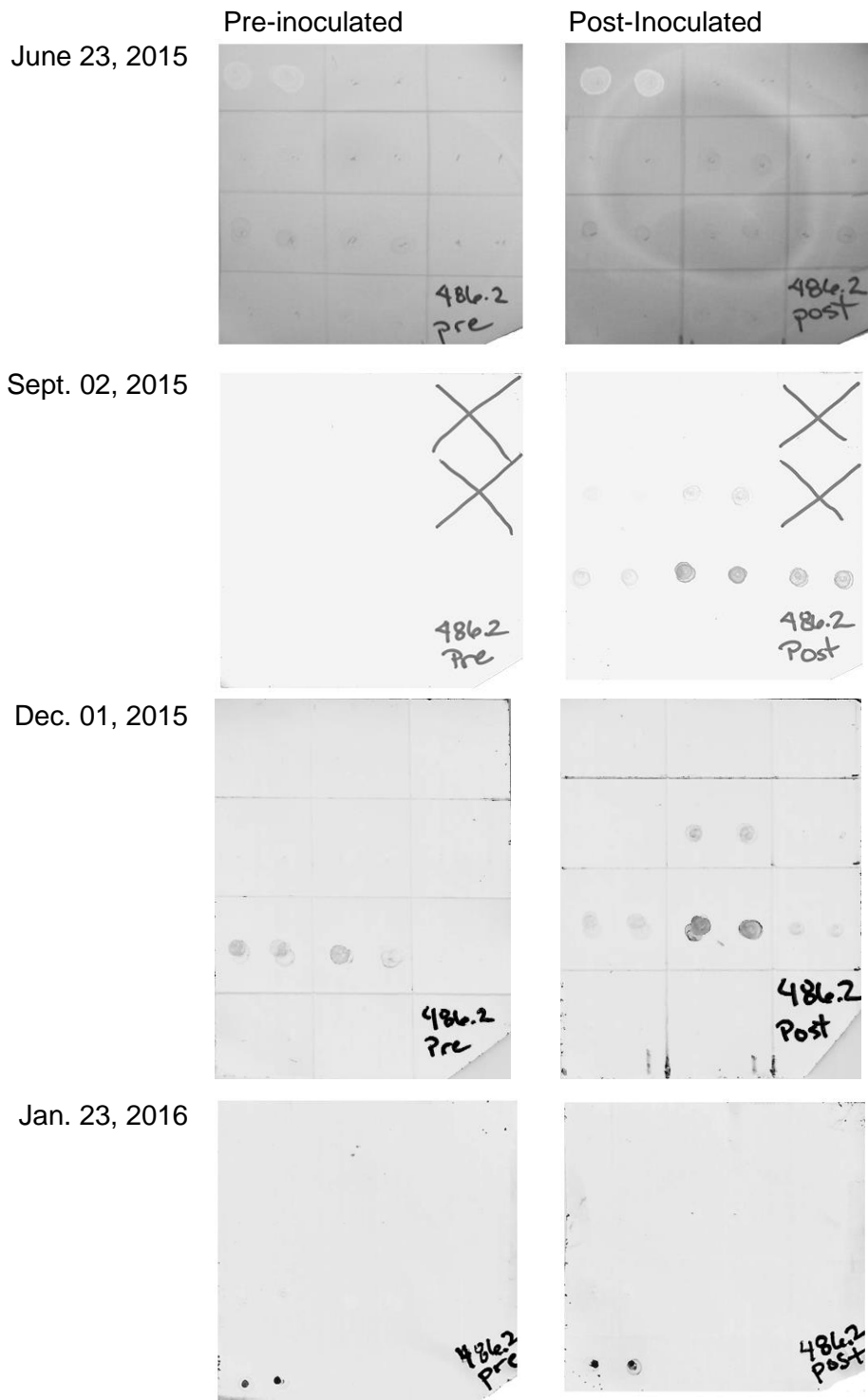


**Figure A3.10** Images of longitudinal dot blots for a C57BL/6 mouse in the O26 serogroup. X's indicate the absence of an antigen blot in that square.

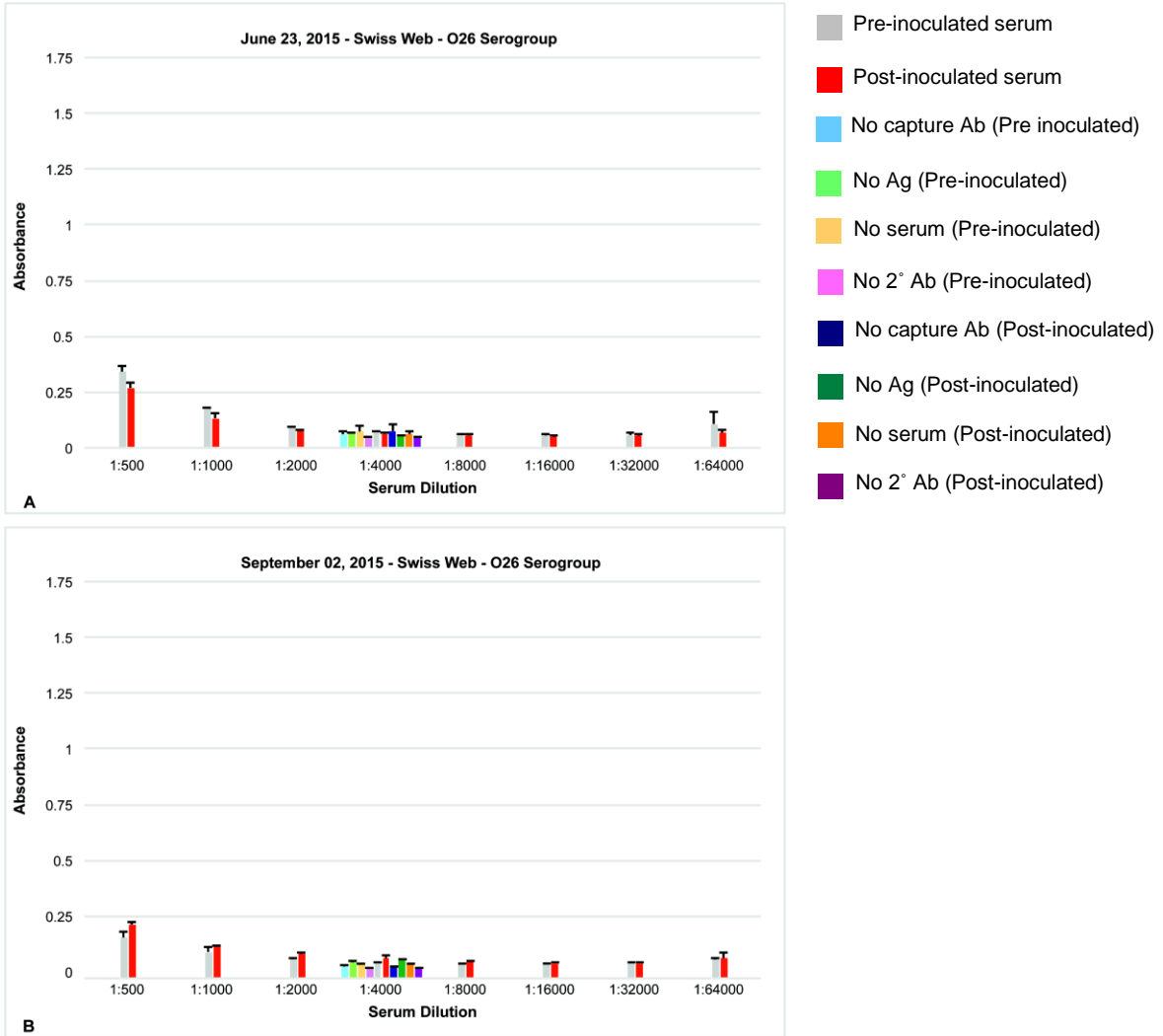


**Figure A3.11 (A-B). ELISA results for a Swiss Webster mouse in O26 serogroup.** A-B. First set of four graphs for serum screens performed over time on a mouse that was repeatedly immunized with serogroup O26 bacterial antigens. C-D. Second set of 2 graphs in the longitudinal serum screen. Graphs C-D appear on the following page.

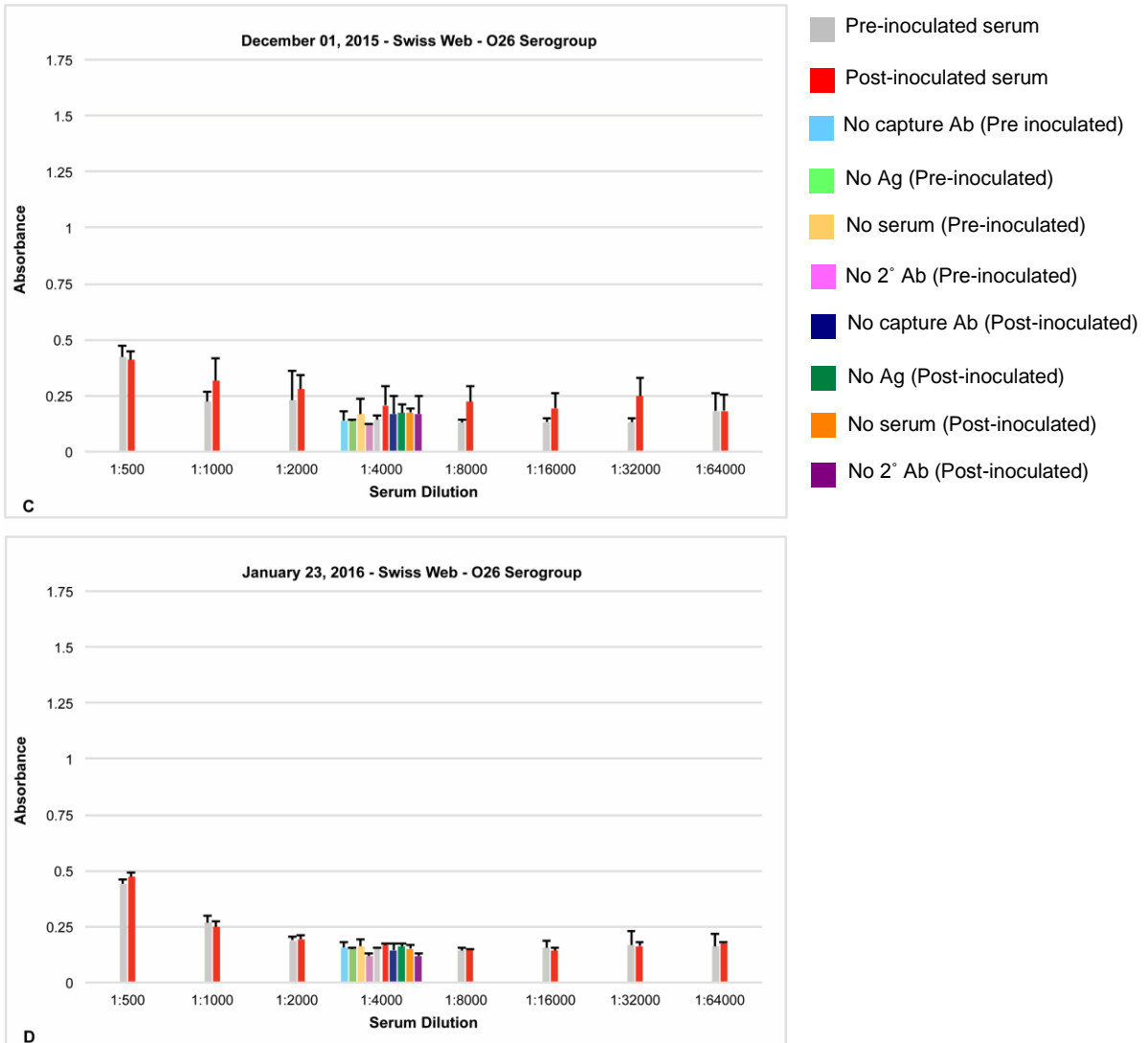


**Figure A3.11 (C-D). ELISA results for a Swiss Webster mouse in O26 serogroup.** C-D. Second set of four graphs for serum screens performed over time on a mouse that was repeatedly immunized with serogroup O26 bacterial antigens. Graphs C-D appear on the previous page.

**Table A3.6 Immunoblot summary analysis of a Swiss Webster mouse inoculated with O26 bacterial antigens.**

		Swiss Webster mouse					
		Pre-Inoculated			Post-Inoculated		
	LPS subtype	Whole LPS	O-ag	Lipid A	Whole LPS	O-ag	Lipid A
June 23, 2015	O111:B4	-	-	-	-	-	-
	O157	-	+	+	+	+	+
	O26	-	-	-	++	++	+
	1x PBS/5% BSA	-	-	-	-	-	-
Sept. 02, 2015	O111:B4	-	-	NA	+	+	+
	O157	+	+	NA	+	++	NA
	O26	+	+	+	+	+++	++
	1x PBS/5% BSA	-	-	-	-	-	-
Dec. 01, 2015	O111:B4	-	-	NA	-	-	NA
	O157	-	-	NA	-	++	NA
	O26	++	++	-	+	+++	+
	1x PBS/5% BSA	-	-	-	-	-	-
Jan. 23, 2016	O111:B4	-	-	NA	+	-	NA
	O157	+	-	NA	-	+	NA
	O26	+	+	-	-	++	-
	1x PBS/5% BSA	++	-	-	++	-	-

No response ' - ', Weak response ' + ', Moderate response ' ++ ', Intense response = ' +++ ', NA = control antigens were not available for testing. PBS control on January 23, 2016 became contaminated during the blotting procedure. Blue highlighted regions indicates the targeted antigen.

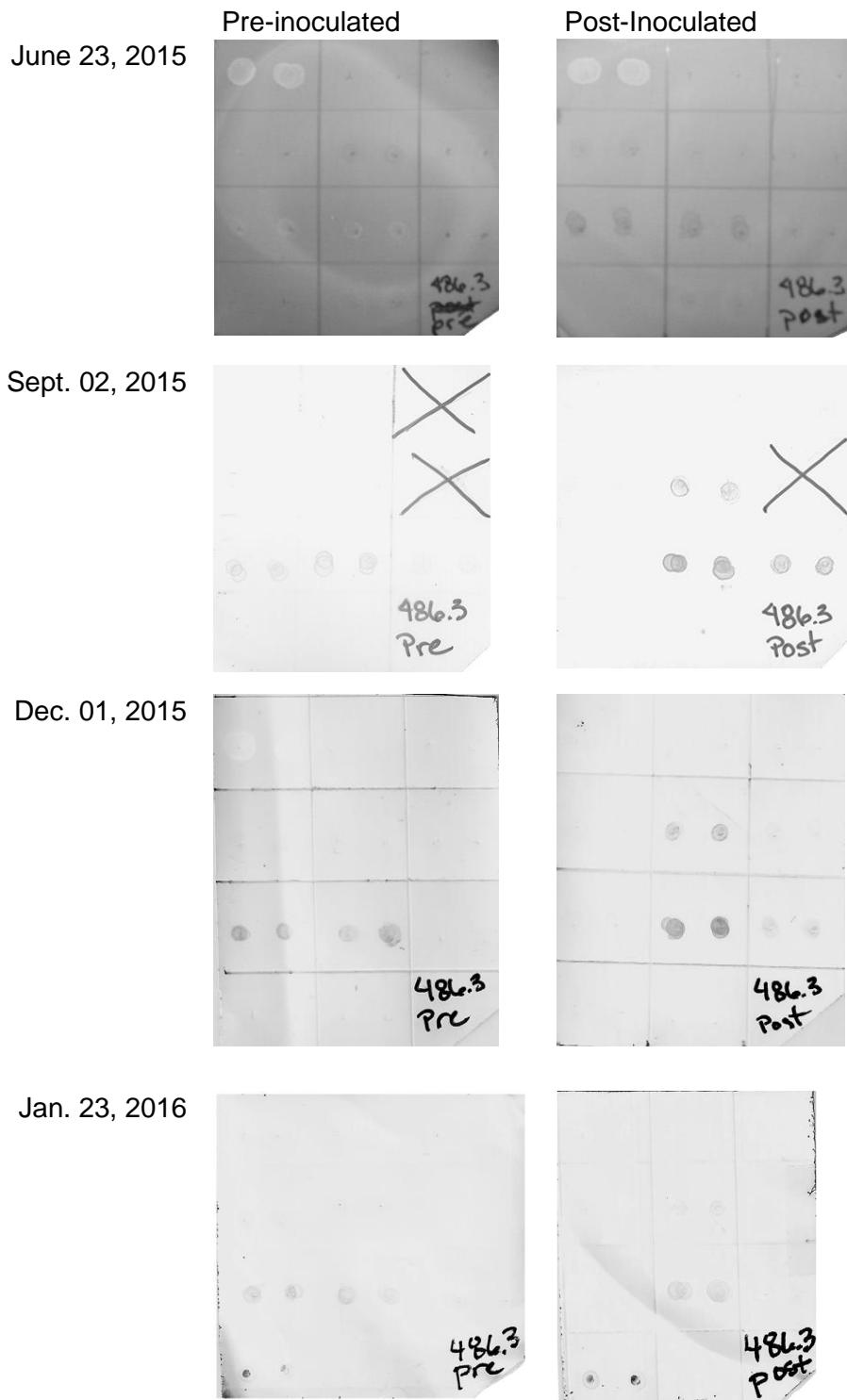


**Figure A3.12 Images of longitudinal dot blots for a Swiss Webster mouse in the O26 serogroup. X's indicate the absence of an antigen blot in that square.**

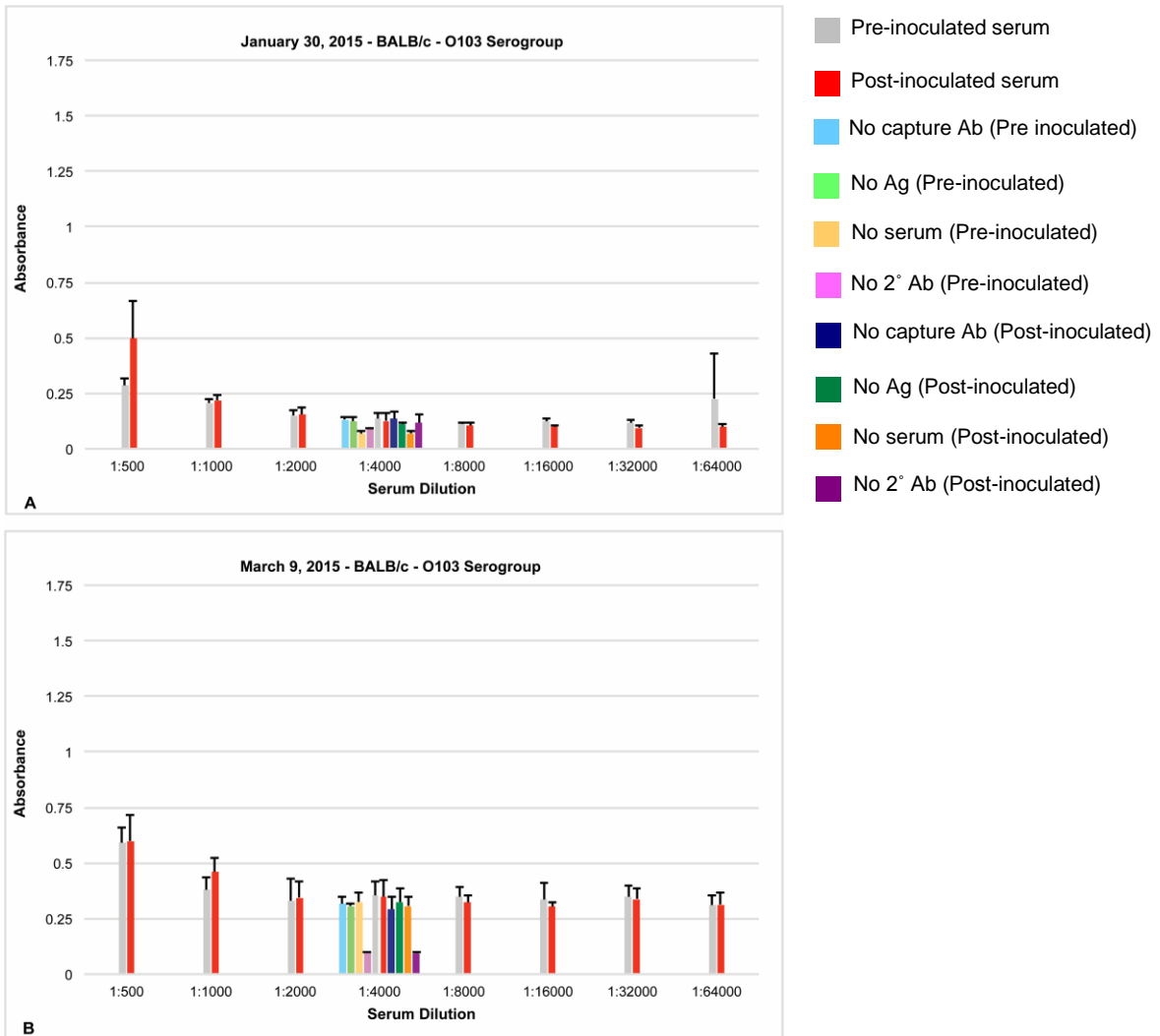


**Figure A3.13 (A-B). ELISA results for a BALB/c mouse in O103 serogroup.** A-B. First set of four graphs for serum screens performed over time on a mouse that was repeatedly immunized with serogroup O103 bacterial antigens. Graphs C-D appear on the following page.

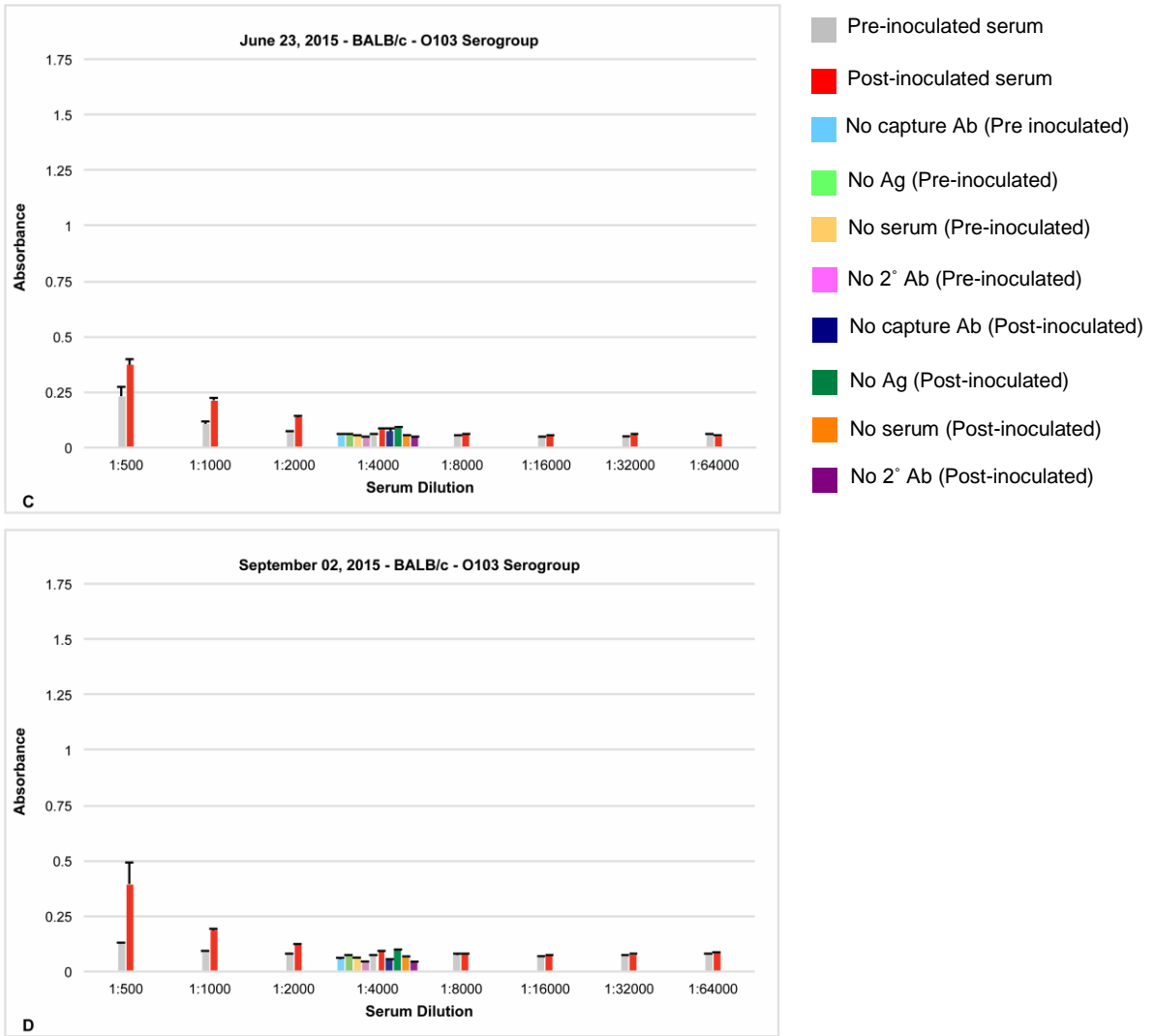
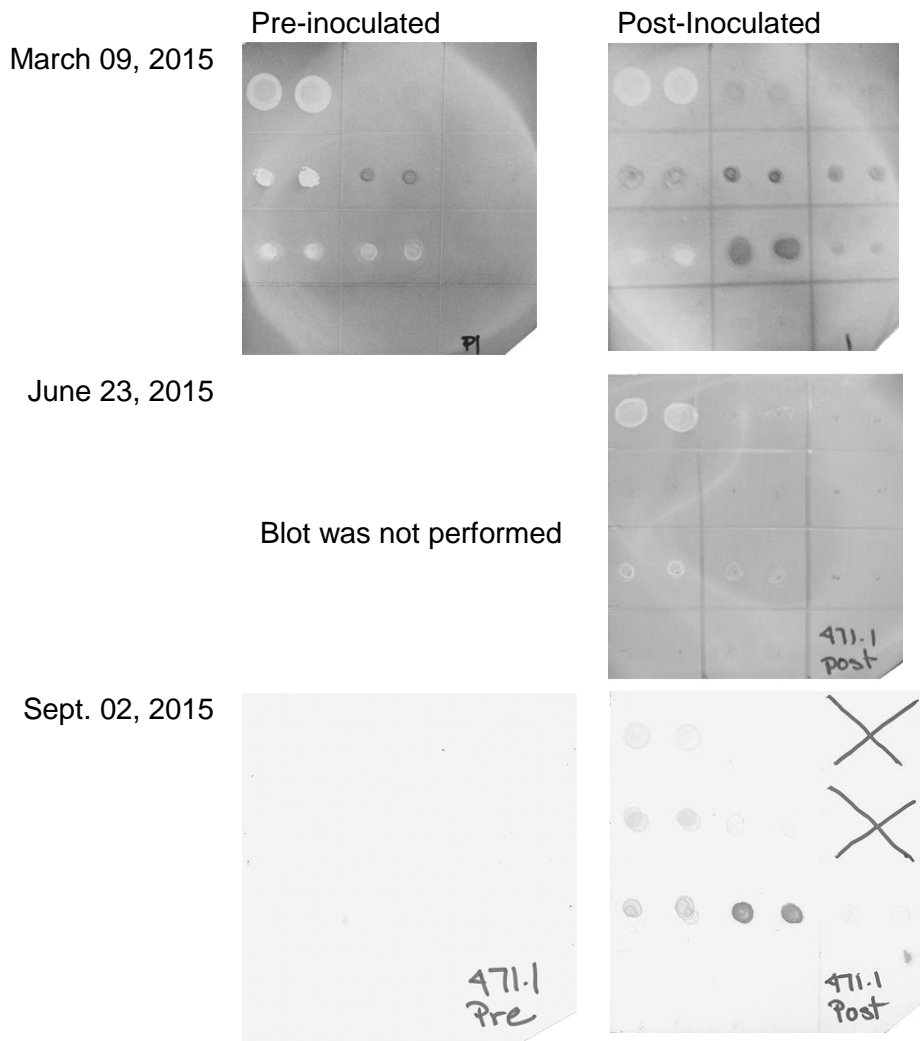


**Figure A3.13 (C-D). ELISA results for a BALB/c mouse in O103 serogroup.** C-D. Second set of four graphs for serum screens performed over time on a mouse that was repeatedly immunized with serogroup O103 bacterial antigens. Graphs A-B appear on the previous page. Mouse was sacrificed to perform a hybridoma fusion.

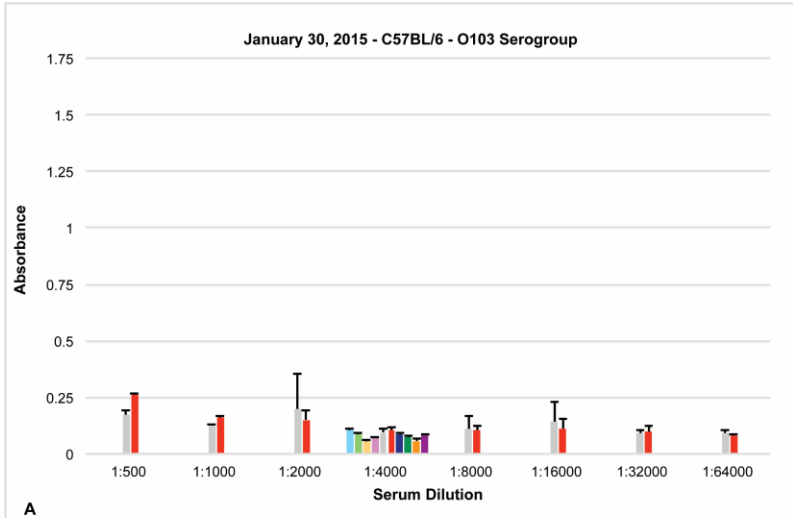
**Table A3.7 Immunoblot summary analysis of a BALB/c mouse inoculated with O103 bacterial antigens.**

		BALB/c mouse					
		Pre-Inoculated			Post-Inoculated		
	LPS subtype	Whole LPS	O-ag	Lipid A	Whole LPS	O-ag	Lipid A
March 09, 2015	O111:B4	+	+	-	+	+	+
	O157	-	++	+	+	+++	+
	O103	-	-	-	-	+++	+
	1x PBS/5% BSA	-	-	-	-	-	-
June 23, 2015	O111:B4	NA	NA	NA	++	-	-
	O157	NA	NA	NA	+	+	-
	O103	NA	NA	NA	+	+	-
	1x PBS/5% BSA	NA	NA	-	-	-	-
Sept. 02, 2015	O111:B4	-	-	NA	+	-	NA
	O157	-	-	NA	++	+	NA
	O103	-	+	-	++	+++	+
	1x PBS/5% BSA	-	-	-	-	-	-

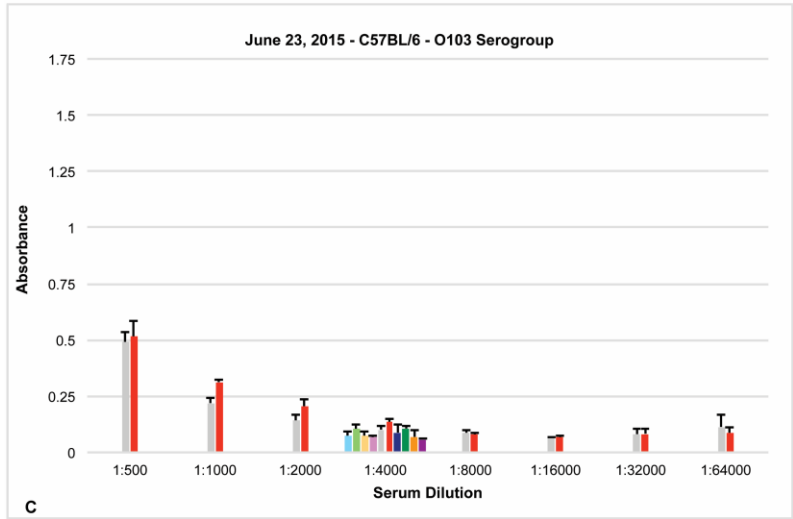
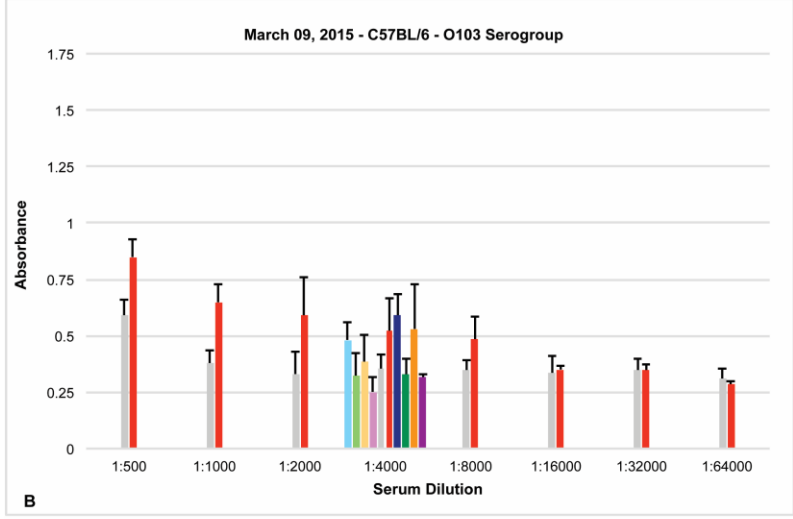
No response '-'; Weak response '+'; Moderate response '++'; Intense response = '+++'; NA = control antigens were not available for testing. June 23, 2015 pre-inoculated blot not performed. Blue highlighted regions indicates the targeted antigen.



**Figure A3.14 Images of longitudinal dot blots for a BALB/c mouse in the O103 serogroup. X's indicate the absence of an antigen blot in that square.**



- Pre-inoculated serum
- Post-inoculated serum
- No capture Ab (Pre inoculated)
- No Ag (Pre-inoculated)
- No serum (Pre-inoculated)
- No 2° Ab (Pre-inoculated)
- No capture Ab (Post-inoculated)
- No Ag (Post-inoculated)
- No serum (Post-inoculated)
- No 2° Ab (Post-inoculated)



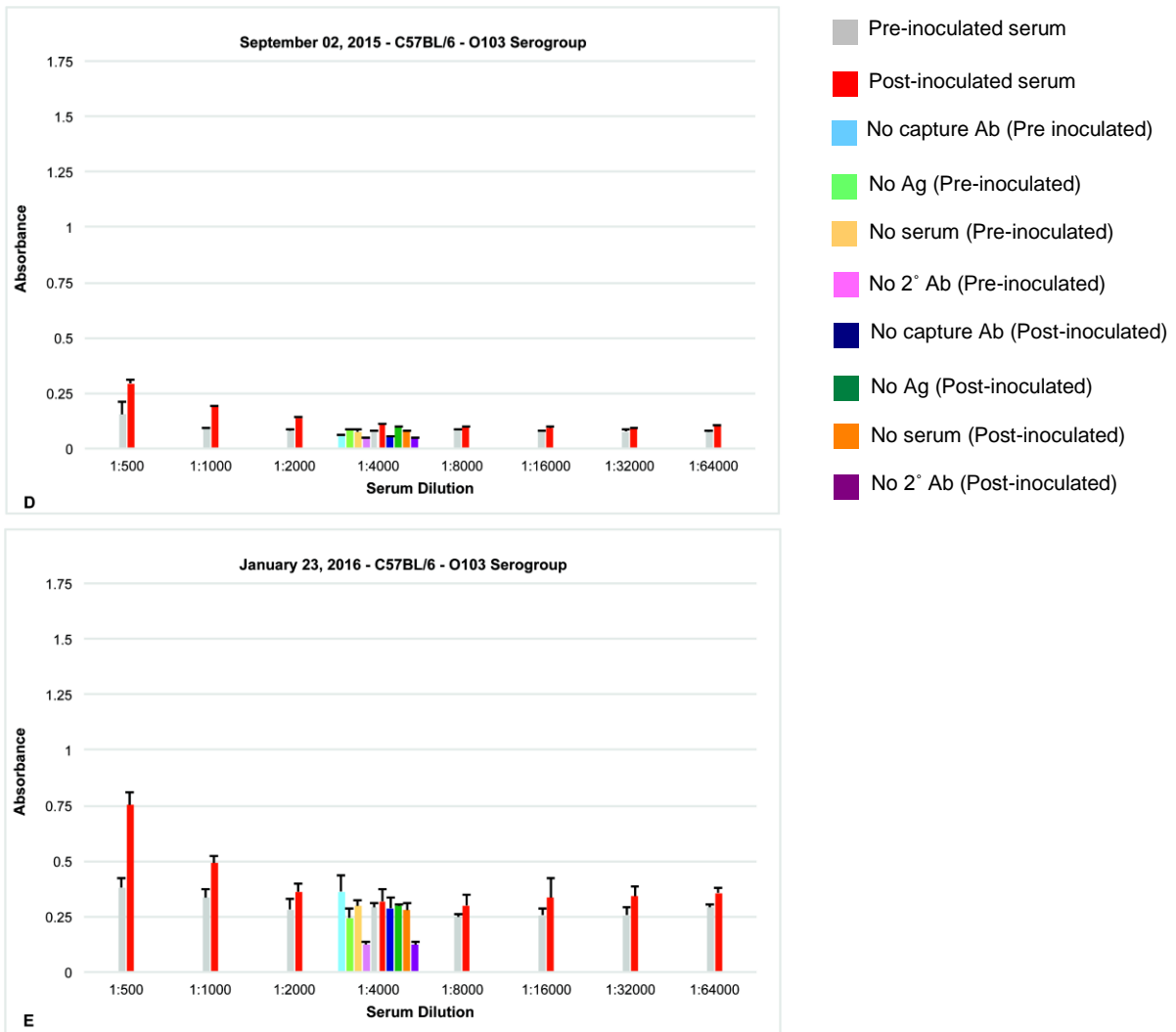
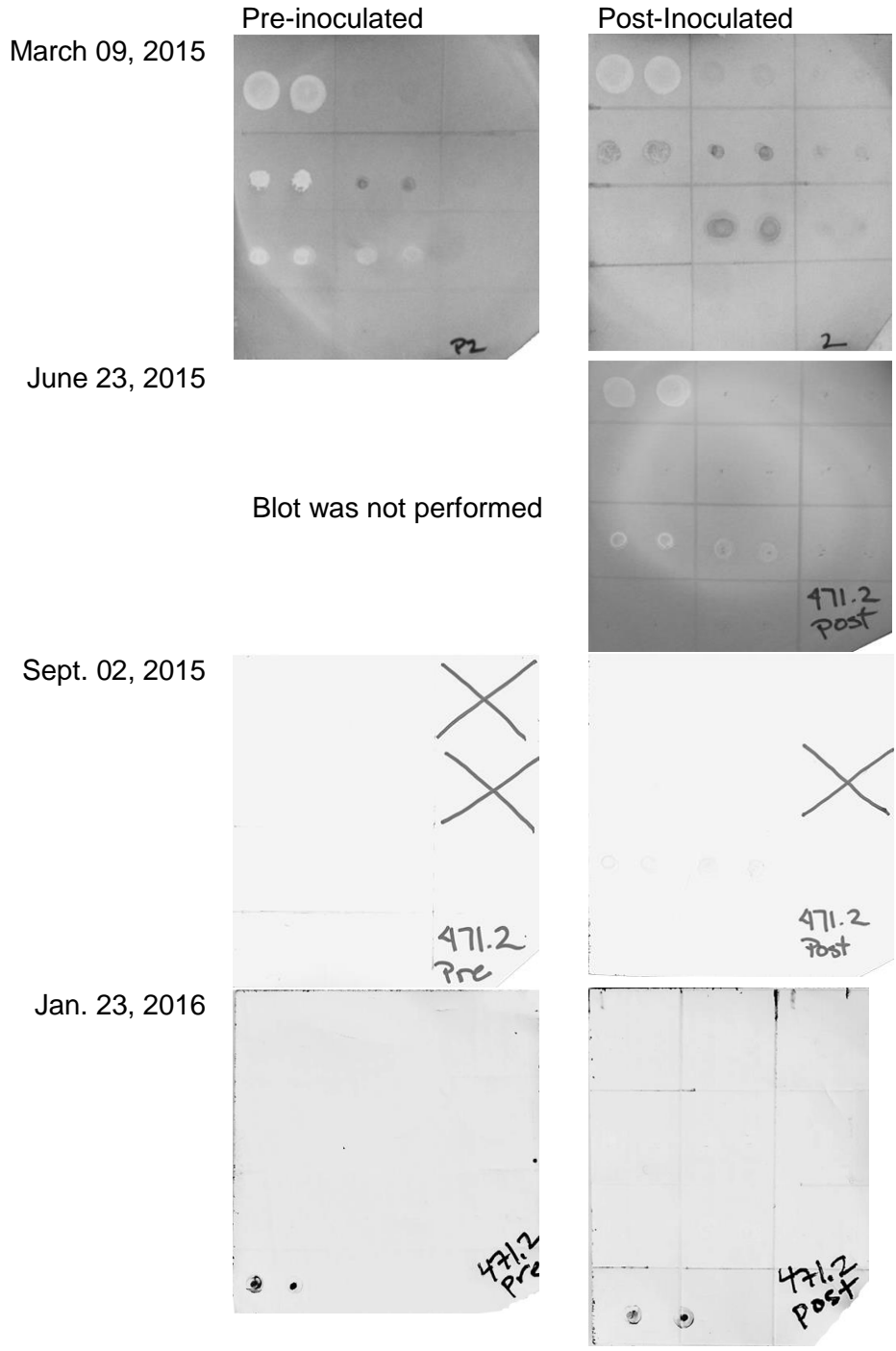


**Figure A3.15. ELISA results for a C57BL/6 mouse in the O103 serogroup.** A-C. Results of first three screens appear on the previous page. D-E. Results of indirect ELISA of 5 serum screens performed over time on a C57BL/6 mouse that was repeatedly immunized with serogroup O103 bacterial antigens.

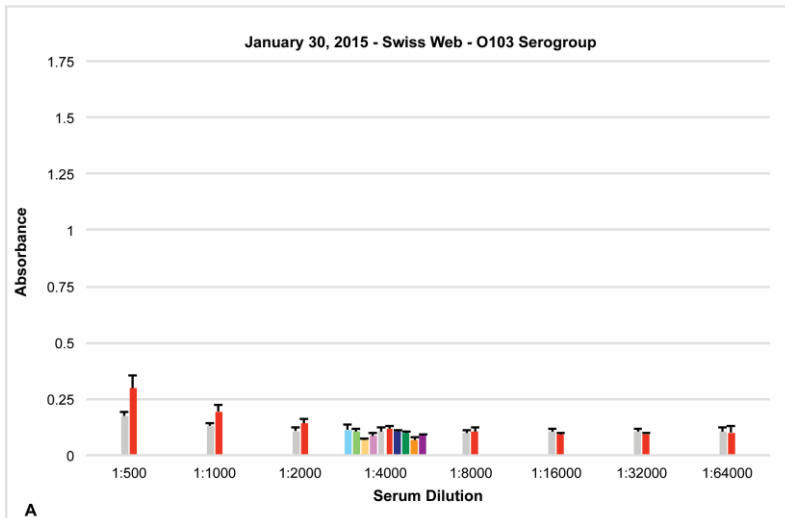
**Table A3.8 Immunoblot summary analysis of C57BL/6 mouse inoculated with O103 bacterial antigens.**

		C57BL/6 mouse					
		Pre-Inoculated			Post-Inoculated		
	LPS subtype	Whole LPS	O-ag	Lipid A	Whole LPS	O-ag	Lipid A
March 09, 2015	O111:B4	+	+	-	+	+	+
	O157	-	+	-	+	++	+
	O103	-	+	-	-	++	+
	1x PBS/5% BSA	-	-	-	-	-	-
June 23, 2015	O111:B4	NA	NA	NA	+	+	-
	O157	NA	NA	NA	+	+	-
	O103	NA	NA	NA	+	+	-
	1x PBS/5% BSA	NA	NA	-	-	-	-
Sept. 02, 2015	O111:B4	-	-	NA	+	-	+
	O157	-	-	NA	+	+	NA
	O103	-	-	-	++	++	+
	1x PBS/5% BSA	-	-	-	-	-	-
Jan. 23, 2016	O111:B4	-	-	NA	-	-	NA
	O157	-	-	NA	-	++	NA
	O103	-	-	-	-	++	+
	1x PBS/5% BSA	++	-	-	+	-	-

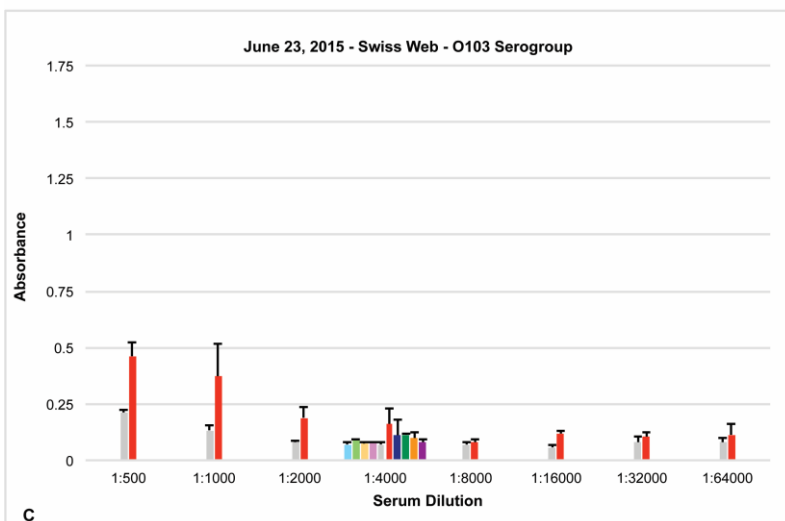
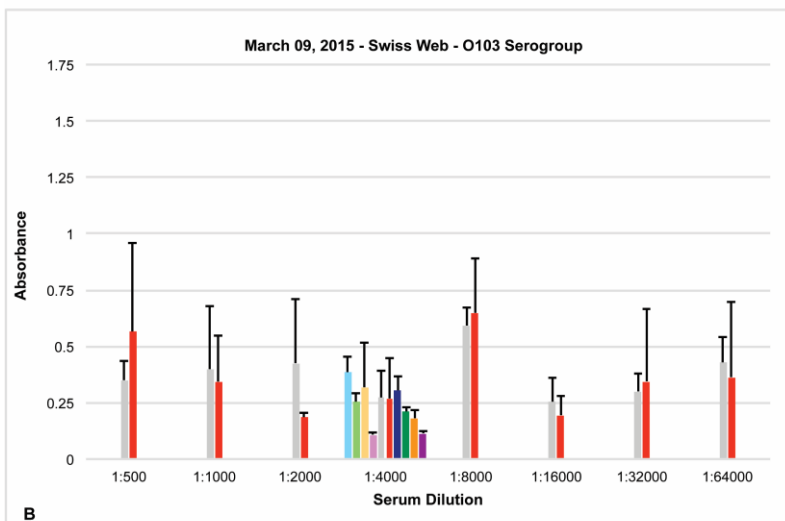
No response ' - ', Weak response ' + ', Moderate response ' ++ ', Intense response = ' +++ ', NA = control antigens were not available for testing. June 23, 2015 pre-inoculated blot not performed. PBS control on January 23, 2016 became contaminated during the blotting procedure. Blue highlighted regions indicates the targeted antigen.



**Figure A3.16 Images of longitudinal dot blots for a C57BL/6 mouse in the O103 serogroup.** X's indicate the absence of an antigen blot in that square. June 23, 2015 pre-inoculated blot was not performed.



- Pre-inoculated serum
- Post-inoculated serum
- No capture Ab (Pre inoculated)
- No Ag (Pre-inoculated)
- No serum (Pre-inoculated)
- No 2° Ab (Pre-inoculated)
- No capture Ab (Post-inoculated)
- No Ag (Post-inoculated)
- No serum (Post-inoculated)
- No 2° Ab (Post-inoculated)



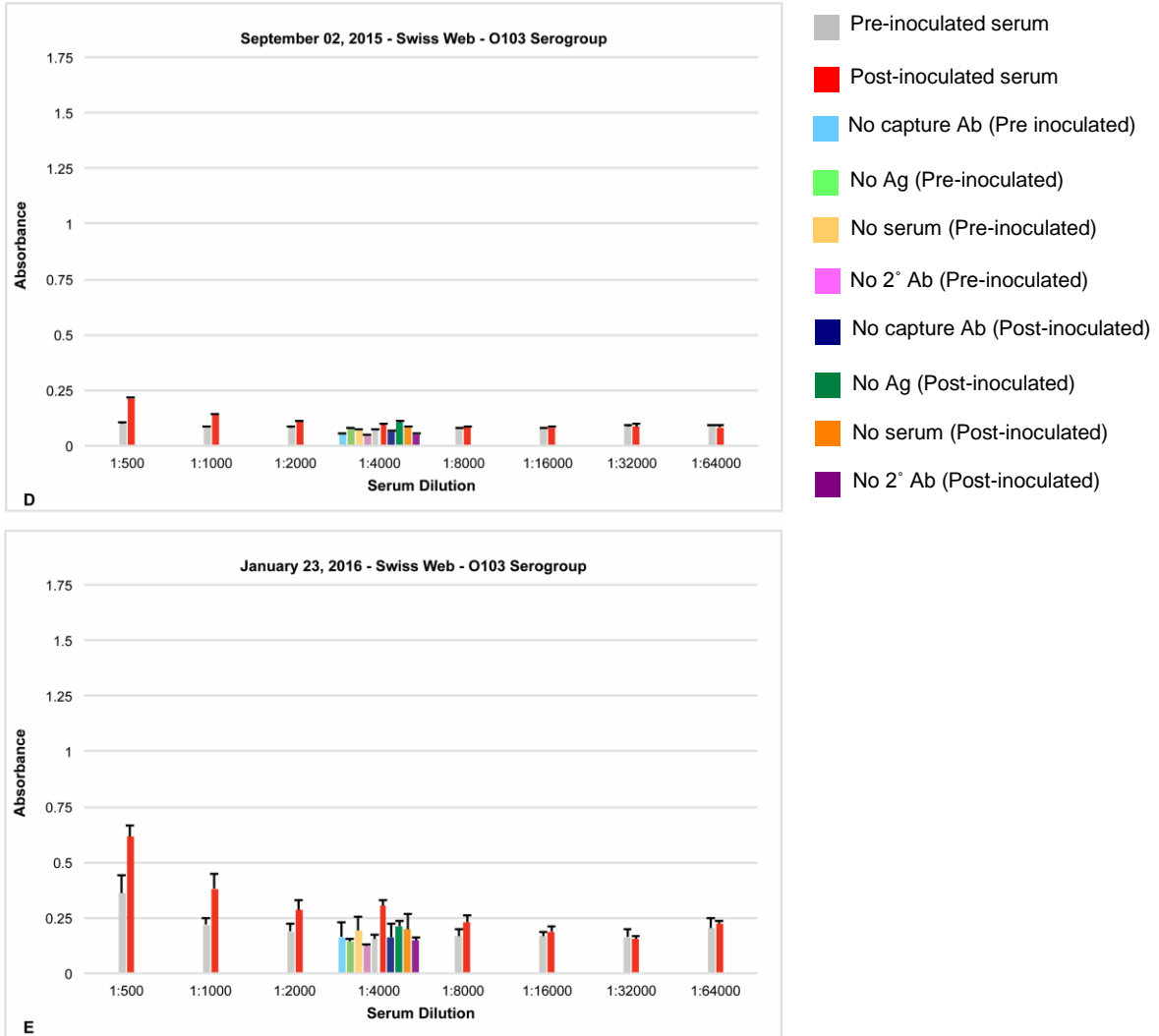


**Figure A3.17. ELISA results for a Swiss Webster mouse in the O103 serogroup.** Five serum screens performed over time on a Swiss Webster mouse that was repeatedly immunized with serogroup O103 bacterial antigens. A-C. Results of first three screens appear on the previous page. D-E. Results of most recent ELISA serum screens.

**Table A3.9 Immunoblot summary analysis of a Swiss Webster mouse inoculated with O103 bacterial antigens.**

		Swiss Webster mouse					
		Pre-Inoculated			Post-Inoculated		
	LPS subtype	Whole LPS	O-ag	Lipid A	Whole LPS	O-ag	Lipid A
March 09, 2015	O111:B4	+	+	-	+	+	+
	O157	-	+	-	+	+++	+
	O103	-	-	-	-	++	+++
	1x PBS/5% BSA	-	-	-	-	-	-
June 23, 2015	O111:B4	NA	NA	NA	+	-	-
	O157	NA	NA	NA	+	+	+
	O103	NA	NA	NA	+	+	+
	1x PBS/5% BSA	NA	NA	-	-	-	-
Sept. 02, 2015	O111:B4	+	-	NA	-	-	+
	O157	-	+	NA	+	++	NA
	O103	-	+	-	-	+++	++
	1x PBS/5% BSA	-	-	-	-	-	-
Jan. 23, 2016	O111:B4	-	-	NA	-	-	NA
	O157	-	-	NA	-	++	NA
	O103	-	-	-	-	++	+
	1x PBS/5% BSA	++	-	-	++	-	-

No response ' - ', Weak response ' + ', Moderate response ' ++ ', Intense response = ' +++ ', NA = control antigens were not available for testing. June 23, 2015 pre-inoculated blot not performed. PBS control on January 23, 2016 became contaminated during the blotting procedure. Blue highlighted regions indicate the targeted antigen

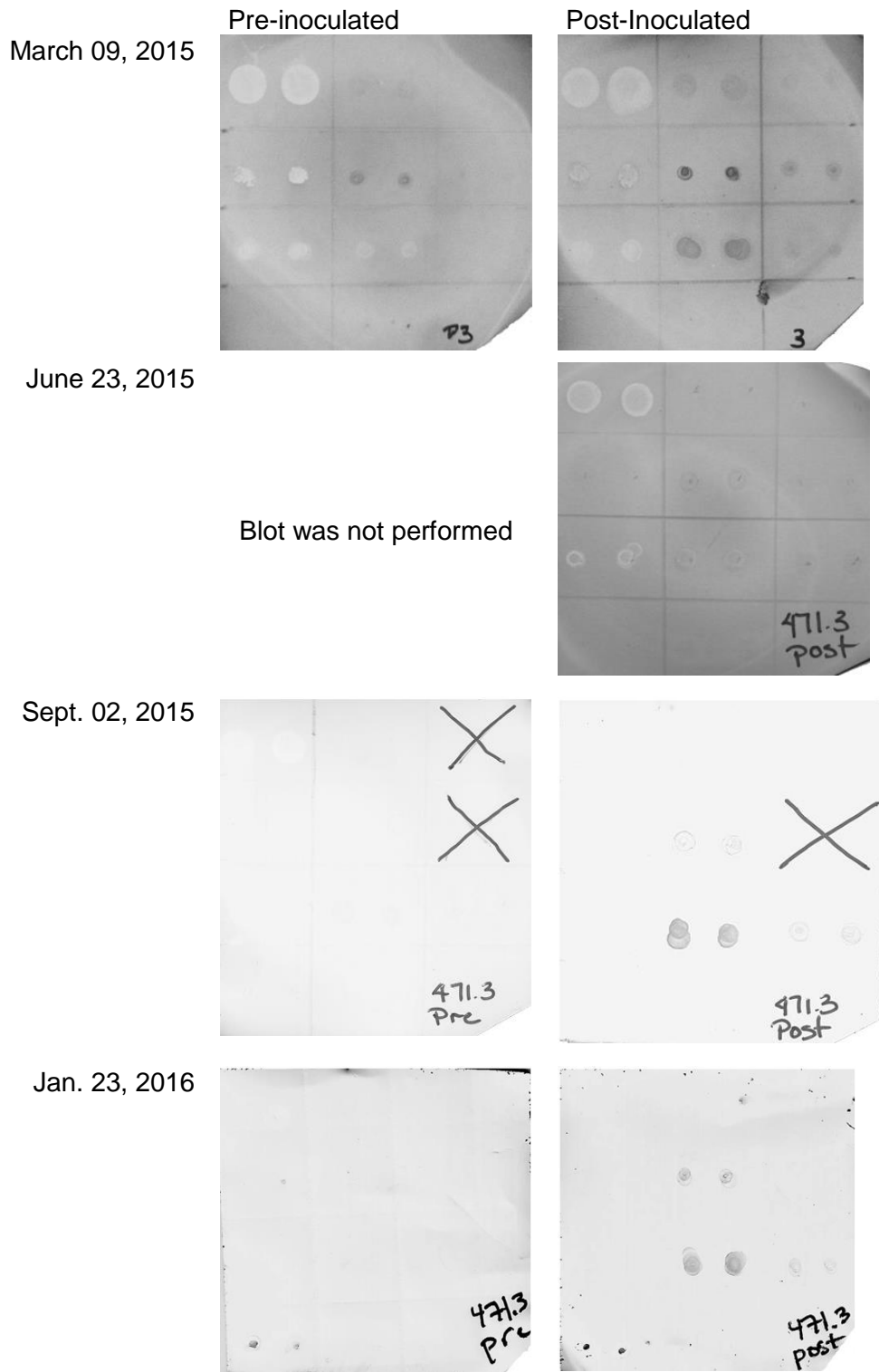


**Figure A3.18** Images of longitudinal dot blots for a Swiss Webster mouse in the O103 serogroup. X's indicate the absence of an antigen blot in that square. June 23, 2015 pre-inoculated blot was not performed.

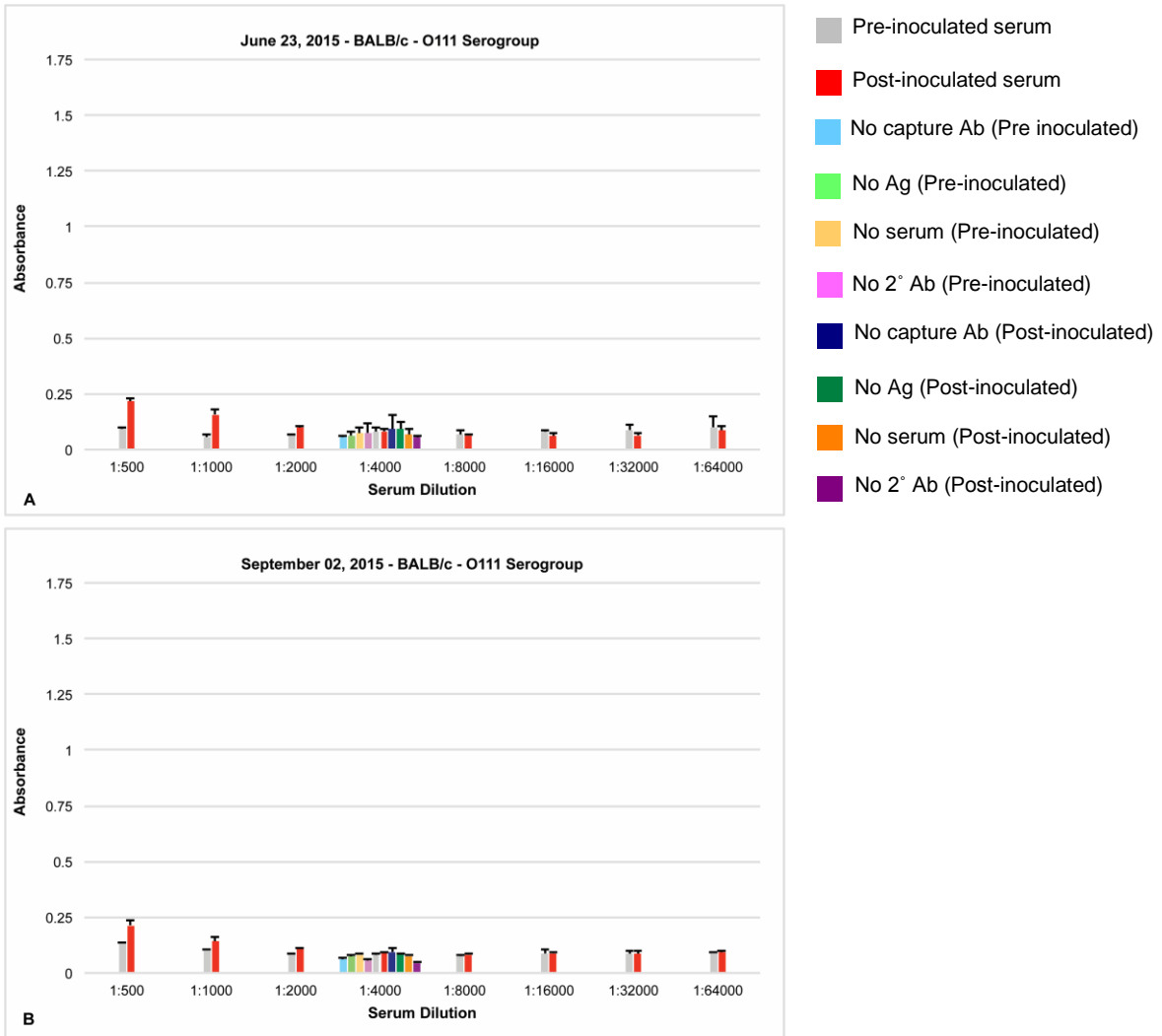


**Figure A3.19. ELISA results for a BALB/c mouse in O111 serogroup.** Results of 2 serum screens performed over time on a BALB/c mouse that was repeatedly immunized with serogroup O111 bacterial antigens. Mouse was selected for hybridoma fusion based on the immunoblot results.

**Table A3.10 Immunoblot summary analysis of a BALB/c mouse inoculated with O111 bacterial antigens.**

BALB/c mouse		Pre-Inoculated			Post-Inoculated		
LPS subtype	Whole LPS	O-ag	Lipid A	Whole LPS	O-ag	Lipid A	
June 23, 2015	O111:B4	-	-	-	-	-	-
	O157	-	+	-	-	+	+
	O111	-	-	-	-	-	+
	1x PBS/5% BSA	-	-	-	-	-	-
Sept. 02, 2015	O111:B4	-	-	-	+	-	NA
	O157	-	-	NA	+	++	NA
	O111	-	+	+	+	++	+++
	1x PBS/5% BSA	-	-	-	-	-	-

No response ' - ', Weak response ' + ', Moderate response ' ++ ', Intense response = ' +++ ', NA = control antigens were not available for testing. Blue highlighted regions indicate the targeted antigen

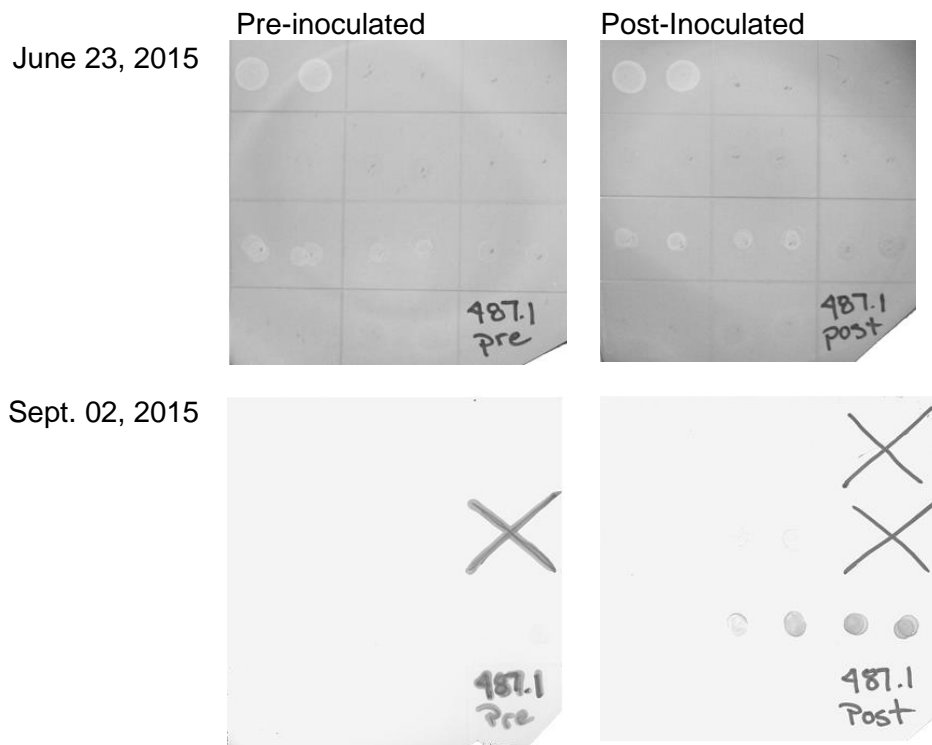


**Figure A3.20 Images of longitudinal dot blots for a BALB/C mouse in the O111 serogroup. X's indicate the absence of an antigen blot in that square.**

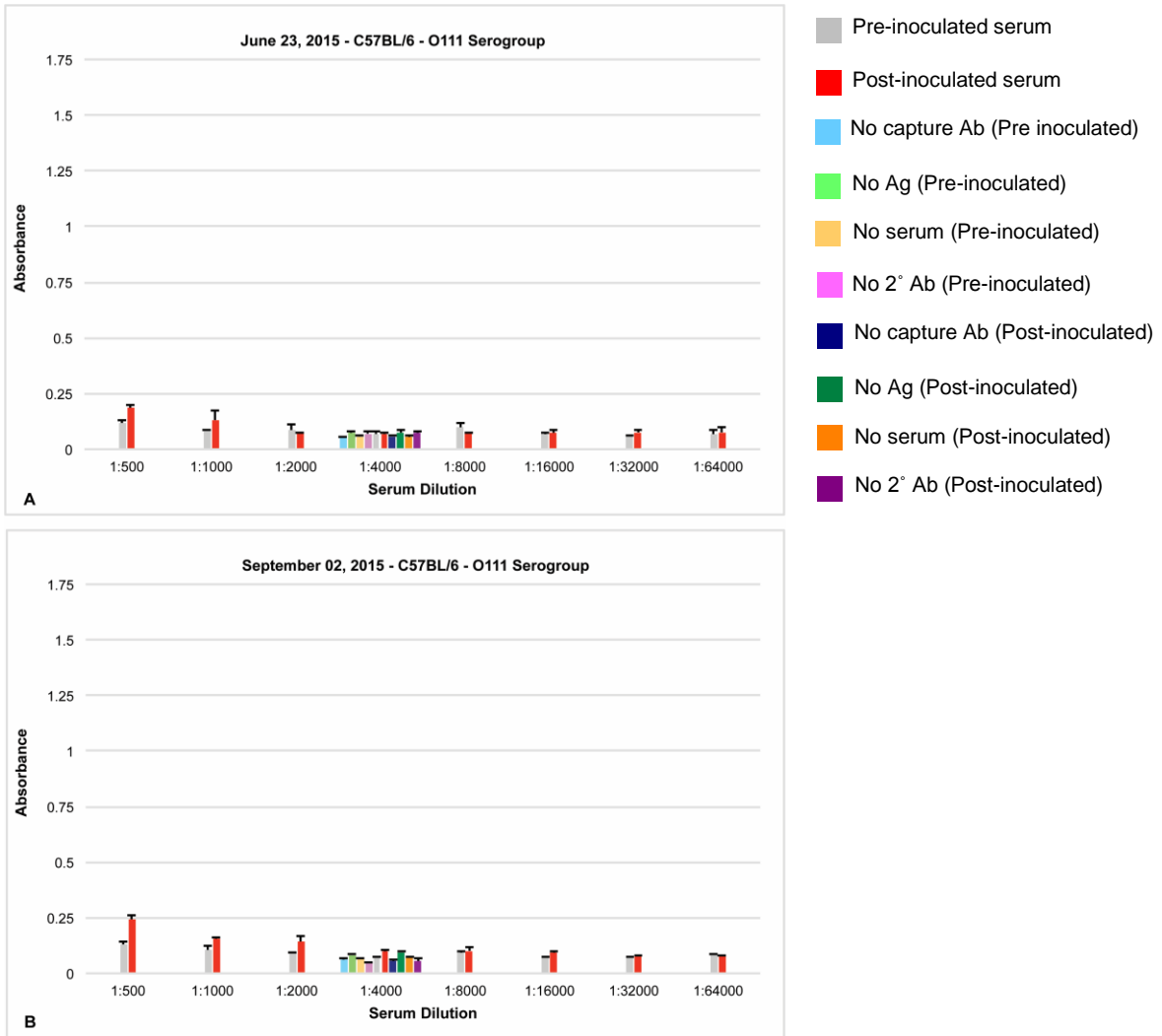


**Figure A3.21. ELISA results for a C57BL/6 mouse in O111 serogroup.** A-B. ELISA results of first two of four serum screens performed over time on a C57BL/6 mouse that was repeatedly immunized with serogroup O111 bacterial antigens. C-D. Second set of results are reported on the following page.

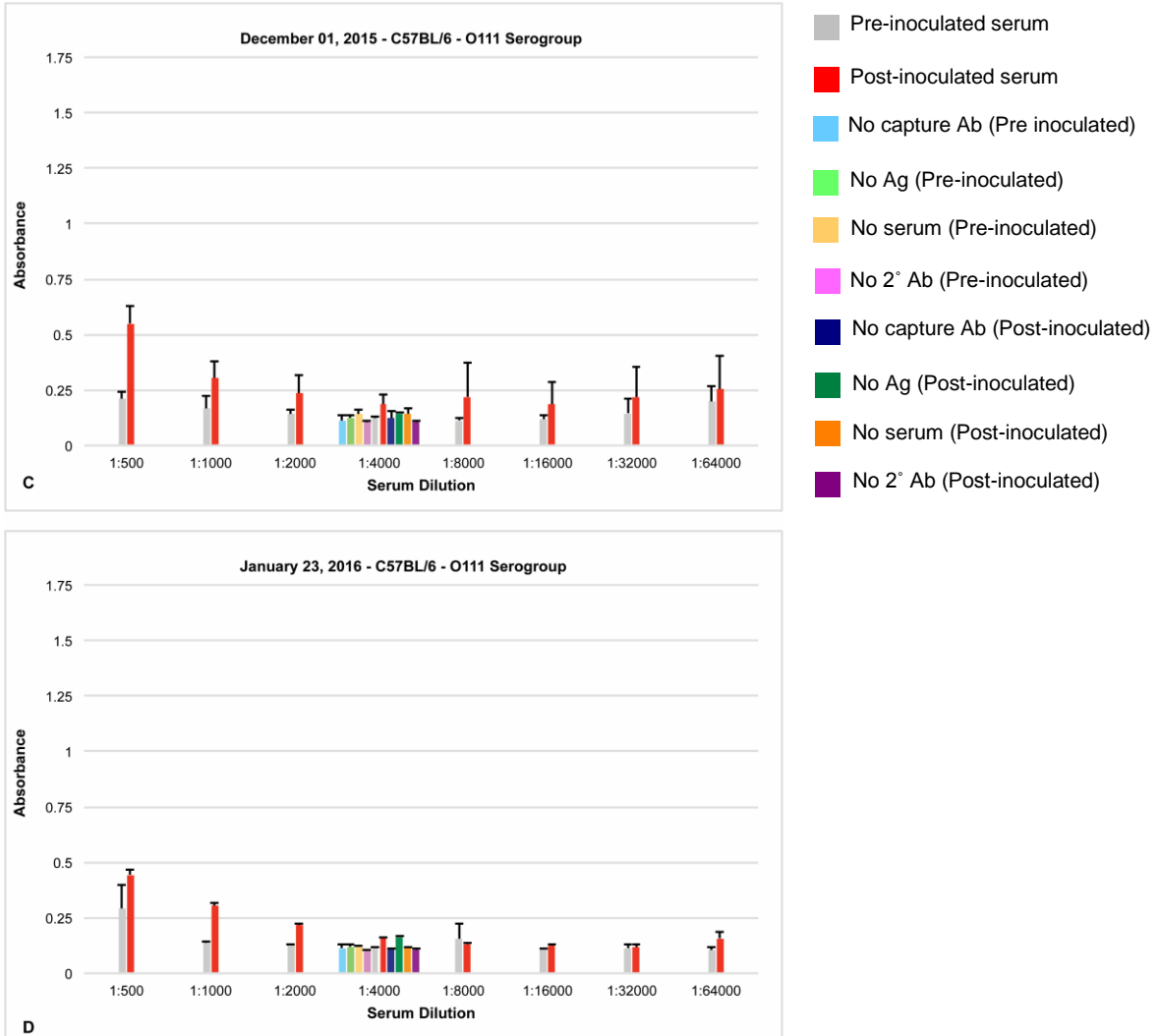


**Figure A3.21. ELISA results for a C57BL/6 mouse in O111 serogroup.** A-B. Reported on previous page. ELISA results of first two of four serum screens performed over time on a C57BL/6 mouse that was repeatedly immunized with serogroup O111 bacterial antigens. C-D. Second set of results for the serum screen.

**Table A3.11 Immunoblot summary analysis of a C57BL/6 mouse inoculated with O111 bacterial antigens.**

		C57BL/6 mouse					
		Pre-Inoculated			Post-Inoculated		
	LPS subtype	Whole LPS	O-ag	Lipid A	Whole LPS	O-ag	Lipid A
June 23, 2015	O111:B4	-	-	-	-	-	-
	O157	-	+	-	-	+	-
	O111	-	+	-	-	-	-
	1x PBS/5% BSA	-	-	-	-	-	-
Sept. 02, 2015	O111:B4	-	-	-	+	-	NA
	O157	-	-	NA	-	+	NA
	O111	-	+	+	-	++	++
	1x PBS/5% BSA	-	-	-	-	-	-
Dec. 01, 2015	O111:B4	-	-	NA	-	-	NA
	O157	-	-	NA	-	+	NA
	O111	-	++	++	-	++	++
	1x PBS/5% BSA	-	-	-	-	-	-
Jan. 23, 2016	O111:B4	-	-	NA	-	-	NA
	O157	-	-	NA	-	+	NA
	O111	-	+	+	-	+	+
	1x PBS/5% BSA	+++	-	-	-	-	-

No response '-'; Weak response '+'; Moderate response '++'; Intense response = '+++'; NA = control antigens were not available for testing. PBS control on January 23, 2016 became contaminated during the blotting procedure. Blue highlighted regions indicate the targeted antigen

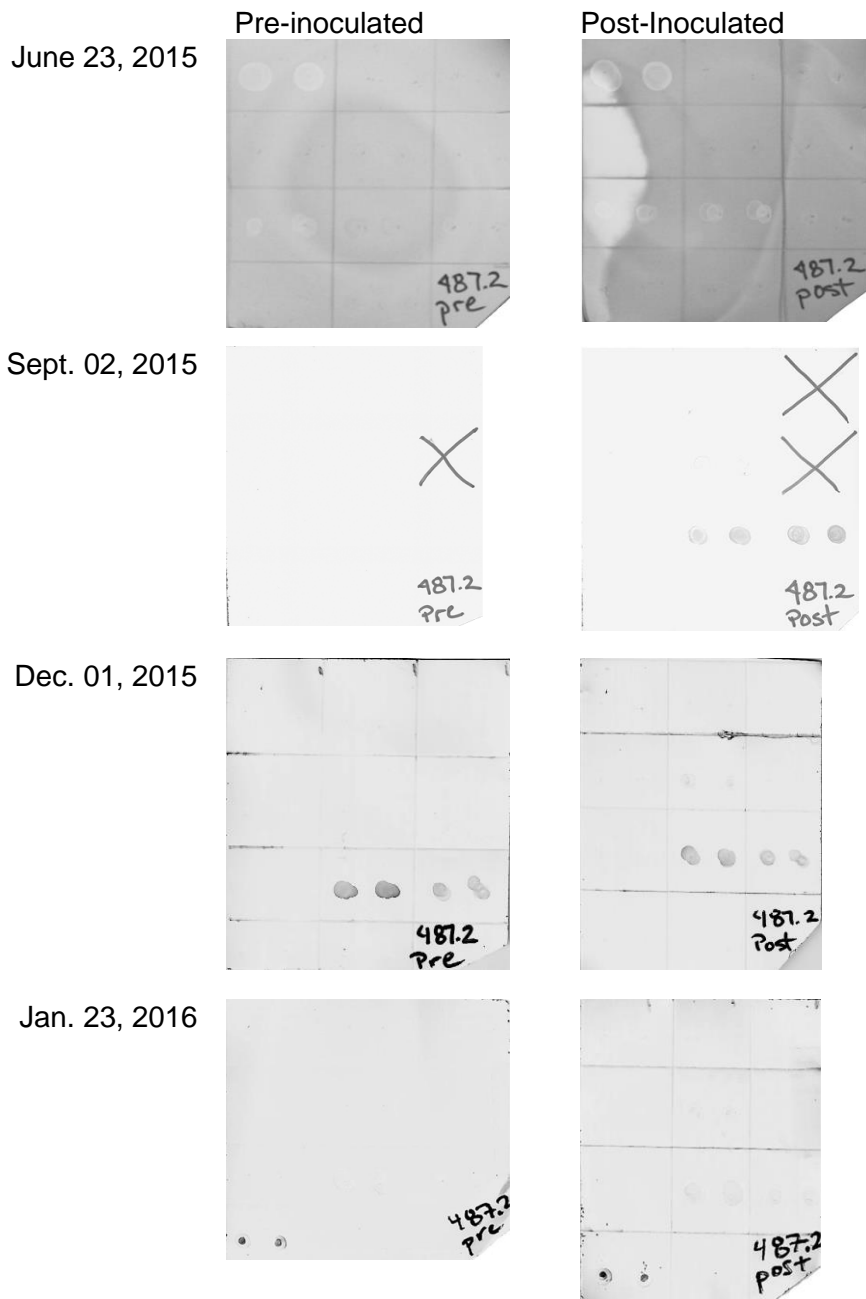


**Figure A3.22 Images of longitudinal dot blots for a C57BL/6 mouse in the O111 serogroup.** X's indicate the absence of an antigen blot in that square.

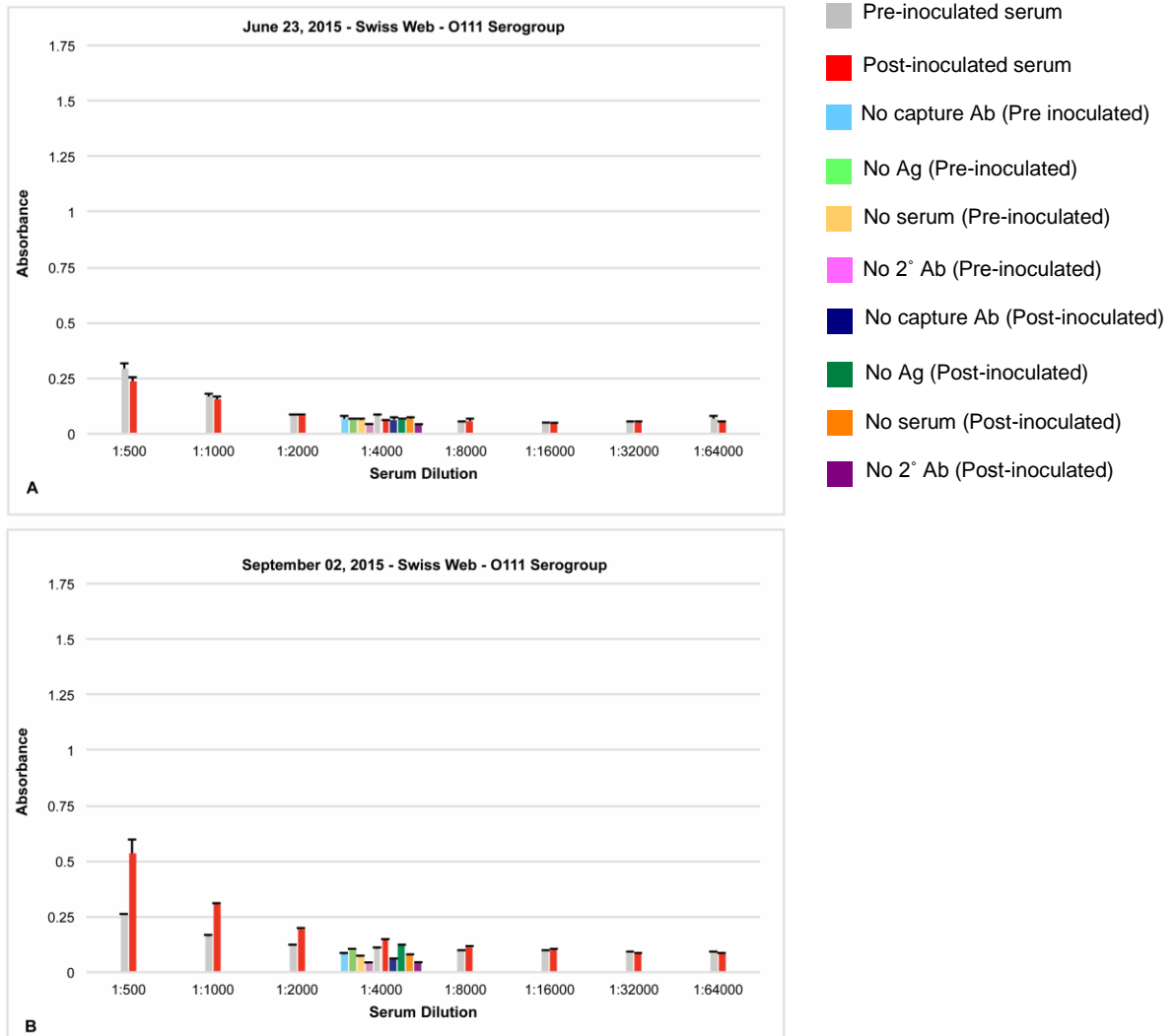


**Figure A3.23. ELISA results for a Swiss Webster mouse in O111 serogroup.** A-B. ELISA results of first two of four serum screens performed over time on a Swiss Webster mouse that was repeatedly immunized with serogroup O111 bacterial antigens. C-D. Second set of results are reported on the following page.

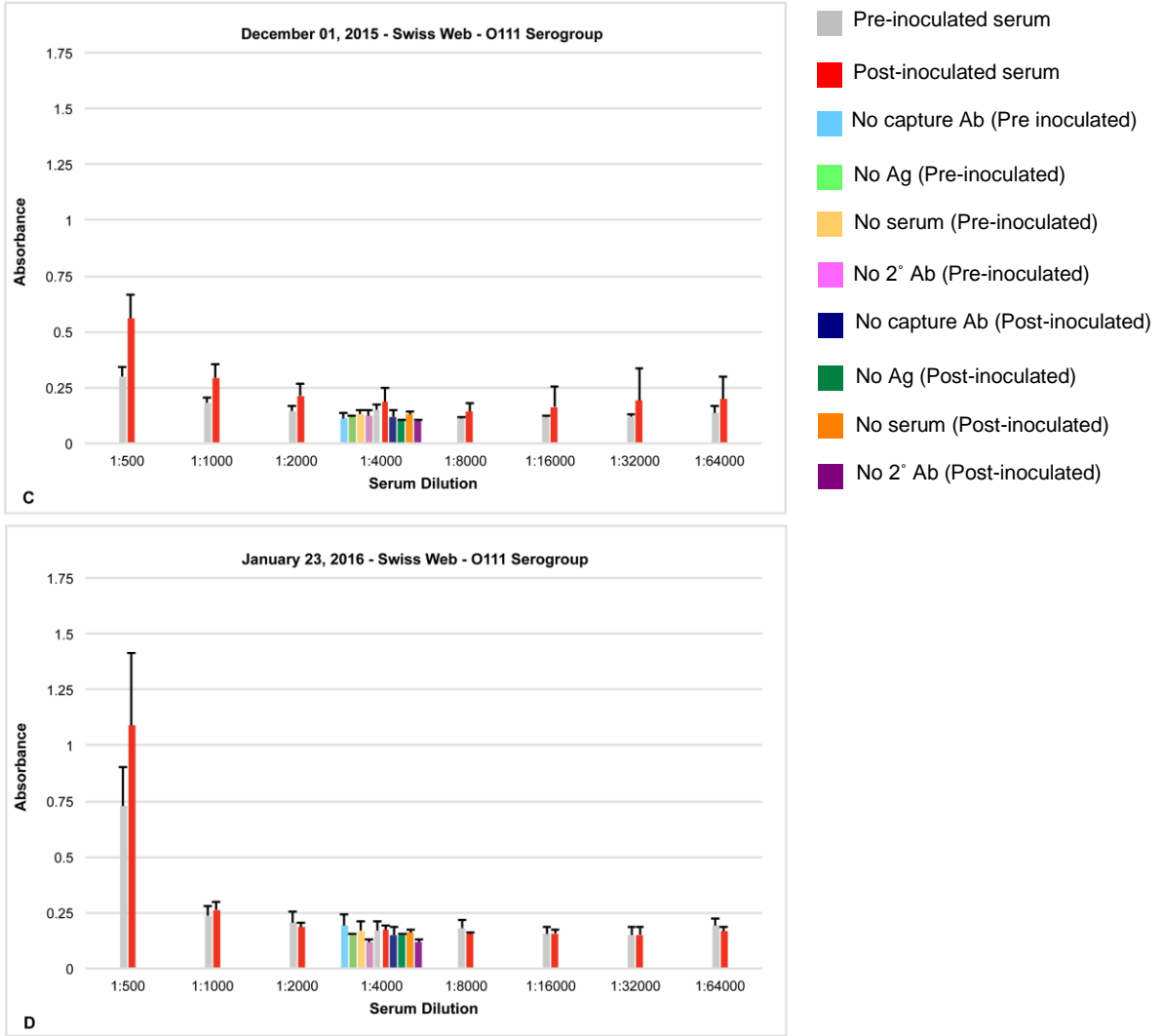
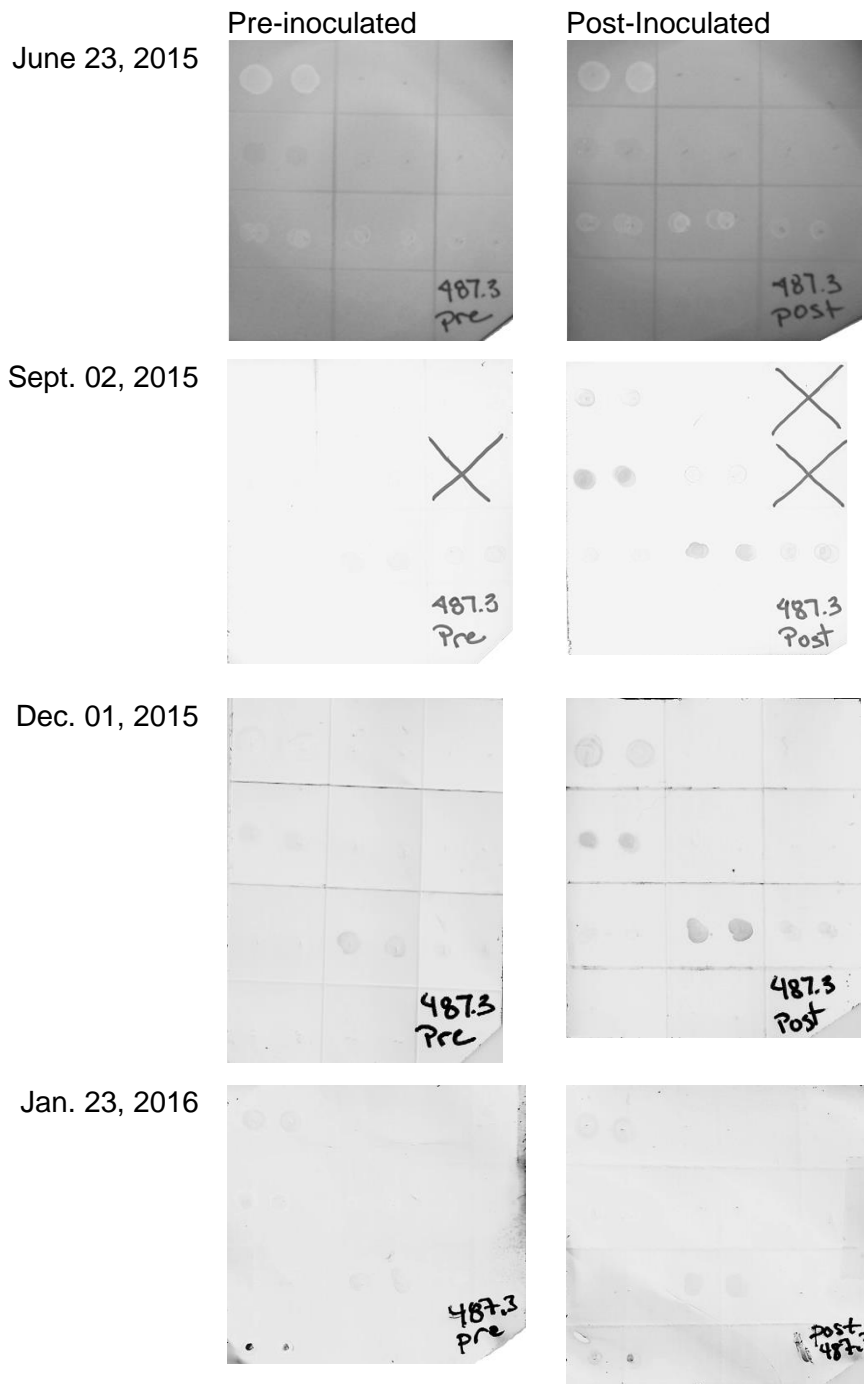


Figure A3.23. ELISA results for a Swiss Webster mouse in O111 serogroup. A-B. Reported on previous page. ELISA results of first two of four serum screens performed over time on a Swiss Webster mouse that was repeatedly immunized with serogroup O111 bacterial antigens. C-D. Second set of results for the serum screen.

**Table A3.12 Immunoblot summary analysis for a Swiss Webster mouse inoculated with O111 bacterial antigens.**

		Swiss Webster mouse					
		Pre-Inoculated			Post-Inoculated		
	LPS subtype	Whole LPS	O-ag	Lipid A	Whole LPS	O-ag	Lipid A
June 23, 2015	O111:B4	-	-	-	-	-	-
	O157	+	+	-	+	+	-
	O111	-	-	-	-	-	-
	1x PBS/5% BSA	-	-	-	-	-	-
Sept. 02, 2015	O111:B4	-	-	-	+	-	NA
	O157	+	+	NA	++	+	NA
	O111	-	+	+	+	++	+
	1x PBS/5% BSA	-	-	-	-	-	-
Dec. 01, 2015	O111:B4	+	-	NA	++	-	NA
	O157	+	-	NA	++	+	NA
	O111	-	+	+	+	++	+
	1x PBS/5% BSA	-	-	-	-	-	-
Jan. 23, 2016	O111:B4	+	-	NA	+	-	NA
	O157	+	+	NA	+	+	NA
	O111	+	+	-	-	+	+
	1x PBS/5% BSA	+++	-	-	++	-	-

No response ' - ', Weak response ' + ', Moderate response ' ++ ', Intense response = ' +++ ', NA = control antigens were not available for testing. PBS control on January 23, 2016 became contaminated during the blotting procedure. Blue highlighted regions indicate the targeted antigen



**Figure A3.24. Images of longitudinal dot blots for a Swiss Webster mouse in the O111 serogroup.** X's indicate the absence of an antigen blot in that square. While subsequent blots are not marked with X's, control Lipid A groups for LPS O111:B4 and O157 were not available for testing.

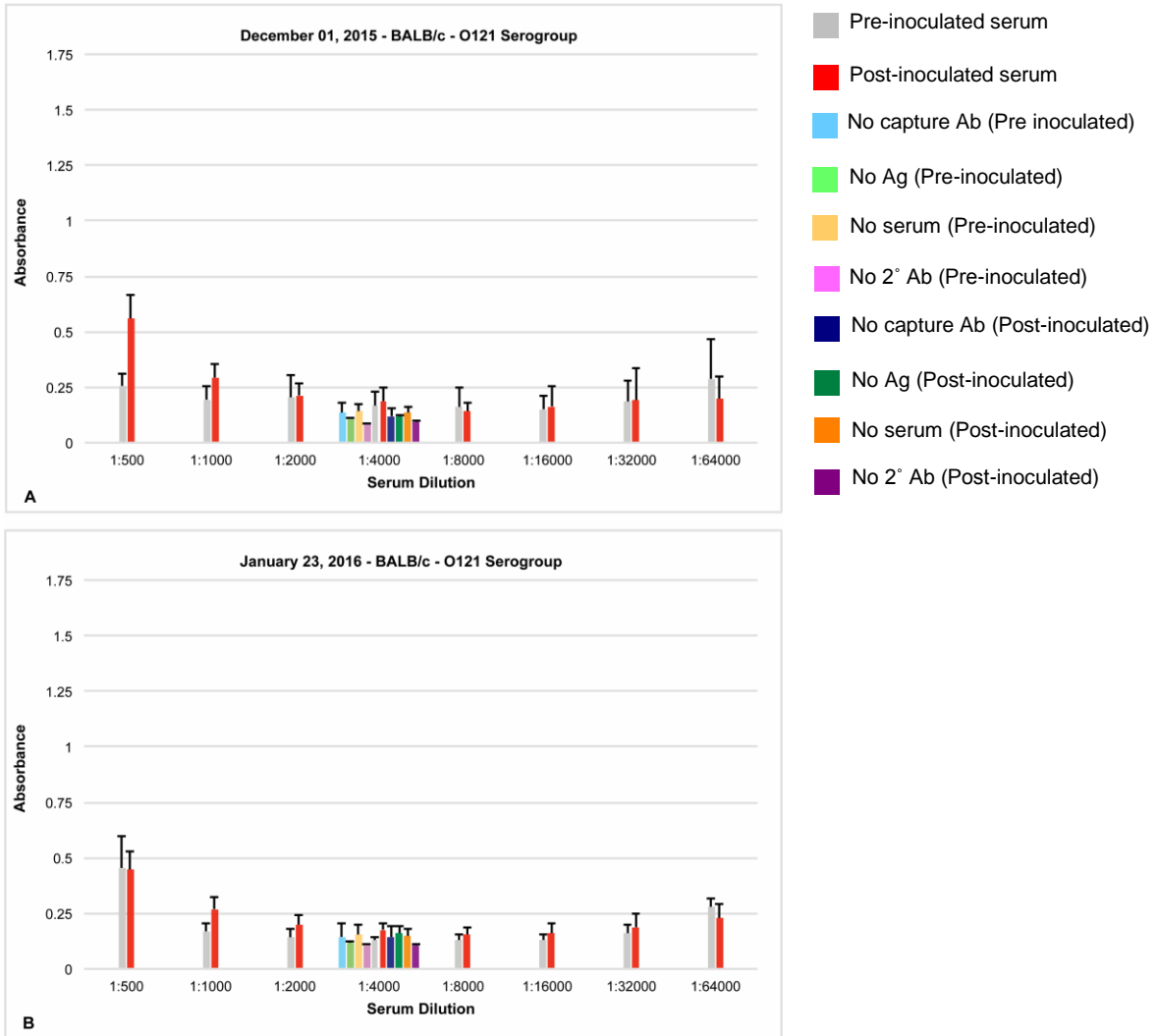


**Figure A3.25.** ELISA graphs for a BALB/c mouse in O121 serogroup. Results of indirect ELISA of 2 serum screens performed over time on a BALB/c mouse that was repeatedly immunized with serogroup O121 bacterial antigens.

**Table A3.13 Immunoblot summary analysis of a BALB/c mouse inoculated with O121 bacterial antigens.**

BALB/c mouse		Pre-Inoculated			Post-Inoculated		
		Whole LPS	O-ag	Lipid A	Whole LPS	O-ag	Lipid A
Dec. 01, 2015	O111:B4	-	-	NA	+	+	NA
	O157	-	-	NA	+	-	NA
	O121	+	NA	NA	+++	NA	NA
	1x PBS/5% BSA	-	-	-	-	-	-
Jan. 23, 2016	O111:B4	-	-	NA	+	-	NA
	O157	+	+	NA	+	++	NA
	O121	-	NA	NA	+	NA	NA
	1x PBS/5% BSA	-	-	-	-	-	-

No response ' - ', Weak response ' + ', Moderate response ' ++ ', Intense response = ' +++ ', NA = control antigens were not available for testing. Immunoblotting procedure was repeated for January 23, 2016 serum screen due to mislabeling of membrane paper. Blue highlighted regions indicate the targeted antigen

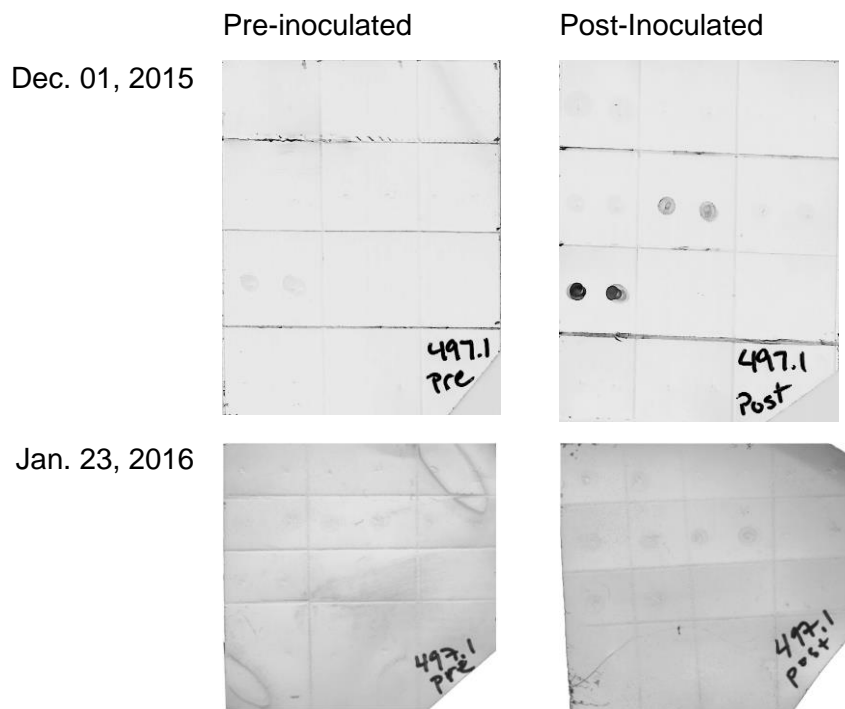


**Figure A3.26 Images of longitudinal dot blots for a BALB/c mouse in the O121 serogroup.** Control O-ag and lipid A antigens were not available for LPS O121. Lipid A antigens were not available for control groups O111:B4 and O157 on either of the test dates.

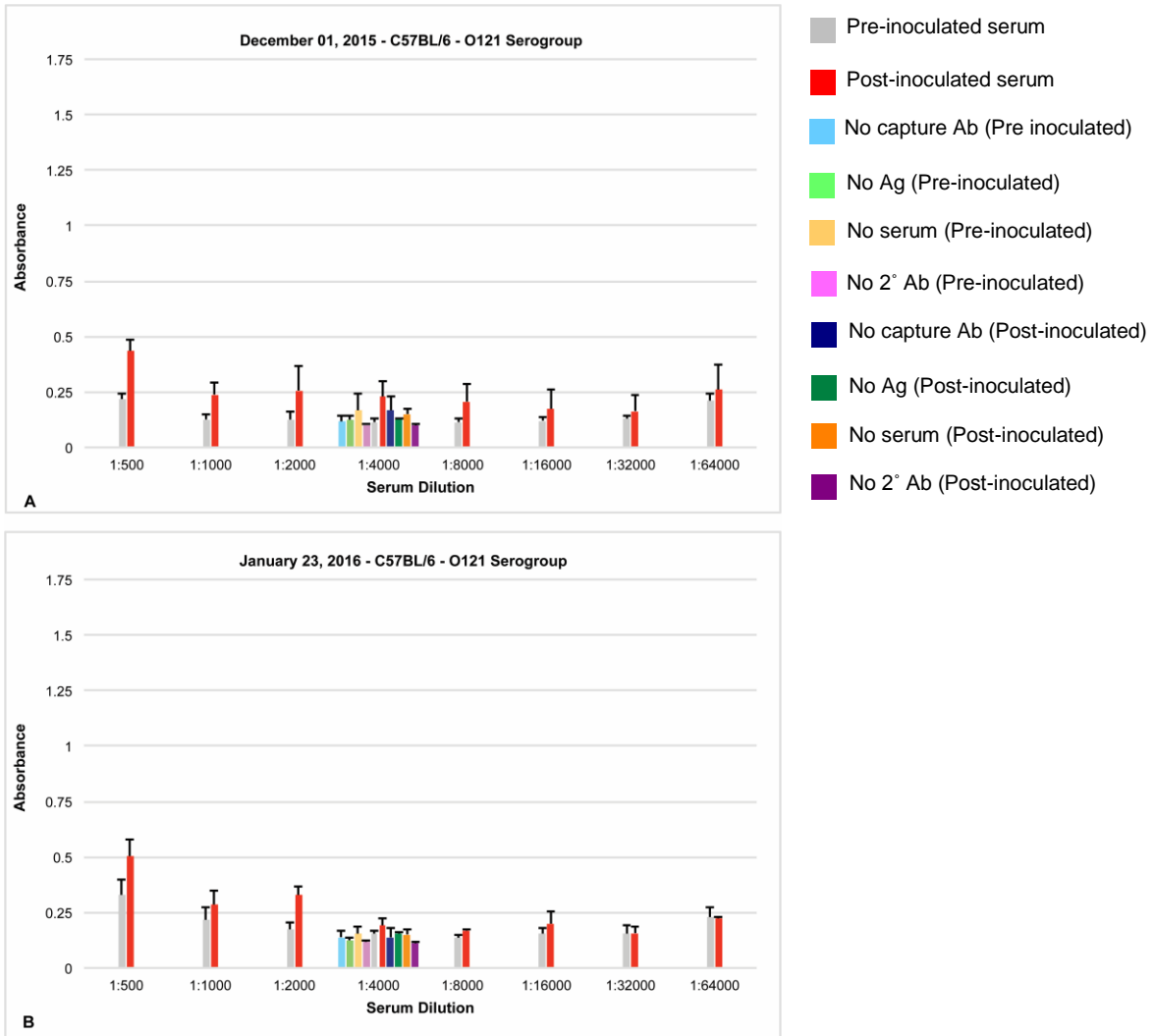


**Figure A3.27. ELISA results for a C57BL/6 mouse in the O121 serogroup.** Results of two serum screens performed over time on a C57BL/6 mouse that was repeatedly immunized with serogroup O121 bacterial antigens.

**Table A3.14 Immunoblot summary analysis of a C57BL/6 mouse inoculated with O121 bacterial antigens.**

C57BL/6 mouse		Pre-Inoculated			Post-Inoculated		
	LPS subtype	Whole LPS	O-ag	Lipid A	Whole LPS	O-ag	Lipid A
Dec. 01, 2015	O111:B4	-	-	NA	-	-	NA
	O157	-	-	NA	+	-	NA
	O121	-	NA	NA	++	NA	NA
	1x PBS/5% BSA	-	-	-	-	-	-
Jan. 23, 2016	O111:B4	-	-	NA	-	-	NA
	O157	-	-	NA	-	-	NA
	O121	-	NA	NA	-	NA	NA
	1x PBS/5% BSA	++	-	-	++	-	-

No response '-'; Weak response '+'; Moderate response '++'; Intense response = '+++'; NA = control antigens were not available for testing. PBS control on January 23, 2016 became contaminated during the blotting procedure. Blue highlighted regions indicate the targeted antigen

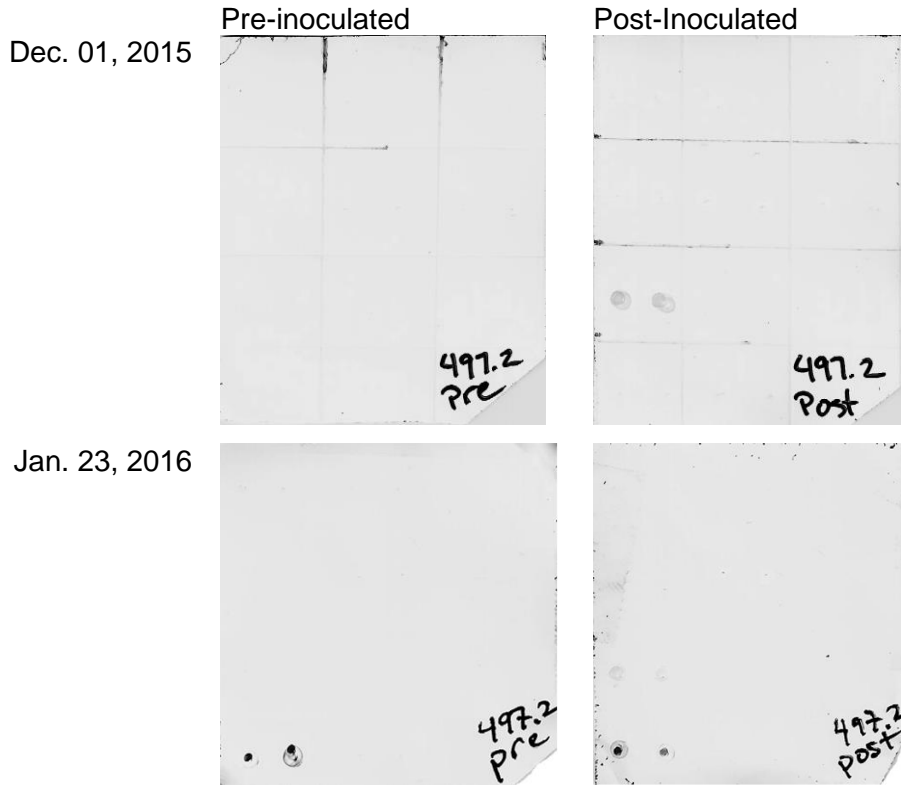


**Figure A3.28 Images of longitudinal dot blots for a C57BL/6 mouse in the O121 serogroup.** Control O-ag and lipid A antigens were not available for LPS O121. Lipid A antigens were not available for control groups O111:B4 and O157.

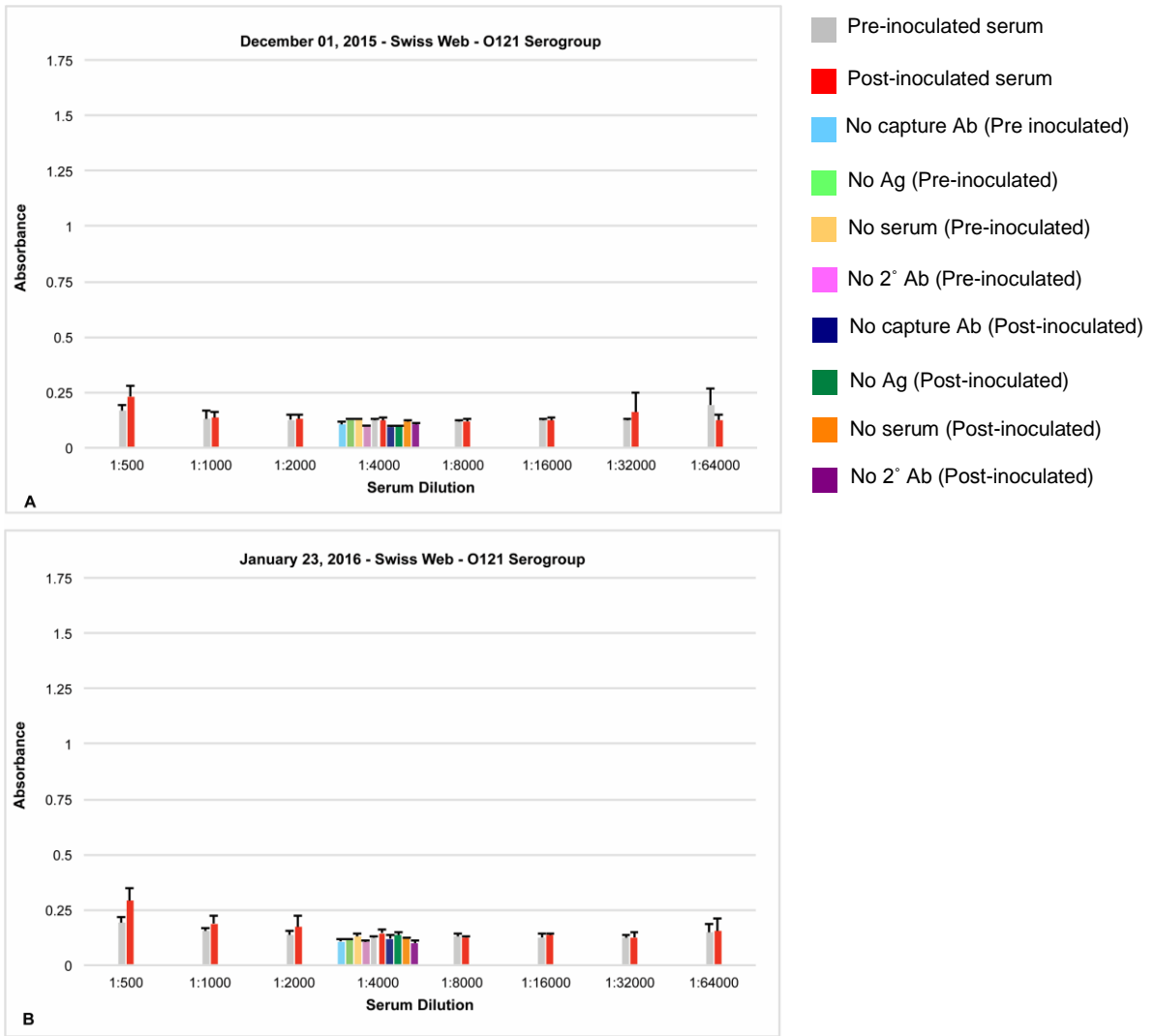


**Figure A3.29. ELISA results for a Swiss Webster mouse in the O121 serogroup.** Results of 2 serum screens performed over time on a Swiss Webster mouse that was repeatedly immunized with serogroup O121 bacterial antigens.

**Table A3.15 Immunoblot summary analysis of a Swiss Webster mouse inoculated with O121 bacterial antigens.**

		Swiss Webster mouse					
		Pre-Inoculated			Post-Inoculated		
	LPS subtype	Whole LPS	O-ag	Lipid A	Whole LPS	O-ag	Lipid A
Dec. 01, 2015	O111:B4	-	-	NA	+	-	NA
	O157	-	-	NA	-	++	NA
	O121	-	NA	NA	+++	NA	NA
	1x PBS/5% BSA	-	-	-	-	-	-
Jan. 23, 2016	O111:B4	-	-	NA	-	-	NA
	O157	-	-	NA	-	-	NA
	O121	-	NA	NA	-	NA	NA
	1x PBS/5% BSA	++	-	-	++	-	-

No response '-'; Weak response '+'; Moderate response '++'; Intense response = '+++'; NA = control antigens were not available for testing. PBS control on January 23, 2016 became contaminated during the blotting procedure. Blue highlighted regions indicate the targeted antigen

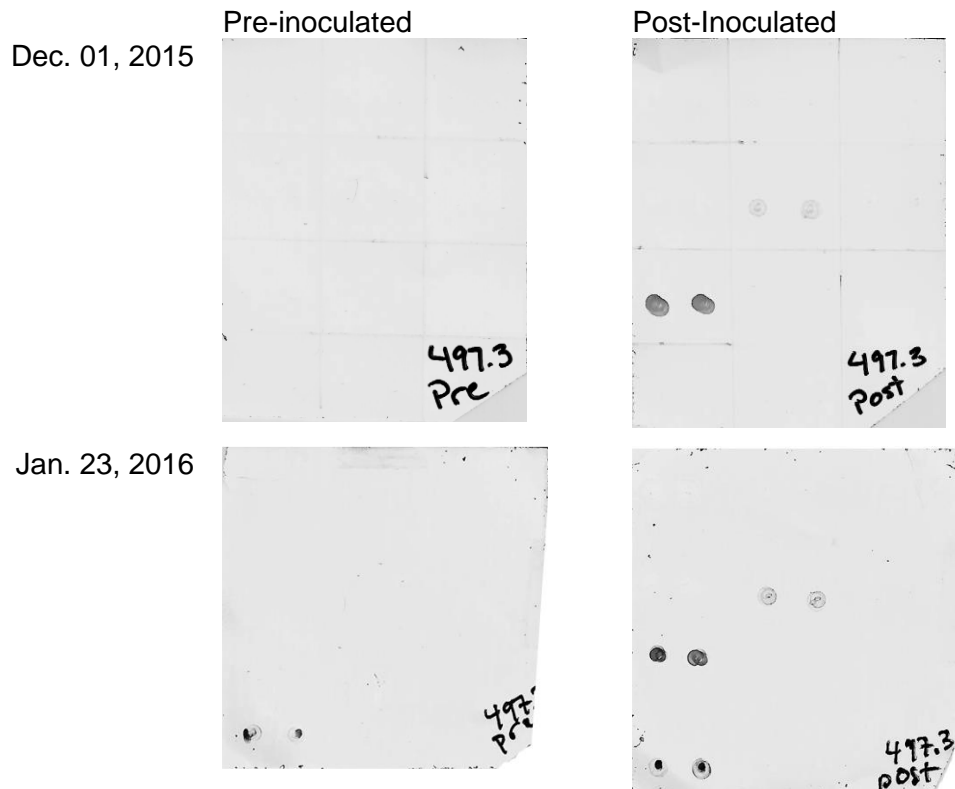


**Figure A3.30 Images of longitudinal dot blots for a Swiss Webster mouse in the O121 serogroup.** Control O-ag and lipid A antigens were not available for LPS O121. Lipid A antigens were not available for control groups O111:B4 and O157.

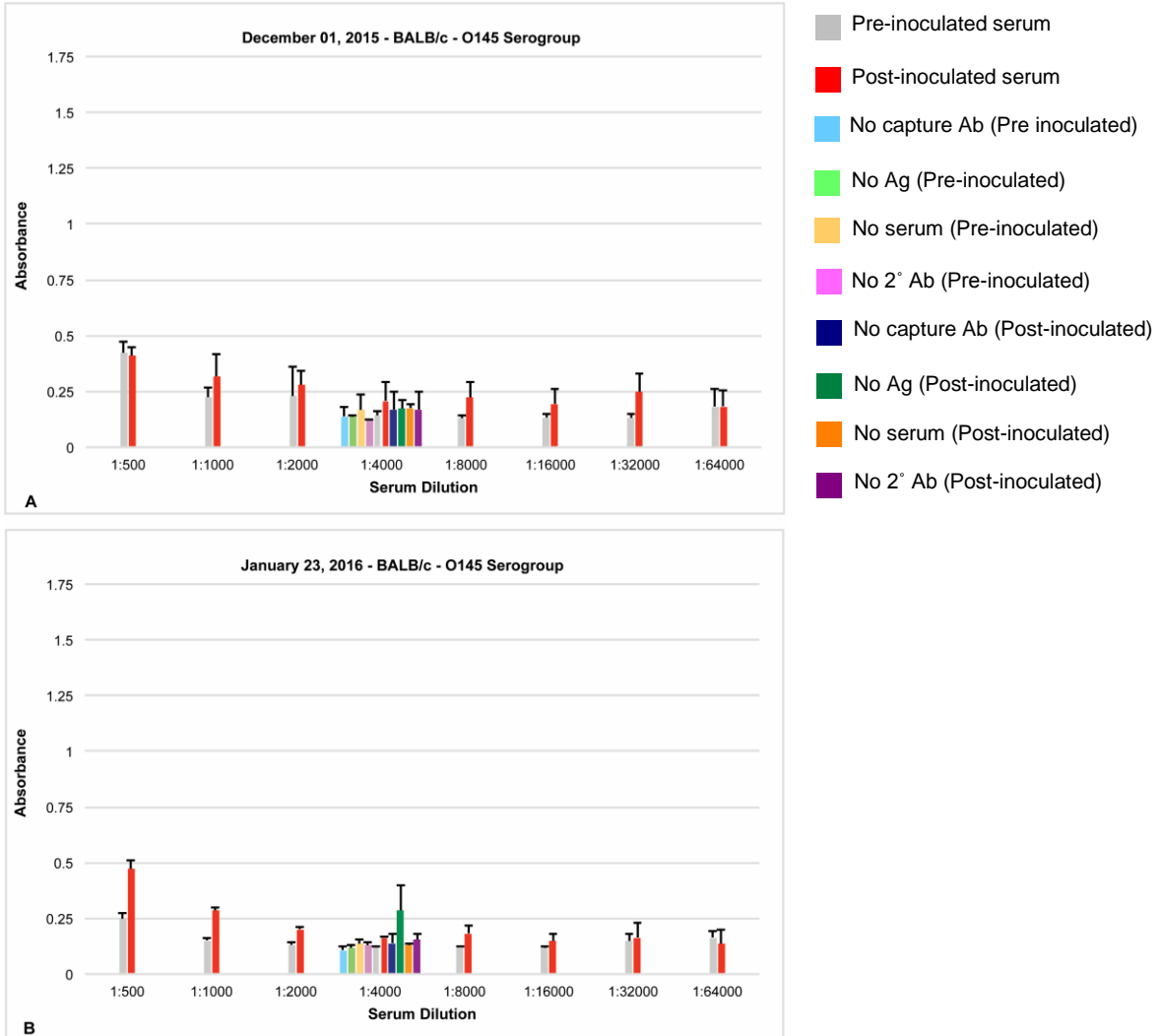


**Figure A3.31. ELISA results for a BALB/c mouse in the O145 serogroup.** Results of serum screens performed over time on a BALB/c mouse that was repeatedly immunized with serogroup O145 bacterial antigens.

**Table A3.16 Immunoblot summary analysis of a BALB/c mouse inoculated with O145 bacterial antigens.**

BALB/c mouse		Pre-Inoculated			Post-Inoculated		
	LPS subtype	Whole LPS	O-ag	Lipid A	Whole LPS	O-ag	Lipid A
Dec. 01, 2015	O111:B4	-	-	NA	+	-	NA
	O157	-	-	NA	+	++	NA
	O145	-	-	-	+	+	-
	1x PBS/5% BSA	-	-	-	-	-	-
Jan. 23, 2016	O111:B4	-	-	NA	+	-	NA
	O157	-	-	NA	+	+	NA
	O145	+	-	NA	+	+	NA
	1x PBS/5% BSA	++	-	-	++	-	-

No response ' - ', Weak response ' + ', Moderate response ' ++ ', Intense response = ' +++ ', NA = control antigens were not available for testing. PBS control on January 23, 2016 became contaminated during the blotting procedure. Blue highlighted regions indicate the targeted antigen

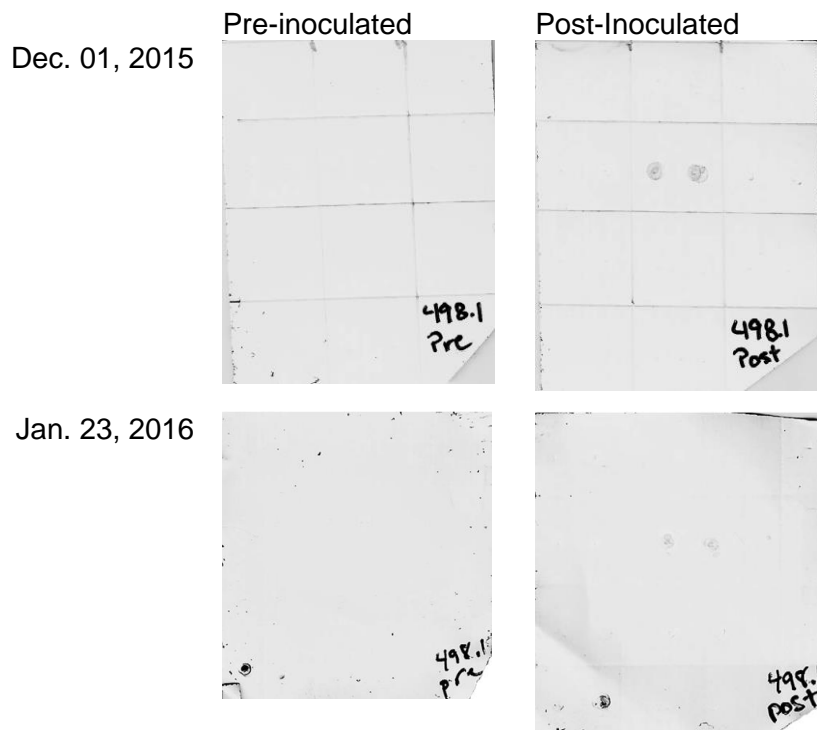


**Figure A3.32 Images of longitudinal dot blots for a BALB/c mouse in the O145 serogroup. Lipid A antigens were not available for control groups O111:B4 and O157.**

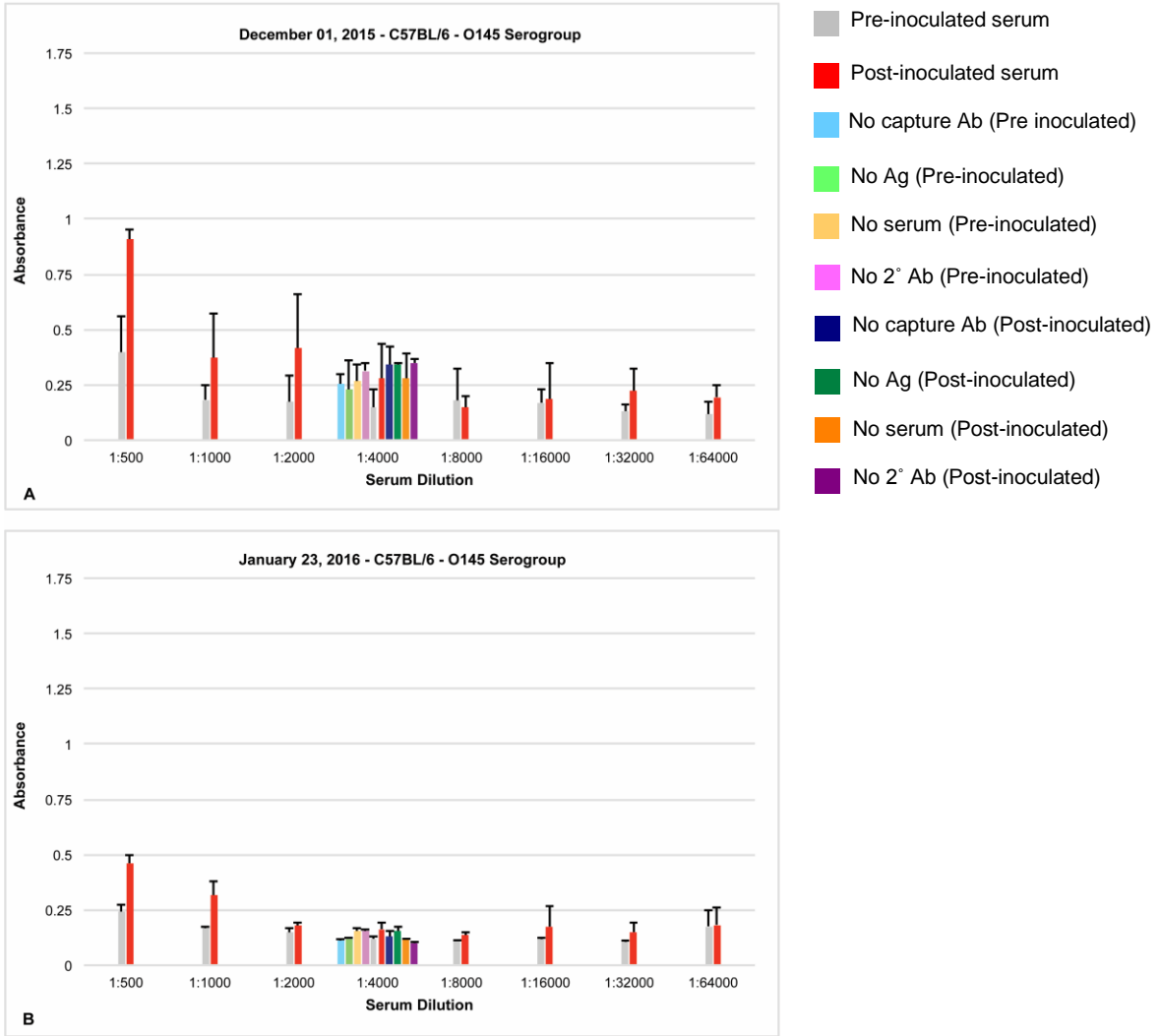


**Figure A3.33. ELISA results for a C57BL/6 mouse in the O145 serogroup.** Results serum screens performed over time on a C57BL/6 mouse that was repeatedly immunized with serogroup O145 bacterial antigens.

**Table A3.17 Immunoblot summary analysis of a C57BL/6 mouse inoculated with O145 bacterial antigens.**

C57BL/6 mouse		Pre-Inoculated			Post-Inoculated		
	LPS subtype	Whole LPS	O-ag	Lipid A	Whole LPS	O-ag	Lipid A
Dec. 01, 2015	O111:B4	-	-	NA	-	+	NA
	O157	-	-	NA	-	++	NA
	O145	-	-	-	+	+	-
	1x PBS/5% BSA	-	-	-	-	-	-
Jan. 23, 2016	O111:B4	-	-	NA	-	-	NA
	O157	-	-	NA	+	++	NA
	O145	-	-	-	+	+	-
	1x PBS/5% BSA	-	-	-	+++	-	-

No response '-'; Weak response '+'; Moderate response '++'; Intense response = '+++'; NA = control antigens were not available for testing. Blue highlighted regions indicate the targeted antigen

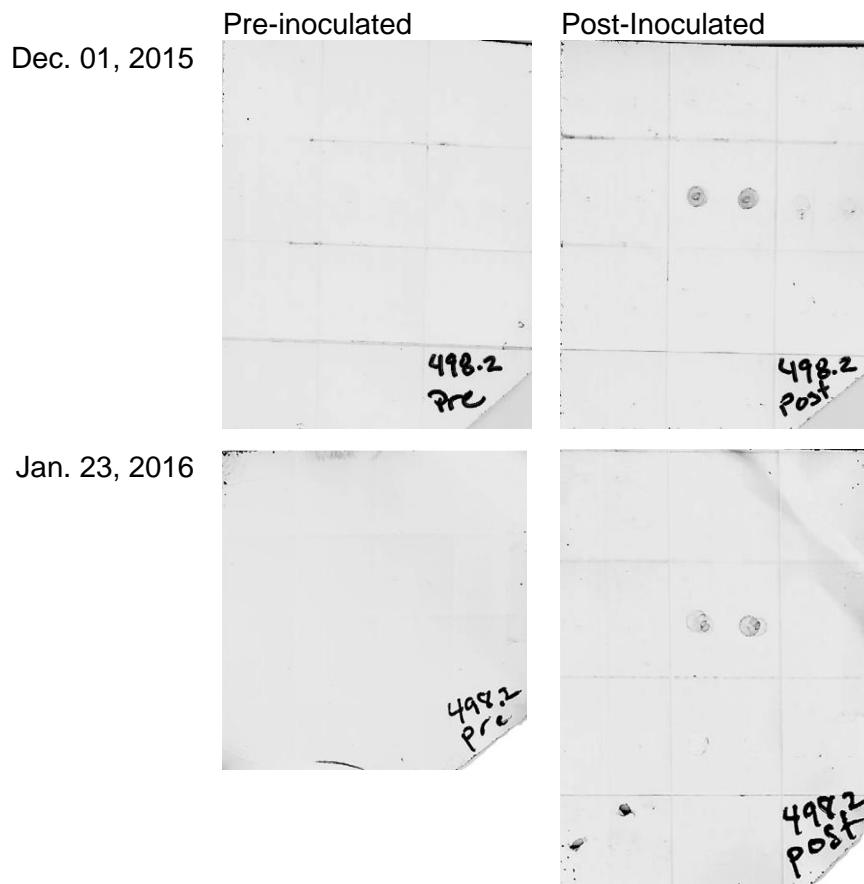


**Figure A3.34. Images of longitudinal dot blots for a C57BL/6 mouse in the O145 serogroup. Lipid A antigens were not available for control groups O111:B4 and O157.**

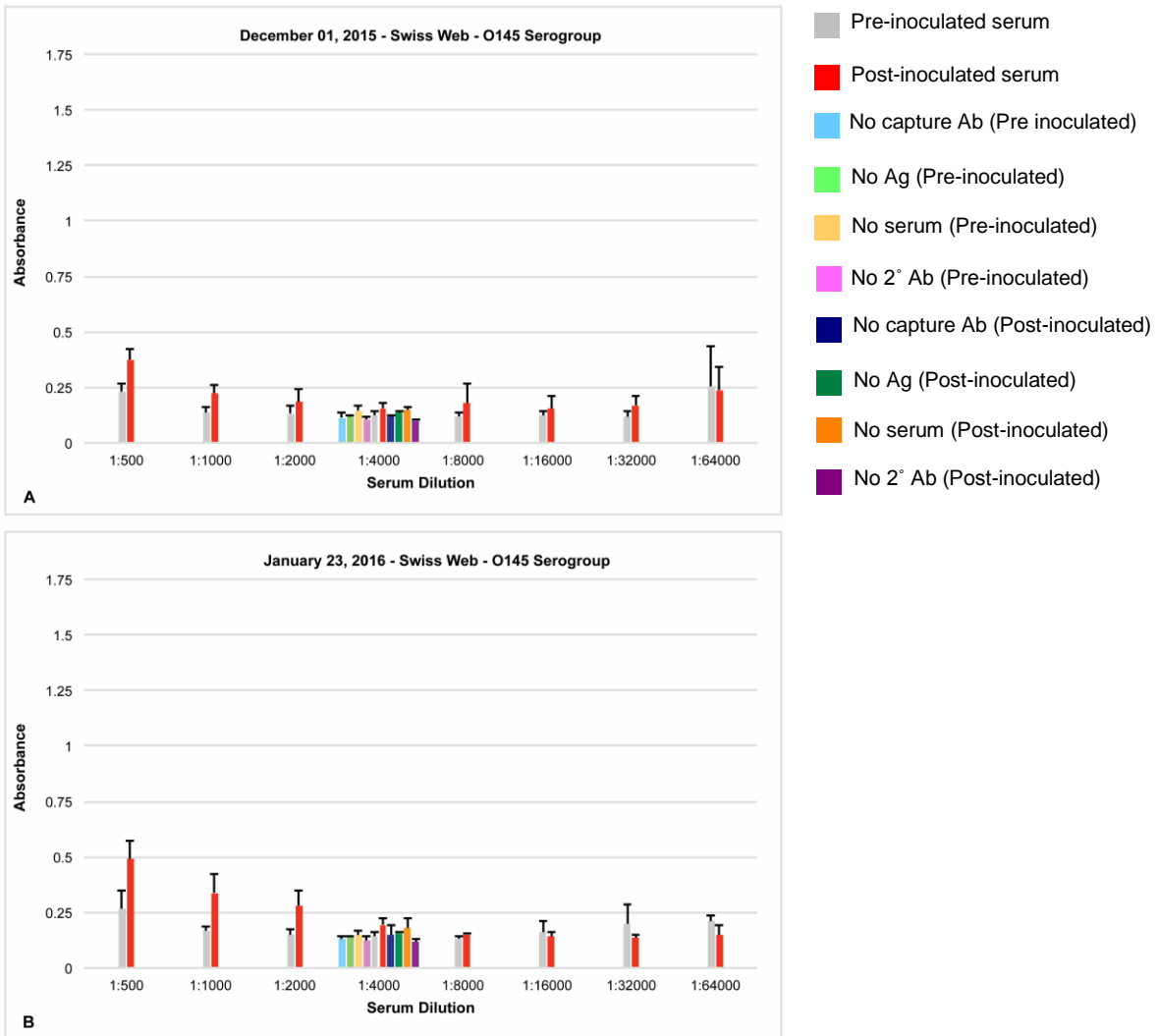
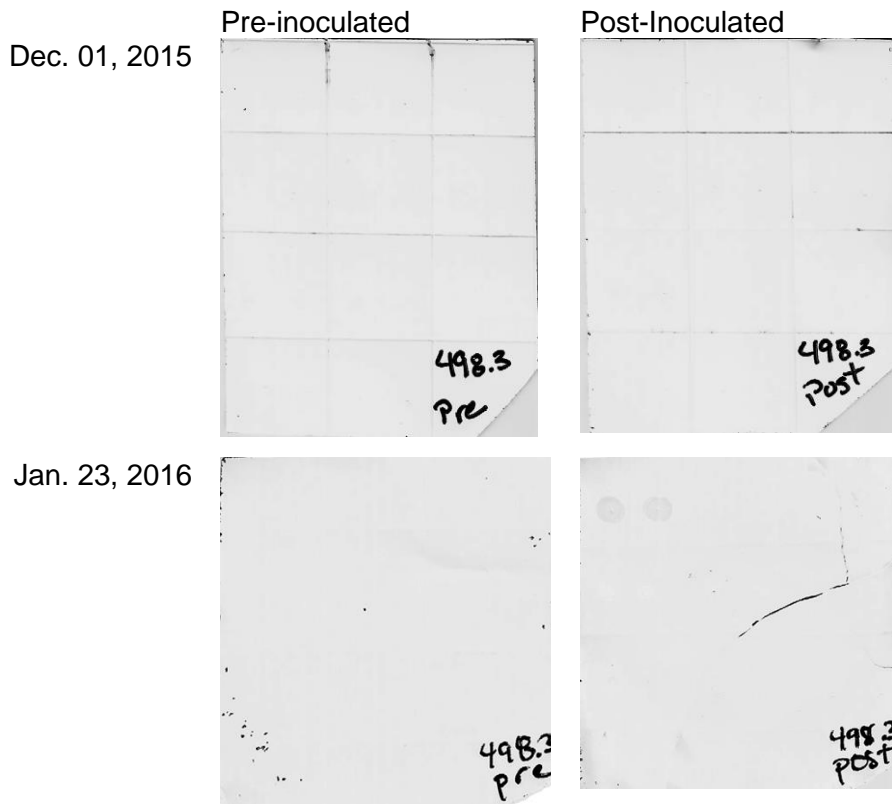


**Figure A3.35. ELISA results for a Swiss Webster mouse in the O145 serogroup.** Results of serum screens performed over time on a Swiss Webster mouse that was repeatedly immunized with serogroup O145 bacterial antigens.

**Table A3.18 Immunoblot summary analysis of a Swiss Webster mouse inoculated with O145 bacterial antigens.**

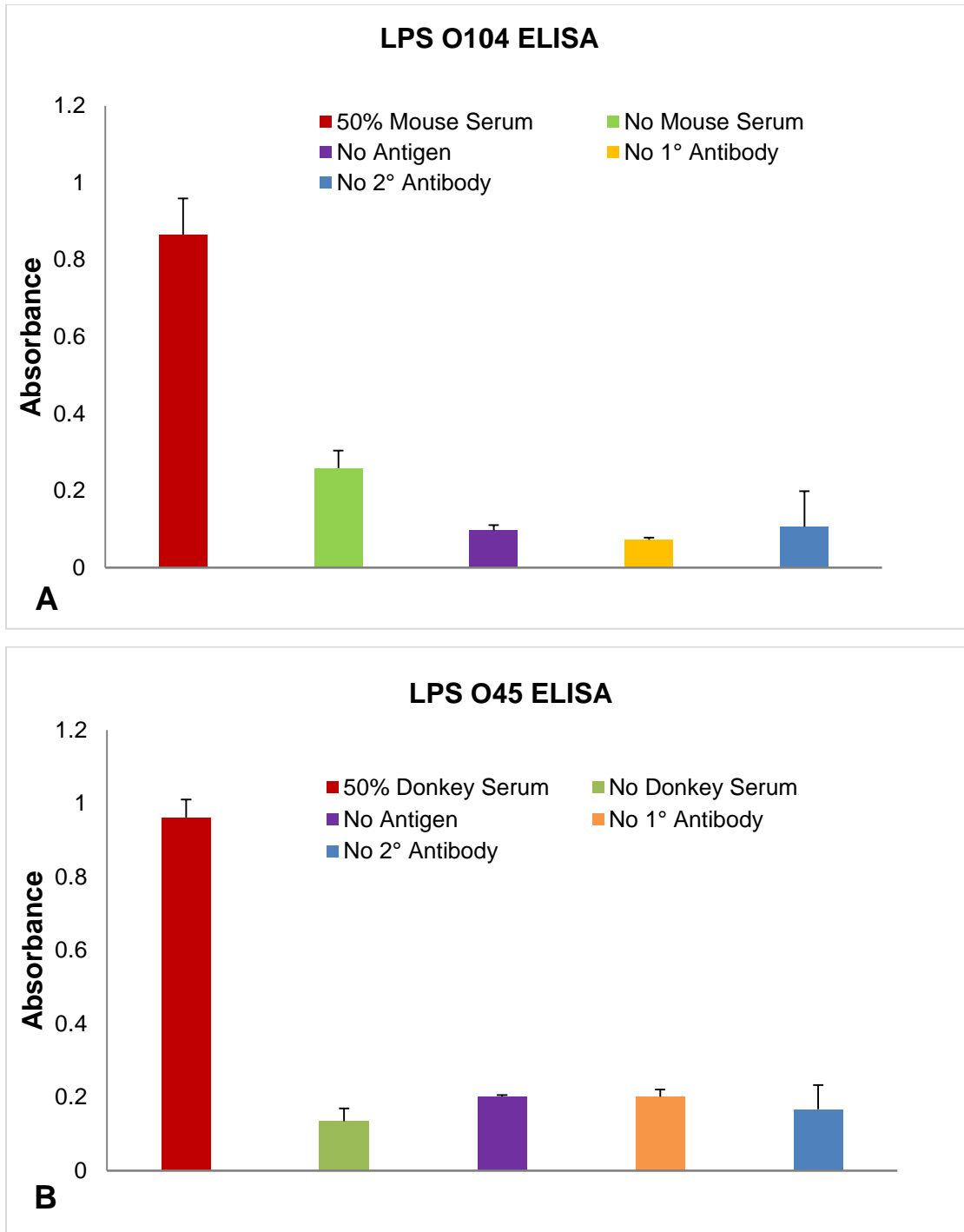
		Swiss Webster					
		Pre-Inoculated			Post-Inoculated		
LPS subtype		Whole LPS	O-ag	Lipid A	Whole LPS	O-ag	Lipid A
Dec. 01, 2015	O111:B4	-	-	NA	-	-	NA
	O157	-	-	NA	-	+	NA
	O145	-	-	-	-	-	-
	1x PBS/5% BSA	-	-	-	-	-	-
Jan. 23, 2016	O111:B4	-	-	NA	+	-	NA
	O157	-	-	NA	+	+	NA
	O145	-	-	NA	-	+	-
	1x PBS/5% BSA	-	-	-	-	-	-

No response '-'; Weak response '+'; Moderate response '++'; Intense response '+++'; NA = control antigens were not available for testing. PBS control on January 23, 2016 became contaminated during the blotting procedure. Blue highlighted regions indicate the targeted antigen

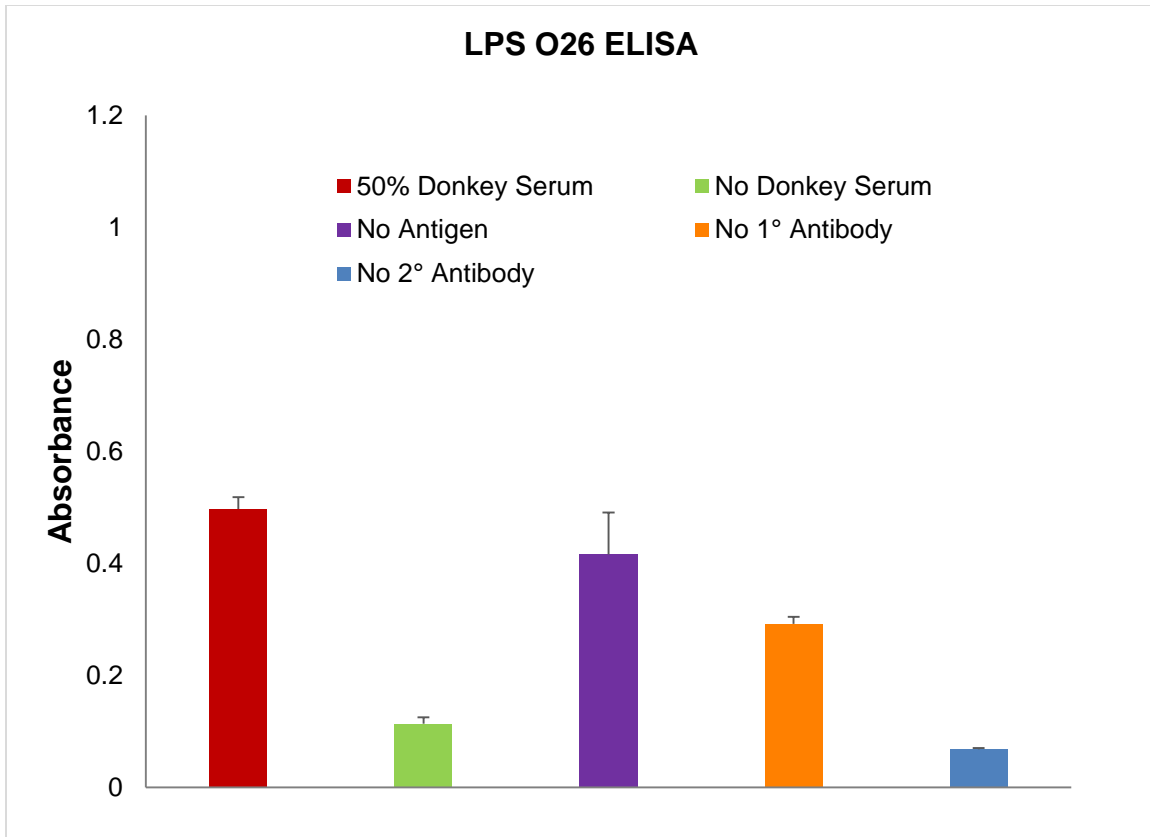


**Figure A3.36. Images of longitudinal dot blots for a Swiss Webster mouse in the O145 serogroup. Lipid A antigens were not available for control groups O111:B4 and O157.**

## Section A4.2 Serum lipoprotein capture ELISAs for LPS



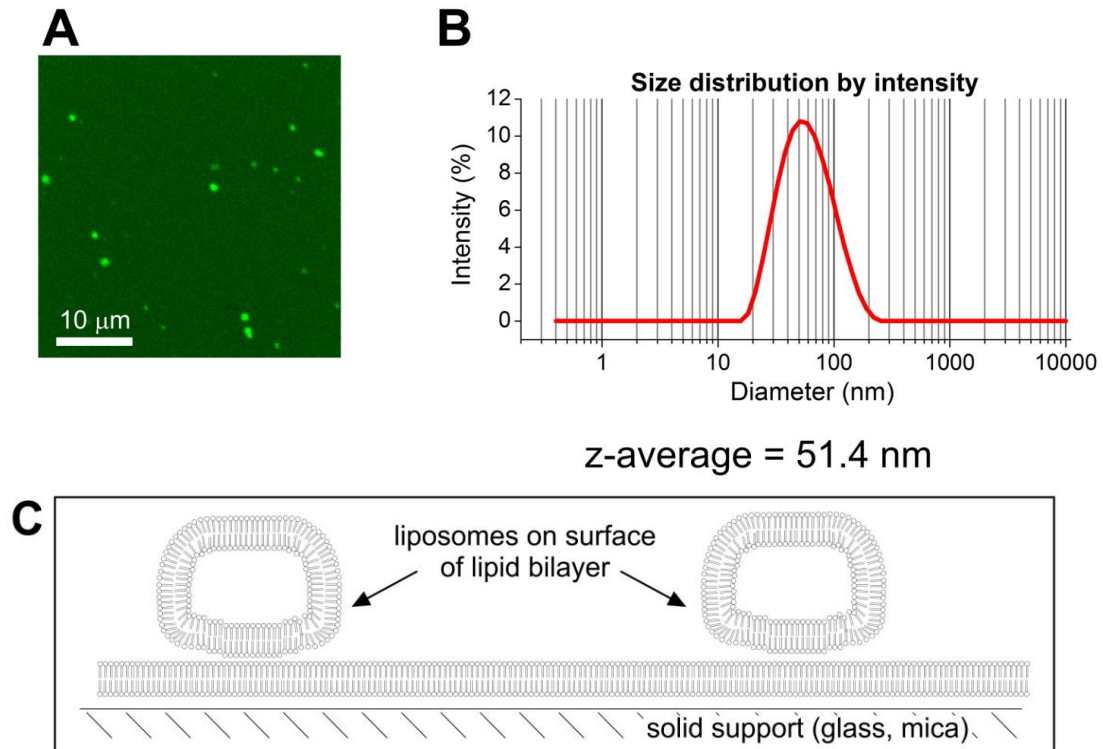
**Figure A3.37. ELISA results for serum functionalized plates.** A. Plate was functionalized with mouse serum and assay tested with LPS O104. B. Results for LPS O45 on a plate functionalized with donkey serum (red bars are specific signal). Results confirm the direct association between LPS and the lipoproteins present in serum. Functionalizing the plates with serum is less labor intensive, more cost effective and provides a physiological presentation of LPS to primary antibodies.



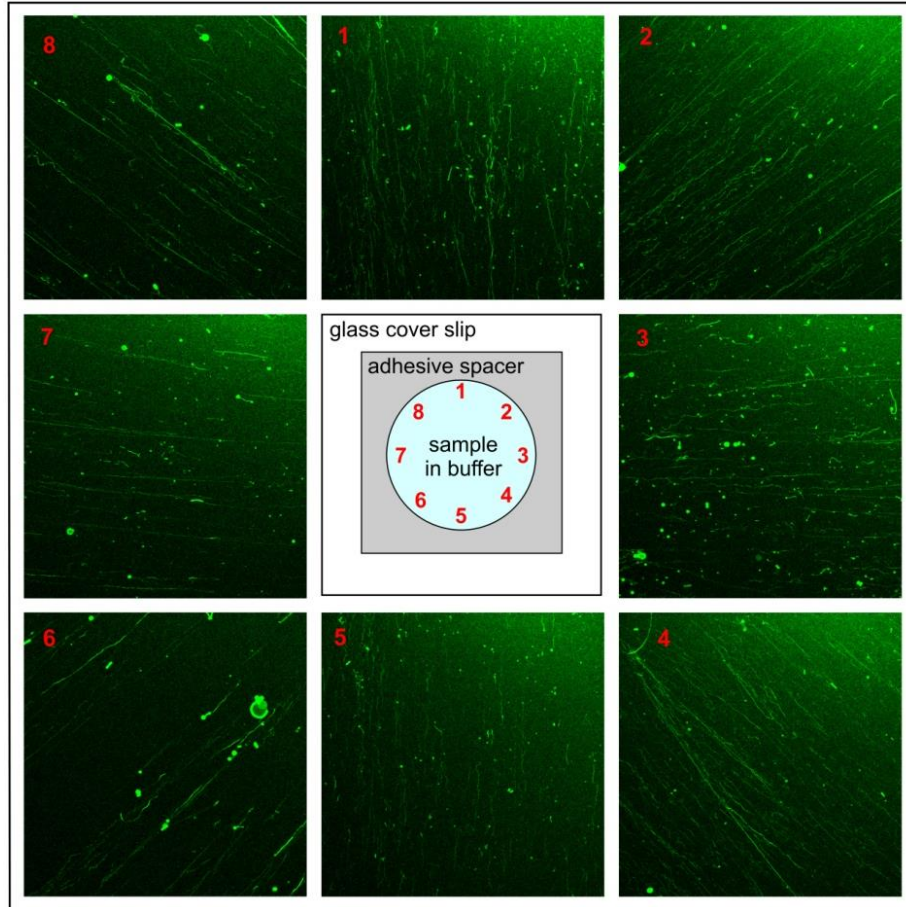
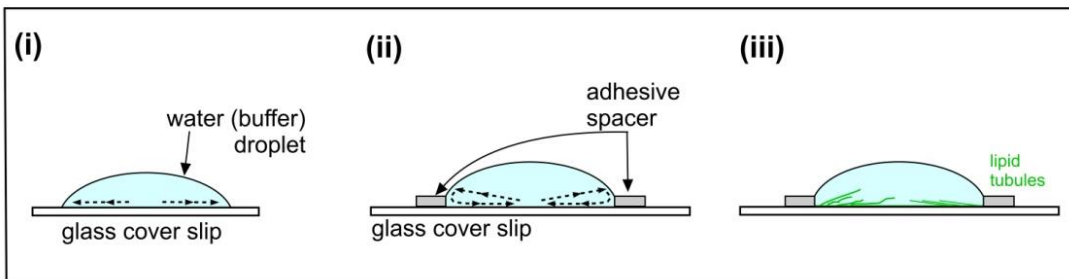
**Figure A3.38. ELISA results for LPS O26 on a serum functionalized plate.** A. Plate was functionalized with donkey serum. (red bars are specific signal) Results demonstrate the low specificity of mAb O26 to its O-ag.

## Appendix 4

### Section A4.1 Supporting images for Chapter 5



**Figure A4.1. Size of surface-associated lipid vesicles.** (A) Representative LSCM image of surface associated vesicles. See Movie S1 for mobility data. (B) Representative dynamic light scattering size distribution (by intensity). (C) Schematic showing proposed surface associated vesicles.

**A****B**

**Figure A4.2. Elongation of lipid tubules.** (A) LSCM fluorescence images acquired of the radial pattern formed by lipid tubules at the edges of the buffer droplet (images 1-8, position labeled on the schematic sample set-up and on the images). A DOPC sLBA (0.5% BODIPY lipids) in PBS was treated with 100  $\mu\text{g}/\text{mL}$  LPS and then images of tubules extending above the sLBA were acquired after approximately 30 min. The tubules were most evident by focusing approximately 2  $\mu\text{m}$  above the surface. (B) Cartoon of possible convection currents causing flow within the buffer droplets. (i) A droplet of water is expected to cause flow in the direction toward the edges of the droplet, driven by evaporation, similar to the “coffee-ring effect”. (ii) Our open droplet set-up, with an imaging spacer which creates boundary walls to the droplet. Complex buffer flows and counter-flows may exist. (iii) These currents serve to stretch out the lipid tubules formed by LPS.

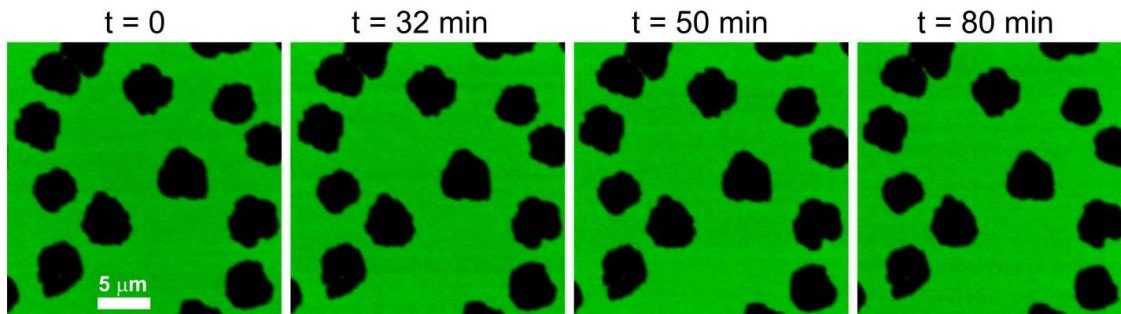


**Figure A4.3. Fluorescence time-course showing that holes are stable.** Time lapse LSCM fluorescence images over the course of 80 min showing the size and shape of holes within the lipid bilayer after LPS treatment. There are no significant changes in the holes.

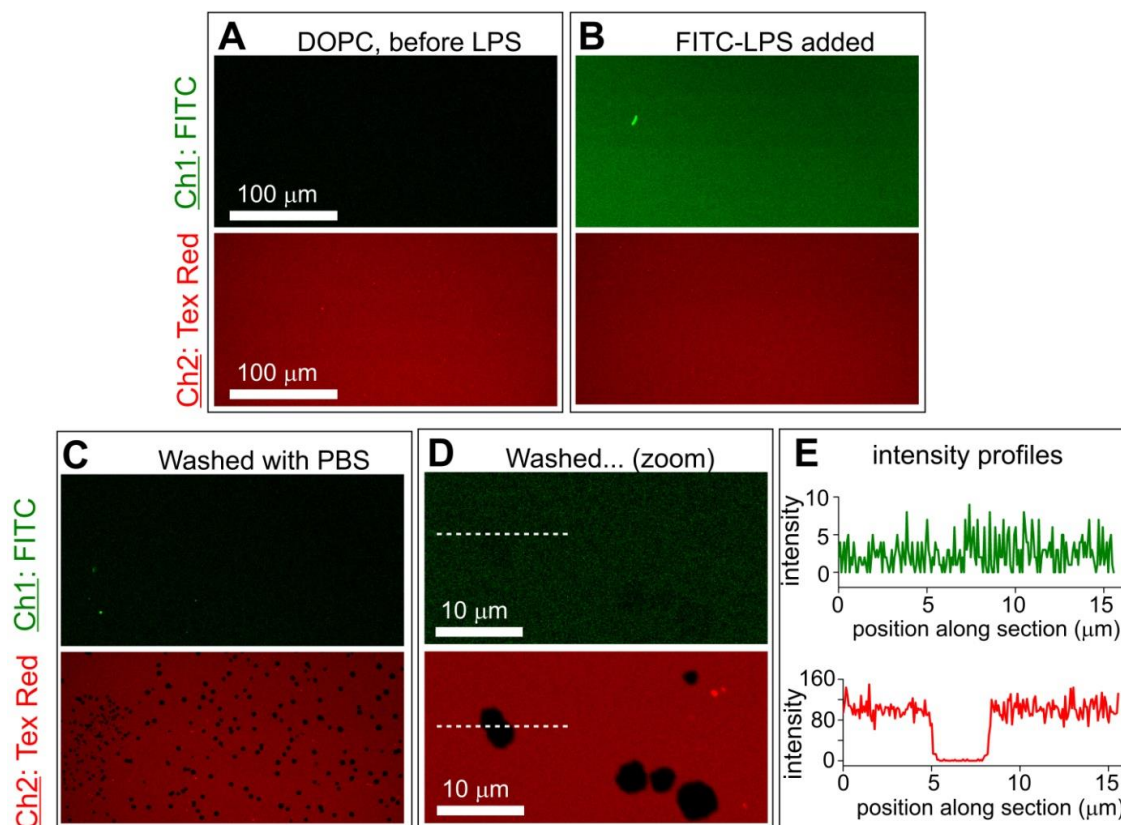


**Figure A4.4. Dual channel LSCM fluorescence images tracking FITC-LPS hole formation.** Upper panels: signal from the FITC-LPS (505-525 nm range); lower panels: signal from the DOPC bilayer doped with 0.5% Texas Red fluorescent lipids (655-755 nm range). Images are shown, (A) before LPS addition, (B) after addition of 100  $\mu\text{g}/\text{mL}$  FITC-LPS in PBS, (C) after 500  $\mu\text{g}/\text{mL}$  FITC-LPS treatment and washing the surface with ten changes of PBS. (D) A higher magnification image from (C), and (E) intensity profiles revealed voids in the Texas Red lipid fluorescence but very low FITC signal with no observable signal difference on or off the holes observed in the matched Texas Red channel.

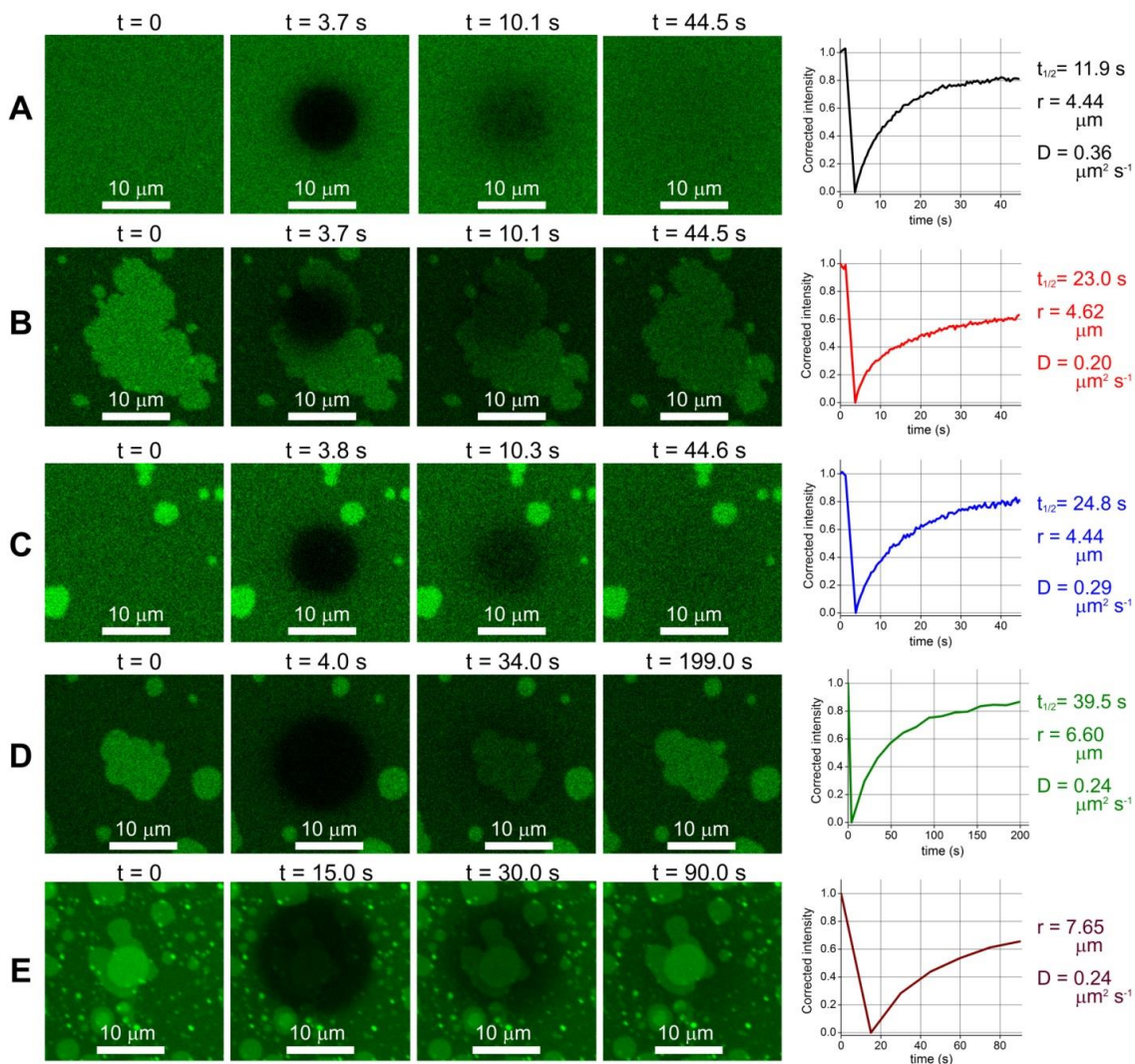


**Figure A4.5. FRAP studies on LPS (Ca<sup>2+</sup>) planar lamellar sheets.** (A) FRAP of a normal DOPC sLBA in Ca<sup>2+</sup> buffer. (B) FRAP of a planar lamellar sheet after LPS (Ca<sup>2+</sup>) treatment. (C) FRAP of the sLBA (nearby planar sheets visible) after LPS (Ca<sup>2+</sup>) treatment. (D) FRAP after bleaching an entire single-layer lamellar sheet. (E) FRAP after bleaching an entire multi-layer lamellar sheet. The corrected intensity vs. time plots show the fluorescence recovery over time in the bleached region. The first measurement post-bleach intensity in the ROI was normalized to zero, correction for any unintended photobleaching over the image series was made\* and the data set was normalized to the pre-bleach intensity (intensity = 1 at t = 0). \*by multiplication of each intensity measurement in the bleach ROI by  $F_{pre}/F_{post}$  in a region of the image that was not bleached, where  $F_{pre}$  = prebleach intensity (t = 0) and  $F_{post}$  = postbleach intensity at each time point. The recovery half-time ( $t(1/2)$ ) was measured from the plots. Diffusion coefficients were then calculated using the formula " $D = 0.22 \cdot r^2 / t(1/2)$ " ( $r$  = radius of bleached area). The diffusion coefficients for the sLBA are similar with a possible slight reduction after LPS(Ca<sup>2+</sup>) treatment. The diffusion coefficient for the planar sheet is significantly lower than that for the sLBA. The diffusion coefficients for bleaching an entire single or multi-lamellar planar sheet are intermediate values.

5  $\mu\text{g}/\text{ml}$  LPS in  $\text{CaCl}_2$  buffer

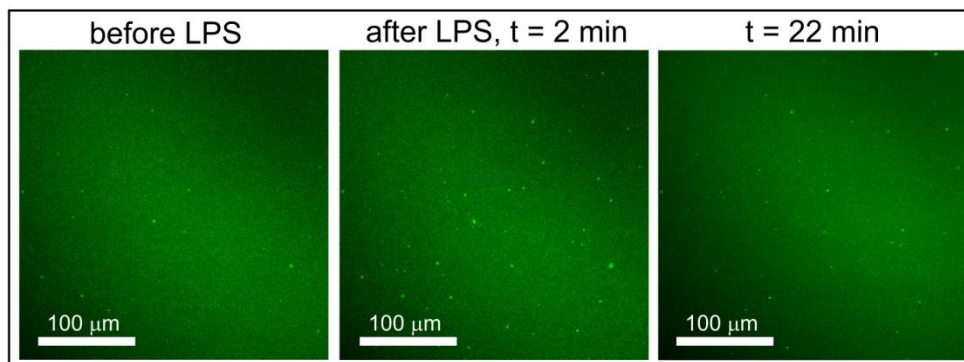


**Figure A4.6. LPS concentration dependence of planar sheet formation.** LSCM fluorescence images of an sLBA before and after addition of 5  $\mu\text{g}/\text{mL}$  LPS in  $\text{Ca}^{2+}$  buffer. Sequential images are shown after 2 min and 22 min after addition of the LPS.

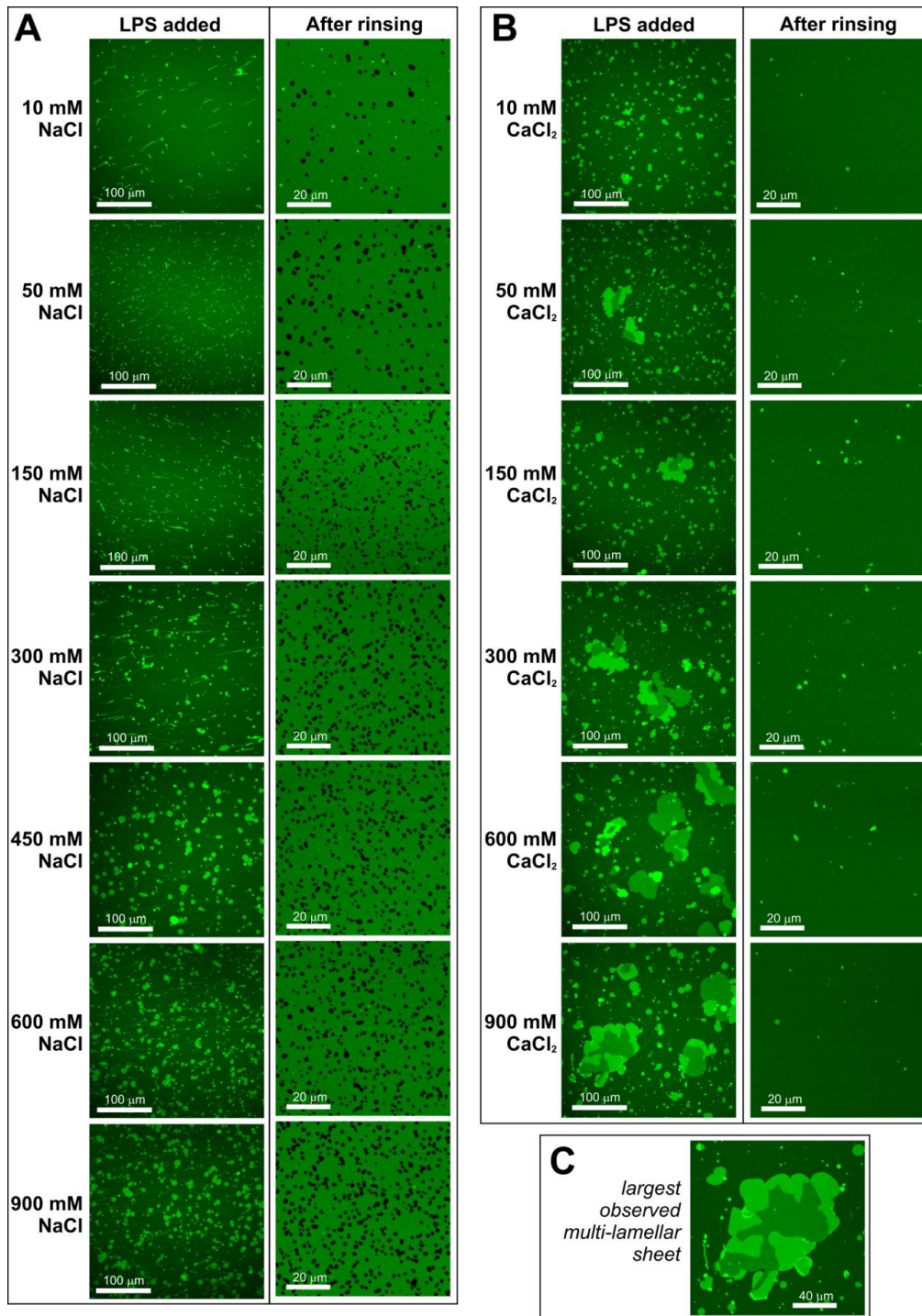


**Figure A4.7. Cation concentration effects on LPS membrane disruption.** (A) Representative LSCM images from showing the effects of LPS in a series of buffers with increasing NaCl concentration. All buffers contained 20 mM TRIS (pH 7.5). sLBAs were treated with 100  $\mu\text{g}/\text{mL}$  LPS and imaged after approximately 15 min after LPS addition (column 1) and after rinsing the surface with fresh buffer (column 2). (B) As in (A), except using a buffer series with  $\text{CaCl}_2$  instead of NaCl. (C) The largest multilamellar lipid patch observed.

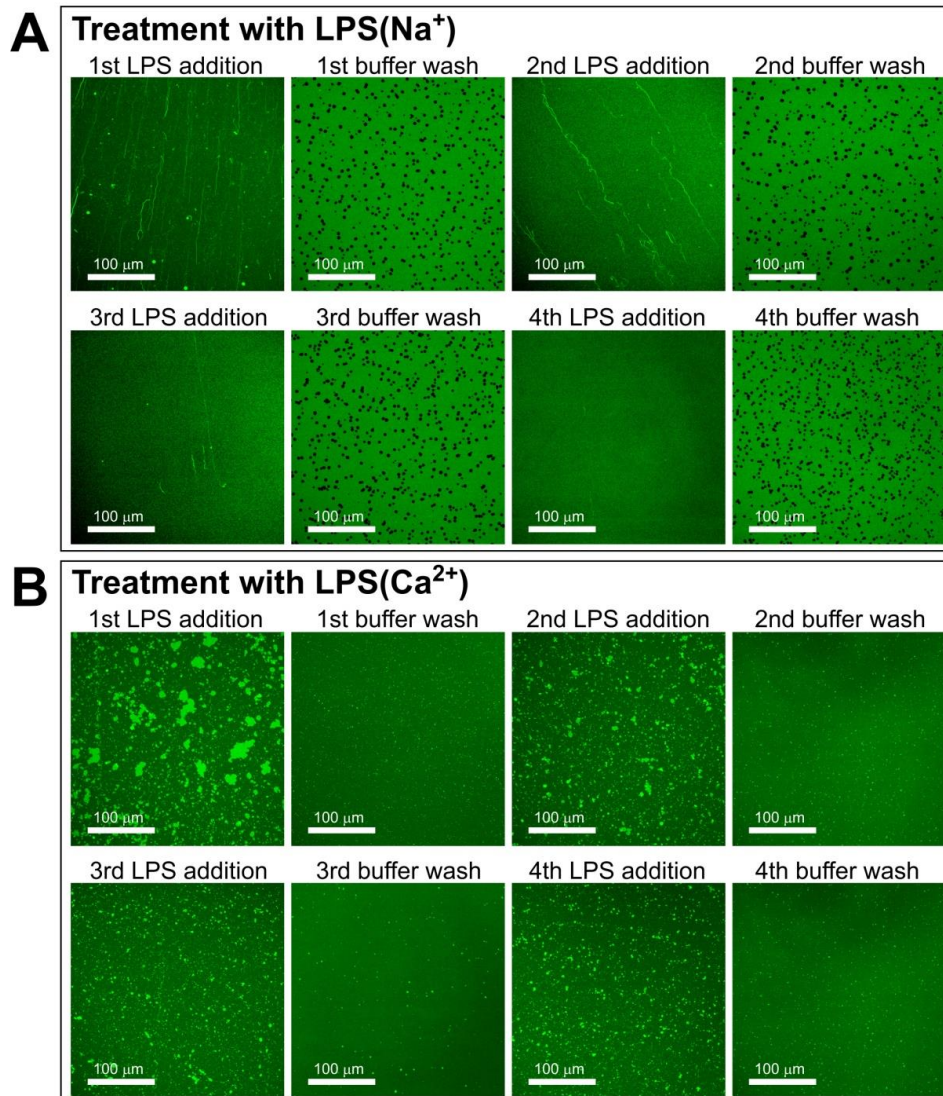


**Figure A4.8. (A) Reduction in lipid tubules and similar hole formation by multiple cycles of LPS treatment.** DOPC sLBAs were incubated with 100  $\mu\text{g}/\text{mL}$  LPS in PBS for 20 min, LSCM images acquired of lipid tubules and then washed with PBS and imaged again. This was repeated until 4 cycles of LPS treatment had been performed. After each LPS treatment lipid tubules were formed and then removed during the buffer wash. Fewer tubules were observed with each LPS treatment, due to the expected depletion of surface-associated vesicles. Note that holes were formed after the first buffer wash and then ‘filled-in’ by the 2nd LPS treatment, probably due to packing of LPS into the holes, joining up with the lipid bilayer, allowing lateral lipid diffusion and ‘healing’ of the holes. However, following the each buffer wash, holes of a similar size and distribution were formed once again, suggesting that hole formation does not depend on surface-associated vesicles, but on the solid-supported lipid bilayer and interaction with LPS. (B) Reduction in planar sheet formation by multiple cycles of LPS treatment. DOPC sLBAs were incubated with 100  $\mu\text{g}/\text{mL}$  LPS in Ca<sup>2+</sup> buffer for 20 min, LSCM images acquired of planar sheets and then washed with Ca<sup>2+</sup> buffer and imaged again. This was repeated until 4 cycles of LPS treatment had been performed. Not all sheets are removed by each buffer wash, but there is a trend to form smaller and fewer planar lamellar sheets with each subsequent LPS treatment.

## Section 4.2. Information for supporting video files

Movies are available for download at <http://dx.doi.org/10.1016/j.bpj.2014.04.016>

**[Movie A4.1. Mobility of surface-associated lipid vesicles.](#)** Time-lapse LSCM series of images showing the motion of surface-associated vesicles on a DOPC sLBA. Total image represents 39.4 x 39.4  $\mu\text{m}$ , interval between images is 1.0 s. Movie is available for download at the following address:  
<http://www.cell.com/cms/attachment/2014949947/2036222547/mmc2.mp4>

**[Movie A4.2. Lipid tubule formation.](#)** Time-lapse LSCM series of images showing treatment of a DOPC sLBA with 100  $\mu\text{g}/\text{mL}$  LPS in PBS. Total image represents 105.3 x 105.3  $\mu\text{m}$ . Series 1 was acquired with continuous image acquisition (1.1 s/ image, no interval) and the droplet of LPS is added to the sample at  $\sim 10$  s (Series 1). Series 2 was then acquired on the same field, with an interval of 15 s, to allow slower processes to be observed. Elapsed time for each series is shown as “T #seconds # milliseconds”. Each image series was contrast-adjusted independently for clarity. Disordered lipid tubules are formed immediately after LPS addition and they extended and stretch out over the course of Series 1 and 2. Note, the overall fluorescence signal is reduced between images “9 s 981 ms” and “12 s 199 ms” (Series 1) because of slight defocusing of the sample due to the physical effect of adding the droplet of LPS at  $\sim 10$  s. Refocusing on the sLBA after imaging reveals a similar sLBA fluorescence before and after LPS addition. Movie is available for download at the following address:

<http://www.cell.com/cms/attachment/2014949947/2036222546/mmc3.mp4>

**[Movie A4.3. Lipid tubule mobility.](#)** Epifluorescence ‘movie’ imaging of a DOPC sLBA after  $\sim 20$  min treatment with 100  $\mu\text{g}/\text{mL}$  LPS in PBS. Total image represents 132 x 132  $\mu\text{m}$ . High lateral mobility of lipid tubules is apparent. Movie is available for download at the following

address:<http://www.cell.com/cms/attachment/2014949947/2036222544/mmc4.mp4>

**[Movie A4.4. Lipid sheet formation and growth.](#)** Time-lapse LSCM series of images showing treatment of a DOPC sLBA with 100  $\mu\text{g}/\text{mL}$  LPS in  $\text{Ca}^{2+}$  buffer. Total image width represents 317.3 x 317.3  $\mu\text{m}$ . Series 1 was acquired with continuous image acquisition (3.3 s/ image, no interval) and the droplet of LPS is added to the sample at  $\sim 9$  s (Series 1). Series 2 was then acquired on the same field, after refocusing (3.3 s/ image, no interval). Series 3 was then acquired with an interval of 30 s, to allow slower processes to be observed. Elapsed time for each series is shown as “T #seconds # milliseconds”. Each image series was contrast-adjusted independently for clarity. Patches of fluorescence, expected to represent planar lipid/LPS lamellae, are formed immediately after LPS addition and expand in size over the course of the video. Note, the overall fluorescence signal is reduced between images “6 s 652 ms” and “13 s 304 ms” (Series 1) because of slight defocusing of the sample due to the physical effect of adding the droplet of LPS at  $\sim 9$  s. Refocusing on the sLBA after imaging reveals a similar sLBA fluorescence before and after LPS addition. Movie is available for download at the following address:

<http://www.cell.com/cms/attachment/2014949947/2036222545/mmc5.mp4>

## Appendix 5

### Section A5.1 Supporting information for Chapter 6

#### A5.1.1 Statistical results

Variability assessment determined that deviations of the logarithm of specific signal remained larger, while those for the background and non-specific binding were commensurate with one another. The ANOVA results (S2 Table) showed that only the type of measurement impacts the variability. It was found that wg# and power also affected variability. AIC modeling determined that all of the variables were significant, but the residuals for the uncertainty of the specific binding were significantly larger, even after LPSc, wg#, and power were accounted for. Regression analysis (**Table A5.3**) showed no significance for any of the analyzed variables (LPSc, wg#, and power), but showed that the uncertainty of the specific binding was greater than four times that of the uncertainty in other types of measurements with a p-value =  $8.77e^{-16}$ . This indicates that the uncertainty in specific binding is significant, but not dependent upon any of the analyzed variables except the inherent variability of LPS itself.

**Table A5.1. ANOVA of variable significance (5%) in relation to logarithm of integrated intensity.**

	DF	Sum Sq	Mean Sq	F Value	Pr(>F)
measurement type	2	62.804	31.402	278.865	< 2.2E <sup>-16</sup>
LPSc	1	1.266	1.266	11.239	0.00109 <sup>#</sup>
wg#	3	1.306	0.435	3.865	0.0113 <sup>#</sup>
power	1	0.52	0.520	4.616	0.0338 <sup>#</sup>
Residuals	112	12.612	0.113		

# indicates numbers with significant p-values for the corresponding coefficient

**Table A5.2. ANOVA of absolute values of residuals.**

	DF	Sum Sq	Mean Sq	F Value	Pr(>F)
measurement type	2	2.691	1.346	45.687	3.10E-15#
LPSc	1	0.028	0.028	0.954	0.331
wg#	3	0.113	0.038	1.279	0.285
power	1	0.053	0.053	1.795	0.183
Residuals	112	3.299	0.029		

# indicates numbers with significant p-values for the corresponding coefficient

**Table A5.3. Regression analysis of residuals for LPS concentration detection.**

Coefficients	Estimate	Std. Error	t – value	Pr ( >   t   )
Intercept	-0.06009	0.15355	-0.391	0.6963
LPSc	0.00013	0.00026	0.521	0.6037
wg1*	0.02712	0.05411	0.501	0.6172
wg2*	0.01488	0.08470	0.307	0.7595
wg3*	0.10956	0.05350	2.048	0.0429#
power	0.00070	0.00052	1.34	0.183
mNSB	0.00378	0.04291	0.088	0.93
mSP	0.40259	0.04291	9.383	8.77E-16#

Residual standard error: 0.17160 on 112 degrees of freedom  
 Multiple R-squared: 0.4666  
 Adjusted R-squared: 0.4332  
 F-statistic: 13.99 on 7 and 112 DF  
 p-value: 6.21E-13

\*wg# is a unique identifying number for an individual waveguide

# indicates numbers with significant p-values for the corresponding coefficient

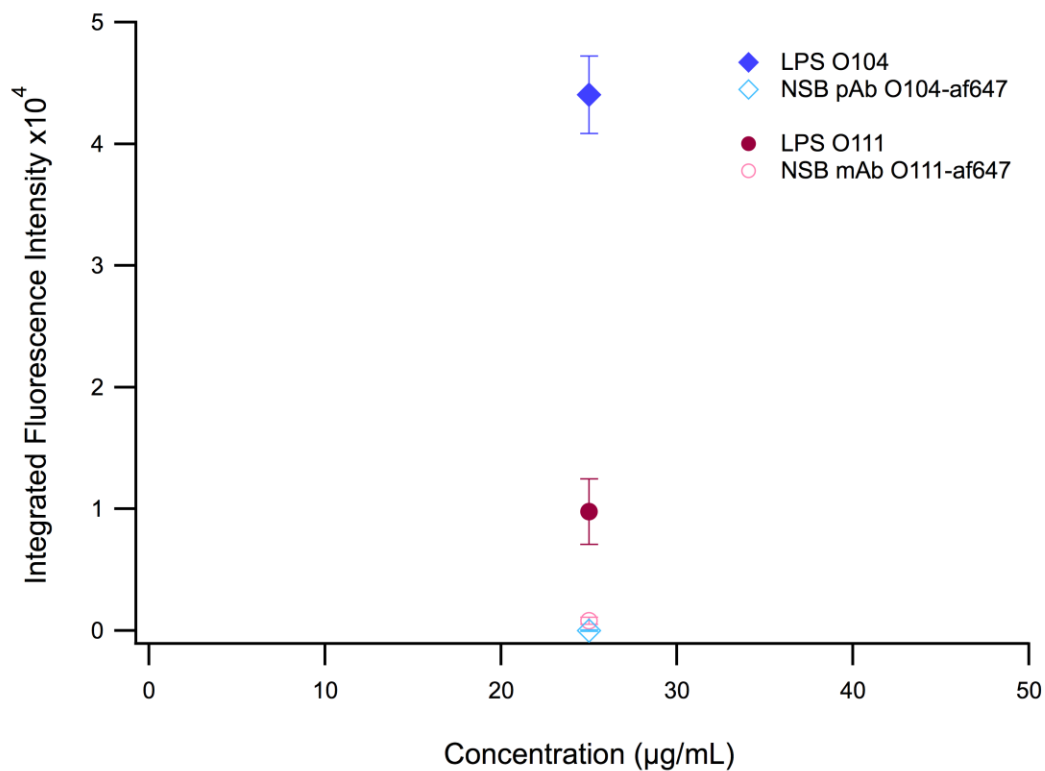


**Figure A5.1. Integrated intensities of O-ag targeted detection of LPS.** Spectra from Figure 6.4 were integrated and plotted to demonstrate the difference in values when using specific antibodies for detection. Error bars indicate standard error of the mean for the average of three replicates.

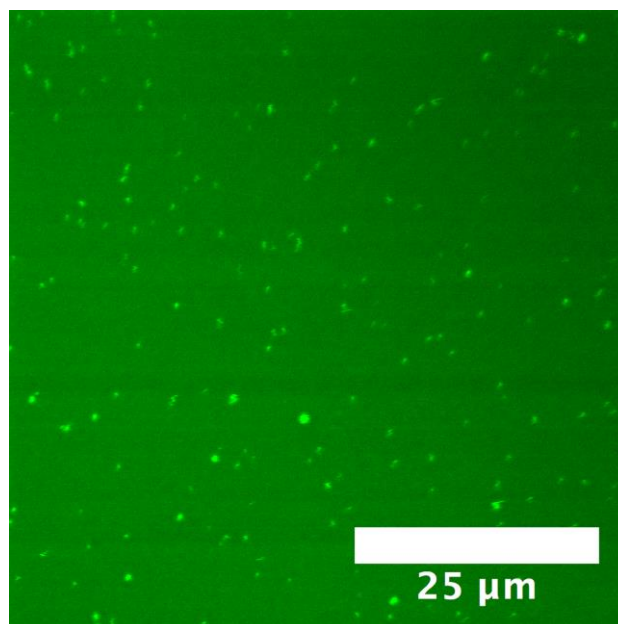


**Figure A5.2. High concentration of LPS O157 in a flow cell.** 100 µg/mL LPS O157 was incubated in the flow cell and rinsed. No hole formation was observed.

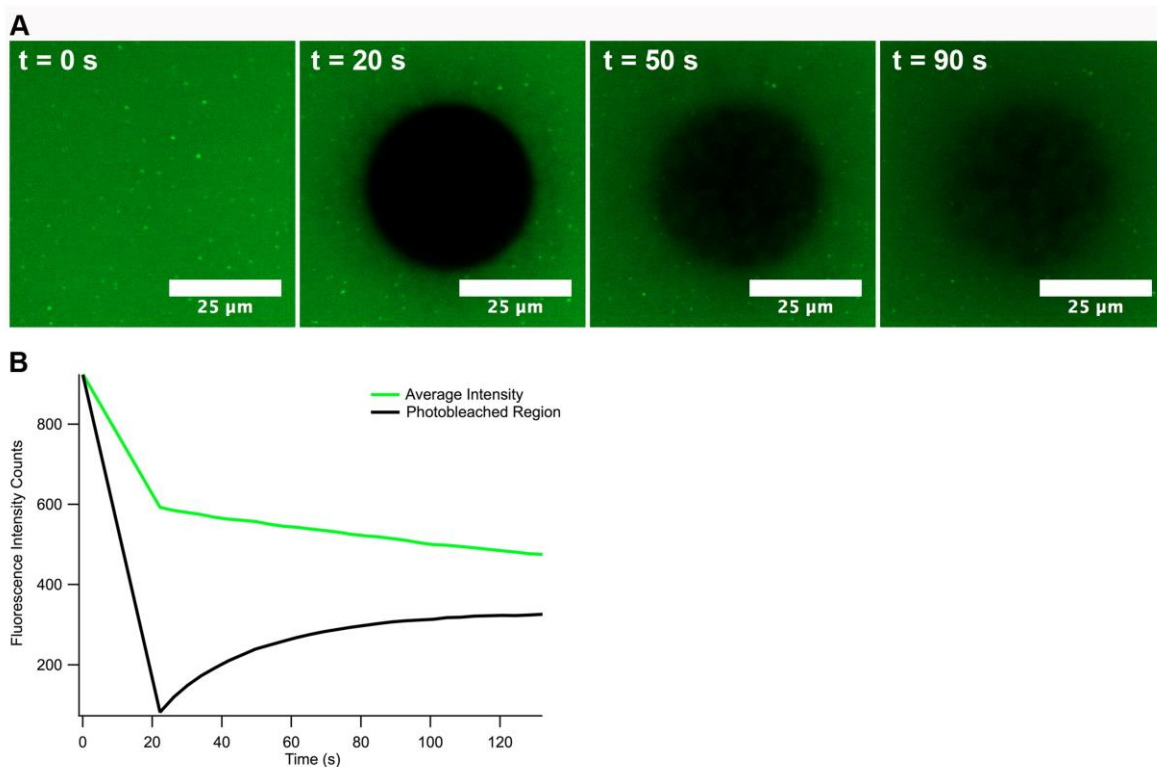


**Figure A5.3. Lateral fluidity of bilayers after incubation with 100  $\mu\text{g}/\text{mL}$  LPS O157 inside a flow cell.** (A) Time lapse series of DOPC-BODIPY bilayers that were photobleached and showed lateral fluidity during recovery. (B) Intensity profile graph of the overall average intensity and the recovery of the photobleached region. Incubating with LPS O157 does not cause hole formation or effect fluidity of the bilayers.

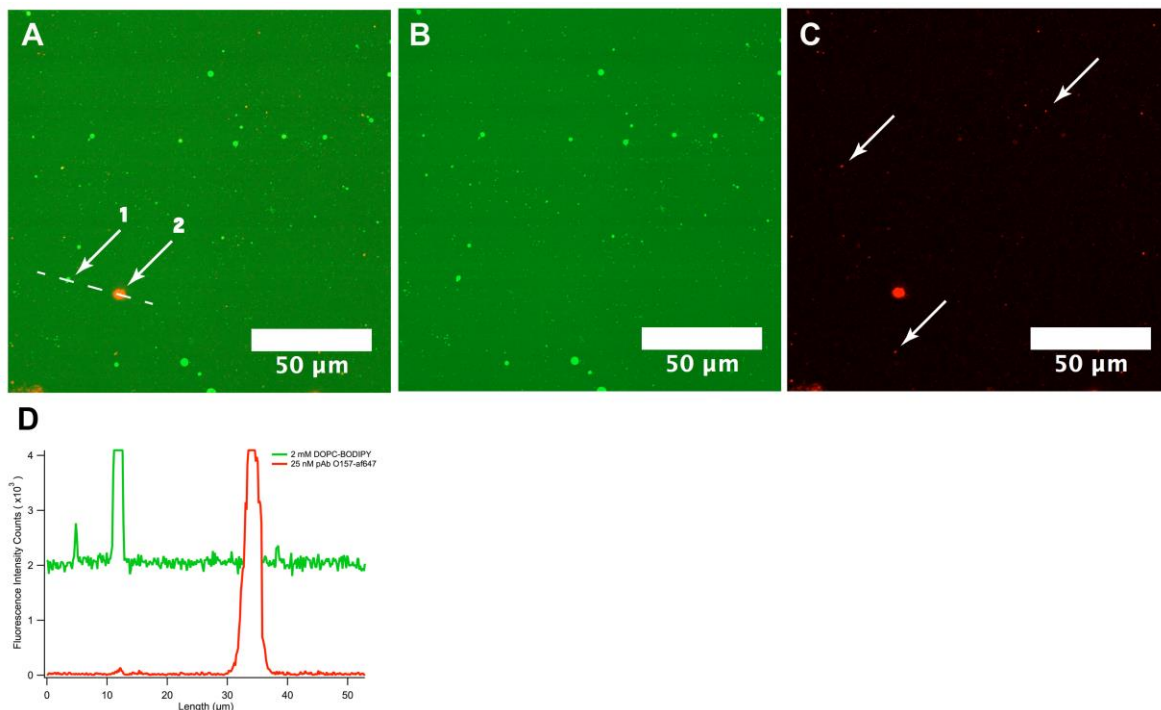


**Figure A5.4. Specific and non-specific binding of pAb O157-af647 inside a flow cell.** (A) Composite 2 channel image of DOPC-BODIPY lipids and pAb O157-af647. White arrows indicate points of fluorescence intensity, and the white dotted line is the region of analysis graphed in D. Arrow 1 is a DOPC-BODIPY surface associated vesicle, and arrow 2 is specific binding of the reporter antibody. (B) Green channel of image A. (C) Red channel of image A. White arrows indicate points of non-specific binding. (D) Line intensity profile of dotted line in image A showing low non-specific binding and saturated intensity of the specific binding. Low NSB and high specific binding events allow for increased signal to noise ratios allowing sensitive detection of LPS membrane insertion.

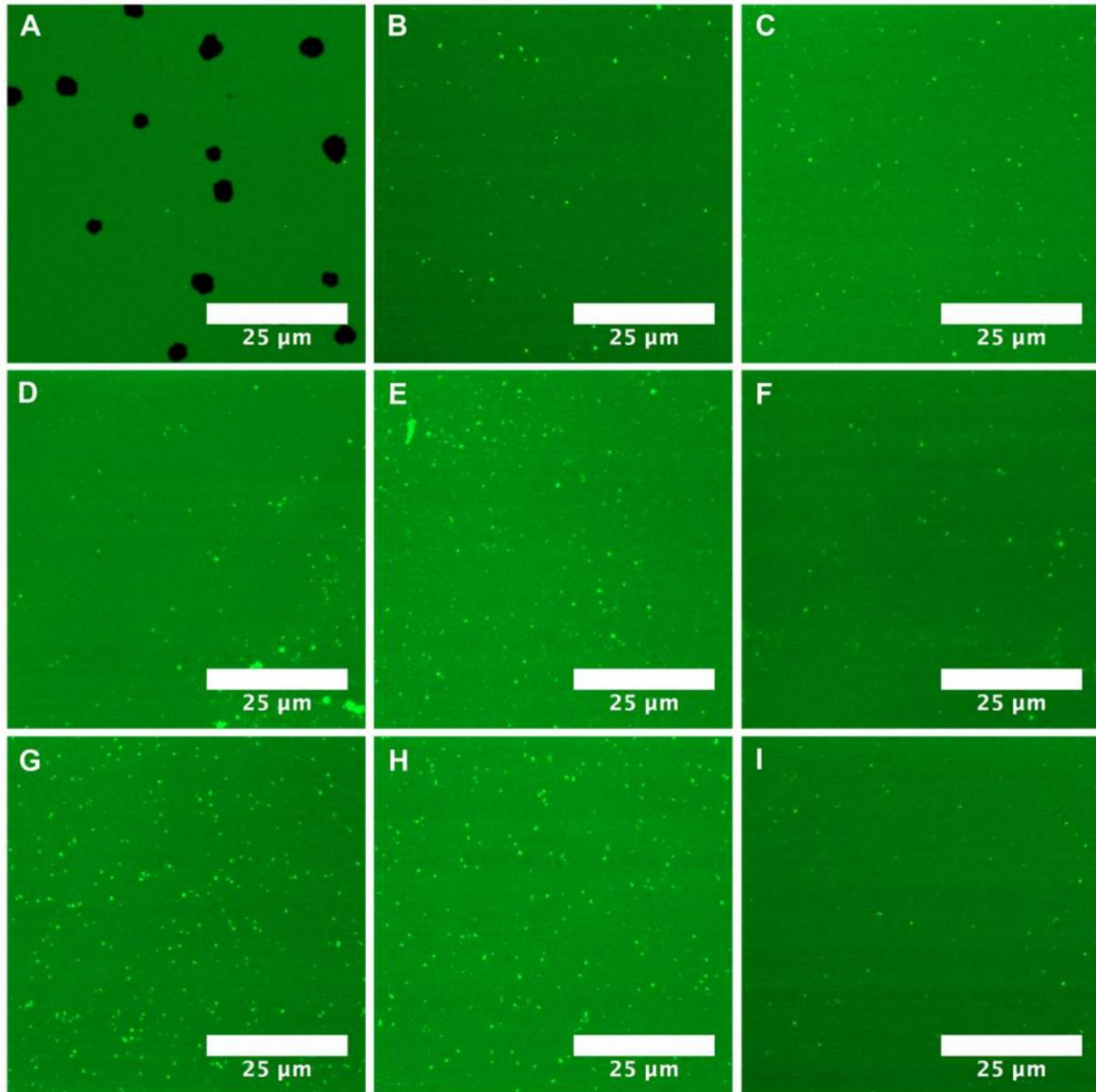


**Figure A5.5. Effects of multiple serogroups of LPS on lipid bilayers.** (A-I) 50  $\mu\text{g}/\text{mL}$  LPS O111:B4, O26, O45, O103, O104, O111, O113, O121, and O145 respectively.

## Section A5.2 Data processing methods

### A5.2.1 Data processing algorithm

The following is a simple algorithm designed to take individual columns of spectral data and take the area under the curve as a function of the change in wavelength. This takes advantage of a built-in Igor Pro 6.3 function called 'areaXY'. Raw and processed data sets are available for download from the publishers website.

### Integration algorithm for spectral data processing.

```
Function BIR5(W, B1, B2, B3, B4, B5, NSB, SP, index) //input function – designed to intergrate input waves B1, B2, B3, B4, B5, NSB, SP where  $\Delta X$  is determined by the  $\Delta W$  – usually about 0.3 nm //The number of input background variables should be altered if using a data set that has more or less responses recorded.
```

```
//Variables
```

```
Wave NSB, SP //non-specific binding and specific binding spectra
```

```
Wave B1, B2, B3, B4, B5 //background spectra
```

```
Wave W //wavelength range scanned
```

```
Variable index
```

```
Make /O/N = 100 NSB_int, SP_int, B1_int, B2_int, B3_int, B4_int, B5_int, ratio //generates the empty waves to allocate the resulting values into //if processing larger data sets (greater than 100 values expected), the size of these waves should be changed accordingly
```

```
NSB_int[index] = areaXY(W, NSB) //calculates the area under the curve of NSB and using the wavelength as the limits of integration...trapezoidal method
```

```
//index is using an assigned value to direct results to a specific location in the wave NSB_int – following commands are engineered in an identical fashion, thus assigning values from one experiment to the same row in each wave
```

```
SP_int[index] = areaXY(W, SP) //calculates the area under the curve of SP and using the wavelength as the limits of integration...trapezoidal method
```

```
B1_int[index] = areaXY (W,B1)
```

```
B2_int[index] = areaXY (W,B2)
```

```
B3_int[index] = areaXY (W,B3)
```

```
B4_int[index] = areaXY (W,B4)
```

```
B5_int[index] = areaXY (W,B5)
```

```
ratio[index] = SP_int[index]/NSB_int[index]
```

```
End
```

### *A5.2.2 Integrated spectral values and data processing method*

Data set is available for download as an excel spreadsheet which contains all the integrated values of the spectral curves and how those values were processed to obtain limits of detection and signal to noise ratios. Data was integrated using IgorPro 7 and algorithm from section A5.2.1.

### *A5.2.3 Raw data of spectral curves*

Data set is available for download as an Excel spreadsheet that contains the spectra collected from a waveguide-based optical biosensor fitted with a USB 2000 Ocean Optics spectrometer. File contains 11 different tabs, and the replicates for each concentration or assay are contained within a single tab. Concentrations are clearly marked, and the waveguide number is written after each replicate number. E.g. N=1/wg#.

## Appendix 6

### Section 6.1 LPS interactions with complex supported lipid bilayers

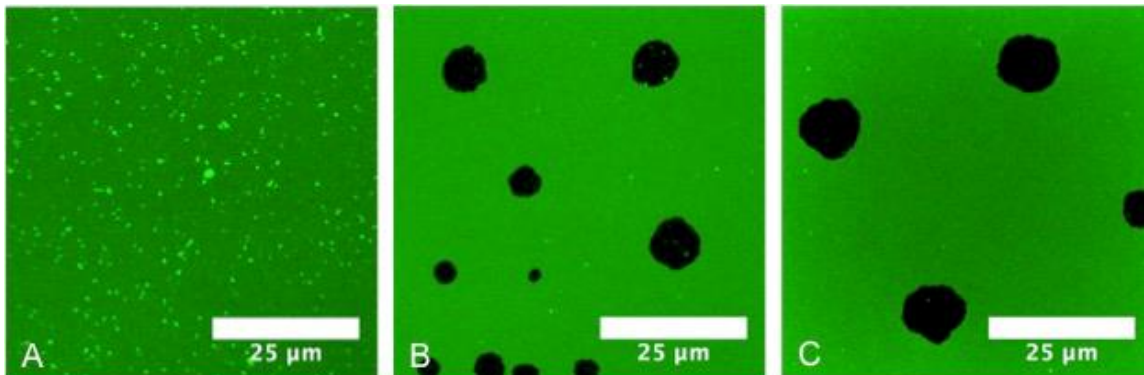


**Figure A6.1. DOPC sLBA controls.** Controls were run simultaneously at room temperature with every experiment. A. DOPC bilayer was imaged throughout the duration of the experiment and rinsed equally as that of the LPS experimental controls. No hole formation or bilayer deformation is noted. FRAP was performed on all sLBAs to ensure bilayer fluidity. B. DOPC lipid bilayer incubated with 50  $\mu\text{g}/\text{mL}$  of LPS for 20 min at R/T. C. DOPC lipid bilayer incubated with 25  $\mu\text{g}/\text{mL}$  LPS for 20 min at R/T.

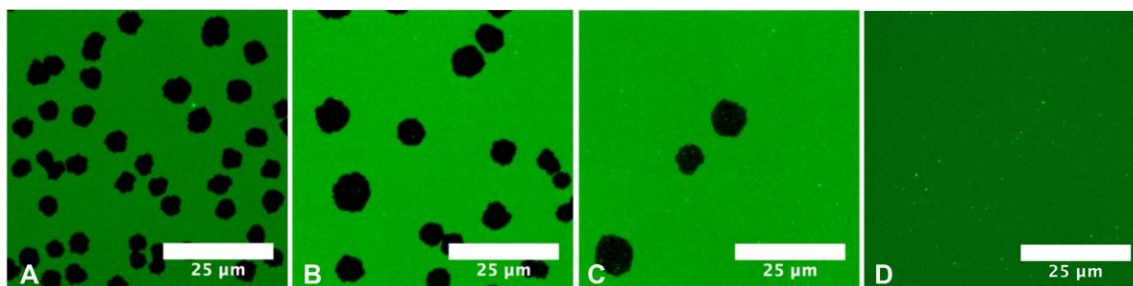


**Figure A6.2. DOPC lipid bilayers with 50% cholesterol.** Bilayers (A-D) were incubated with 200, 100, 50, and 25  $\mu\text{g}/\text{mL}$  LPS O111:B4 (respectively) for 20 min at R/T and then rinsed and imaged.

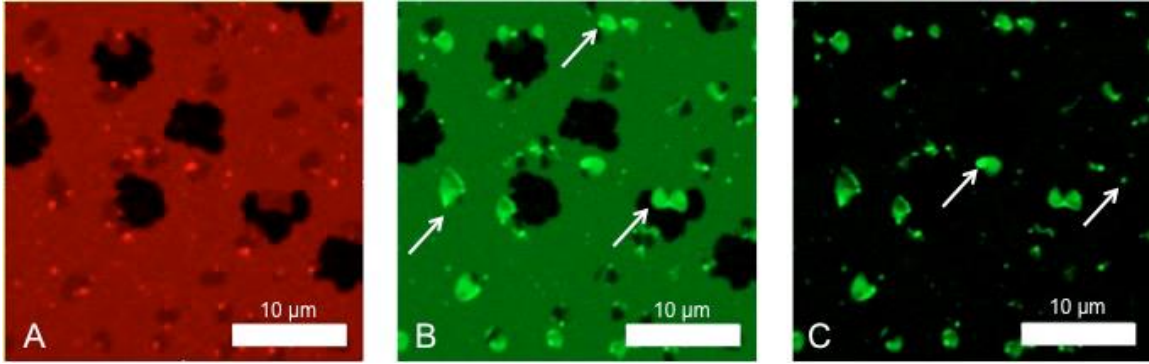


**Figure A6.3. Lipid bilayers labeled with TR enriched with 50% NBD-cholesterol.** To ensure incorporation of cholesterol, NBD-labeled cholesterol was used for imaging with TR lipids. Bilayer was incubated with 200 µg/mL LPS for 20 min. A. Red channel shows red lipids and hole formation. Bright red spots occur due to the overlap of excitations of Texas Red and NBD. B. Green channel with white arrows. Arrows show some of the localized cholesterol. C. Composite channel with the red background subtracted out. Arrows again indicate the presence of cholesterol in the lipids.

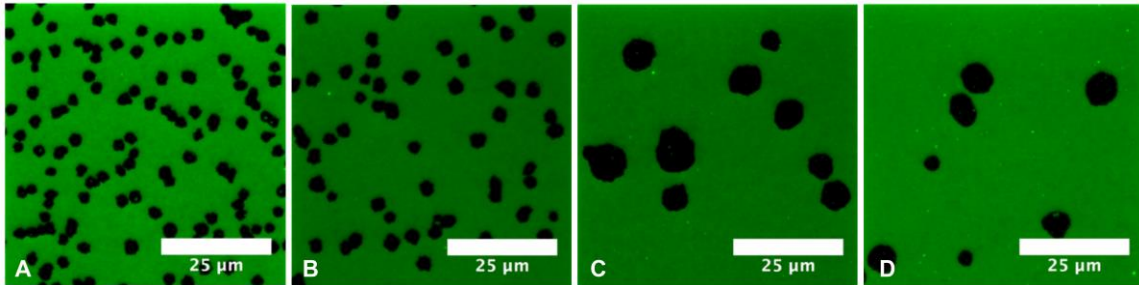


**Figure A6.4 DOPC lipid bilayers with 5% Sphingomyelin.** Bilayers (A-D) were incubated with 200, 100, 50, and 25 µg/mL (respectively) LPS O111:B4 for 20 min at R/T and then rinsed and imaged.

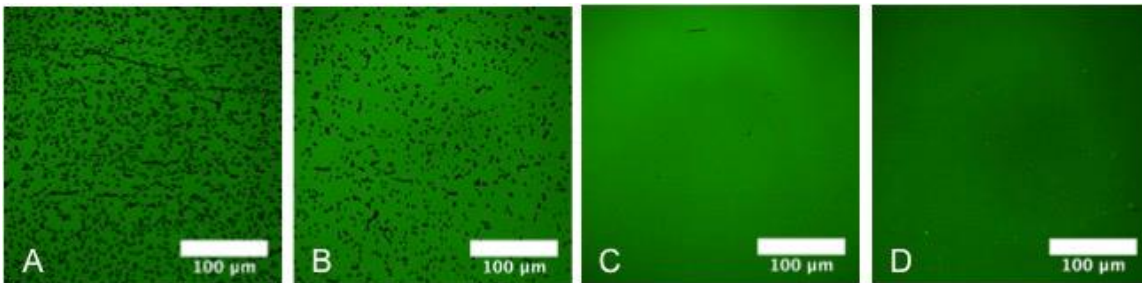


**Figure A6.5. Zoomed out image of lipid bilayers with 5% sphingomyelin and 50% cholesterol.** Bilayers (A-D) were incubated with 200, 100, 50, and 25 µg/mL (respectively) LPS O111:B4 for 20 min at R/T and then rinsed and imaged. C-D. Both 50 and 25 µg/mL LPS bilayers show the presence of very small, infrequent holes, which may be an artifact of washing.

When we combined 5% sphingomyelin with 25% cholesterol in our sLBA mixtures (**Figure A6.6**), LPS-induced hole formation was highly asymmetric both in the pattern and size of the holes formed (**Figure A6.6 A-B**), as compared to all other holes formations that we noted in the bilayers. It is evident that there are divided regions between holes of larger size and less frequency, as compared to other regions where holes are much smaller, but more frequent. We also witnessed unusual patterns in the hole formation, and highly localized regions of fluorescence intensity when incubating with 50 µg/mL LPS (**Figure A6.6 E-F**). In our previous studies, these regions of intensity have demonstrated to be lipid vesicles, which recover after photobleaching. However, FRAP of these isolated regions did not result in fluorescence recovery after 5 minutes, indicating little to no lateral mobility between the lipid architectures. The incorporation of a fluorescently labeled sphingomyelin is a logical next step to analyze the distribution of the molecule within the bilayer, and determine the interaction that LPS has with the molecule. This particular ratio of lipids (5% sphingomyelin/25% cholesterol) is more physiologically relevant in comparison to the higher levels of cholesterol, however investigating a ratio of 15% sphingomyelin/25% cholesterol would probably be the most representative of a cell membrane exposed to LPS. As yet, this system indicates that cholesterol is capable of inhibiting hole formation at lower concentrations of LPS, while sphingomyelin is not. Even optimizing the ratio of the two to conditions that are more biomimetic may not completely inhibit this mechanism, as data with sphingomyelin shows no inhibition. This is compelling evidence that hole formation in cell membranes may be possible. Thus, investigating this system fully could lead to interesting insights into LPS signaling in the presence of lipid rafts and membrane architectures.

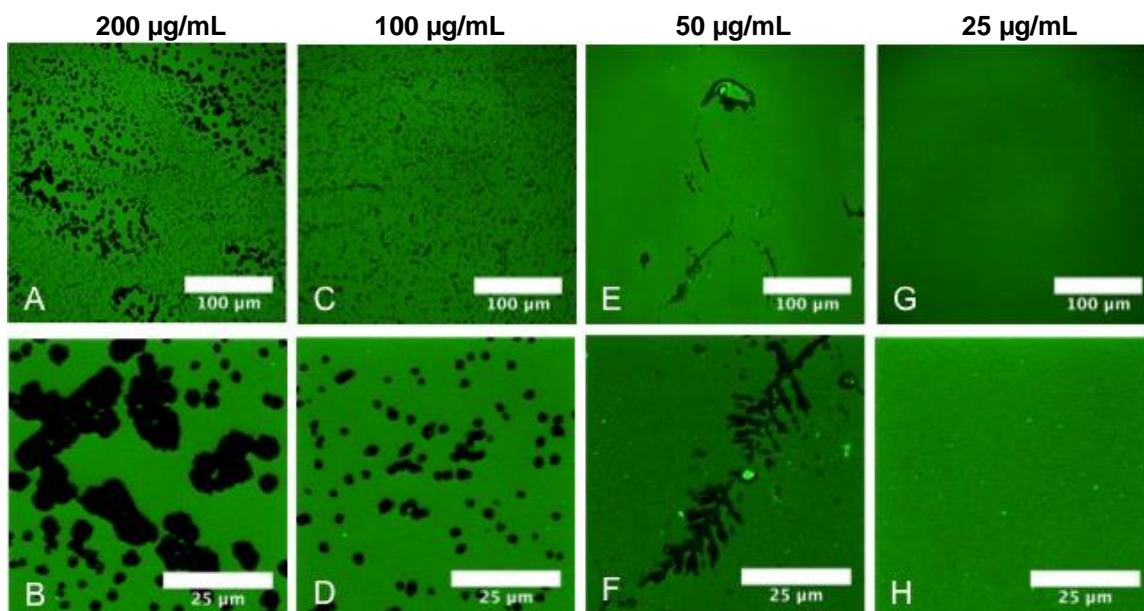


**Figure A6.6. Bilayers enriched with 5% sphingomyelin and 25% cholesterol.** Incubated decreasing (left to right) concentrations of LPS for 20 min at room temperature. Top row: images using 1x magnification. Bottom row: Images taken at 5x magnification of some of defects seen.

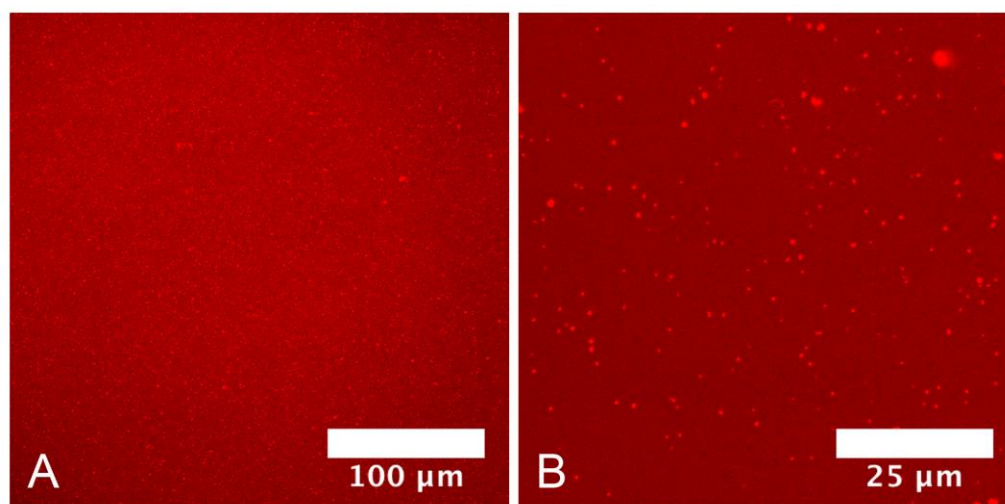


**Figure A6.7. Lipid bilayers controls for elevated temperature studies.** A. Bilayer imaged at 37 °C and then imaged again under 5x magnification (B). No defects were observed.

Section A6.2 Effect of murine serum on LPS-induced cytokine expression

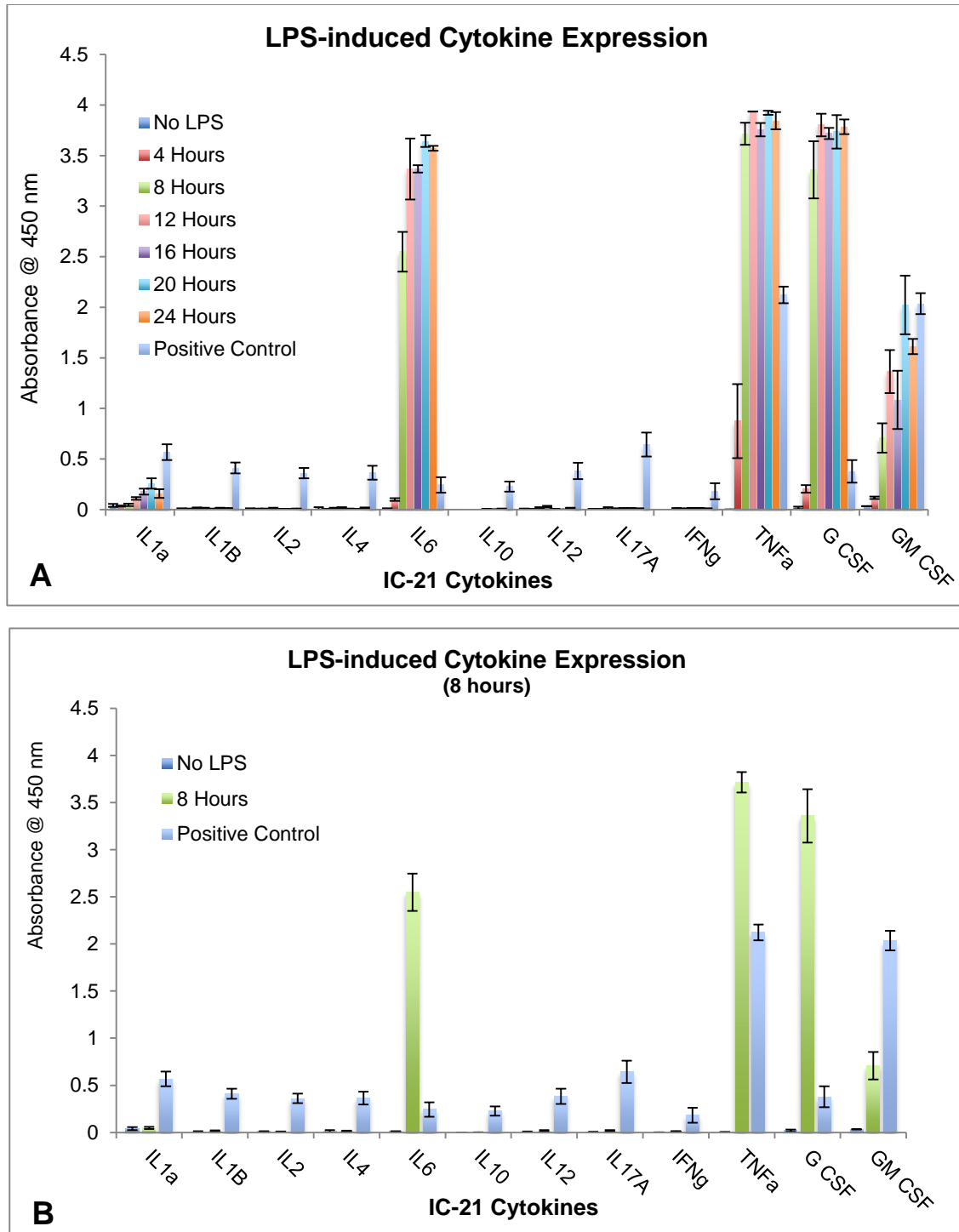


**Figure A6.8. LPS-induced cytokine expression in IC-21 cells.** A. A time point study in a 12-plex kit was used with 100 ng/mL LPS to determine the optimum time necessary to look at cytokine expression. B. The 8 hour time point was selected from the time point study and re-graphed for clarity. Results are plotted as the mean absorbance of three replicates with standard deviation error bars.

LPS spiked into serum and allowed to incubate overnight previous to dosing cells, was determined to have a minimally measurable cytokine effect on the IC-21 (TLR4 positive) cell line as compared to the LPS negative control. While it was evident that inflammatory cytokines were being expressed at levels above the negative control in some cases (IL-1 $\alpha$ , IL-1b, IL-17a, G-CSF), the general trend was that we could not determine the difference between the serum control and the experimental group of serum spiked with LPS. This dictated methods for the following experiment and determined that LPS should be added to the serum immediately prior to dosing the cells.

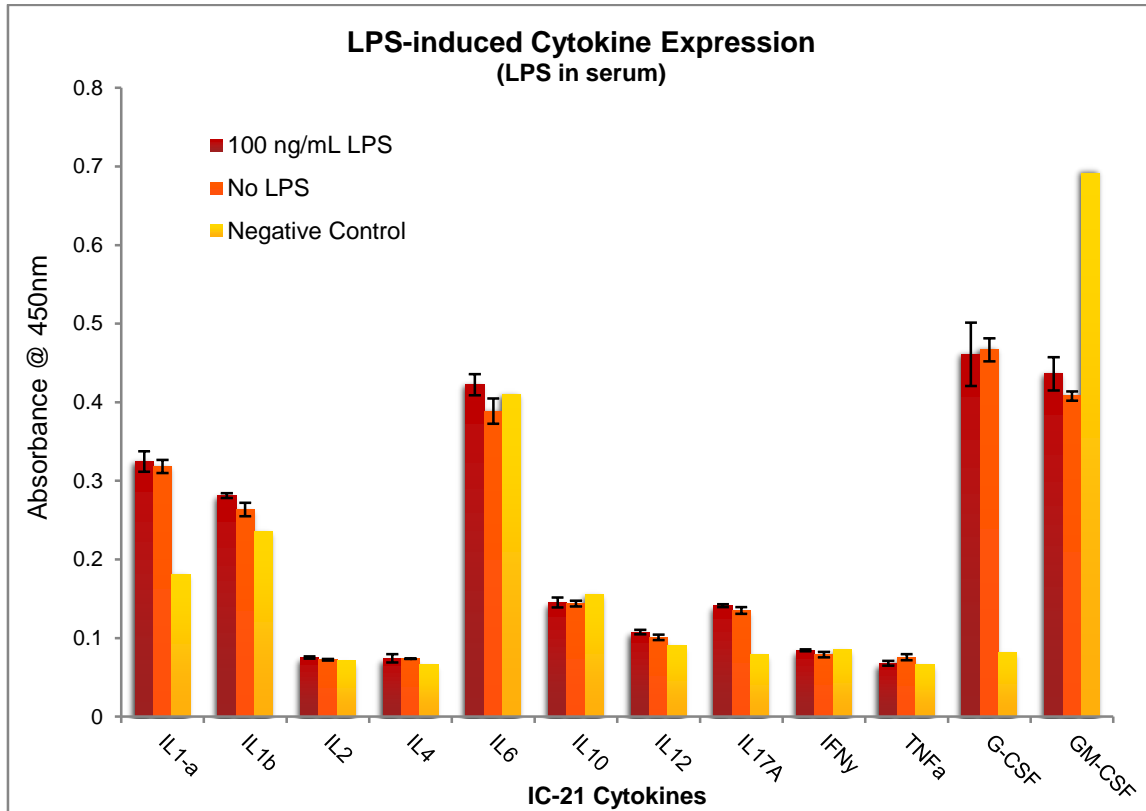


**Figure A6.9. Cytokine expression of IC-21 cells when LPS is presented to cells in serum.** LPS was spiked into mouse serum and allowed to incubated overnight prior to introduction to cells. After an 8 hour incubation period, no cytokine expression above the negative (no cytokine) control could be detected. Results are plotted as the mean absorbance of three replicates with standard deviation error bars.

Mean fluorescence intensity (MFI) of cytokine standards was processed using a 5 parameter logistic equation (**Equation A6.1**). Equations were generated for each set of cytokine standards (each microplate had its own set of standards) using an

online tool (myassays.com). The 5 parameter logistic fit (5PL) is suitable for quantitative analysis of asymmetric data results, which is often the case in biological data. The samples are first corrected by subtracting the mean of the blank measurements (in this case 0 pg/mL was used as the blank). The data points are then plotted as concentration versus the corrected MFI (**Figure A6.10**), and then the 5PL is made through the data points. The concentrations of the expressed cytokines can then be determined by using the 5PL fit. One of the limitations of the 5PL method is that data points outside of the range of the upper and lower asymptotes cannot be directly calculated. This is the reason some blank spaces appear in **Tables A6.3, A6.4, and A6.6**. The 5PL fit equation is as follows:

$$f(x) = D + \frac{A - D}{[1 + (\frac{x}{C})^b]^m}$$

**Equation 1**

Where **A** is the minimum MFI value (lower asymptote), **b** is the Hill slope, **C** is the inflection point on the curve, **D** is the maximum MFI value (upper asymptote), and **m**, is the asymmetry factor. This equation can then be solved for **x**, which is the concentration of cytokine. However, to get **x** is a rather laborious calculation, and therefore by using software to determine these values, we minimize the chances for errors in the calculations. Values for each variable in the equation for the five primary inflammatory cytokines are shown in **Table A6.1** and **Table A6.2**, along with the calculated R<sup>2</sup> value for each fit. Different values were obtained as each kit came with a set of standards to run in duplicate on individual plates.

**Table A6.1 Values for the variables in the cytokine standards determined from the 5 parameter logistic fit using the controls on the 23ScCr plate.**

Variable	IL-1 $\alpha$	TNF $\alpha$	IL-6	IL-12	IFN $\gamma$
A	11.07	16.66	64.14	11.19	42.30
B	1.16	1.15	1.051	1.14	1.22
C	2337	142368	9405	12391	3397
D	9977	2090	35679	29674	39261
M	1.01	715.98	1.002	1.00	1.01
R <sup>2</sup>	0.998	0.970	0.998	0.999	0.999

**Table A6.2 Values for the variables in the cytokine standards determined from the 5 parameter logistic fit using the controls on the IC-21 plate.**

Variable	IL-1 $\alpha$	TNF $\alpha$	IL-6	IL-12	IFN $\gamma$
A	-17.8215	-8.19711	-3.79875	5.34817	42.2976
b	1.00079	1.03838	0.929849	1.03272	1.21926
C	4387.19	750.53	24188.2	25083.8	3396.78
D	14344.2	3564.72	64856.6	50619.4	39260.9
m	1	1.02497	0.998988	1.00075	1.00965
R <sup>2</sup>	0.973	0.919	0.982	0.995	0.999

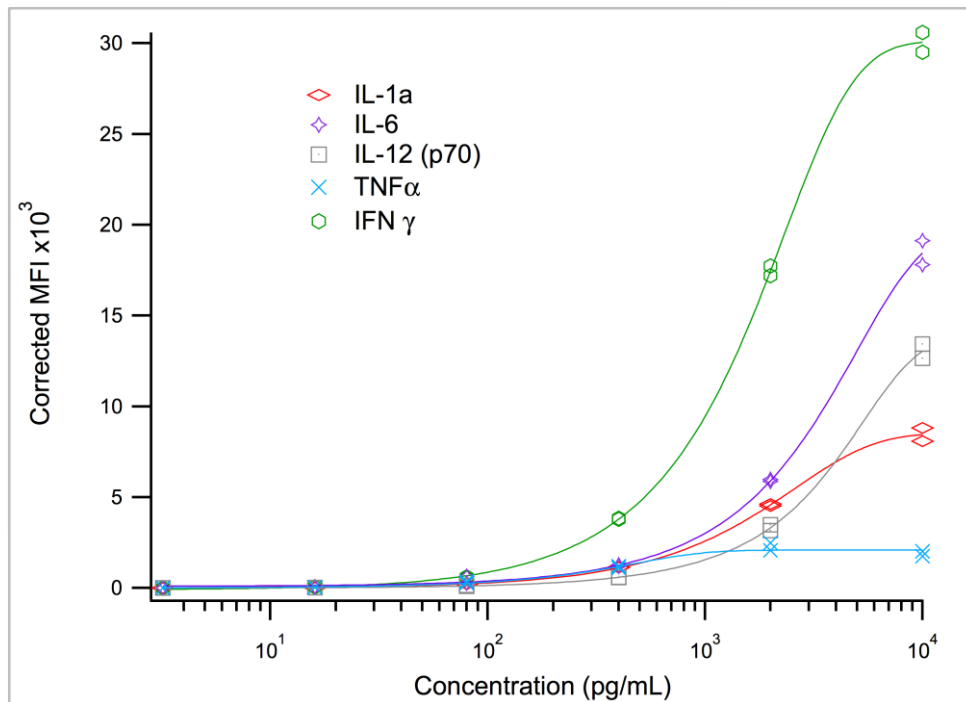


**Figure A6.10. Standard curves for murine cytokines using the Milliplex XMap 25-plex kit.** Results for duplicates of the standards were processed using a 5 parameter logistic and plotted on a semi-log scale against the corrected mean fluorescence intensity (MFI).

**Table A6.3. Calculated cytokine expression in pg/mL using serum variants**

Test Group	IC-21 - TLR4 (+) cells					23ScCr - TLR4 (-) cells				
	IL-1 $\alpha$	TNF $\alpha$	IL-6	IL-12	IFN $\gamma$	IL-1 $\alpha$	TNF $\alpha$	IL-6	IL-12	IFN $\gamma$
serum	9.738	2.604	7.483	-	6.484	4.346	-	81.978	-	0.670
serum + LPS	12.615	3.260	13.71	-	9.318	2.975	-	86.497	-	-
'no serum'	9.841	2.522	0.459	-	0.956	7.632	-	-	-	-
'no serum' + LPS	90.964	26.814	52.63	1.452	2.701	6.534	-	-	-	-
d.serum	37.106	149.86	505.6	5.953	11.780	14.782	16.688	41.197	-	6.836
d.serum + LPS	79.586	226.02 0	1204	8.668	16.881	10.252	9.360	9.167	-	4.146

**Table A6.4 Values for the variables in chemokine standards determined from the 5 parameter logistic fit using the controls on the IC-21 plate.**

Variable	RANTES	MIP-2	MIP-1b	MIP-1a	KC	MCP-1	IP-10	IL-9	G-CSF	GM-CSF
A	41.99	-5.572	-4.204	9.305	-69.68	-12.54	138.34	3.589	6.535	4.465
b	1.213	1.543	1.494	1.287	0.929	1.375	1.382	1.266	0.922	2.002
C	93.20	2761	936.8	7151	2118	2713	1473	19399	13096	4241
D	8480	18815	14541	41700	21980	17399	32202	12337	28327	28388
m	0.654	1	1	1	0.993	0.993	1.012	1	0.999	1.005
R <sup>2</sup>	.903	0.914	0.930	0.935	0.956	0.999	0.990	0.999	0.918	0.970

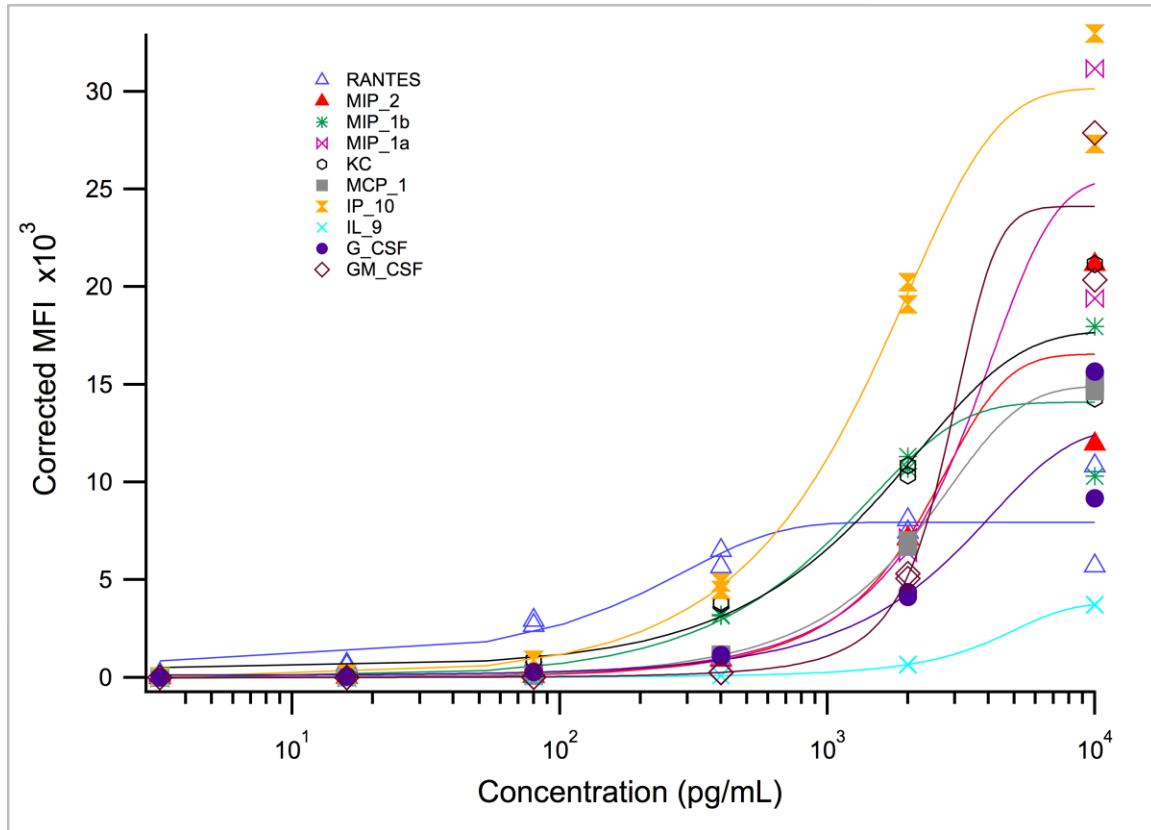


**Figure A6.11. Standard curves for other murine cytokines/chemokines.** Obtained using the Milliplex XMap 25-plex kit. Results for duplicates of the standards from the IC-21 plate were processed using a 5 parameter logistic and plotted on a semi-log scale against the corrected mean fluorescence intensity (MFI).

### Section A6.3 The effect of FBS on cytokine expression

The addition of 50% FBS to cells in an attempt to detach the cells from the tissue culture treated surfaces produced an unexpected response. We also examined FBS as a control presentation method of LPS in our cytokine panels. Firstly, we did not observe any de-adherence of IC-21 cells from the culture surface as was observed when using mouse serum. This negated the possibility of using this as a new method to remove cells. However, the presentation of LPS in FBS produced a dramatic response both in TLR4(+) and TLR4(-) cell lines (**Figure A6.11 C,D**), especially in comparison to the experiments performed in mouse serum (**Figure A6.11 A,B**) Significant levels of IL-1 $\alpha$ , TNF $\alpha$ , and IL-6 were produced in the FBS + LPS group. Calculated concentrations can be found in **Table A6.4**. The FBS + LPS test group is very interesting in that it produces elevated levels as compared

to the mouse serum. These results pose some interesting questions about the lipoprotein composition of FBS, and whether it would offer a similar protective effect in bovine cells as mouse serum does to murine cells. This is another important point for the design of *in vitro* studies as FBS is a commonly used supplement and usually the serum of choice for many cell lines. Studies that use FBS in experiments for different animal cell lines should be particularly aware of the potential for altered effects due to serum choice.

**Table A6.5. Calculated cytokine expression in pg/mL using FBS and normal murine serum**

Test Group	IC-21 - TLR4 (+) cells					23ScCr - TLR4 (-) cells				
	IL-1 $\alpha$	TNF $\alpha$	IL-6	IL-12	IFN $\gamma$	IL-1 $\alpha$	TNF $\alpha$	IL-6	IL-12	IFN $\gamma$
'no serum'	9.841	2.522	0.459	-	0.956	7.632	-	-	-	-
serum	9.738	2.604	7.483	-	6.484	4.346	-	81.978	-	0.670
serum + LPS	12.615	3.260	3.329	-	9.318	2.975	-	86.497	-	-
50% FBS	6.403	2.357	0.214	-	0.253	7.02	-	-	-	-
50% FBS + LPS	318.1	87.52	1736	14.33	7.695	12.99	5.793	603.2	6.92	-

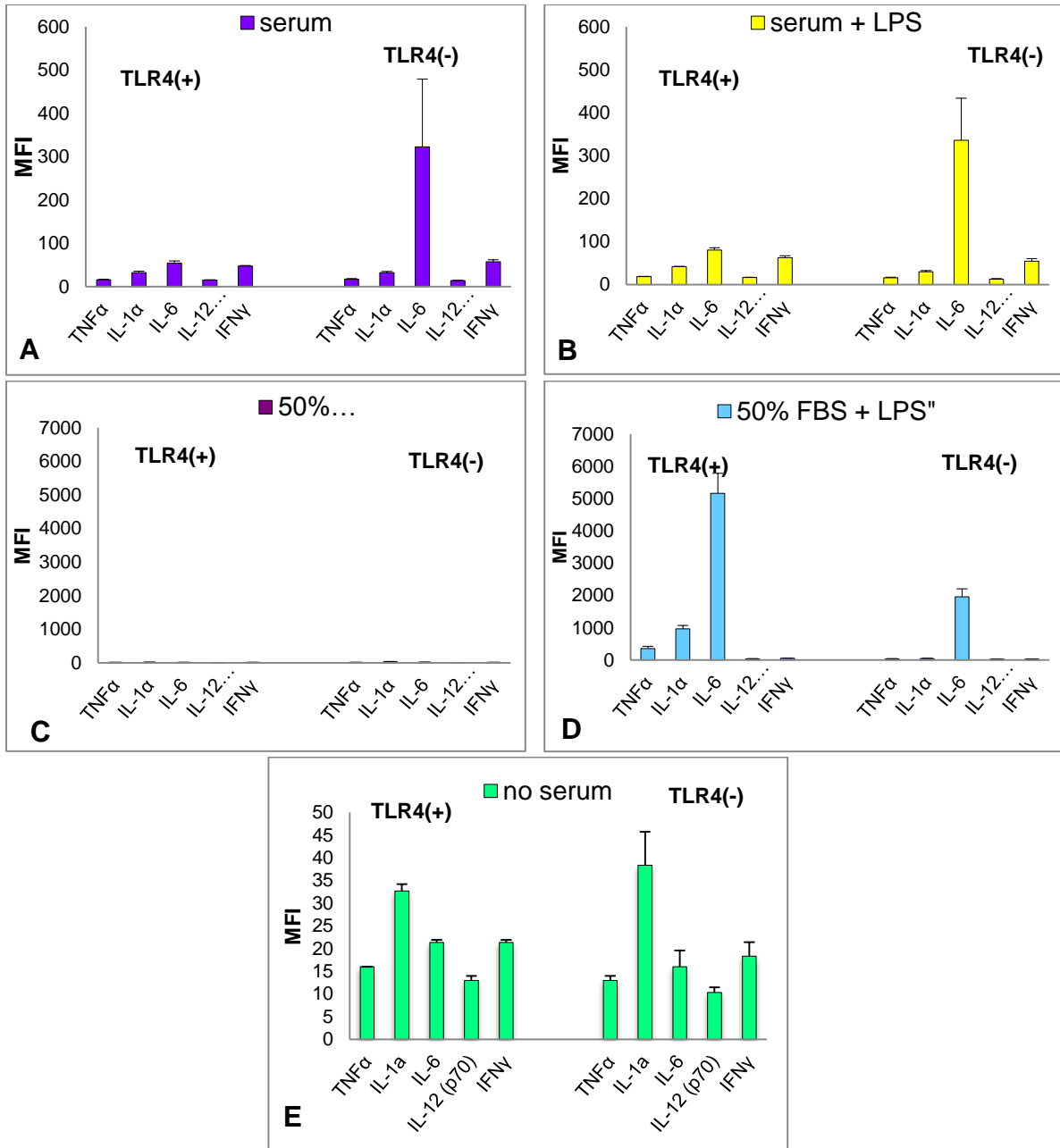


**Figure A6.12 The effect of 50% FBS on cytokine expression.** Proinflammatory cytokines were measured using the 25-plex kit to determine if FBS had a detrimental effect on cells. A-B 50% mouse serum and 50% mouse serum with LPS. C-D 50% FBS with and without LPS. E. No serum, buffer control. We spiked serum with LPS and discovered that FBS spiked with LPS results in a much higher inflammatory response than mouse serum spiked with LPS.